Development of Novel Nuclease Inhibitors as Potential Anticancer Agents

A thesis submitted to the University of Oxford for the degree of Doctor of Philosophy

Marcin Bieliński

St Peter's College

Department of Chemistry

University of Oxford

Hilary Term 2022

Abstract

Development of Novel Nuclease Inhibitors as Potential Anticancer Agents

Marcin Bieliński, St Peter's College

Thesis submitted for the degree of Doctor of Philosophy, Hilary Term 2022

SNM1A and SNM1B are 5' to 3' exonucleases that are involved in the repair of DNA interstrand crosslinks (ICLs); the endonuclease SNM1C is involved in the repair of DNA double strand breaks via non-homologous end-joining. Cells depleted in SNM1A and SNM1B show increased sensitivity toward clinically used ICL inducing drugs, such as cisplatin or mitomycin C and those cells depleted in SNM1C display increased sensitivity towards ionising radiation. Inhibitors of SNM1A, SNM1B, and SNM1C could potentiate the effects of these commonly used cancer drugs or prevent the development of resistance to them.

A high-throughput screen was carried out to identify SNM1 hits for use as a foundation for the development of new inhibitors. Building on these hits, sets of structural analogues were synthesised to investigate structure-activity relationships (SAR). The developed compounds were initially tested using a fluorescence-based assay, with activity for apparent inhibitors being validated by radioactive gel-based assays.

The hydroxamic acid group was identified as a pharmacophore targeting the active site of SNM1 nucleases. Initial sets of hydroxamate-based compounds inhibited all three SNM1 nucleases, demonstrating no selectivity. By application of iterative rounds of SAR analysis informed by crystallographic data, improved hydroxamate-based inhibitors were developed.

The work culminated in a series of compounds that selectively inhibits SNM1B with IC_{50}s in the low nanomolar range. Although potent inhibition was observed against purified, recombinant SNM1B, achieving a similar result in human cell lines was more challenging despite the use of a prodrug strategy.

Overall, the work reveals that potent and selective inhibition of human SNM1 nuclease isoforms is viable. Future work can focus on optimising the cellular potency of SNM1 inhibitors.

Acknowledgements

First of all, I would like to thank Prof Christopher Schofield for offering me this challenging, yet rewarding, project and for his assistance throughout its development. Additionally, I would like to thank our collaborators, Prof Peter McHugh and Prof Opher Gileadi, without whom this project would not be possible.

I am grateful to all members of the Schofield group, especially Jurgen, Karina, Daniel, Tika, Klem and Tom, for all the insightful discussions about science and everything else. I am also thankful to all members of Peter's and Opher's labs, especially Hannah and Lucy, who helped me survive through the endless hours spent on testing inhibitors and proofreading this thesis; Lia and Joe, who contributed with beautiful crystal structures.

I want to thank the SBM CDT and all the partners for funding. I am also thankful to all fellow SBM students with whom I shared this journey.

Finally, I am thankful to my wife, Joanna, who always supported me even when she felt left out because I focused too much on my project. Also, a huge thank you to my family back home in Poland.

Table of Contents

Abbreviations

°C	degree Celsius
δ	chemical shift
(6-4)PP	pyrimidone (6-4) photoproduct
8-oxo-G	8-oxo-guanine
Å	Angstrom
ADP	adenosine diphosphate
AlkB	α-ketoglutarate-dependent DNA repair protein B
alt-NHEJ	alternative NHEJ
AMP	adenosine monophosphate
anh.	anhydrous
app	apparent
aq	aqueous
AP	apurinic/apyrimidinic
APE1	apurinic endonuclease 1
APTX	aprataxin
Ar	aryl
ATM	ataxia telangiectasia mutated
ATP	adenosine triphosphate
ATR	ATM and Rad3-related
BER	base excision repair
BHQ	black hole quencher 1
Bn	benzyl
br	broad (NMR)
BRCA	breast cancer early onset
c-NHEJ	classical NHEJ
CO	crossover
conc.	concentrated
CPD	cyclobutane pyrimidine dimers
CPSF	cleavage and polyadenylation specificity factor
CASP	CPSF, Artemis, SNM1, PSO2
d	doublet (NMR)
D-loop	displacement loop
DCM	dichloromethane
DDR	DNA damage response
dHJ	double Holliday junction
DIPEA	*N*-diisopropylethylamine
DMA	dimethylacetamide
DMF	dimethylformamide
DMSO	dimethylsulfoxide
DNA	deoxyribonucleic acid
DNA-PK	DNA-dependent protein kinase
DNA-PKcs	DNA-PK catalytic subunit
DNase	deoxyribonuclease
DSB	double strand break

dsDNA	double stranded DNA
DSBR	double strand break repair
ELF	European Lead Factory
ELAC	ElaC ribonuclease Z
EME1	essential meiotic structure-specific endonuclease 1
equiv.	equivalent
ESI	electrospray ionisation
Et	ethyl
EtOAc	ethyl acetate
EXO1	exonuclease 1
FA	Fanconi anemia
FAN1	FANCI-associated nuclease 1
FEN1	flap endonuclease 1
FITC	fluorescein isothiocyanate
GG-NER	global genome NER
h	hour(s)
HDAC	histone deacetylase
HPLC	high performance liquid chromatography
HR	homologous recombination
HRMS	high resolution mass spectrometry
HTS	high-throughput screening
IC_{50}	half maximal inhibitory concentration
ICL	interstrand crosslink
IDL	insertion and deletion loops
INT	integrator complex
IR	infrared
J	coupling constant
LC-MS	liquid chromatography coupled mass spectrometry
LIG	DNA ligase
lit.	literature
LRMS	low resolution mass spectrometry
M	molar
M1G	pyrimido[1,2-a]purin-10(3H)-one
MBL	metallo-β-lactamase
Me	methyl
MGMT	O^6-methylguanine DNA methyltransferase
MHz	megahertz
min	minute(s)
MMR	missmatch repair
MRE11	meiotic recombination 11 homolog A
MRN	MRE11-RAD50-NSB1
mRNA	messenger RNA
MS	mass spectrometry
MUS81	methyl methanesulfonate ultraviolet sensitive gene clone 81
m/z	mass to charge
NCO	non-crossover

NER	nucleotide excision repair
NHEJ	non-homologous end joining
NHS	*N*-hydroxysuccinamide
NMR	nuclear magnetic resonance
p	quintet (NMR)
PALB2	partner and localizer of BRCA2
PARP	poly(ADP-ribose) polymerase
PCNA	proliferating cell nuclear antigen
Pd/C	palladium on carbon
PlKK	phosphatidylinositol 3-kinase-like protein kinases
PNKP	polynucleotide kinase 3′ phosphatase
Pol	polymerase
PSO	psoralen derivative sensitive
q	quartet (NMR)
RAD23B	UV excision repair protein RAD23 homolog B
RFC	replication factor C
RMI1	RecQ-mediated genome instability protein 1
RNA	ribonucelic acid
RNAP	RNA polymerase
ROS	reactive oxygen species
RP HPLC	reversed-phase HPLC
RPA	replication protein A
RT	room temperature
RTEL1	regulator Of telomere elongation helicase 1
s	singled (NMR)
SAR	structure activity relationship
sat.	saturated
SBL	serine-β-lactamase
SDSA	synthesis-dependent strand annealing
SNM1	sensitive to nitrogen mustard 1
snRNA	small nuclear RNA
SSB	single strand break
ssDNA	single stranded DNA
SSBR	single-strand break repair
t	triplet (NMR)
TC-NER	transcription coupled NER
TEA	triethylamine
TFA	trifluoroacetic acid
TFIIH	transcription factor II Human
THF	tetrahydrofuran
TLC	thin-layer chromatography
TLS	translesion synthesis
TMBS	trimethylbromosilane
TOP	DNA topoisomerase
tRNA	transfer RNA
UV	ultraviolet

v	volume
wt.	weight
XP	Xeroderma pigmentosum
XRCC1	X-ray repair cross-complementing protein

Chapter 1. Introduction

1.1. Threats to genome integrity

Every day, in each cell in the human body, thousands of spontaneous and induced DNA damaging events occur, caused by both endogenous and exogenous sources.[1] Accumulation of such DNA damage can lead to apoptosis or genome instability, resulting in the development of cancer, neurodegenerative diseases, and ageing.[2, 3]

1.1.1. Endogenous sources of DNA damage

Under physiological conditions, the stability of DNA is at constant risk. The presence of appropriately located water molecules can lead to hydrolysis of *N*-glycosidic bonds and cleavage of nucleic acid bases, resulting in apurinic/apyrimidinic (AP) sites; DNA depurination is 500 times more frequent than DNA depyrimidination.[4,5] Single-strand breaks (SSBs) may occur via β-elimination and cleavage of a 3′ phosphodiester bond in case if the AP site is not repaired.[6] Furthermore, hydrolysis of cytosine leads to deamination, thus fascitilating the formation of a mismatch base pair or a point mutation.[7]

Reactive oxygen species (ROS), such as hydrogen peroxide, superoxide radicals, or hydroxyl radicals, are byproducts of many normal metabolic processes. While ROS can cause many different types of DNA lesions, the two most common ones are SSBs and the oxidation of guanine into 8-oxo-guanine (8-oxo-G).[8, 9] Additionally, ROS can cause lipid peroxidation that results in the formation of reactive aldehydes products, such as malondialdehyde or 4-hydroxynonenal. These aldehydes can cause the formation of mutagenic base adducts (e.g. pyrimidopurinone (M1G)) and DNA crosslinks

(**Figure 1.1**).[10,11] Errors in physiological processes involving nucleic acids, such as DNA replication, can lead to insertion, deletion, or mismatch of base pairs in the DNA.[12]

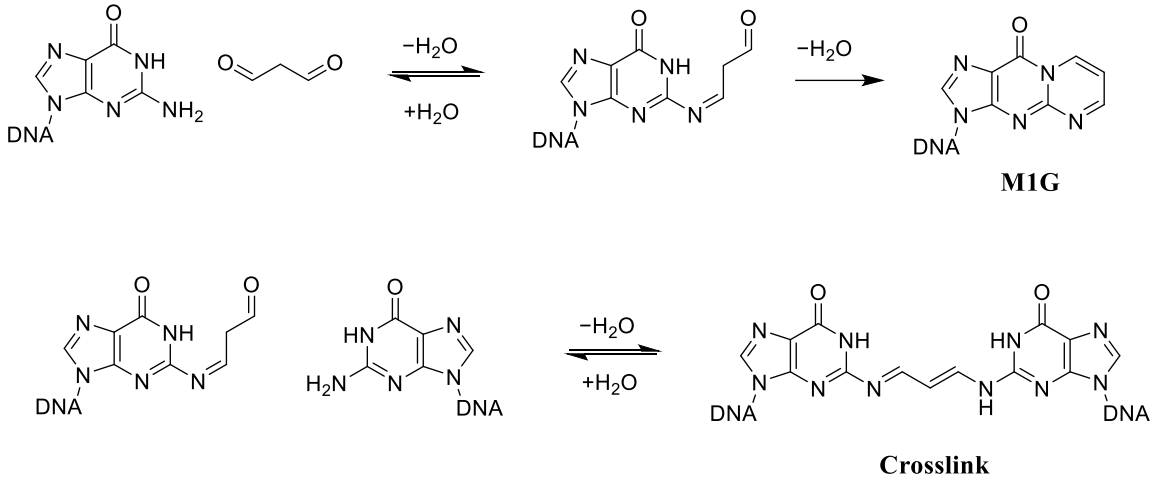

Figure 1.1: *Summary of reactions of malondialdehyde with DNA.*

1.1.2. Exogenous sources of DNA damage

On top of all the DNA lesions caused by endogenous physiological factors, DNA damage can be induced by a myriad of environmental factors. Ultraviolet (UV) radiation from the sun can cause dimerisation of pyrimidines to form cyclobutane pyrimidine dimers (CPDs) or pyrimidine-pyrimidone (6-4) photoproducts ((6-4)PPs).[13] These lesions primarily occur between two adjacent thymidine bases, potentially impeding replication or causing misreading of the DNA. Ionising radiation, which has higher energy than the UV radiation from the sunlight, not only does generate ROS, but also induces double-strand breaks (DSBs).[14,15] DSBs are very carcinogenic partly because they can lead to genome rearrangement, making them one of the most lethal DNA lesions. Since ionising radiation has the ability to slow cell division or cause cellular death, it is commonly used in radiotherapy to treat cancerous tumours.[16]

Many environmental pollutants—from tobacco smoke or the combustion of fossil fuels, amongst others—are cancerogenic.[17, 18] Similarly to ionising radiation, chemical DNA damaging agents, which can covalently bind to the DNA, are used in cancer treatment because of their cytotoxicity.[19] Clinically used DNA crosslink inducing chemotherapeutics include cisplatins, nitrogen mustards, and mitomycin C (**Figure 1.2**). These drugs primarily generate mono-base adducts or intrastrand cross-links between adjacent bases. On rare occasions, they can also generate interstrand crosslinks (ICLs) between two strands of the DNA duplex.[20,21] ICLs are particularly cytotoxic, with about 20−40 ICLs being lethal to a cell.[22] Most commonly, ICL inducing agents react with nitrogens at N2 or N7 position in guanines.[23] Reaction mechanisms for the formation of DNA interstrand crosslinks by cisplatins, nitrogen mustards, and mitomycin C are shown in **Figure 1.3**.

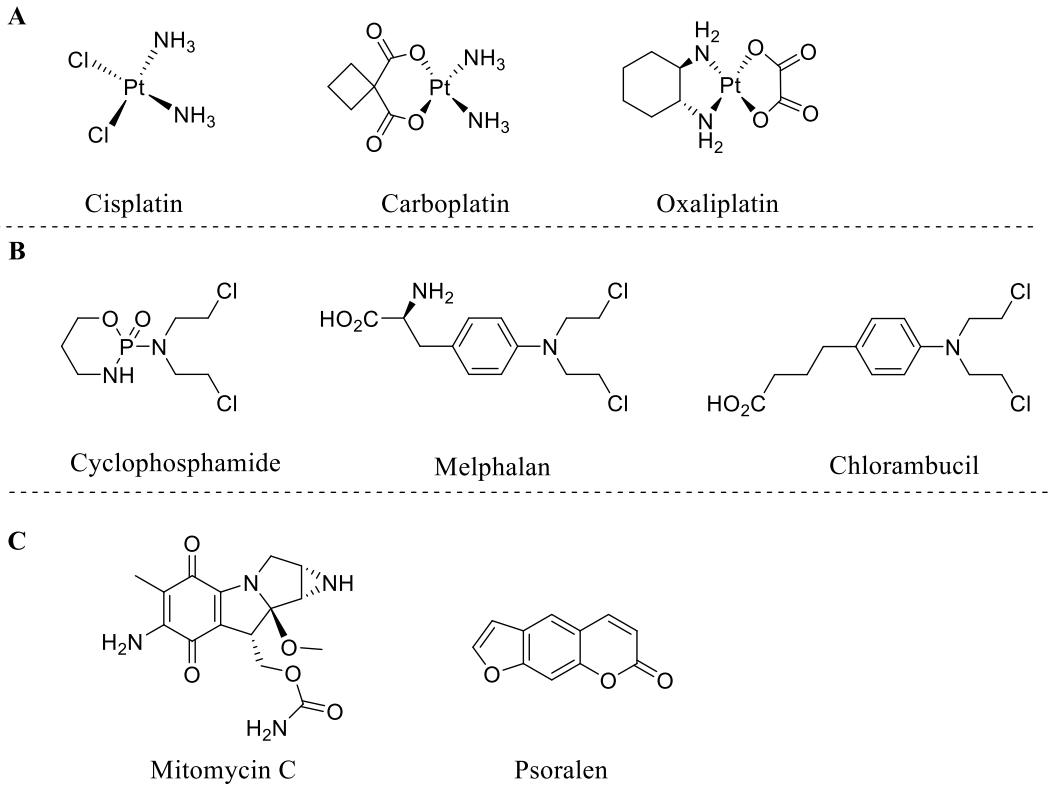

Figure 1.2: *DNA crosslink inducing agents.* ***A:*** *Cisplatins;* ***B:*** *Nitrogen mustards;* ***C:*** *Other types of crosslinking agents.*

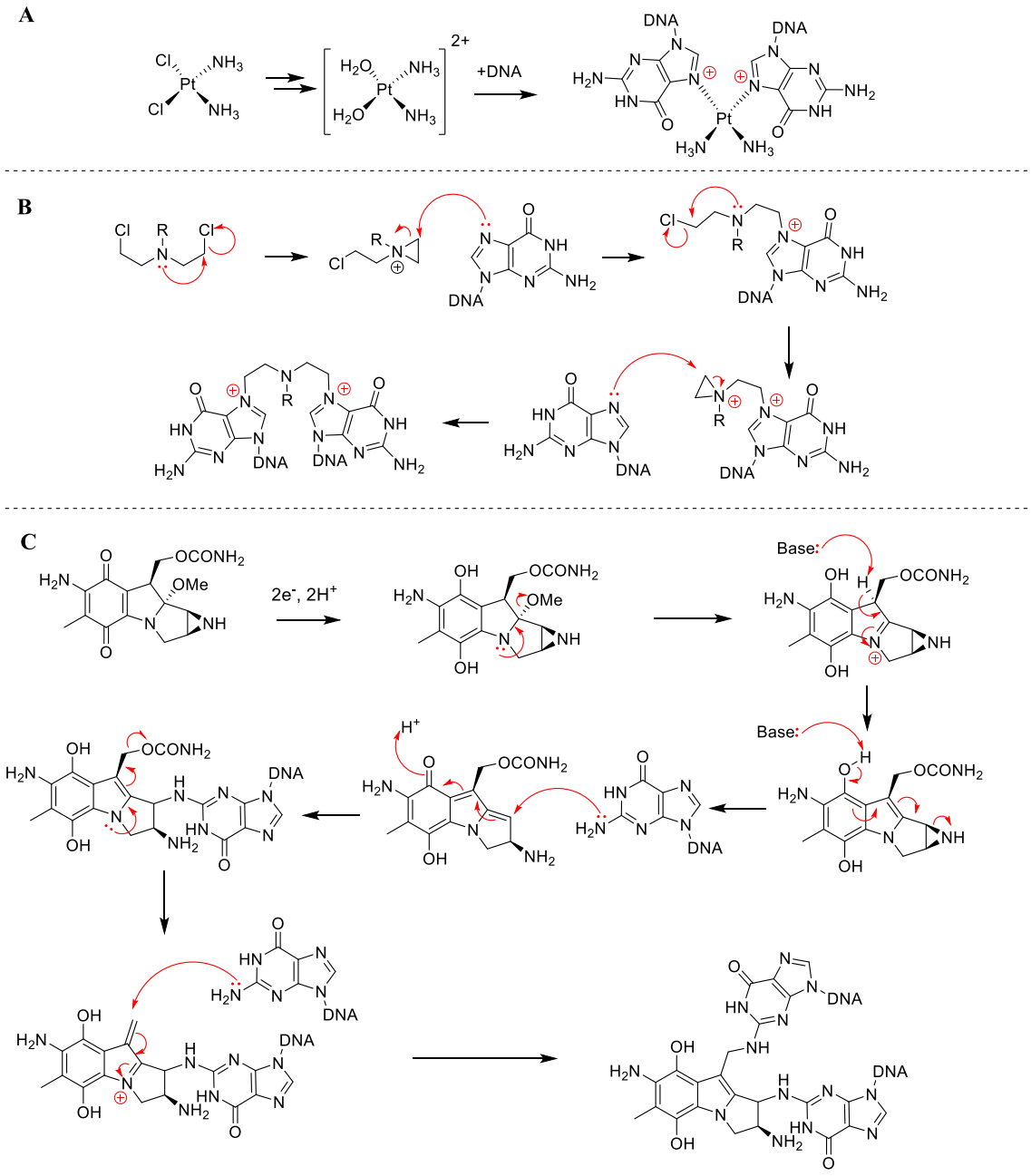

Figure 1.3: *Reaction scheme for ICL formation by* ***A****: Cisplatins;* ***B****: Nitrogen mustard;* ***C****: Mitomycin C.*

1.2. DNA damage response processes

The continuous formation of lesions in the DNA, caused by endogenous and environmental factors, has forced cells to evolve and develop a DNA damage response (DDR) processes to maintain genome integrity.[24] The DDR machinery senses specific lesions and initiates a

signalling cascade response. The latter can trigger apoptosis, senescence, alteration of gene expression, or a DNA repair pathway, depending on the extent and type of DNA damage in the genome. In eukaryotic DDR poly(ADP-ribose) polymerases (PARPs) and phosphatidylinositol 3 kinase-like protein kinases (PlKKs), including ataxia telangiectasia mutated (ATM), ATM and Rad3 related (ATR), and DNA-dependent protein kinase (DNA-PK), play important roles.[25,26] While ATR and PARP enzymes are primarily involved in the repair of SSBs, ATM and DNA-PK are mainly involved in the repair of DSBs.[27]

1.2.1. DNA damage repair pathways

Repair of specific DNA lesions occurs in many different ways, ranging from simple chemical reversals of a lesion to complex multistep pathways of DNA repair. Enzymes that can directly reverse chemical changes of DNA include photolyases (not active in humans), methyltransferases, and demethylases. For example, (6-4)DNA photolyase catalyses bond breakage in (6-4)PPs dimer to reform initial monomers.[28] O^6-Methylguanine DNA methyltransferase (MGMT) and the α-ketoglutarate-dependent DNA repair protein B (AlkB) can demethylate methylated DNA bases, lesions that are caused by endogenous and exogenous methylating agents. While MGMT reverses methylation of the *O*-methylated DNA base using nucleophilic cysteine, the AlkB dioxygenase oxidatively demethylates *N*-methylated bases. [29,30]

To repair other DNA lesions, cells have developed several complex repair pathways. These include base excision repair (BER), nucleotide excision repair (NER), translesion synthesis (TLS), mismatch repair (MMR), single-strand break repair (SSBR) and double-strand break repair (DSBR), as well as interstrand crosslink (ICL) repair pathways. Each

pathway has multiple steps with many proteins involved in the repair, and with several proteins typically being involved in repairing more than one type of lesion.[31]

1.2.1.1. Base excision repair

Base excision repair is used to repair chemically modified DNA bases (*e.g.* alkylated, deaminated, or oxidised bases) or AP sites caused by depurination and depyrimidination (**Figure 1.4**).[32] The initial step in BER is excision of the damaged base by DNA glycosylase to generate an AP site. Excision can be done by monofunctional DNA glycosylase, which only catalyses the hydrolysis of the *N*-glycosidic bonds to remove the damaged base, or by bifunctional DNA glycosylase, which can additionally catalyse β-elimination and cleavage at 3′ position of the AP site. The next step is the incision of the DNA backbone at the 5′ position of the AP site by apurinic endonuclease 1 (APE1).[33] The repair pathways then split into two subpathways, short patch and long patch BER.[34] In the short patch BER, the DNA polymerase β (Polβ) fills the gap with a single new base. In case the AP site is not removed, Polβ additionally hydrolysis 3′ phosphodiester bond via its deoxyribosephosphodiesterase activity.[35] Finally, the DNA is ligated by the X-ray cross-complementing 1 (XRCC1) and DNA ligase (LIG3α) complex.

Long-patch BER pathway occurs when after incision Polε or Polδ performs DNA polymerisation incorporating multiple nucleotides.[36] Next, excision of the newly formed 5′ flap is catalysed by flap endonuclease 1 (FEN1). In the final step, ligation is completed by LIG1 to complete the DNA repair.[37]

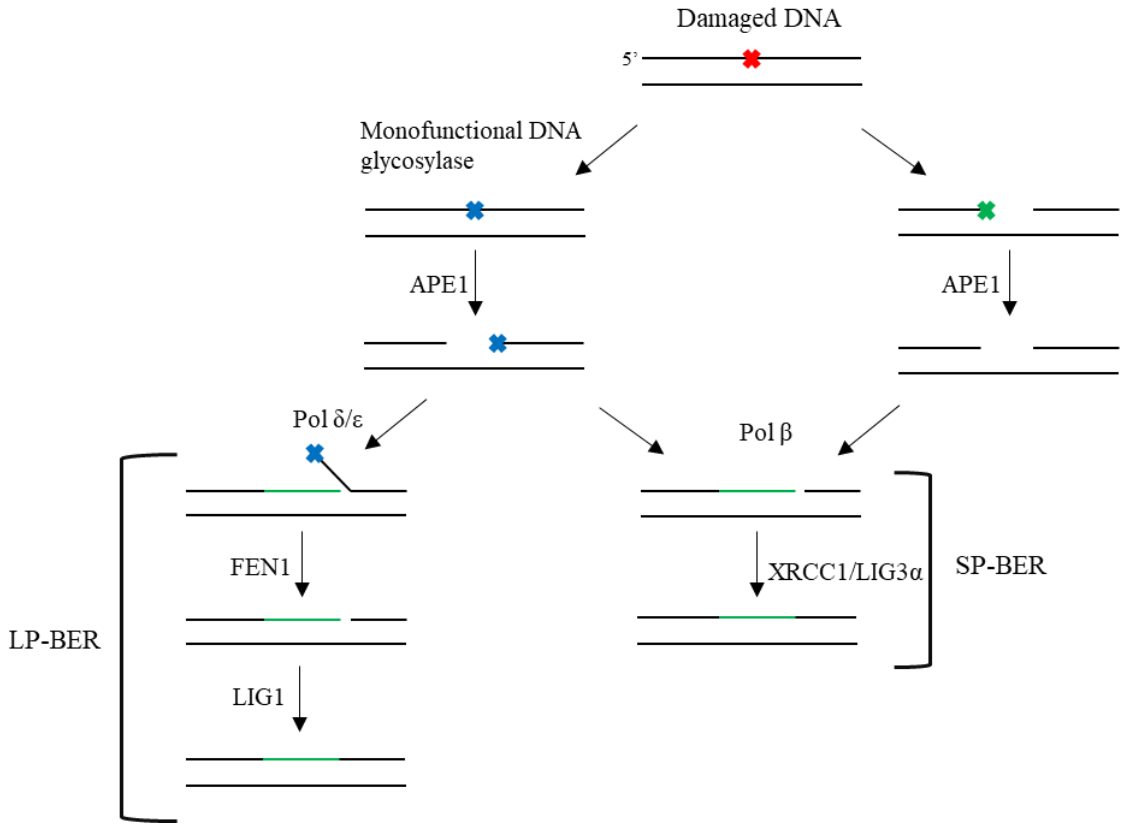

Figure 1.4: *Scheme of BER pathway. X: Damaged base. X: AP site. X: α,β-unsaturated aldehyde or 3′ phosphate. Green line: newly incorporated DNA sequence. SP-BER: short-patch base excision repair. LP-BER: long-patch base excision repair.*

1.2.1.2. Nucleotide excision repair

Whilst BER repairs small non-helix-distorting lesions, NER targets bulky lesions that distort the DNA helix.[38] Common helix distorting lesions are M1G produced by reaction with malondialdehyde and UV induced CDPs and (6-4)PPs. Nucleotide excision repair (**Figure 1.5**) may occur via two subpathways: global genome NER (GG-NER) and transcription coupled NER (TC-NER); the only difference between them is the damage recognition step and the recruitment of initial repair factors.[39,40]

NER is initiated by recognition of DNA damage. The recognition step can be triggered by the xeroderma pigmentosum complementation group C (XPC)/UV excision repair protein RAD23 homolog B (RAD23B) complex or due to RNA Polymerase II (RNAPII) stalling.

The XPC/RAD23B complex and RNAP are involved in GG-NER and TC-NER pathways, respectively. Following the recognition step, the transcription factor II Human (TFIIH) complex is recruited to the lesion, and helicases separate the DNA duplex around the lesion to form a transcription bubble.[41] After the formation of the DNA bubble, XPG, XPA, and replication protein A (RPA) proteins bind to the DNA and form a pre-incision complex.[42] XPA facilitates recruitment of XPF-excision repair cross-complementing 1 (XPF-ERCC1). RPA binds and protects undamaged single-stranded DNA, whereas XPF-ERCC1 and XPG endonuclease make incisions to remove the nucleotide fragment with the lesion. The gap is then filled by Polδ, ε, or κ with the assistance of proliferating cell nuclear antigen (PCNA) and replication factor c (RFC).[43] Finally, the process is completed when the nick in the DNA backbone is ligated by XRCC1/LIG3α complex or LIG1.

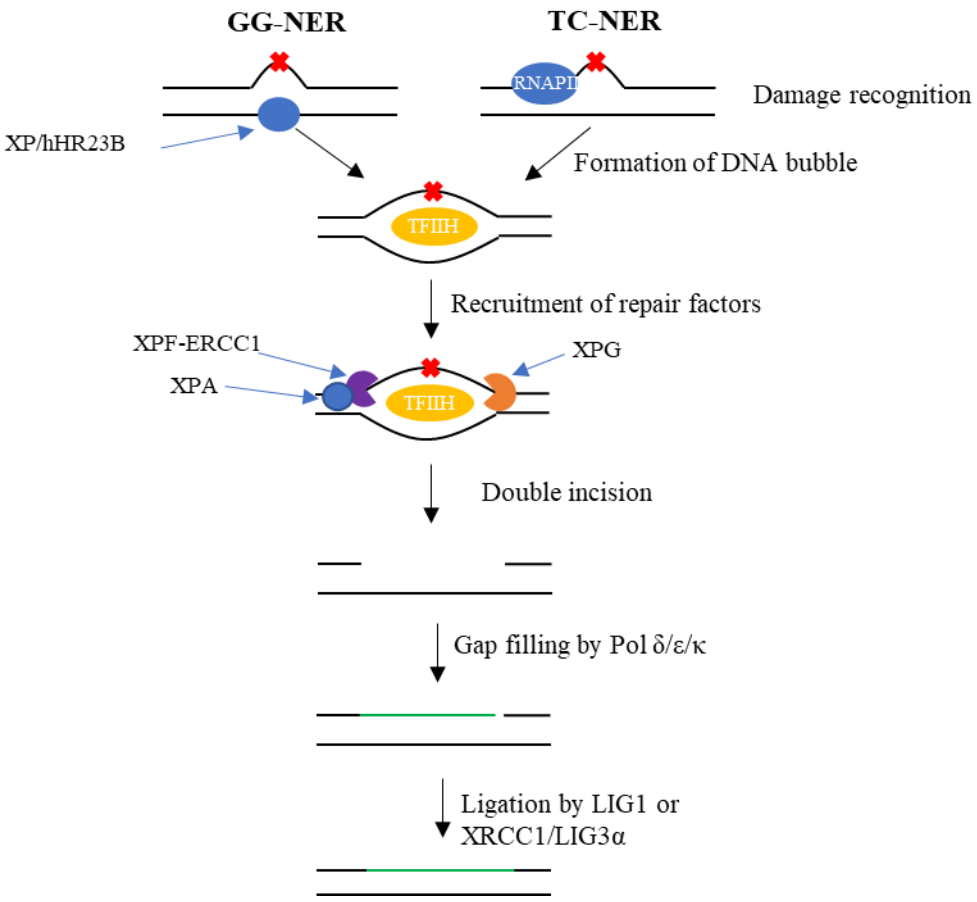

Figure 1.5: *Scheme for the NER pathway. X: Damaged base. Green line: newly incorporated DNA sequence.*

1.2.1.3. Translesion synthesis

Translesion synthesis, while not being a repair mechanism in itself, plays an essential role in preventing stalling of DNA replication and collapse of replication fork due to lesions in DNA, such as pyrimidine dimers or AP sites.[44] When a DNA polymerase stalls due to DNA lesions, a specialised translesion polymerase is recruited.[45] Translesion polymerases facilitate the insertion of correct nucleic bases opposite to the DNA damage site. Due to a lack of proofreading ability, the translesion polymerases are more error-prone and have lower fidelity relative to regular polymerases.[46] Therefore, switching back to a regular polymerase is favourable after bypassing DNA lesions. The DNA lesion is later repaired using one of the DNA repair pathways, *i.e.* NER or BER.

1.2.1.4. Mismatch repair

Mismatch repair (**Figure 1.6**) is a process responsible for repairing mispaired, deleted, and inserted DNA bases formed during DNA replication or homologous recombination.[47] MMR is initiated by recognition of DNA lesions by MutSα and MutSβ heterodimers. MutSα is responsible for recognising mispaired bases and short insertion and deletion loops (IDLs) (1-2 bases long), whilst MutSβ recognises long IDLs (+2 bases long).[48, 49] MutLα is then recruited by MutSα/β and makes an incision on the damaged strand. RFC and PCNA are involved in coordinating the incision.[50] After the incision is made, exonuclease 1 (EXO1) removes the lesion in the 5′ to 3′ direction via its exonuclease activity.[51] Finally, the gap is filled by Polδ, and LIG1 ligates the nick in the DNA. Cells with defective MMR have higher rates of mutations and tumour formation.[52]

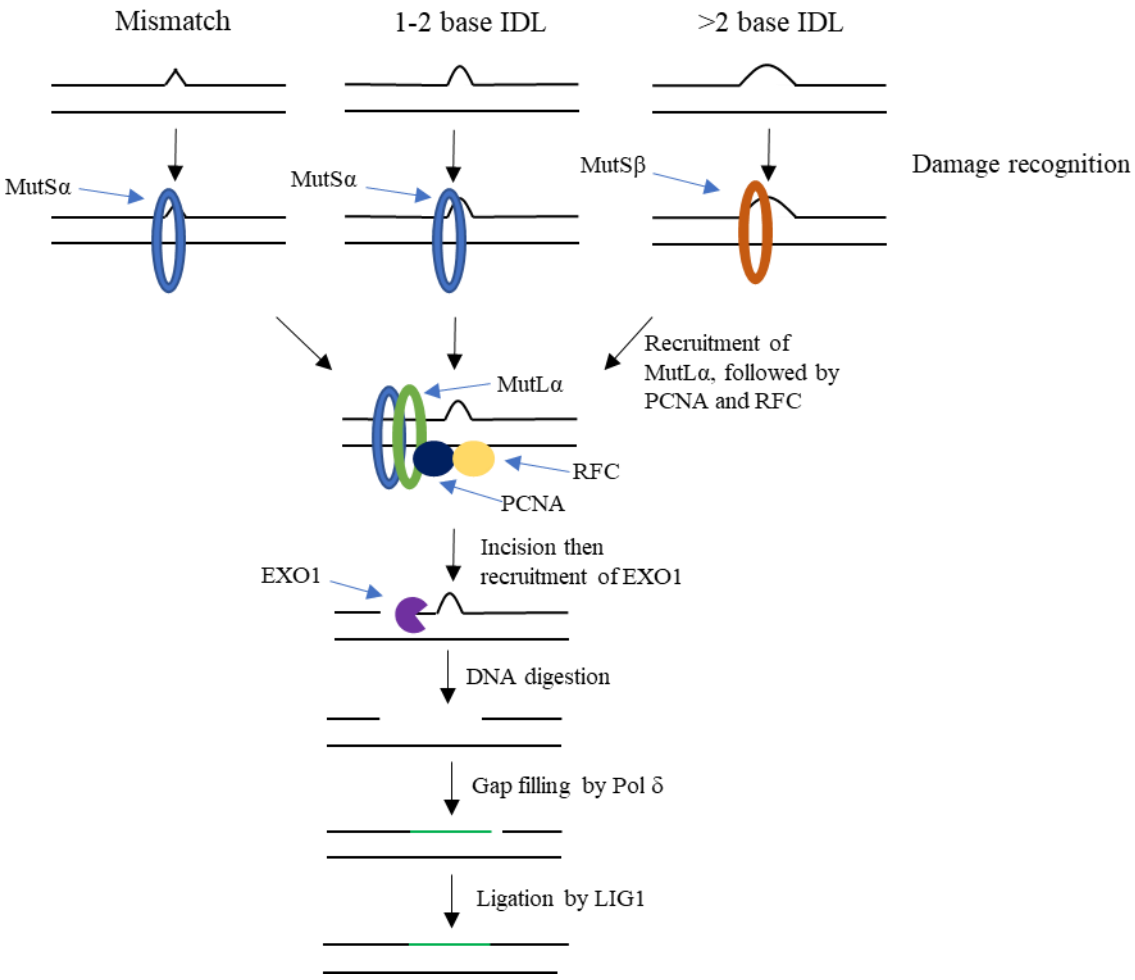

Figure 1.6: *Scheme for the mismatch repair pathway. Green line: newly incorporated DNA sequence.*

1.2.1.5. Single-strand break repair

Single-strand breaks, alongside depurination, are the most frequent DNA lesions.[53] The majority of SSBs are repaired via global SSB repair.[54] The repair process is initiated by detecting DNA damage, primarily performed by PARP1.[55] Before the gap in the DNA backbone can be filled, DNA ends need to be restored to 5′ phosphate and 3′ hydroxyl. Therefore, if any end is damaged (*e.g.* due to adduct on the phosphate or loss of 5′ phosphate), it must be processed for the DNA ends to be compatible for polymerisation and ligation. The enzymes involved in the DNA end processing depend on the type of damage. Common enzymes involved in this step include phosphatases, kinases, nucleases (APE1), or

polymerases.[56,57,58] The next two steps include gap filling and ligation. Similarly to the BER pathway, these final steps can happen via either a short patch or a long patch subpathway, described previously in **Section 1.2.1.1**. If SSBs are not repaired, they may lead to the formation of hazardous DSBs.[59]

1.2.1.6. Double-strand break repair

Double-strand break repair can happen via one of two major pathways: non-homologous end joining (NHEJ) and homologous recombination (HR). Since the homologous chromosome is required for the HR, it can only occur in the S and G_2 phases of the cell cycle. NHEJ may occur at any stage of the cell cycle. The choice between the pathways depends not only on the cell cycle phase but also on the nature of the DSB and the availability of the DNA ends.[60]

NHEJ is a repair pathway in which two ends of the DSB are directly ligated. NHEJ repair occurs via two subpathways: classical-NHEJ (c-NHEJ) or alternative NHEJ (alt-NHEJ) pathways, shown in **Figure 1.7**.[61] C-NHEJ repair is initiated by recognition of DSB by Ku70-Ku80 heterodimer, which later forms a complex with DNA-PK catalytic subunit (DNA-PKcs). Ku heterodimer stabilises the DNA ends and keeps them close together, while DNA-PKcs phosphorylates downstream substrates using its kinase activity.[62] Then, similarly to SSB repair, the DNA ends need to be processed to produce 5′ phosphate and 3′ hydroxyl groups, which are necessary for ligation.[63] DNA processing is primarily done by sensitive to nitrogen mustard 1C (SNM1C also known as Artemis), which removes damaged nucleotides using endonuclease activity.[64] Other common end processing enzymes include polynucleotide kinase 3′ phosphatase (PNKP) and aprataxin (APTX). PNKP phosphorylates 5′ ends and dephosphorylates 3′ ends, whilst APTX removes adenosine monophosphate (AMP) adducts.[65,66] Once the ends are processed, any gap created upon DSB or by end

processing is filled by Pol μ or λ.[67] Finally, the DNA ends are ligated by the XRCC4-LIG4 complex.[68]

Alternative NHEJ, also known as microhomology-mediated end joining, is activated when other pathways are unavailable. Alt-NHEJ is initiated by PARP1 recognising the DSBs. PARP1 modifies and recruits downstream factors.[69] In the next step, short ssDNA overhangs are generated by the resection of nucleotides. Meiotic recombination 11 homolog A (MRE11), EXO1, and FEN1 are implicated to be involved in this short-range resection process.[70] Following formation of the overhangs, they are annealed, guided through sequence homology.[71] Flaps that result from the annealing are cleaved by endonucleases, such as XPF/ERCC1 or FEN1.[72] Any remaining gaps are then filled by Pol θ, β, μ, or λ. Finally, XRCC1/LIG3 or LIG1 ligates the two strands.[73] Alt-NHEJ is much more error-prone than other DSB repair pathways as it can remove large portions of DNA sequence.[74]

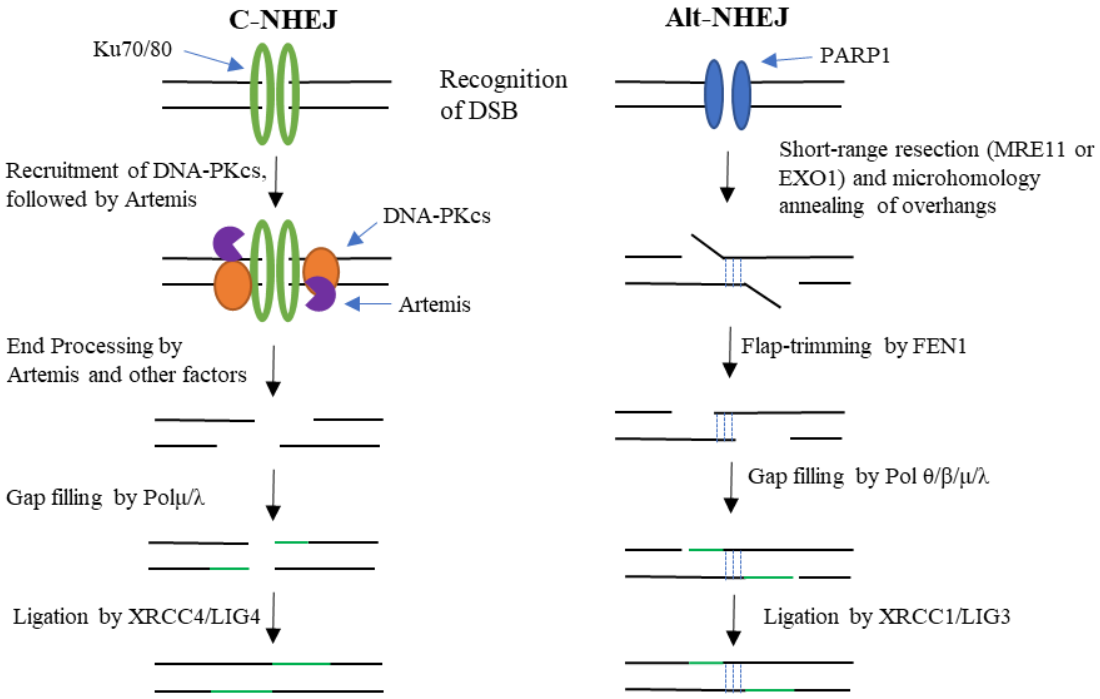

Figure 1.7: *Scheme of classical and alternative non-homologous recombination. Green line: newly incorporated DNA sequence.*

Homologous recombination (HR) is a high fidelity DSB repair process as it uses a template from a homologous chromosome. HR consists of several subpathways; the main two subpathways of HR discussed here are synthesis-dependent strand annealing (SDSA) and double strand break repair (DSBR), shown in **Figure 1.8**.[75] The SDSA and DSBR subpathways have the same initial pathway but diverge in the final steps. The HR repair is initiated when the MRN (MRE11-RAD50-NSB1) complex detects DSB and binds the end of DNA break.[76] MRN then activates ATM, which is involved in recruiting downstream factors. MRE11, together with EXO1 or the DNA replication ATP-dependent helicase/nuclease (DNA2) in conjunction with the Bloom's syndrome protein (BLM) helicase, digest a short chain of DNA in a 5′ to 3′ direction and produces 3′ overhangs.[77] RPA then binds the ssDNA resulting in the unwinding of the overhangs and activation of ATR, which recruits downstream factors through phosphorylation. Partner and localiser of BRCA2 (PALB2) and breast cancer 2 early onset (BRCA2) then mediate displacement of RPA in a RAD51-dependent manner.[78] The RAD51-DNA complex is able to invade homologous DNA duplex and form a displacement loop (D-loop). The polymerisation is primarily performed by replicative Pol δ, but other translational polymerases have been implicated in this process.[79] At this point, there are different possible outcomes, resulting in either crossover (CO) or non-crossover (NCO) products.[80]

In one pathway, the D-loop can dissociate via strand displacement, and the newly synthesised strand may anneal back to the original DNA strand. D-Loop dissociation is a part of the SDSA pathway; it is dependent on the helicase activities of BLM and regulator of telomere elongation helicase 1 (RTEL1) and results in an NCO product.[81]

If the D-loop does not dissociate, a second DNA strand may form another D-loop and generate a double Holliday-junction (dHJ). The dHJ can be separated via the dissolution or resolution process. In the dissolution of dHJ, the branch migration is catalysed by the topoisomerase activity of the BLM, DNA topoisomerase 3α (TOP3α), and RecQ-mediated genome instability protein 1 (RMI1) complex, leading solely to the formation of NCO products.[82] In the resolution of the dHJ, strands are separated by structure-specific endonucleases, such as methyl methanesulfonate ultraviolet sensitive gene clone 81 (MUS81) and essential meiotic structure-specific endonuclease 1 (EME1) complex.[83] Although resolution can lead to both NCO and CO products, this process mainly results in the formation of CO products.[84]

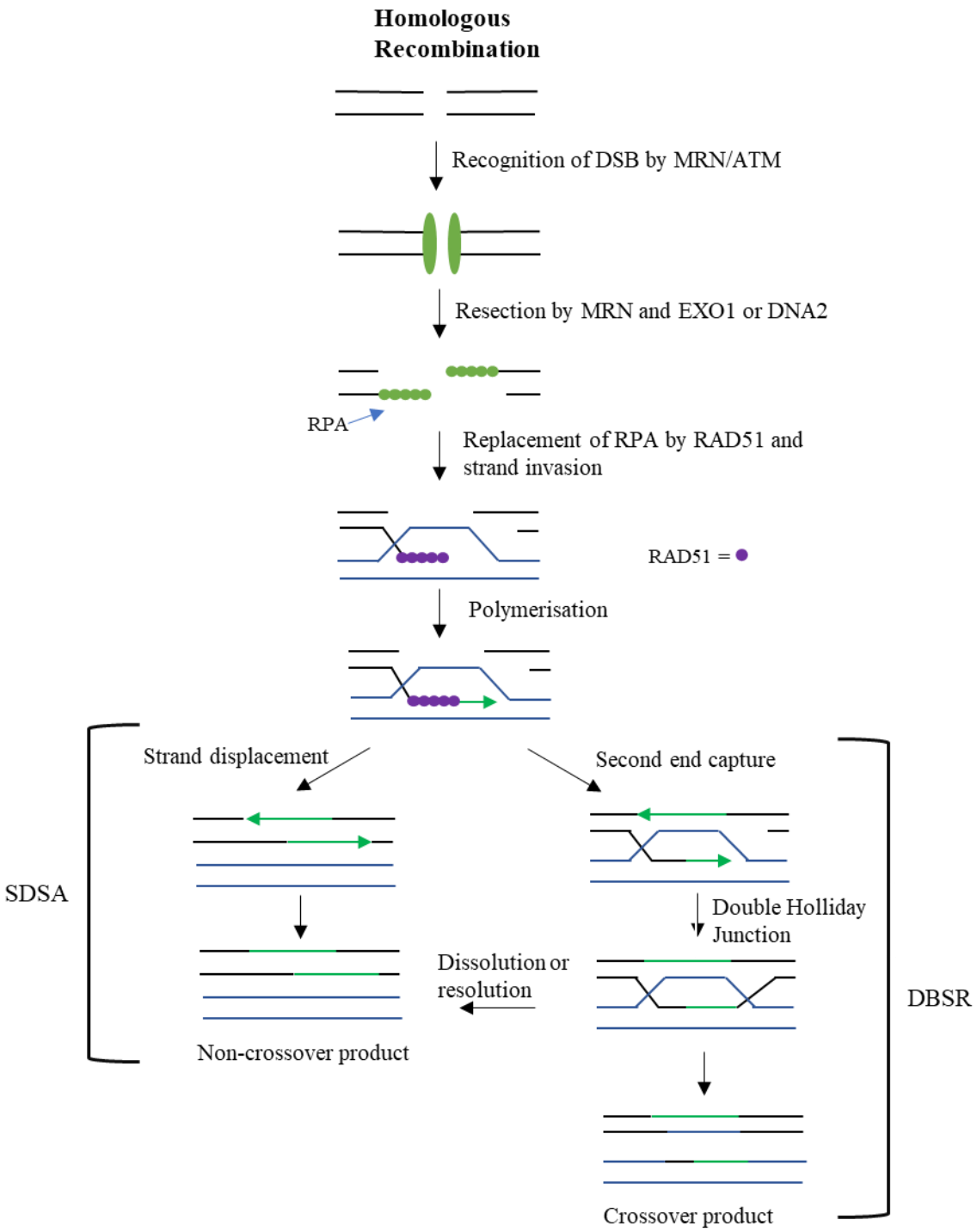

Figure 1.8: *Scheme of homologous recombination. Green line: newly incorporated DNA sequence. Blue lines: DNA duplex from the sister chromatid.*

Two other subpathways involved in HR are the single-strand annealing and the break-induced replication pathways. Efficient and accurate homologous recombination is

vital for genome integrity, and inefficient HR can be oncogenic. Mutations in BRCA1 and BRCA2 genes, which play an essential role in regulating HR, may increase the risk of ovarian and breast cancer.[85]

1.2.1.7. Interstrand crosslink repair

Interstrand crosslinks are highly cytotoxic as they covalently tether two DNA duplex strands preventing DNA separation, thereby blocking the process of DNA transcription and replication.[86] While the ICL repair pathways in humans have not been fully defined, simpler models (using yeast or bacterial cells) and studies on Fanconi anaemia (FA) provide valuable insight.

FA is a rare genetic disease that increases the probability of cancer development and sensitivity towards ICL inducing agents. 21 FA genes, including BRCA1 and BRCA2, are associated with ICL sensitivity and are involved in ICL repair.[87] Other repair pathways—TLS, NER, and HR—are involved in repairing ICLs. ICL repair can be either replication dependent or replication independent. [88] The pathway of ICL repair is dependent on the phase of the cell cycle, with a majority of ICL repair occurring in the S-phase during the DNA replication.[89] Due to the complexity of the ICL repair and lack of a definite repair pathway, a simplified version of ICL repair will be explained in this section. The scheme for the ICL repair is shown in **Figure 1.9**.

During S-phase, ICL repair is initiated when a single replication fork collisions with an ICL or during a dual collision of converging replication forks.[90,91] FA proteins mediate this repair process; these proteins help in recognising the lesion, stabilising the replication fork, activating downstream factors, and removing the ICL.[92] Once the lesion is detected and the

replication fork is stabilised, the ICL is unhooked. ICL unhooking is an essential step in ICL repair, and several nucleases have been implicated in this incision and unhooking process.[93] The current results suggest that XPF-ERCC1, MUS81-EME1 and SLX1-SLX4 nucleases may be involved in the incision at position 5′ to the ICL. [94] Some studies indicate that following the initial incision, a subsequent incision at a position 3′ to the ICL resulting in unhooking is performed by FANCI-associated nuclease 1 (FAN1). SNM1A and SNM1B are also indicated to be involved in the unhooking process, either through the digestion past the crosslink following the first incision, or the digestion of nucleotides in the unhooked ICL adduct, thus releasing the ICL containing fragment.[95] After unhooking of ICL is complete, TLS is performed to bypass the lesion. Finally, the lesion is probably removed by NER and HR repairs the double strand break.[96]

In the G_0 and G_1 phases of the cell cycle, ICL repair occurs in a replication-independent manner.[97] This process is connected to the NER pathway, and NER repair factors are involved in recognising and removing the lesion.[98] After detecting the ICL, XPF-ERCC1 and XPG make a double incision to unhook the ICL. It has been suggested that SNM1A may be involved in unhooking and processing to produce monobase adduct.[99] Then, the TLS is performed to fill a gap formed by the double incision. Finally, NER is performed to remove the lesion.

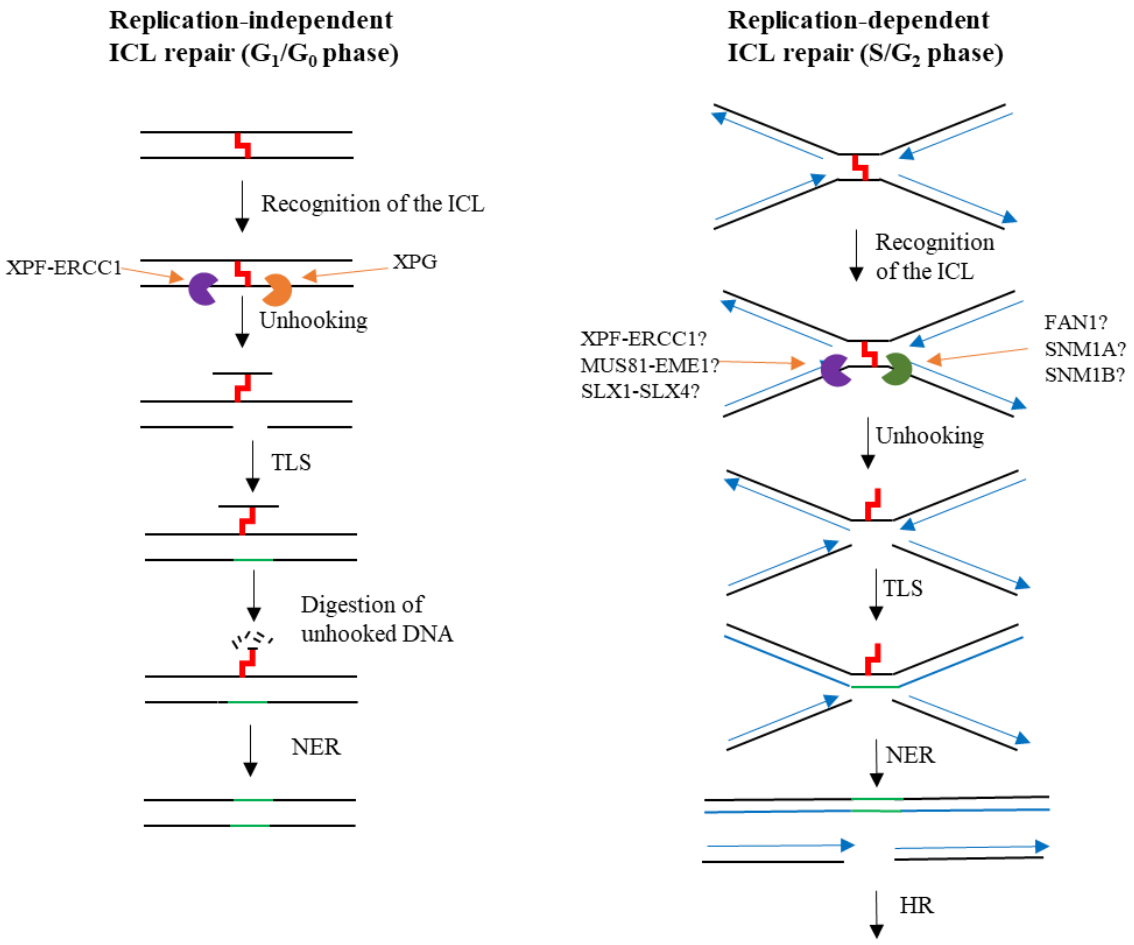

Figure 1.9: *Scheme of Interstrand cross-link repair. Red zigzag: interstrand crosslink. Green line: newly incorporated DNA sequence during the repair. Blue lines: DNA produced during the replication.*

1.2.2. DNA damage repair as a target in cancer therapy

The success of PARP inhibitors in cancer treatment has created a paradigm shift by demonstrating that targeting DNA repair is a feasible therapeutic target.[100] Due to the importance of PARP proteins in recognising the SSBs and activating factors involved in SSB repair, inhibition of PARP results in the reduced repair of SSBs.[101] PARP inhibitors, such as Olaparib or Rucaparib, not only sensitise cancer cells to chemotherapeutics and ionising radiation but are also the first clinically approved drugs that exploit the synthetic lethality.[102] Synthetic lethality occurs when a dysfunction of two or more proteins leads to apoptosis, while dysfunction in each individual gene is tolerated.[103] This can be taken advantage of in

cancer therapy, whereby inhibition of a protein can lead to a cell death if its synthetic lethal partner protein is not functional. A normal cell, however, can still function in these circumstances because its other proteins remain functional. In the case of PARP inhibitors, the synthetic lethal relationship between PARP and BRCA1 or BRCA2 is exploited. Due to the importance of PARP proteins in recognising the SSBs and activating factors involved in SSB repair, inhibition of PARP results in the reduced repair of SSBs. Unrepaired SSBs lead to the formation of DSB during replication; accordingly, PARP inhibition induces the formation of DSB. In the case of cells with defective HR repair due to BRCA1 or BRCA2 mutations, the increase of DSBs caused by PARP inhibition leads to an increased reliance on NHEJ-mediated repair pathways. Iterative cycles of DNA replication together with the excessive use of NHEJ results in increased levels of mutational burden and subsequent cell death. Therefore, PARP inhibitors can selectively kill cancer cells with BRCA1 or BRCA2 mutations often found in ovarian or breast cancers.[104]

The success of PARP inhibitors encourages the development of inhibitors against other proteins involved in DNA repair pathways. This includes nucleases, which play an essential role in the majority of DNA repair pathways, with many nucleases involved in more than one pathway.[105] Additionally, tumours are able to develop resistance towards DNA damaging therapies through the upregulation of DNA repair pathways. Accordingly, the development of nuclease inhibitors might be beneficial from the perspective of cancer treatment as they may sensitise cancer cells towards ionising radiation (*e.g.* SNM1C or MRE11) or crosslink inducing agents such as cisplatin or Mitomycin C (*e.g.* SNM1A/B, FEN1 or XPF-ERCC1).[106, 107] Studies suggest that inhibiting specific nucleases (*e.g.* MRE11 or FEN1) may induce synthetic lethality in BRCA depleted cells. [108,109]

1.3. Human metallo-β-lactamase fold nucleases

Metallo-β-lactamase (MBL) fold proteins were first observed in bacteria and are primarily known for their roles in β-lactam antibacterial resistance.[110] However, subsequent research has identified at least 18 human MBL-fold proteins that contain conserved motifs in their active site similar to those observed in bacterial MBLs.[111] Members of the MBL superfamily contain the characteristic αββα MBL-fold domain.[112] These enzymes are primarily zinc or iron-dependent proteins. Human MBL-fold proteins possess a variety of functions, including small molecule metabolism and nucleic acid processing.[113] Nine hMBL-fold proteins belong to the DNA/RNA interacting subfamily, out of which three enzymes are involved in DNA repair using their nuclease activity (SNM1A/B/C), whilst the remaining enzymes process RNA (ELAC1, ELAC2, CPSF73, CPSF100, INTS9, and INTS11).[114] SNM1A and SNM1B are exonucleases, whereas SNM1C is an endonuclease. ElaC ribonuclease Z 1/2 (ELAC1/2) belongs to the RNAse Z family and process the 3′ end of tRNA via endoribonuclease activity.[115] CPSF73 and CPSF100 dimerise to form the cleavage and polyadenylation specific factor (CPSF) complex that processes 3′ ends of mRNA.[116] While CPSF73 exhibits exoribonuclease and endoribonuclease activity, CPSF100 does not show any nuclease activity.[117] Similarly to CPSF100, Integrator complex subunit 9 (INT9) does not possess catalytic activity. Int9, together with endoribonuclease Int11, are part of the Integrator complex that processes 3′ ends of snRNA.[118] Out of the DNA/RNA interacting subfamily of hMBLs, a self-defining β-CASP (CPSF, Artemis, SNM1, PSO2) family can be further identified. Human MBL fold enzymes containing the β-CASP domain include SNM1A/B/C, CPSF73 and Int11.[119] Based on the structural data, the β-CASP domain inserts in between

the MBL domain and the catalytic core is located at the interface between these two domains.[120]

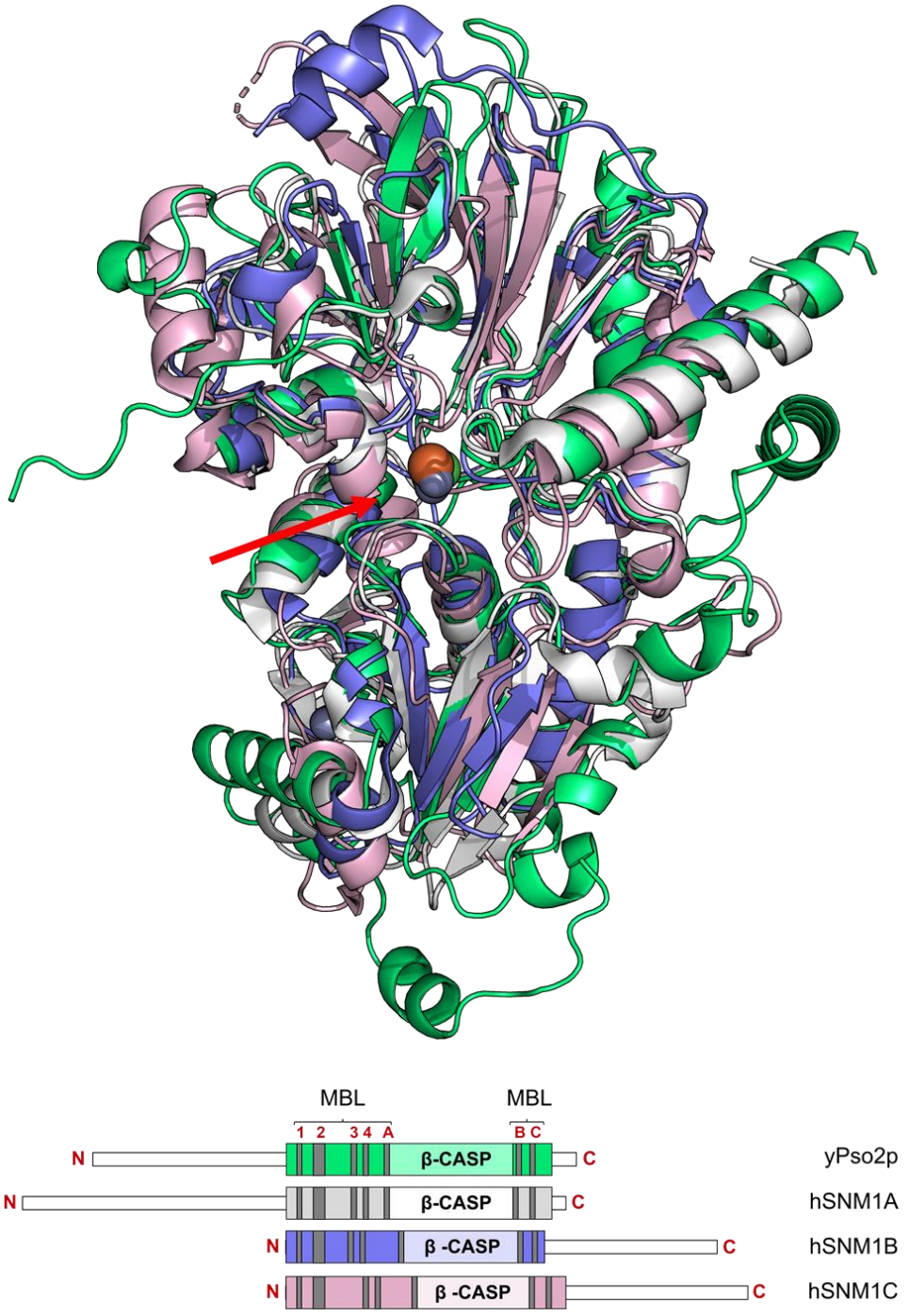

Figure 1.10: Top: *Overlay of structures of the human SNM1A (5Q1N) In white, SNM1B (7A1F) in blue, SNM1C (7AF1) in pink, and yeast Pso2 (Alphafold entry E7F457) in green. The metal ions coordinated in the active sites are shown in the sphere indicated by the red arrow.* ***Bottom:*** *Cartoon representation of sequence*

alignment for human SNM1A, SNM1B, SNM1C and yeast Pso2, showing the MBL and β-CASP domains. The conserved MBL motifs are labelled 1–4, and β-CASP family motifs, A–C.

The first enzyme from the SNM1 family was identified in yeast, *i.e.* sensitive to psoralen (PSO2).[121] PSO2 belongs to the MBL/β-CASP protein family and is specifically essential for ICL repair in yeast. SNM1A/B/C are human orthologues of yeast PSO2 and have a high level of amino acid sequence similarity that results in conserved motifs in both the MBL and β-CASP domains. SNM1A is most similar to PSO2 with 48% sequence similarity, while SNM1B has 33% similarity to PSO2.[122, 123] The overlay of structures of the SNM1A, SNM1B, SNM1C, and PSO2 is shown in **Figure 1.10**. The proposed phosphodiester hydrolysis mechanism by SNM1 nucleases is analogous to that proposed for the hydrolyses of β-lactams by bacterial MBLs (**Figure 1.11**).[124,125] In both catalytic reactions, the hydroxyl group, activated by zinc ions, performs a nucleophilic attack that leads to hydrolysis of either the β-lactam or a phosphodiester bond.[126]

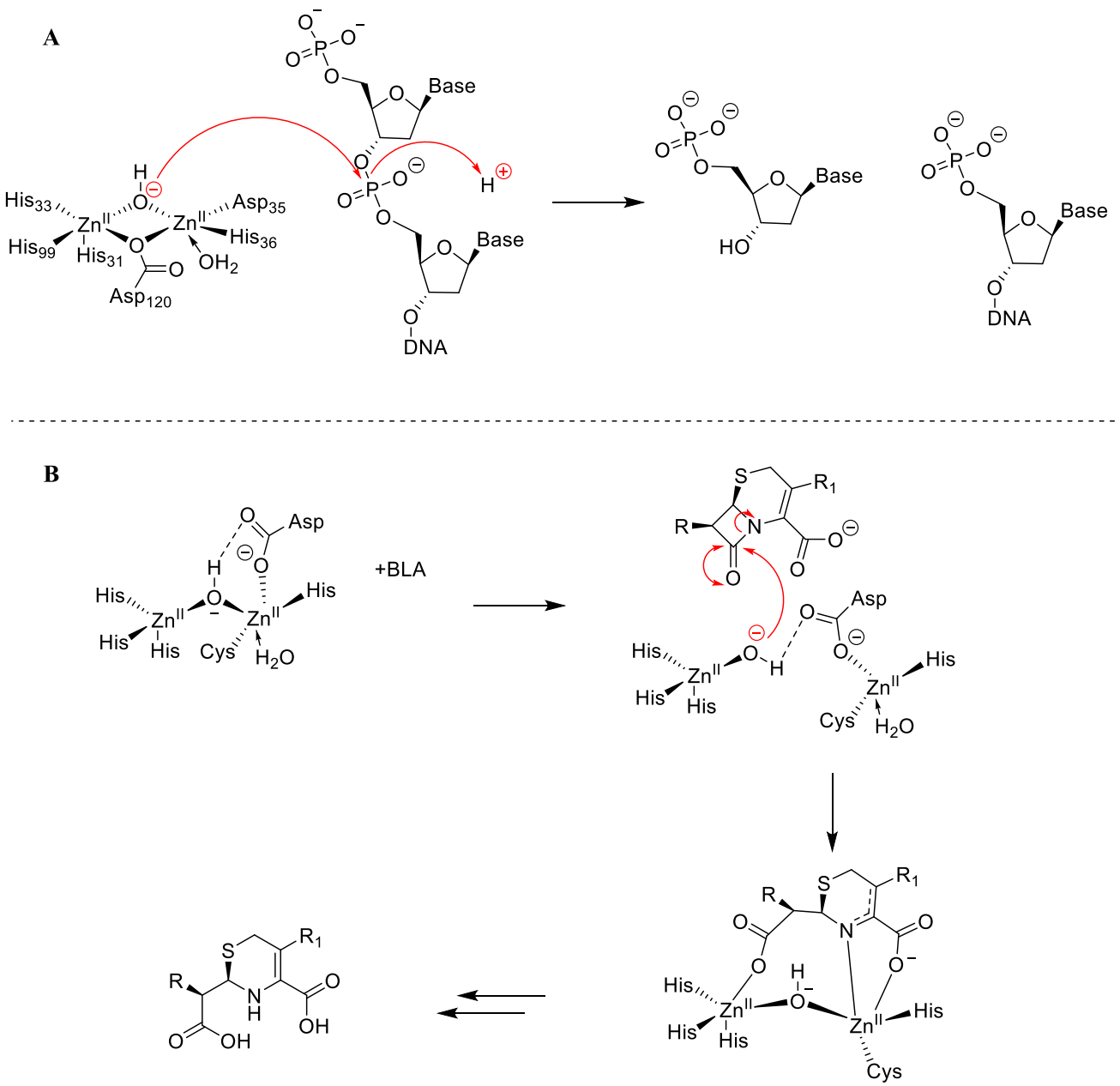

***Figure 1.11: A**: Proposed scheme for hydrolysis of phosphodiester bond by SNM1B. **B**: Scheme for hydrolyses of β-lactam by bacterial MBL.*

1.3.1. SNM1A

SNM1A is a 5′ to 3′ directed exonuclease. As discussed in **Section 1.2.1.7**, SNM1A is implicated in the unhooking step of ICL repair.[127] While the function of SNM1A is not fully elucidated, experimental results strongly speak for its importance in ICL repair. Ectopic expression of SNM1A in PSO2 mutants partially restores the resistance to ICL inducing

agents.[128] Hypersensitivity towards ICL inducing agents (mitomycin C or cisplatin) was observed in SNM1A depleted DT40 cells.[129] Similarly, the enhanced sensitivity towards mitomycin C was observed in mice with the knockout mSNM1A gene.[130] While both SNM1A and SNM1B are believed to digest crosslinked nucleotides in ICL repair, the evidence primarily points to SNM1A. However, redundancy between SNM1A and SNM1B was indicated, as depletion of both nucleases results in higher sensitivity towards ICL inducing agents than when only one gene is depleted.[131]

1.3.2. SNM1B (Apollo)

SNM1B is closely related to SNM1A. It is a 5′ to 3′ directed exonuclease, and similarly to SNM1A, SNM1B depletion sensitises cells towards ICL inducing agents.[132] In addition to the SNM1B being implicated in ICL repair, probably the best characterised cellular function of SNM1B is in telomere maintenance.[133] Initial studies on SNM1B found that it interacts with the telomeric repeat-binding factor (TRF2), a component of the shelterin nucleoprotein complex.[134] The shelterin complex stabilises the formation of t-loops, a structure formed by strand invasion of 3′ overhangs, which help protect DNA ends. The 3′ overhangs requisite for t-loop formation are believed to be generated by the 5′−3′ exonuclease activity of SNM1B. Studies with SNM1B knockout mouse embryo fibroblasts have shown that lack of SNM1B leads to telomere dysfunction and chromatid fusion, confirming the importance of SNM1B in telomere maintenance.[135] Additionally, patients with a mutation in SNM1B suffered bone marrow failure due to impaired DNA repair and telomer instability.[136]

1.3.3. SNM1C (Artemis)

While SNM1A/B function as exonucleases, SNM1C is a structure-specific endonuclease. SNM1C is capable of cleaving DNA loops, flaps, gaps, hairpins, and overhangs.[137,138] DNA-PKcs complexes with, and phosphorylates SNM1C, which activates its endonuclease activity. As described in **Section 1.2.1.6,** SNM1C plays an essential role in non-homologous end-joining repair. As NHEJ factors are involved in V(D)J recombination, a process that produces T cell receptors and B cell antibodies, SNM1C defects may lead to severe combined immunodeficiency.[139,140] SNM1C is considered a promising anticancer target as cell lines with depleted SNM1C have increased sensitivity towards ionising radiation. Additionally studies show that inhibition of SNM1C in tumors may activate tumor protein p53, which could lead to tumor regression.[141]

1.4. Metallo-β-Lactamase inhibitors

1.4.1. Bacterial MBL inhibitors

β-Lactams are the most widely used class of antibiotics.[142] However, the rise of antimicrobial resistance puts these antibiotics at risk of becoming ineffective and threatens public health.[143] β-Lactamase can be classified into four categories based on sequence and structure: the nucleophilic serine-β-lactamases (class A, C, and D) and the metallo-β-lactamases (class B).[144] While inhibitors of serine-β-lactamases are widely used clinically, the development of MBL inhibitors is explored to a much lesser extent. Clinically used inhibitors for serine-β-lactamases (SBL) include Clavulanic acid, Avibactam, and Vaborbactam.[145]

Bacterial metallo-β-lactamases can be divided into 3 sub-classes: B1, B2 and B3. Both B1 and B3 contain two zinc ions in the active site, while B2 enzymes are mono zinc ion enzymes.[146] Since the B1 sub-class emerged as the most clinically substantial, this sub-class is a primary target for the development of new inhibitors.[147] Amongst others, members of the B1 sub-class include NDM-1, VIM-2, and IMP-1.[148] The majority of bacterial MBL inhibitors can be classified as either metal chelators (i.e. thiols, *N*-heterocyclic carboxylic acids, or sulfonamides) or transition state analogues (boronates).

1.4.1.1. Thiol inhibitors of MBLs

Thiol-based inhibitors bind to the active site of MBL using their free thiol group, which binds zinc(II) ions and displaces catalytic water in the active site.[149] In addition to a thiol group, most of these inhibitors poses a carboxylic acid functional group. The presence of carboxylic acid not only allows for interactions with polar amino acid residues but also, based on crystal structures, it can be observed that the oxygen atom in carboxylic acid can bind one of the zinc (II) ions.[150] The importance of the carboxylic acid group in inhibitors likely reflects the presence of a carboxylic acid functional group or equivalent sulphonic acid in the majority of β-lactam antibiotics. Known thiol-base MBL inhibitors include dimercaprol, L-captopril, bisthiazolidines and thioenolates, shown in **Figure 1.12**.[151,152]

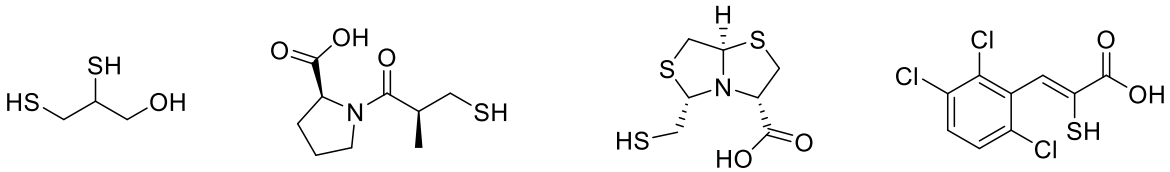

Figure 1.12: *Structures of thiol-based inhibitors of bacterial MBLs. From left to right: dimercaprol, L-captopril, bisthiazolidine and thioenolate.*

1.4.1.2. *N*-Heterocyclic carboxylic acid MBL inhibitors

An important category of metal-chelating bacterial MBL inhibitors is *N*-heterocyclic carboxylic acid inhibitors. These inhibitors are derivatives of various heterocycles, such as picolinic acid, 4-thiazolecarboxylic acid, and indole-2-carboxylate, shown in **Figure 1.13**.[153] A common feature for this class is the adjacent positioning of carboxylic acid and nitrogen in the heteroaromatic ring. The importance of nitrogen and carboxylic acid chelators can be seen in the crystal structure of picolinic acid-based inhibitors with CphA and ANT431 with VIM-2, as both functional groups chelate a single zinc(II) atom.[154] In contrast to what has been observed for thiol and sulfonamide based inhibitors, the catalytic water bridged between two zinc(II) atoms from the VIM-2 was not displaced by ANT431. [155]

Recently, a series of novel and potent inhibitors with an indole-2-carboxylate core has been developed against a broad range of bacterial MBLs. The binding mode of these inhibitors was revealed using crystallographic studies with the B1 MBLs VIM-1 and VIM-2. Similarly to what has been seen in other *N*-heterocyclic carboxylic, the carboxylic acid in the indole-2-carboxylate is involved in chelating metal ion in the active site. However, instead of chelating the metal ion, the nitrogen atom forms a hydrogen bond with the water bridging between the two active site metal ions.[156]

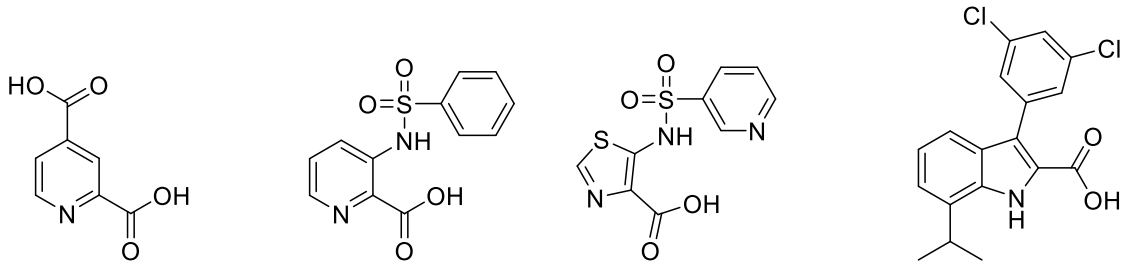

2,4-PDCA ANT431 InC

Figure 1.13: *Structures of N-heterocyclic carboxylic acid inhibitors of bacterial MBLs. IncC: indole-2-carboxylates.*

1.4.1.3. Sulfonamide MBL inhibitors

Sulfonamides are a recently emerging class of MBL inhibitors, shown in **Figure 1.14**.[157] With this class of inhibitors, sulfonamide acts as the primary zinc chelating functional group. Like free sulfur in thiols, the free nitrogen in sulfonamide can chelate both zinc (II) ions and displace the bridged water.[158,159] Again, a common characteristic of these inhibitors is a carboxylic acid side chain involved in the binding through the chelation of one of the zinc (II) ions.

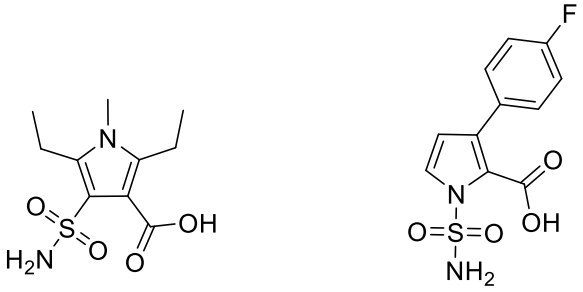

Figure 1.14: *Structures of Sulfonamide inhibitors of bacterial MBLs.*

1.4.1.4. Bicyclic boronate MBL inhibitors

Bicyclic boronates are potentially the most exciting class of MBL inhibitors, as they present a broad spectrum of β-lactamase inhibition and are able to inhibit both MBLs and SBLs.[160] Boron's near unique property to readily interchange hybridisation between sp^2 and sp^3 in water enables these compounds to mimic β-lactam substrate (sp^2) and high energy tetrahedral intermediate (sp^3) binding, shown in **Figure 1.15**. Based on structural data, the tetrahedral (sp^3) form of the boronic acid is bound to the active site, where it can displace the bridged water and act as a transition state analogue.[161,162] A promising inhibitor within this class is Taniborbactam which is currently in phase III of clinical trials.[163]

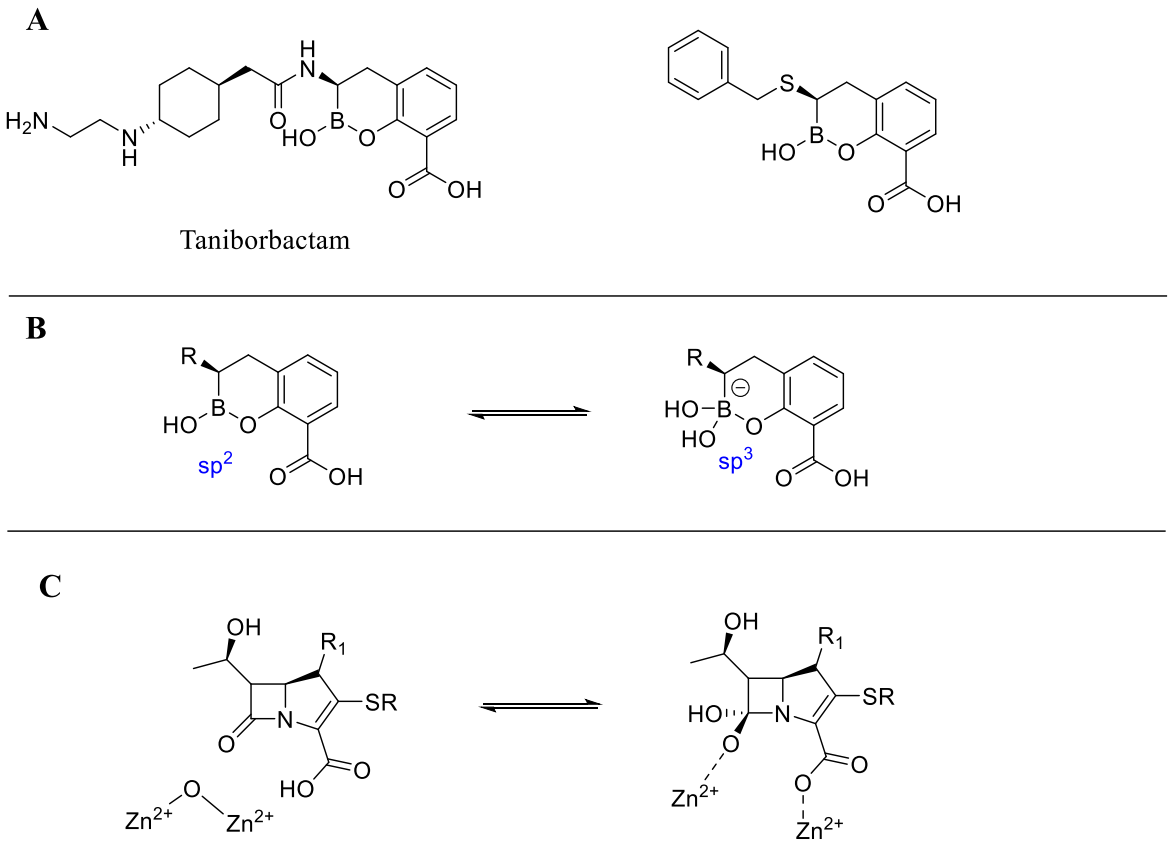

Figure 1.15: A: *Structures of boronate inhibitors of bacterial MBLs.* ***B:*** *Boronates interchange between two hybridisation states.* ***C:*** *Rection of β-lactam with MBL and formation of high energy tetrahedral intermediate.*

1.4.2. Protozoan MBL inhibitors

Acoziborole (**Figure 1.16**) is a novel boronate-based drug active against *T.b. gambiense*—a parasite responsible for causing African sleeping sickness—which is currently in clinical trials.[164] Although acoziborole was developed using phenotypic screening, a further investigation identified mRNA processing as a primary target, and CPSF73 is suspected to be its molecular target.[165] Although no crystal structure of acoziborole bound to CPSF73 is available, molecular docking studies have been carried out to investigate its potential binding mode.[166] Based on the docking model, the acoziborole boron atom reacts with a water molecule that bridge the two zinc (II) ions in the active site, leading to tetrahedral

coordination around the boron atom and sp^3 hybridisation. The tetrahedral coordination of the boron is proposed to mimic the phosphate group of the RNA substrate of CPSF73.

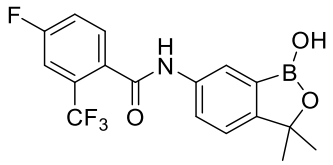

Figure 1.16: *Structure of Acoziborole.*

1.4.3. Human MBL fold enzyme inhibitors

Probably the most thoroughly investigated human MBL inhibitor is JTE-607, shown in **Figure 1.17**.[167] Although this compound was known to inhibit cytokine synthesis for more than 20 years, the mechanism of action was unknown for a long time. In further phenotypic screening, JTE-607 was shown to inhibit the growth of Ewing's sarcoma and acute myeloid leukaemia.[163] By using compound-immobilised affinity chromatography CPSF73 was identified as a direct target of JTE-607. Additionally, it was determined that JTE-607 acts as a prodrug activated upon hydrolysis of ethyl ester.[168] The crystal structure of hydrolysed JTE-607 bound CPSF73 showed that the inhibitor binds to the interfacial cavity between β-CASP and MBL domains in close proximity to active site zinc (II) ions but does not interact with the metal ions directly. It is suggested that hydrolysed JTE-607 may partially mimic the binding mode of the pre-mRNA substrate.[169]

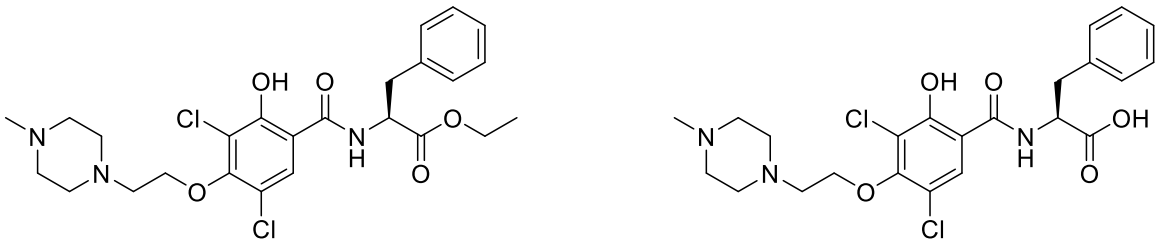

Figure 1.17: *Structure of JTE-607 prodrug (Left) and hydrolysed JTE-607 (Right)*

The development of inhibitors against human MBL nucleases appears to have been rather unsuccessful to date, with only a limited number of inhibitors reported in the literature. Most of them target SNM1A nuclease and do not exhibit high potency. One of the first reported inhibitors of SNM1A and SNM1B nucleases were cephalosporins, a class of β-lactam antibiotics.[170] Among the screened cephalosporins, ceftriaxone (**Figure 1.18A**) was the most potent inhibitor of SNM1A and B. This finding implied an interesting chemical relationship between SNM1 nucleases and true MBLs. However, recent crystal structures appear to undermine the proposed similarities between the two families of enzymes concerning cephalosporin binding.[167] While true MBLs bind to β-lactam ring, this was not the case for SNM1A. In the ceftriaxone-bound SNM1A structure (PDB: 5NZW), ceftriaxone binds to a single metal in the active site via two oxygens from the cyclic diamide sidechain.[171]

The McGouran group have attempted to develop nucleoside-based inhibitors against SNM1A. A library of nucleosides with modifications at 5′ and 3′ positions was screened as SNM1A inhibitors. Their study identified weakly potent hydroxamic acid, squaramide and thiosquaramide as potential metal-chelating pharmacophores that target SNM1A. [172,173] Selected nucleoside-based inhibitors of SNM1A are shown in **Figure 1.18B**.

A recent high-throughput screen of bioactive compounds against SNM1A was rather unfruitful; selected hits are shown in **Figure 1.18C**.[174] Out of nine hits, four were later identified as potential DNA binders. One of the hits was aurintricarboxylic acid, a known non-specific nuclease inhibitor. In most of these hits, a common feature was catechol moiety, which might be another metal-chelating pharmacophore targeting SNM1A.

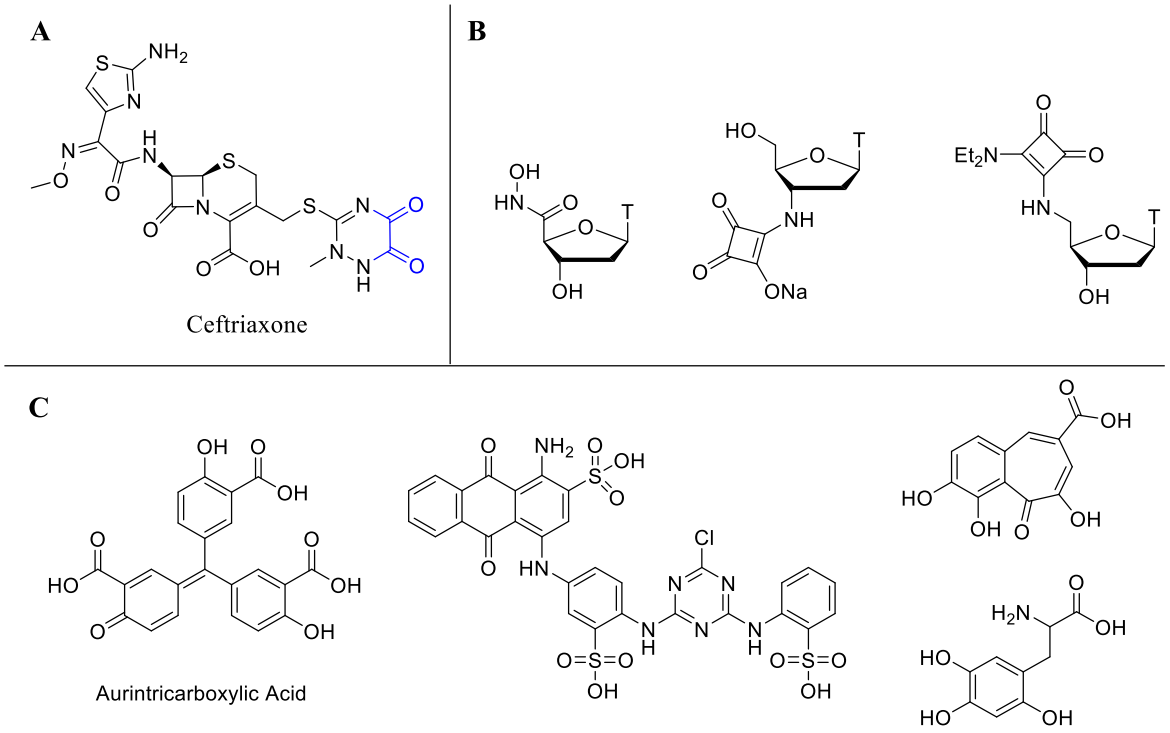

Figure 1.18: A: *Structure of Ceftriaxone. Carbonyls involved in binding metal in the active site of SNM1A are marked in blue.* ***B:*** *Nucleoside based inhibitors of SNM1A from McGouran group.* ***C:*** *Hits identified by HTS of bioactive compounds. T: Thymine*

1.5. Human nuclease inhibitors

Although nucleases are attractive therapeutic targets, especially in cancer treatment, the development of human nuclease inhibitors is still in its early stage, with few compounds being tested in preclinical trials or used as chemical probes. There is a wide range of mechanisms through which the nuclease activity can be inhibited. Since most nucleases are metalloenzymes, metal chelators are common inhibitors of them. Examples of inhibitors that mimic the nucleic acid substrate are also known. While most inhibitors target the active site of the nucleases, targeting protein-protein interactions between nucleases and other factors involved in the DNA repair pathway can be just as effective.

1.5.1. Metal-binding nuclease inhibitors

The prevailing characteristic among metal-chelating nuclease inhibitors is the presence of oxygen-based functional groups, including carbonyls, hydroxamates, catechols, or carboxylic acids. 2,4-Diketobutyric acid inhibitors and their structural analogues have been developed against FEN1 and XPG, shown in **Figure 1.19**.[175] The exact binding mode of 2,4-diketobutyric acid inhibitors are unknown but based on structural studies of highly related HIV integrase inhibitors, one may propose that 2,4-diketobutyric acids similarly chelate metals in the active site of nucleases.[176]

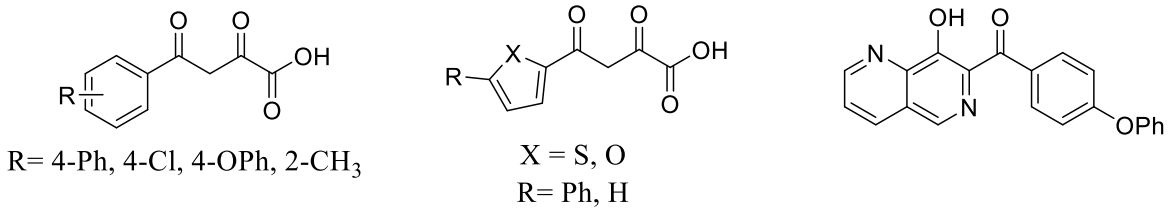

Figure 1.19: *Structure of 2,4-diketobutyric acid-based inhibitors (compounds on the left and middle) and their structural analogue (compound on the right).*

The *N*-hydroxyimide appears to be particularly effective as a pharmacophore against a broad range of nucleases. Compounds with this functional group have been shown to inhibit FEN1, XPG, ERCC1-XPF and DNase.[177] Although selectivity was an initial issue, selective and cellularly active inhibitors against FEN1 were reported (**Figure 1.20**). [178,] While FEN1 inhibitors did not reach clinical trials, they ended up being useful biochemical tools. These inhibitors were used to further validate FEN1 as a possible druggable target in cancer treatment.[179] FEN1 inhibitors helped identify sensitive cancer cell lines and synthetic lethality genetic interactions. The *N*-hydroxyimide (FEN1-IN-1) have been shown to bind to two metals in the active site of FEN1 via two carbonyl groups and a hydroxyl group. In

the crystal structure (PDB: 5FV7), each oxygen from the carbonyl group chelated to one out of two Mg^{2+} ions, while the hydroxyl group was bridged between both metal ions.[180]

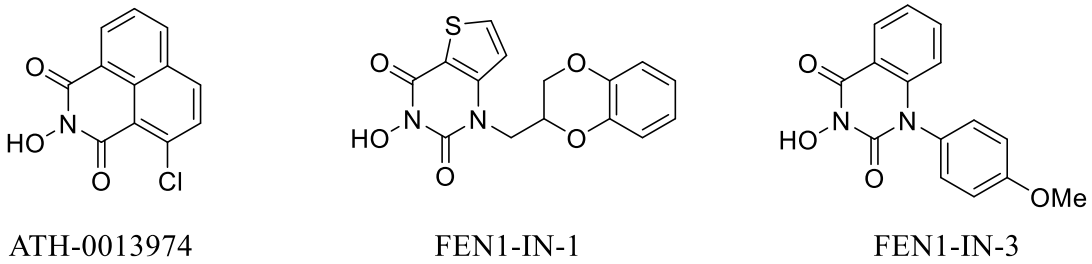

Figure 1.20: *Structure of ATH-0013974 (initial hit) and FEN1 inhibitors 1 and 3.*

Catechols, 3-hydroxypyridones and hydroxypyrimidinones have been reported to inhibit ERCC1-XPF, shown in **Figure 1.21**.[181] As these motifs are known, metal chelators, it can be proposed that they bind metal ions in the active site. While catechol based inhibitors encouragingly inhibited DNA repair in cell-based assays, the tested hydroxypyrimidinones did not. [182] Additionally, as the N-hydroxyimide and hydroxypyrimidinone are structurally similar, hydroxypyrimidinones inhibit both FEN1 and ERRC1-XPF, with a higher selectivity towards the latter nuclease.

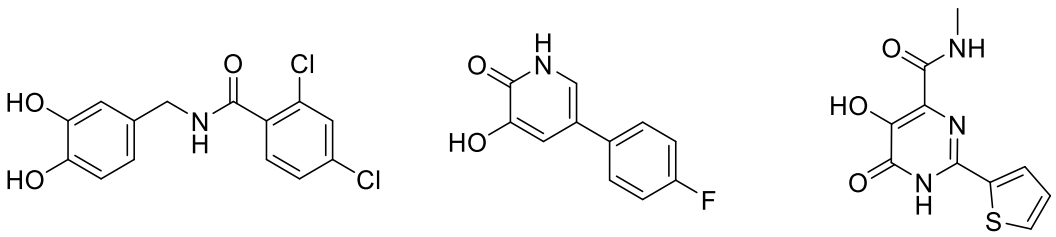

Figure 1.21: *Structure of catechol (left), 3-hydroxypyridone (middle) and hydroxypyrimidone (right) based inhibitors of ERCC1-XPF.*

7-Nitroindole-2-carboxylic acid (CRT0044876) was identified as an inhibitor of APE1, shown in **Figure 1.22**.[179] Molecular modelling predicts that carboxylic acid binds the metal in the active site. This model suggests that carboxylic acid can be used as another metal-binding pharmacophore in nuclease inhibitors.[183]

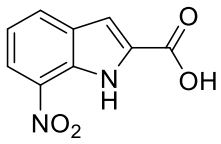

Figure 1.22: *Structure of 7-Nitroindole-2-carboxylic acid (CRT0044876) inhibitor of APE1*

1.5.2. Nuclease inhibitors mimicking nucleic acid substrate

Using HTS, arylstibonic acids (**Figure 1.23**) were identified as inhibitors of APE1 nuclease activity.[180] Molecular modelling suggests that the arylstibonic acids mimic the abasic site in DNA, a substrate for APE1. The stibonic acid and carboxylic acid in the compound are proposed to mimic the phosphate backbone in the DNA.[184]

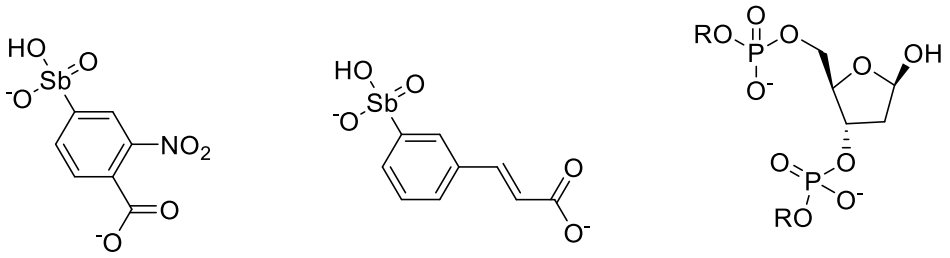

Figure 1.23: *Structure arylstibonic acid inhibitors of APE1 (left and middle) and abasic DNA, a substrate for APE1 (right).*

1.5.3. Nuclease inhibitors targetting protein-protein interactions

Since heterodimerisation of ERCC1-XPF is required for endonuclease activity, the protein-protein interface between ERCC1 and XPF is an attractive medicinal chemistry target. Virtual screening was used to isolate druggable binding sites and identify potential hit compounds that inhibit dimerisation of ERCC1-XPF through binding to XPF protein.[185] In the follow-up work, a computer-aided drug design was employed to develop improved inhibitors of ERCC1-XPF protein-protein interaction.[186] Inhibitors binding to XPF (**Figure 1.24.A**) showed promising results in cell-based assays, as they sensitised cells to the UV irradiation and ICL inducing agent cyclophosphamide, cisplatin, and mitomycin C.[187,188]

Another strategy to inhibit ERCC1-XPF DNA repair activity involved targeting the interaction between ERCC1 and XPA. While XPA is not required for endonuclease activity, XPA-ERCC1 interaction is essential for the proper NER function since XPA recruits ERCC1 to the damage site.[189] Like in the identification of ERCC1-XPF protein-protein interaction inhibitors, virtual screening was used to identify inhibitors targeting XPA-ERCC1 interaction.[190] The structure of inhibitor binding XPA is shown in **Figure 1.24B**.

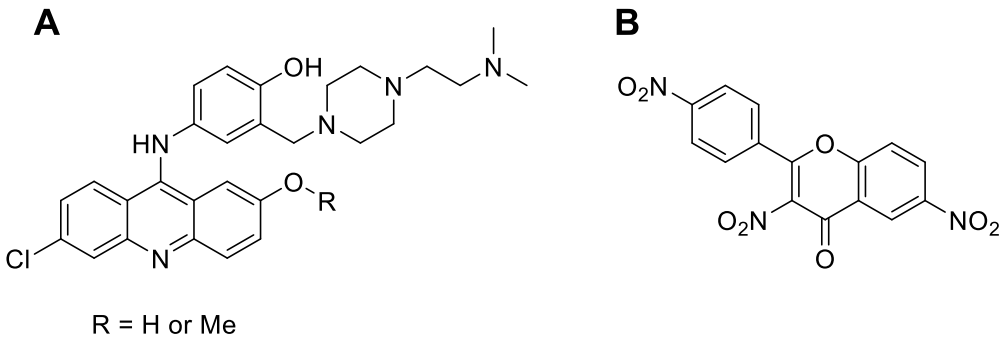

Figure 1.24: *Structure of protein-protein interaction inhibitors.* ***A:*** *XPF binders.* ***B:*** *XPA binder.*

1.5.4. MRE-11 inhibitor

Using a forward genetic screen, mirin was identified as an inhibitor of MRN (Mre11–Rad50–Nbs1 complex); later, it was reported to selectively inhibits exonuclease activity of MRE11.[191] Using structural data, a chemical library of mirin derivatives was developed. From this new library of inhibitors, a more potent exonuclease activity inhibitor (PFM39) was identified. A selective endonucleases activity inhibitor (PFM03) was also found, as shown in **Figure 1.25**. The binding mode of these inhibitors was identified by using x-ray crystallography. Instead of binding to the active site, the results imply that mirin derived inhibitors bind in close proximity to the active site and impede the path of DNA towards the active site. Selective inhibitors of both endonuclease and exonucleases activity allowed for

further evaluation of MRN function and provided insight into the regulation of pathway choices.[192]

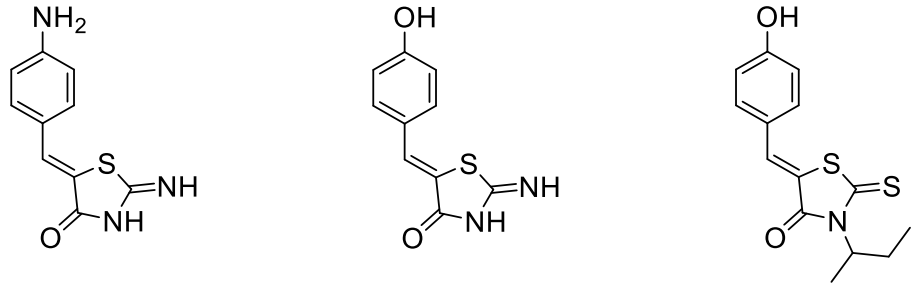

Figure 1.25: *Structures of Mre11 inhibitors.*

1.6. Research aims of the work described in this thesis

While the precise biological functions of human MBL nucleases SNM1A, B and C are not yet fully understood, these enzymes are essential for maintaining genome integrity, whilst their depletion leads to either chemosensitisation or radiosensitisation.[129] Therefore, developing small-molecule inhibitors against these enzymes is believed to be beneficial for further the investigation of functional roles of these nucleases in DNA repair, or as sensitising agents in cancer treatment.

This project has aimed at the development of potent and selective inhibitors of a human MBL nucleases that could be tested in cellular assays and used for target validation. Since all three nucleases—SNM1A, SNM1B, and SNM1C—play essential physiological roles and are potential pharmaceutical targets, inhibitor development is not restricted to a single enzyme. Although the project's primary focus was on developing inhibitors against SNM1A, it was envisaged that selected inhibitors showing promising results should also be tested against SNM1B/C. In case any inhibitor, or set of inhibitors, shows a substantially better

potency against SNM1B/C than SNM1A, it was considered that the project could shift focus towards one of the other enzymes.

Prior to this work, an extensive high-throughput screen of 400,000 compounds had been performed against SNM1A. 22 hits were identified, thus providing a foundation for developing new inhibitors. Taking these hits as a starting point, it was proposed for the structural analogues to be synthesised in order to investigate the structure-activity relationship (SAR). The study of SAR will help improve the inhibitors and understand potential structural differences between the enzymes that might be exploited to achieve selectivity. In addition to testing inhibitors by using in-vitro assays, it was envisaged that inhibitors could be soaked into SNM1A/B/C crystals or co-crystallised with SNM1A/B/C to obtain inhibitor bound crystal structures.

It was also intended that potential inhibitor libraries would be tested throughout the project to identify new pharmacophores and inhibitors targeting human MBL nucleases. The libraries investigated include known metalloenzyme inhibitors, metal binders, and in-house compounds.

1.7. References

[1] T. Lindahl, *Nature*, 1993, **362**, 709-715.
[2] D. K. Jeppesen, V. A. Bohr and T. Stevnsner, *Progress in Neurobiology*, 2011, **94**, 166-200.
[3] W. P. Roos, A. D. Thomas and B. Kaina, *Nature Reviews Cancer*, 2016, **16**, 20-33.
[4] L. A. Loeb and B. D. Preston, *Annual Review of Genetics*, 1986, **20**, 201-230.
[5] T. Lindahl and B. Nyberg, *Biochemistry*, 1972, **11**, 3610-3618.
[6] V. Bailly and W. G. Verly, *Nucleic Acids Research*, 1988, **16**, 9489-9496.
[7] S.-I. Yonekura, N. Nakamura, S. Yonei and Q.-M. Zhang-Akiyama, *Journal of Radiation Research*, 2009, **50**, 19-26.

[8] J. Cadet and J. R. Wagner, *Cold Spring Harbor Perspectives in Biology*, 2013, **5**, a012559-a012559.
[9] A.-G. Bourdat, T. Douki, S. Frelon, D. Gasparutto and J. Cadet, *Journal of the American Chemical Society*, 2000, **122**, 4549-4556.
[10] L. J. Marnett, *Mutat Res*, 1999, **424**, 83-95.
[11] J. P. Plastaras, J. N. Riggins, M. Otteneder and L. J. Marnett, *Chemical Research in Toxicology*, 2000, **13**, 1235-1242.
[12] E. Viguera, D. Canceill and S. D. Ehrlich *The EMBO Journal*, 2001, **20**, 2587-2595.
[13] D. L. Mitchell and R. S. Nairn, *Photochemistry and Photobiology*, 1989, **49**, 805-819.
[14] P. O'Neill and P. Wardman, *International Journal of Radiation Biology*, 2009, **85**, 9-25.
[15] J. Vignard, G. Mirey and B. Salles, *Radiother Oncol*, 2013, **108**, 362-369.
[16] R. Baskar, K. A. Lee, R. Yeo and K.-W. Yeoh, *International Journal of Medical Sciences*, 2012, **9**, 193-199.
[17] H. Yu, *Journal of Environmental Science and Health, Part C*, 2002, **20**, 149-183.
[18] S. S. Hecht, *JNCI Journal of the National Cancer Institute*, 1999, **91**, 1194-1210.
[19] Y. Huang and L. Li, *Transl Cancer Res*, 2013, **2**, 144-154.
[20] Y. Zou, B. Van Houten and N. Farrell, *Biochemistry*, 1994, **33**, 5404-5410.
[21] S. M. Rink and P. B. Hopkins, *Biochemistry*, 1995, **34**, 1439-1445.
[22] P. D. Lawley and D. H. Phillips, *Mutation Research/Fundamental and Molecular Mechanisms of Mutagenesis*, 1996, **355**, 13-40.
[23] P. A. Muniandy, J. Liu, A. Majumdar, S.-T. Liu and M. M. Seidman, *Critical Reviews in Biochemistry and Molecular Biology*, 2010, **45**, 23-49.
[24] S. P. Jackson and J. Bartek, *Nature*, 2009, **461**, 1071-1078.
[25] A. Sancar, L. A. Lindsey-Boltz, K. Unsal-Kacmaz and S. Linn, *Annu Rev Biochem*, 2004, **73**, 39-85.
[26] J.-C. Amé, V. Rolli, V. Schreiber, C. Niedergang, F. Apiou, P. Decker, S. Muller, T. Höger, J. M.-D. Murcia and G. De Murcia, *Journal of Biological Chemistry*, 1999, **274**, 17860–17868.
[27] J. W. Harper and S. J. Elledge, *Molecular Cell*, 2007, **28**, 739-745.
[28] Z. Liu, L. Wang and D. Zhong, *Physical Chemistry Chemical Physics*, 2015, **17**, 11933-11949.
[29] B. Kaina, M. Christmann, S. Naumann and W. P. Roos, *DNA Repair*, 2007, **6**, 1079-1099.
[30] P. Ø. Falnes, A. Klungland and I. Alseth, *Neuroscience*, 2007, **145**, 1222-1232.
[31] N. Chatterjee and G. C. Walker, *Environmental and Molecular Mutagenesis*, 2017, **58**, 235-263.
[32] D. Wilson III and V. Bohr, *DNA Repair*, 2007, **6**, 544-559.
[33] B. Demple and J.-S. Sung, *DNA Repair*, 2005, **4**, 1442-1449.
[34] A. B. Robertson, A. Klungland, T. Rognes and I. Leiros, *Cell. Mol. Life Sci.*, 2009, **66**, 981-993.

[35] R. A. O. Bennett, D. M. Wilson, D. Wong and B. Demple, *Proceedings of the National Academy of Sciences*, 1997, **94**, 7166-7169.
[36] U. Sattler, P. Frit, B. Salles and P. Calsou, *EMBO reports*, 2003, **4**, 363–367.
[37] B. Pascucci, M. Stucki, Z. O. Jónsson, E. Dogliotti and U. Hübscher, *Journal of Biological Chemistry*, 1999, **274**, 33696–33702.
[38] M. Kusakabe, Y. Onishi, H. Tada, F. Kurihara, K. Kusao, M. Furukawa, S. Iwai, M. Yokoi, W. Sakai and K. Sugasawa, *Genes and Environment*, 2019, **41**.
[39] I. O. Petruseva, A. N. Evdokimov and O. I. Lavrik, *Acta Naturae*, 2014, **6**, 23-34.
[40] M. Fousteri and L. H. Mullenders, *Cell Research*, 2008, **18**, 73-84.
[41] A. H. Sarker, S. E. Tsutakawa, S. Kostek, C. Ng, D. S. Shin, M. Peris, E. Campeau, J. A. Tainer, E. Nogales and P. K. Cooper, *Molecular Cell*, 2005, **20**, 187–198.
[42] F. Coin, V. Oksenych, V. Mocquet, S. Groh, C. Blattner and J. M. Egly, *Molecular Cell*, 2008, **31**, 9-20.
[43] T. Ogi, S. Limsirichaikul, R. M. Overmeer, M. Volker, K. Takenaka, R. Cloney, Y. Nakazawa, A. Niimi, Y. Miki, N. G. Jaspers, L. H. F. Mullenders, S. Yamashita, M. I. Fousteri and A. R. Lehmann, *Molecular Cell*, 2010, **37**, 714-727.
[44] J. E. Sale, *Cold Spring Harbor Perspectives in Biology*, 2013, **5**, a012708-a012708.
[45] A. Lehmann, A. Niimi, T. Ogi, S. Brown, S. Sabbioneda, J. Wing, P. Kannouche and C. Green, *DNA Repair*, 2007, **6**, 891–899.
[46] J. E. Sale, A. R. Lehmann and R. Woodgate, *Nature Reviews Molecular Cell Biology*, 2012, **13**, 141-152.
[47] P. Modrich, *Journal of Biological Chemistry*, 2006, **281**, 30305-30309.
[48] J. Genschel, S. J. Littman, J. T. Drummond and P. Modrich, *Journal of Biological Chemistry*, 1998, **273**, 19895-19901.
[49] F. Palombo, I. Iaccarino, E. Nakajima, M. Ikejima, T. Shimada and J. Jiricny, *Current Biology*, 1996, **6**, 1181-1184.
[50] A. Pluciennik, L. Dzantiev, R. R. Iyer, N. Constantin, F. A. Kadyrov and P. Modrich, *Proceedings of the National Academy of Sciences*, 2010, **107**, 16066-16071.
[51] D. X. Tishkoff, N. S. Amin, C. S. Viars, K. C. Arden and R. D. Kolodner, *Cancer Res*, 1998, **58**, 5027-5031.
[52] J. R. Eshleman and S. D. Markowitz, *Human Molecular Genetics*, 1996, **5**, 1489-1494.
[53] M. Hossain, Y. Lin and S. Yan, *International Journal of Molecular Sciences*, 2018, **19**, 2389.
[54] K. W. Caldecott, *Nature Reviews Genetics*, 2008, **9**, 619-631.
[55] A. E. O. Fisher, H. Hochegger, S. Takeda and K. W. Caldecott, *Molecular and Cellular Biology*, 2007, **27**, 5597-5605.
[56] T. A. Winters, W. D. Henner, P. S. Russell, A. McCullough and T. J. Jorgensen, *Nucleic Acids Research*, 1994, **22**, 1866-1873.

[57] A. Jilani, D. Ramotar, C. Slack, C. Ong, X. M. Yang, S. W. Scherer and D. D. Lasko, *Journal of Biological Chemistry*, 1999, **274**, 24176-24186.
[58] Y. Matsumoto and K. Kim, *Science*, 1995, **269**, 699-702.
[59] A. Kuzminov, *Proceedings of the National Academy of Sciences*, 2001, **98**, 8241-8246.
[60] R. Scully, A. Panday, R. Elango and N. A. Willis, *Nature Reviews Molecular Cell Biology*, 2019, **20**, 698-714.
[61] K. K. Chiruvella, Z. Liang and T. E. Wilson, *Cold Spring Harbor Perspectives in Biology*, 2013, **5**, a012757-a012757.
[62] J. R. Walker, R. A. Corpina and J. Goldberg, *Nature*, 2001, **412**, 607-614.
[63] M. Weinfeld, R. S. Mani, I. Abdou, R. D. Aceytuno and J. N. M. Glover, *Trends in Biochemical Sciences*, 2011, **36**, 262–271.
[64] H. H. Y. Chang and M. R. Lieber, *Nucleic Acids Research*, 2016, **44**, 4991-4997.
[65] N. K. Bernstein, R. S. Williams, M. L. Rakovszky, D. Cui, R. Green, F. Karimi-Busheri, R. S. Mani, S. Galicia, C. A. Koch, C. E. Cass, D. Durocher, M. Weinfeld and J. N. M. Glover, *Molecular Cell*, 2005, **17**, 657-670.
[66] I. Ahel, U. Rass, S. F. El-Khamisy, S. Katyal, P. M. Clements, P. J. McKinnon, K. W. Caldecott and S. C. West, *Nature*, 2006, **443**, 713-716.
[67] K. Ramadan, I. V. Shevelev, G. Maga and U. Hübscher, *Journal of Molecular Biology*, 2004, **339**, 395-404.
[68] U. Grawunder, M. Wilm, X. Wu, P. Kulesza, T. E. Wilson, M. Mann and M. R. Lieber, *Nature*, 1997, **388**, 492-495.
[69] M. Audebert, B. Salles and P. Calsou, *Biochemical and Biophysical Research Communications*, 2008, **369**, 982-988.
[70] S. Sharma, S. M. Javadekar, M. Pandey, M. Srivastava, R. Kumari and S. C. Raghavan, *Cell Death & Disease*, 2015, **6**, e1697-e1697.
[71] A. Sallmyr and A. E. Tomkinson, *Journal of Biological Chemistry*, 2018, **293**, 10536–10546.
[72] A. Ahmad, A. R. Robinson, A. Duensing, E. Van Drunen, H. B. Beverloo, D. B. Weisberg, P. Hasty, J. H. J. Hoeijmakers and L. J. Niedernhofer, *Molecular and Cellular Biology*, 2008, **28**, 5082-5092.
[73] L. Liang, L. Deng, S. C. Nguyen, X. Zhao, C. D. Maulion, C. Shao and J. A. Tischfield, *Nucleic Acids Research*, 2008, **36**, 3297-3310.
[74] M. Bétermier, P. Bertrand and B. S. Lopez, *PLoS Genetics*, 2014, **10**, e1004086.
[75] X. Li and W.-D. Heyer, *Cell Research*, 2008, **18**, 99-113.
[76] T. H. Stracker and J. H. J. Petrini, *Nature Reviews Molecular Cell Biology*, 2011, **12**, 90-103.
[77] A. V. Nimonkar, J. Genschel, E. Kinoshita, P. Polaczek, J. L. Campbell, C. Wyman, P. Modrich and S. C. Kowalczykowski, *Genes & Development*, 2011, **25**, 350-362.
[78] R. B. Jensen, A. Carreira and S. C. Kowalczykowski, *Nature*, 2010, **467**, 678-683.

[79] L. Maloisel, F. Fabre and S. Gangloff, *Molecular and Cellular Biology*, 2008, **28**, 1373-1382.
[80] K. Mitchel, H. Zhang, C. Welz-Voegele and S. Jinks-Robertson, *Molecular Cell*, 2010, **38**, 211-222.
[81] E. J. Uringa, J. L. Youds, K. Lisaingo, P. M. Lansdorp and S. J. Boulton, *Nucleic Acids Research*, 2011, **39**, 1647-1655.
[82] E. P. Mimitou and L. S. Symington, *Trends in Biochemical Sciences*, 2009, **34**, 264-272.
[83] J. M. Svendsen and J. W. Harper, *Genes & Development*, 2010, **24**, 521-536.
[84] T. Allers and M. Lichten, *Cell*, 2001, **106**, 47-57.
[85] M. Jasin, *Oncogene*, 2002, **21**, 8981-8993.
[86] D. M. Noll, T. M. Mason and P. S. Miller, *Chemical Reviews*, 2006, **106**, 277–301.
[87] R. Ceccaldi, P. Sarangi and A. D. D'Andrea, *Nature Reviews Molecular Cell Biology*, 2016, **17**, 337-349.
[88] H. L. Williams, M. E. Gottesman and J. Gautier, *Trends in Biochemical Sciences*, 2013, **38**, 386-393.
[89] R. J. Legerski, *Environmental and Molecular Mutagenesis*, 2010, **51**, 540-551.
[90] L. J. Niedernhofer, A. S. Lalai and J. H. J. Hoeijmakers, *Cell*, 2005, **123**, 1191-1198.
[91] P. Knipscheer, M. Räschle, A. Smogorzewska, M. Enoiu, T. V. Ho, O. D. Schärer, S. J. Elledge and J. C. Walter, *Science*, 2009, **326**, 1698-1701.
[92] J. Zhang, J. M. Dewar, M. Budzowska, A. Motnenko, M. A. Cohn and J. C. Walter, *Nature Structural & Molecular Biology*, 2015, **22**, 242-247.
[93] Q. Li, K. Dudas, G. Tick and L. Haracska, *Front Cell Dev Biol*, 2021, **9**, 699966.
[94] C. Clauson, O. D. Scharer and L. Niedernhofer, *Cold Spring Harbor Perspectives in Biology*, 2013, **5**, a012732-a012732.
[95] U. B. Abdullah, J. F. McGouran, S. Brolih, D. Ptchelkine, A. H. El-Sagheer, T. Brown and P. J. McHugh, *The EMBO Journal*, 2017, **36**, 2047-2060.
[96] J. M. Hinz, *Environmental and Molecular Mutagenesis*, 2010, **51**, 582-603.
[97] H. L. Williams, M. E. Gottesman and J. Gautier, *Mol Cell*, 2012, **47**, 140-147.
[98] R. D. Wood, *Environmental and Molecular Mutagenesis*, 2010, **51**, 520-526.
[99] T. Iyama, S. Y. Lee, B. R. Berquist, O. Gileadi, V. A. Bohr, M. M. Seidman, P. J. McHugh and D. M. Wilson, *Nucleic Acids Research*, 2015, **43**, 247-258.
[100] M. J. O'Connnor, *Molecular Cell*, 2015, **60**, 547-560.
[101] M. Rouleau, A. Patel, M. J. Hendzel, S. H. Kaufmann and G. G. Poirier, *Nature Reviews Cancer*, 2010, **10**, 293-301.
[102] C. J. Lord and A. Ashworth, *Science*, 2017, **355**, 1152-1158.
[103] S. M. B. Nijman, *FEBS Letters*, 2011, **585**, 1–6.
[104] M. K. Weil and A. P. Chen, *Current Problems in Cancer*, 2011, **35**, 7-50.
[105] Z. Bartosova and L. Krejci, *FEBS Letters*, 2014, **588**, 2446-2456.

[106] Y.-Y. Wang, A. C. Hung, S. Lo, Y.-C. Hsieh and S.-S. F. Yuan, *Cancer Letters*, 2021, **514**, 1-11.
[107] S. Arora, A. Kothandapani, K. Tillison, V. Kalman-Maltese and S. M. Patrick, *DNA Repair*, 2010, **9**, 745-753.
[108] E. Guo, Y. Ishii, J. Mueller, A. Srivatsan, T. Gahman, C. D. Putnam, J. Y. J. Wang and R. D. Kolodner, *Proceedings of the National Academy of Sciences*, 2020, **117**, 19415-19424.
[109] S. Ying, F. C. Hamdy and T. Helleday, *Cancer Research*, 2012, **72**, 2814-2821.
[110] K. Bush and J. F. Fisher, *Annual Review of Microbiology*, 2011, **65**, 455–478.
[111] S. M. Diene, L. Pinault, V. Keshri, N. Armstrong, S. Khelaifia, E. Chabrière, G. Caetano-Anolles, P. Colson, B. La Scola, J.-M. Rolain, P. Pontarotti and D. Raoult, *Scientific Reports*, 2019, **9**.
[112] C. Bebrone, *Biochemical Pharmacology*, 2007, **74**, 1686–1701.
[113] I. Pettinati, J. Brem, S. Y. Lee, P. J. McHugh and C. J. Schofield, *Trends Biochem. Sci.*, 2016, **41**, 338–355.
[114] Z. Dominski, *Critical Reviews in Biochemistry and Molecular Biology*, 2007, **42**, 67-93.
[115] S. Schiffer, S. Rosch and A. Marchfelder, *The EMBO Journal*, 2002, **21**, 2769-2777.
[116] C. R. Mandel, S. Kaneko, H. Zhang, D. Gebauer, V. Vethantham, J. L. Manley and L. Tong, *Nature*, 2006, **444**, 953-956.
[117] N. G. Kolev, T. A. Yario, E. Benson and J. A. Steitz, *EMBO reports*, 2008, **9**, 1013–1018.
[118] T. R. Albrecht and E. J. Wagner, *Molecular and Cellular Biology*, 2012, **32**, 1112-1123.
[119] I. Callebaut D. Moshous, J. P. Mornon, J. P de Villartay, *Nucleic Acids Research*, 2002, **30**, 3592-3601.
[120] B. Mir-Montazeri, M. Ammelburg, D. Forouzan, A. N. Lupas and M. D. Hartmann, *Journal of Structural Biology*, 2011, **173**, 191–195
[121] J. A. P. Henriques and E. Moustacchi, *Genetics*, 1980, **95**, 273-288.
[122] I. Demuth and M. Digweed, *Mutation Research/DNA Repair*, 1998, **409**, 11-16.
[123] M. Schmiester and I. Demuth, *Oncotarget*, 2017, **8**, 48398-48409.
[124] H. T. Baddock, J. A. Newman, Y. Yosaatmadja, M. Bielinski, C. J. Schofield, O. Gileadi and P. J. McHugh, *Nucleic Acids Research*, 2021, **49**, 9294–9309.
[125] A. R. Palacios, M.-A. Rossi, G. S. Mahler and A. J. Vila, *Biomolecules*, 2020, **10**, 854.
[126] B. Sengerová, C. K. Allerston, M. Abu, S. Y. Lee, J. Hartley, K. Kiakos, C. J. Schofield, J. A. Hartley, O. Gileadi and P. J. McHugh, *Journal of Biological Chemistry*, 2012, **287**, 26254-26267.
[127] H. T. Baddock, Y. Yosaatmadja, J. A. Newman, C. J. Schofield, O. Gileadi and P. J. McHugh, *DNA Repair*, 2020, **95**, 102941.
[128] A. Hazrati, M. Ramis-Castelltort, S. Sarkar, L. J. Barber, C. J. Schofield, J. A. Hartley and P. J. McHugh, *DNA Repair*, 2008, **7**, 230-238.

[129] M. Ishiai, M. Kimura, K. Namikoshi, M. Yamazoe, K. Yamamoto, H. Arakawa, K. Agematsu, N. Matsushita, S. Takeda, J. M. Buerstedde and M. Takata, *Mol Cell Biol*, 2004, **24**, 10733-10741.
[130] M. L. Dronkert, J. de Wit, M. Boeve, M. L. Vasconcelos, H. van Steeg, T. L. Tan, J. H. Hoeijmakers and R. Kanaar, *Mol Cell Biol*, 2000, **20**, 4553-4561.
[131] K. Nojima, H. Hochegger, A. Saberi, T. Fukushima, K. Kikuchi, M. Yoshimura, B. J. Orelli, D. K. Bishop, S. Hirano, M. Ohzeki, M. Ishiai, K. Yamamoto, M. Takata, H. Arakawa, J.-M. Buerstedde, M. Yamazoe, T. Kawamoto, K. Araki, J. A. Takahashi, N. Hashimoto, S. Takeda and E. Sonoda, *Cancer Research*, 2005, **65**, 11704-11711.
[132] I. Demuth, M. Digweed and P. Concannon, *Oncogene*, 2004, **23**, 8611-8618.
[133] M. Schmiester and I. Demuth, *Oncotarget*, 2017, **8**, 48398-48409.
[134] B. D. Freibaum and C. M. Counter, *Journal of Biological Chemistry*, 2008, **283**, 23671-23676.
[135] Y. C. Lam, S. Akhter, P. Gu, J. Ye, A. Poulet, M.-J. Giraud-Panis, S. M. Bailey, E. Gilson, R. J. Legerski and S. Chang, *The EMBO Journal*, 2010, **29**, 2230-2241.
[136] L. Kermasson, D. Churikov, A. Awad, R. Smoom, E. Lainey, F. Touzot, S. Audebert-Bellanger, S. Haro, L. Roger, E. Costa, M. Mouf, A. Bottero, M. Oleastro, C. Abdo, J.-P. De Villartay, V. Géli, Y. Tzfati, I. Callebaut, S. Danielian, G. Soares, C. Kannengiesser and P. Revy, *Blood*, 2022, **139**, 2427-2440.
[137] Y. Ma, U. Pannicke, K. Schwarz and M. R. Lieber, *Cell*, 2002, **108**, 781-794.
[138] Y. Ma, K. Schwarz and M. R. Lieber, *DNA Repair*, 2005, **4**, 845-851.
[139] D. Moshous, I. Callebaut, R. De Chasseval, B. Corneo, M. Cavazzana-Calvo, F. Le Deist, I. Tezcan, O. Sanal, Y. Bertrand, N. Philippe, A. Fischer and J.-P. De Villartay, *Cell*, 2001, **105**, 177-186.
[140] J. Mansilla-Soto and P. Cortes, *Journal of Experimental Medicine*, 2003, **197**, 543-547.
[141] X. Zhang, Y. Zhu, L. Geng, H. Wang and R. J. Legerski, *Oncogene*, 2009, **28**, 2196 2204.
[142] K. Bush and P. A. Bradford, *Cold Spring Harbor Perspectives in Medicine*, 2016, **6**, a025247.
[143] J. M. Munita and C. A. Arias, *Microbiology Spectrum*, 2016, **4**, 481-511.
[144] K. Bush and G. A. Jacoby, *Antimicrobial Agents and Chemotherapy*, 2010, **54**, 969–976.
[145] C. L. Tooke, P. Hinchliffe, E. C. Bragginton, C. K. Colenso, V. H. A. Hirvonen, Y. Takebayashi and J. Spencer, *J Mol Biol*, 2019, **431**, 3472-3500.
[146] M.-R. Meini, L. I. Llarrull and A. J. Vila, *FEBS Letters*, 2015, **589**, 3419–3432.
[147] M. F. Mojica, R. A. Bonomo and W. Fast, *Current Drug Targets*, 2016, **17**, 1029-1050.
[148] M. P. S. Booth, M. Kosmopoulou, L. Poirel, P. Nordmann and J. Spencer, *PLOS ONE*, 2015, **10**, e0140059.
[149] J. Brem, S. S. van Berkel, D. Zollman, S. Y. Lee, O. Gileadi, P. J. McHugh, T. R. Walsh, M. A. McDonough and C. J. Schofield, *Antimicrobrial Agents amd Chemotherapy*, 2016, **60**, 142-150.

[150] P. Hinchliffe, M. M. González, M. F. Mojica, J. M. González, V. Castillo, C. Saiz, M. Kosmopoulou, C. L. Tooke, L. I. Llarrull, G. Mahler, R. A. Bonomo, A. J. Vila and J. Spencer, *Proceedings of the National Academy of Sciences*, 2016, **113**, E3745-E3754.
[151] F.-M. Klingler, T. A. Wichelhaus, D. Frank, J. Cuesta-Bernal, J. El-Delik, H. F. Müller, H. Sjuts, S. Göttig, A. Koenigs, K. M. Pos, D. Pogoryelov and E. Proschak, *Journal of Medicinal Chemistry*, 2015, **58**, 3626-3630.
[152] J. Brem, S. S. Van Berkel, W. Aik, A. M. Rydzik, M. B. Avison, I. Pettinati, K.-D. Umland, A. Kawamura, J. Spencer, T. D. W. Claridge, M. A. McDonough and C. J. Schofield, *Nature Chemistry*, 2014, **6**, 1084-1090.
[153] N. Wade, K. H. M. E. Tehrani, N. C. Brüchle, M. J. Haren, V. Mashayekhi and N. I. Martin, *ChemMedChem*, 2021, **16**, 1651–1659.
[154] L. E. Horsfall, G. Garau, B. M. Lienard, O. Dideberg, C. J. Schofield, J. M. Frere and M. Galleni, *Antimicrobrial Agents and Chemotherapy*, 2007, **51**, 2136-2142.
[155] S. Leiris, A. Coelho, J. Castandet, M. Bayet, C. Lozano, J. Bougnon, J. Bousquet, M. Everett, M. Lemonnier, N. Sprynski, M. Zalacain, T. D. Pallin, M. C. Cramp, N. Jennings, G. Raphy, M. W. Jones, R. Pattipati, B. Shankar, R. Sivasubrahmanyam, A. K. Soodhagani, R. R. Juventhala, N. Pottabathini, S. Pothukanuri, M. Benvenuti, C. Pozzi, S. Mangani, F. De Luca, G. Cerboni, J.-D. Docquier and D. T. Davies, *ACS Infectious Diseases*, 2019, **5**, 131-140.
[156] J. Brem, T. Panduwawala, J. U. Hansen, J. Hewitt, E. Liepins, P. Donets, L. Espina, A. J. M. Farley, K. Shubin, G. G. Campillos, P. Kiuru, S. Shishodia, D. Krahn, R. K. Leśniak, J. Schmidt, K. Calvopiña, M.-C. Turrientes, M. E. Kavanagh, D. Lubriks, P. Hinchliffe, G. W. Langley, A. F. Aboklaish, A. Eneroth, M. Backlund, A. G. Baran, E. I. Nielsen, M. Speake, J. Kuka, J. Robinson, S. Grinberga, L. Robinson, M. A. McDonough, A. M. Rydzik, T. M. Leissing, J. C. Jimenez-Castellanos, M. B. Avison, S. Da Silva Pinto, A. D. Pannifer, M. Martjuga, E. Widlake, M. Priede, I. Hopkins Navratilova, M. Gniadkowski, A. K. Belfrage, P. Brandt, J. Yli-Kauhaluoma, E. Bacque, M. G. P. Page, F. Björkling, J. M. Tyrrell, J. Spencer, P. A. Lang, P. Baranczewski, R. Cantón, S. P. McElroy, P. S. Jones, F. Baquero, E. Suna, A. Morrison, T. R. Walsh and C. J. Schofield, *Nature Chemistry*, **2021**, DOI: 10.1038/s41557-021-00831-x.
[157] N. Ooi, V. E. Lee, N. Chalam-Judge, R. Newman, A. J. Wilkinson, I. R. Cooper, D. Orr, S. Lee and V. J. Savage, *Journal of Antimicrobial Chemotherapy*, 2021, **76**, 460-466.
[158] J. Wachino, W. C. Jin, K. Kimura, H. Kurosaki, A. Sato and Y. Arakawa, *Mbio*, 2020, **11**.
[159] A. J. M. Farley, Y. Ermolovich, K. Calvopiña, P. Rabe, T. Panduwawala, J. Brem, F. Björkling and C. J. Schofield, *ACS Infectious Diseases*, 2021, **7**, 1809-1817.
[160] S. T. Cahill, R. Cain, D. Y. Wang, C. T. Lohans, D. W. Wareham, H. P. Oswin, J. Mohammed, J. Spencer, C. W. G. Fishwick, M. A. McDonough, C. J. Schofield and J. Brem, *Antimicrobial Agents and Chemotherapy*, 2017, **61**, AAC.02260-02216.

[161]A. Krajnc, J. Brem, P. Hinchliffe, K. Calvopiña, T. D. Panduwawala, P. A. Lang, J. J. A. G. Kamps, J. M. Tyrrell, E. Widlake, B. G. Saward, T. R. Walsh, J. Spencer and C. J. Schofield, *Journal of Medicinal Chemistry*, 2019, **62**, 8544-8556.

[162] A. Parkova, A. Lucic, A. Krajnc, J. Brem, K. Calvopiña, G. W. Langley, M. A. McDonough, P. Trapencieris and C. J. Schofield, *ACS Infectious Diseases*, 2020, **6**, 1398-1404.

[163] ClinicalTrials.gov. Safety and Efficacy Study of Cefepime/VNRX-5133 in Patients With Complicated Urinary Tract Infections. https://clinicaltrials.gov/ct2/show/NCT03840148

[164] R. T. Jacobs, B. Nare, S. A. Wring, M. D. Orr, D. Chen, J. M. Sligar, M. X. Jenks, R. A. Noe, T. S. Bowling, L. T. Mercer, C. Rewerts, E. Gaukel, J. Owens, R. Parham, R. Randolph, B. Beaudet, C. J. Bacchi, N. Yarlett, J. J. Plattner, Y. Freund, C. Ding, T. Akama, Y. K. Zhang, R. Brun, M. Kaiser, I. Scandale and R. Don, *PLoS Neglected Tropical Diseases*, 2011, **5**, e1151.

[165] D. Begolo, I. M. Vincent, F. Giordani, I. Pöhner, M. J. Witty, T. G. Rowan, Z. Bengaly, K. Gillingwater, Y. Freund, R. C. Wade, M. P. Barrett and C. Clayton, *PLOS Pathogens*, 2018, **14**, e1007315.

[166] R. J. Wall, E. Rico, I. Lukac, F. Zuccotto, S. Elg, I. H. Gilbert, Y. Freund, M. R. K. Alley, M. C. Field, S. Wyllie and D. Horn, *Proceedings of the National Academy of Sciences*, 2018, **115**, 9616-9621.

[167] M. Kakutani, K. Takeuchi, I. Waga, H. Iwamura and K. Wakitani, *Inflammation Research*, 1999, **48**, 461-468.

[168] J. Kakegawa, N. Sakane, K. Suzuki and T. Yoshida, *Biochemical and Biophysical Research Communications*, 2019, **518**, 32-37.

[169] N. T. Ross, F. Lohmann, S. Carbonneau, A. Fazal, W. A. Weihofen, S. Gleim, M. Salcius, F. Sigoillot, M. Henault, S. H. Carl, J. B. Rodríguez-Molina, H. R. Miller, S. M. Brittain, J. Murphy, M. Zambrowski, G. Boynton, Y. Wang, A. Chen, G. J. Molind, J. H. Wilbertz, C. G. Artus-Revel, M. Jia, F. A. Akinjiyan, J. Turner, J. Knehr, W. Carbone, S. Schuierer, J. S. Reece-Hoyes, K. Xie, C. Saran, E. T. Williams, G. Roma, M. Spencer, J. Jenkins, E. L. George, J. R. Thomas, G. Michaud, M. Schirle, J. Tallarico, L. A. Passmore, J. A. Chao and R. E. J. Beckwith, *Nature Chemical Biology*, 2020, **16**, 50-59.

[170] S. Y. Lee, J. Brem, I. Pettinati, T. D. W. Claridge, O. Gileadi, C. J. Schofield and P. J. McHugh, *Chemical Communications*, 2016, **52**, 6727-6730.

[171] Y. Yosaatmadja, H. T. Baddock, J. A. Newman, M. Bielinski, A. E. Gavard, S. M. M. Mukhopadhyay, A. A. Dannerfjord, C. J. Schofield, P. J. McHugh and O. Gileadi, *Nucleic Acids Research*, 2021, **49**, 9310-9326.

[172] W. Doherty, E.-M. Dürr, H. T. Baddock, S. Y. Lee, P. J. McHugh, T. Brown, M. O. Senge, E. M. Scanlan and J. F. McGouran, *Organic & Biomolecular Chemistry*, 2019, **17**, 8094-8105.

[173] M. Berney, W. Doherty, W. T. Jauslin, M. T Manoj, E.-M. Dürr and J. F. McGouran, *Bioorganic & Medicinal Chemistry*, 2021, **46**, 1163-69
[174] B. Buzon, R. A. Grainger, C. Rzadki, S. Y. M. Huang and M. Junop, *ACS Omega*, 2021, **6**, 9352-9361.
[175] L. N. Tumey, B. Huck, E. Gleason, J. Wang, D. Silver, K. Brunden, S. Boozer, S. Rundlett, B. Sherf, S. Murphy, A. Bailey, T. Dent, C. Leventhal, J. Harrington and Y. L. Bennani, *Bioorganic & Medicinal Chemistry Letters*, 2004, **14**, 4915-4918.
[176] T. Kawasuji, T. Yoshinaga, A. Sato, M. Yodo, T. Fujiwara and R. Kiyama, *Bioorgan Med Chem*, 2006, **14**, 8420-8429.
[177] L. N. Tumey, D. Bom, B. Huck, E. Gleason, J. Wang, D. Silver, K. Brunden, S. Boozer, S. Rundlett, B. Sherf, S. Murphy, T. Dent, C. Leventhal, A. Bailey, J. Harrington and Y. L. Bennani, *Bioorganic & Medicinal Chemistry Letters*, 2005, **15**, 277-281.
[178] E. Guo, Y. Ishii, J. Mueller, A. Srivatsan, T. Gahman, C. D. Putnam, J. Y. J. Wang and R. D. Kolodner, *Proceedings of the National Academy of Sciences*, 2020, **117**, 19415-19424.
[179] T. A. Ward, P. J. McHugh and S. T. Durant, *PLOS ONE*, 2017, **12**, e0179278.
[180] J. C. Exell, M. J. Thompson, L. D. Finger, S. J. Shaw, J. Debreczeni, T. A. Ward, C. McWhirter, C. L. B. Siöberg, D. M. Molina, W. M. Abbott, C. D. Jones, J. W. M. Nissink, S. T. Durant and J. A. Grasby, *Nat Chem Biol*, 2016, **12**, 815-821.
[181] T. M. Chapman, K. J. Gillen, C. Wallace, M. T. Lee, P. Bakrania, P. Khurana, P. J. Coombs, L. Stennett, S. Fox, E. A. Bureau, J. Brownlees, D. W. Melton and B. Saxty, *Bioorganic & Medicinal Chemistry Letters*, 2015, **25**, 4097-4103.
[182] T. M. Chapman, C. Wallace, K. J. Gillen, P. Bakrania, P. Khurana, P. J. Coombs, S. Fox, E. A. Bureau, J. Brownlees, D. W. Melton and B. Saxty, 2015, **25**, 4104-4108.
[183] S. Madhusudan, F. Smart, P. Shrimpton, J. L. Parsons, L. Gardiner, S. Houlbrook, D. C. Talbot, T. Hammonds, P. A. Freemont, M. J. E. Sternberg, G. L. Dianov and I. D. Hickson, *Nucleic acids research*, 2005, **33**, 4711.
[184] L. A. Seiple, J. H. Cardellina, R. Akee and J. T. Stivers, *Molecular Pharmacology*, 2008, **73**, 669-677.
[185] L. P. Jordheim, K. H. Barakat, L. Heinrich-Balard, E. L. Matera, E. Cros-Perrial, K. Bouledrak, R. El Sabeh, R. Perez-Pineiro, D. S. Wishart, R. Cohen, J. Tuszynski and C. Dumontet, 2013, **84**, 12-24.
[186] F. Gentile, A. H. Elmenoufy, G. Ciniero, D. Jay, F. Karimi-Busheri, K. H. Barakat, M. Weinfeld, F. G. West and J. A. Tuszynski, *Chemical Biology & Drug Design*, 2020, **95**, 460-471.
[187] A. H. Elmenoufy, F. Gentile, D. Jay, F. Karimi-Busheri, X. Yang, O. M. Soueidan, C. Weilbeer, R. S. Mani, K. H. Barakat, J. A. Tuszynski, M. Weinfeld and F. G. West, *Journal of Medicinal Chemistry*, 2019, **62**, 7684-7696.

[188] G. Ciniero, A. H. Elmenoufy, F. Gentile, M. Weinfeld, M. A. Deriu, F. G. West, J. A. Tuszynski, C. Dumontet, E. Cros-Perrial and L. P. Jordheim, *Cancer Chemotherapy and Pharmacology*, 2021, **87**, 259–267.
[189] F. Gentile, J. A. Tuszynski and K. H. Barakat, *Journal of Molecular Graphics and Modelling*, 2016, **65**, 71-82.
[190] K. H. Barakat, L. P. Jordheim, R. Perez-Pineiro, D. Wishart, C. Dumontet and J. A. Tuszynski, *PLoS ONE*, 2012, **7**, e51329.
[191] D. Aude, B.-C. Louise, M. S. Rose, P. M. Ami, L. Ji-Hoon, L. N. Matthew, K. Levy, J. Maria, B. Richard, T. P. Tanya and G. Jean, *Nature Chemical Biology*, 2008, **4**, 119.
[192] A. Shibata, D. Moiani, A. S. Arvai, J. Perry, S. M. Harding, M. M. Genois, R. Maity, S. Van rossum-Fikkert, A. Kertokalio, F. Romoli, A. Ismail, E. Ismalaj, E. Petricci, M. J. Neale and R. G. Bristow, *Molecular Cell*, 2014, **53**, 7-18.

Chapter 2. Cyclic *N*-hydroxyimide inhibitors

2.1. Initial hits against SNM1A

Prior to the initiation of the work described in this thesis, an extensive high-throughput screen (HTS) using a fluorescence-based assay of 400,000 compounds had been performed against SNM1A by the European Lead Factory (ELF) in collaboration with the University of Oxford (unpublished results). The HTS led to the identification of 22 potential hit compounds. Following the HTS, attempts were undertaken to obtain inhibitor-bound structures by soaking the inhibitors into crystals of SNM1A. Compounds **3** and **9** were the only hits found to bind to SNM1A and to successfully yield crystal structures (**Figure 2.1**). The structure of **3** is strikingly similar to the reported FEN1 inhibitors mentioned in **Section 1.5.1**.

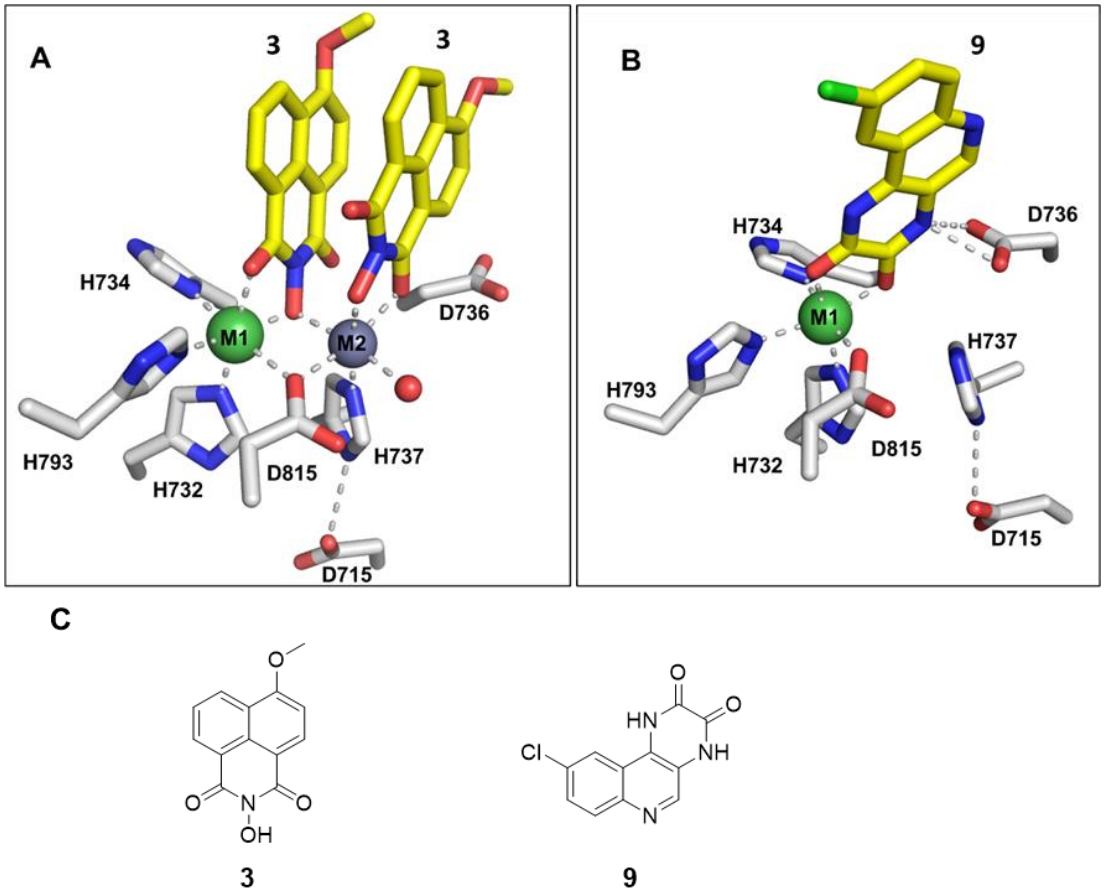

Figure 2.1: *Inhibitor hit molecules from the HTS in complex with SNM1A* ***A:*** *View from a crystal structure of hit* ***3*** *bound to the active site of SNM1A.* ***B:*** *View from a crystal structure of hit* ***9*** *bound to the active site of SNM1A.* ***C:*** *Structure of hits* ***3*** *and* ***9****.* ***M1****: Nickel.* ***M2****: Zinc.*

The crystal structure reveals that compounds **3** and **9** both chelate metal ions in the active site using their oxygen atoms, with octahedral coordination around each metal ion. Whilst the SNM1A structure complexed with **3** bound has two metal ions present in the active site, only one metal ion is present in the structure with **9**. In the crystal structures, metal ion M1 was assigned as nickel (II), and M2 was assigned as zinc (II). By contrast, two zinc (II) ions are generally considered to be the physiologically relevant metals, though this has not yet been demonstrated to be the case *in vivo*.[1] Structures of SNM1A with only the first potential metal ion binding site occupied are also common, raising questions about the biologically relevant metal ions.[2]

Interestingly, for the crystal structure with the hit **3**, there are two molecules of **3** bound to the active site. The two molecules of **3** apparently stack with each other at a distance of ~3.6 angstrom (Å), indicating a possible pi-stacking interaction between the two molecules. Both molecules of **3** chelate the active site metal ions using their cyclic hydroxymate pharmacophore. The *N*-hydroxyl group of one of the molecules of **3** bridges between the two metal ions displacing the catalytic water molecule. A similar mode of ligation and displacement of catalytic water was previously observed for thiol or sulfonamide-based inhibitors of true MBLs described in **Chapter 1**.[3,4] Additionally, it can be observed that one of the **3** molecules displaces the Asp736, which normally chelates the **M2** metal ion. There are no other substantial interactions between molecule **3** and SNM1A in the crystal structure complex, with more than 3.5 Å distance between molecule **3** and any amino acid residue side chain.

Inhibitor **9** chelates metal ion **M1** in the active site using two catechol oxygens from the cyclic diamide sidechain. Additionally, there might a be hydrogen bonding interaction between oxygens in Asp736 and one of the amide nitrogens from molecule **9** as there is a distance of 2.8 Å between these atoms.

After obtaining structural data, compounds **3** and **9** were resynthesised for validation studies because the ELF provided only limited quantities. Additionally, compound **5**, a structural isomer of **3**, was synthesised as there was a discrepancy between the report from ELF and the obtained structural data for **3**. The initial report from ELF stated that compound **5**, which has a methoxy group at the *meta*-position, was tested in the HTS. At the same time, based on the structural data, the ELF supplied to Oxford compound **3**, which has a methoxy group

at the *para*-position, instead of compound **5**. The synthesis of compounds **3**, **5**, and **9** were based on previously published synthetic routes (**Figure 2.2**).[5,6,7]

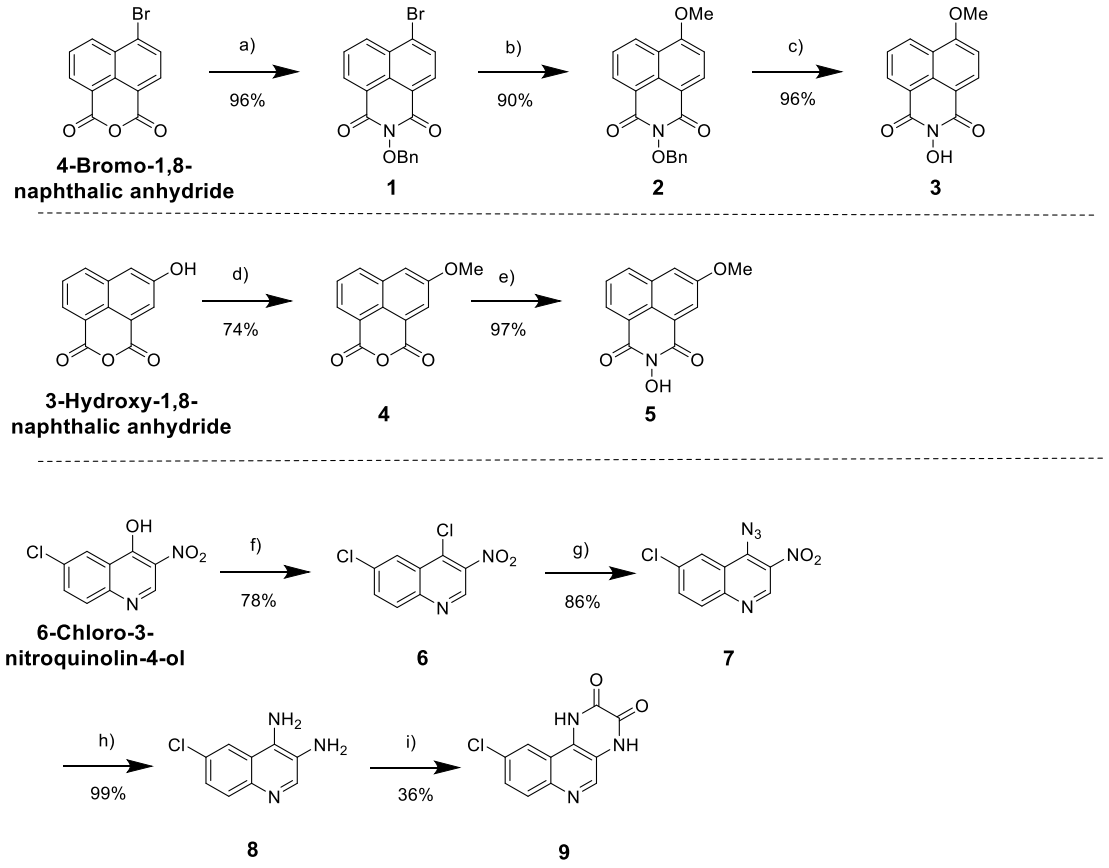

Figure 2.2: *Scheme for synthesis of inhibitors **3**, **5** and **9**. Conditions for each step:* ***a)*** *$NH_2OBn.HCl$, pyridine, reflux, 2 h;* ***b)*** *NaOMe, $CuSO_4$, MeOH, reflux, 12 h;* ***c)*** *Pd/C, H_2, DMA, RT, 4 h;* ***d)*** *SO_4Me_2, K_2CO_3, acetone, reflux 3 h;* ***e)*** *$NH_2OH.HCl$, pyridine, reflux, 1 h;* ***f)*** *$SOCl_2$, DMF, DCM, reflux 2 h;* ***g)*** *NaN_3, DMF, RT, 2 h;* ***h)*** *Raney nickel, H_2, MeOH, RT, 1 h;* ***i)*** *diethyl oxalate, reflux, 2 h.*

The synthesis of hit **3** from commercially available 4-bromo-1,8-naphthalic anhydride was very efficient, with each step having excellent yield (≥ 90%) with an overall yield of 83% over 3 steps. In step **a)**, 4-bromo-1,8-naphthalic anhydride was reacted with *O*-benzylhydroxylamine to form **1** via a condensation reaction, using pyridine as a solvent, base, and nucleophilic catalyst. In step **b)**, compound **1** was converted into **2** via nucleophilic aromatic substitution using sodium methoxide as nucleophile and copper(II) sulfate as a catalyst. Following the synthesis, compounds **1** and **2** were purified using filtration with the

washing of the solid precipitate to remove any soluble impurities. Finally, in step **c)**, the benzyl protecting group in compound **2** was removed by hydrogenation to produce hit **3**. Hydrogen gas and palladium on carbon catalyst was used for benzyl deprotection. After hydrogenation, compound **3** was purified by filtration.

The synthesis of hit **5** from commercially available 3-hydroxy-1,8-naphthalic anhydride was relatively efficient, proceeding in an overall yield of 72% after 2 steps. In step **d)**, the hydroxyl group, from 3-hydroxy-1,8-naphthalic anhydride, was methylated using dimethyl sulfate as an alkylating agent and potassium carbonate as a base to produce compound **4**. Compound **4** was synthesised at a good yield of 74% in step **d)**. Next, in step **e)**, **4** was reacted with hydroxylamine to produce hit **5** via a condensation reaction, using pyridine as a solvent, base, and nucleophilic catalyst. Step **e)** was performed at an excellent yield of 97%. Both **4** and **5** were purified by filtration with washing of the precipitate to remove soluble impurities.

Hit **9** was synthesised from commercially available 6-chloro-3-nitroquinolin-4-ol with an overall yield of 24% after 4 steps. First, in step **f)**, intermediate **6** was synthesised from 6-chloro-3-nitroquinolin-4-ol by converting the hydroxyl group into chloride using thionyl chloride as a chlorinating agent and DMF as a catalyst. Compound **6** was purified using extraction and column chromatography. The yield of step **f)** was 78%. In step **g)**, **6** was converted into **7** via aromatic nucleophilic substitution of chloride at position 4 with azide. Sodium azide was used as the source of the azide. While two chloride atoms were present in the intermediate **6**, the substitution reaction was only observed at position 4, which is more reactive due to the adjacent nitro group. In step **g)** compound **7** was purified using extraction and was synthesised in a good yield of 86%. Next, in step **h)**, compound **7** was converted

into **8** via hydrogenation. Initially, it was attempted to perform hydrogenation using palladium on carbon as a catalyst, but this resulted in an additional reduction of the chloride at position 6. Use of Raney nickel catalyst instead of palladium on carbon resulted in a more selective hydrogenation reaction with a reduction of only the azide and nitro groups. Step **h)** resulted in a nearly quantitative yield of 99%, and compound **8** could be obtained by filtration. Finally, in step **i)**, compound **8** reacted with diethyl oxalate using cyclocondensation reaction to produce hit **9**. In step **i)**, hit **9** was produced in a very poor yield of 36%. Hit **9** was purified using filtration and solvent wash to remove soluble impurities.

All three compounds, **3**, **5**, and **9**, were tested using real-time fluorescence and radioactive gel-based assays against SNM1A (**Figure 2.4**). The conditions used for the fluorescence-based assay and the gel-based assay were the same as in previously published work.[8]

The real-time fluorescence-based method is an enzyme activity-based assay. The assay employs SNM1A or other MBL nuclease (SNM1B or SNM1C) and a chemically modified oligonucleotide as a substrate. The substrate used for fluorescence-based assay with SNM1A or SNM1B was a 20-nucleotide ssDNA labelled with fluorescein isothiocyanate (FITC) at the 5′ end and black-hole quencher 1 (BHQ) 8 nucleotides away. In the plate reader, the FITC is excited using radiation at a 495 nm wavelength, and the fluorescence emission is quenched by BHQ. Upon digestion of the oligonucleotide substrate in the 5′ to 3′ direction by either SNM1A or SNM1B exonuclease activity, FITC-labelled nucleotide is released. As the FITC labelled nucleotide is released, the fluorescence emission is no longer quenched by BHQ, and the fluorescence at 515 nm wavelength is emitted, as shown in **Figure 2.3**. The 515 nm fluorescence emission is measured at 15-time points over 35 minutes. The rate of

increase of the fluorescence intensity represents the enzymatic activity of the nuclease. The real-time fluorescence-based assay gives quantitative results as it precisely measures the fluorescence emission at fixed time points and shows the enzyme activity over a specific duration.

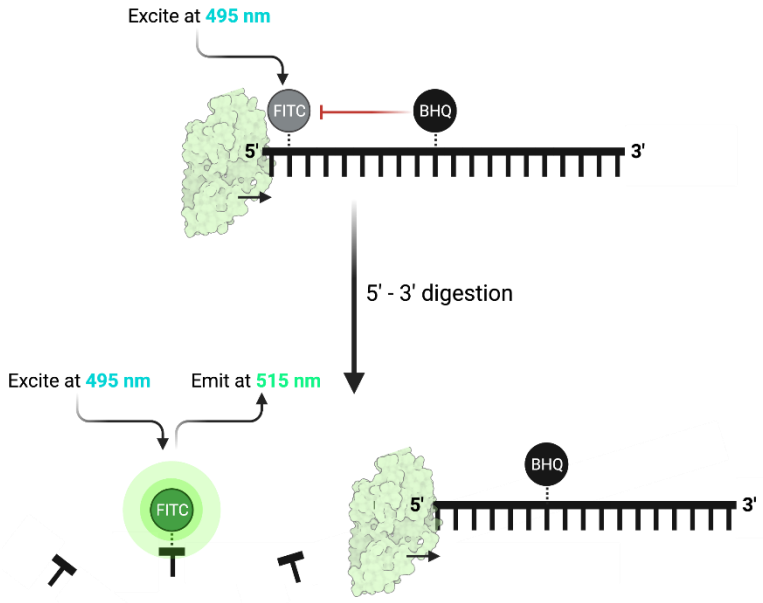

Figure 2.3: *Schematic for the real-time fluorescence assay.*

Similarly to fluorescence-based assay, the radioactive gel-based assay is also an enzyme activity-based method. The substrate used for the gel-based assay was either a 21 or 50 nucleotides long ssDNA containing phosphorus-32 (^{32}P) at the 3' end. In the radioactive gel-based assay, SNM1A, B, or C, nuclease together with the radiolabeled DNA substrate were allowed to react for 40 min. Over the reaction time, the nuclease digests the DNA substrate to produce oligonucleotides of various lengths. After 40 min, the enzymatic reaction is quenched, and electrophoresis gel is run to separate the products of the nuclease digestion. Measurement of the radioactive decay of the ^{32}P allows for the identification of specific DNA bands on the electrophoresis gel. The obtained products and the extent of digestion by SNM1 nuclease can be determined using the radioactive gel-based assay. While the

radioactive gel-based assay gives less quantitative results, it uses a much more physiologically relevant substrate than the fluorescence-based assay. The radioactive gel-based assay was mainly used to validate inhibitors, firstly identified by a fluorescence-based assay.

The gel-based assay and real-time fluorescence assay are independent methods of examining the nuclease activity of the enzyme as they show different readouts. The fluorescence assay measures only the digestion of a single nucleotide that results in fluorescence emission. In contrast, in the radioactive gel-based assay, we can see various products of digestion, and therefore, digestion of multiple nucleotides can be observed. Since the real-time fluorescence assay results are more quantitative, this assay was primarily used to plot dose-response curves and calculate the IC_{50} value for each inhibitor. In the dose-response curves, the y-axis is labelled as "Percentage Response", which stands for the percentage of fluorescence observed, where 100% is the maximum fluorescence observed when substrated is treated by an enzyme with no inhibitor present, and 0% is the background fluorescence of the untreated probe. The fluorescence observed corresponds to the enzyme activity. The x-axis is labelled as "Log(Concentration/M)", in which "Concentration" stands for the concentration of inhibitors used. Additionally, the real-time fluorescence assay is faster and more high-throughput than the gel-based assay, and therefore it was a preferred method for testing larger sets of compounds.

Half maximal inhibitory concentration (IC_{50}) is a measure of inhibitor potency, indicating the concentration of an inhibitor at which there is 50% biological activity. Throughout the project, IC_{50} values were used to quantify the potency of inhibitors.

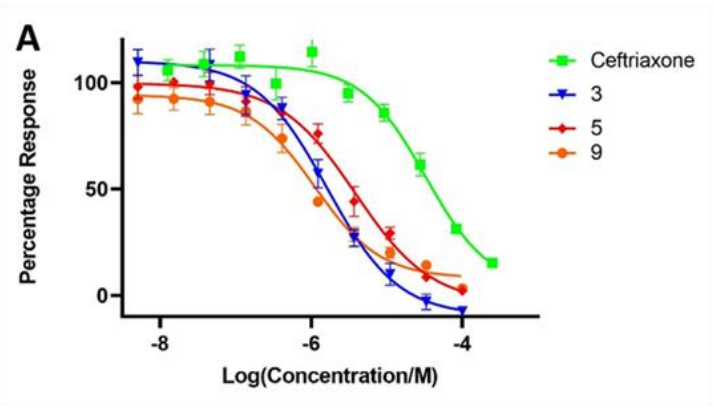

B

Compound	IC_{50}/μM
Ceftriaxone	32
3	2.4
5	2.9
9	2.0

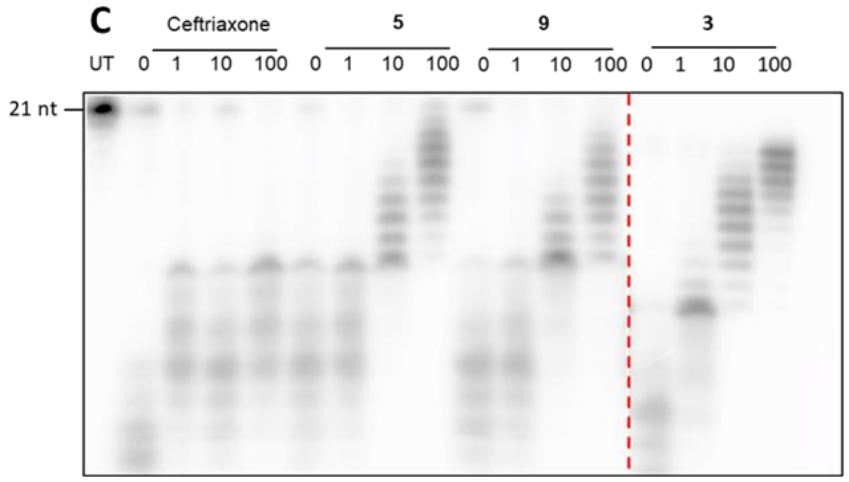

Figure 2.4: A: *Dose-response curve plotted using the data from real-time fluorescence assay for inhibitor testing against SNM1A. Concentrations used [SNM1A] = 0.5 nM and [DNA] = 25 nM.* ***B****: IC_{50} values calculated for each inhibitor.* ***C****: Representing gel image from radioactive gel-based assay against SNM1A. Concentrations used [SNM1A] = 0.8 nM and [DNA (21-mer)] = 100 nM. The indicated concentrations are in μM. UT: untreated. A red dotted line is used to separate images taken from 2 separate gels.*

Hit compounds **3**, **5** and **9** were tested against SNM1A, together with ceftriaxone as a positive control inhibitor, by using both the real-time fluorescence-based and gel-based assays (**Figure 2.4**).[7] All three hits (**3**, **5** and **9**) were more inhibitory than ceftriaxone, one of the most potent SNM1A inhibitors reported in the literature.[7] The newly identified hits inhibited SNM1A with nearly identical potencies with IC_{50}s measured in the low micromolar range; **3** = 2.4 μM, **5** = 2.9 μM, and **9** = 2.0 μM. With the gel-based assay, SNM1A was partially inhibited when using 10 and 100 μM concentrations of **3**, **5** and **9**. Because compounds **3**, **5** and **9** have IC_{50} values within the same range and all showed very similar

inhibition on the gel-based assay, it was not possible to identify one of them as the most potent hit.

Hits **3**, **5**, and **9,** together with ceftriaxone were further tested against SNM1A from another batch of enzyme purified using non-standard conditions, without immobilised metal affinity chromatography (IMAC) (**Figure 2.5**). IMAC is a standard protein purification procedure that uses immobilised metal ions, primarily nickel (II) ions, to separate proteins and purify the particular protein of interest. The metal ions from the IMAC column can leach out and affect the metal content in the enzymes.[9] Non-IMAC SNM1A protein samples were purified using HiTrap SP FF, ion exchange chromatography, instead of the IMAC. SNM1A purified with IMAC has a mixture of iron, nickel and zinc in the active site, while the batch purified without IMAC contains iron and zinc ions, the presence of ions was measured using ICP-MS (Inductive coupled plasma mass spectrometry). At the same time, it is widely predicted that zinc ions are naturally present in SNM1A, though this has not been demonstrated *in vivo*.[1] SNM1A purified without IMAC, was only used for assay presented in **Figures 2.5** and **3.2**, for all other assay proteins purfied using IMAC were used, as this purification method was much more efficient.

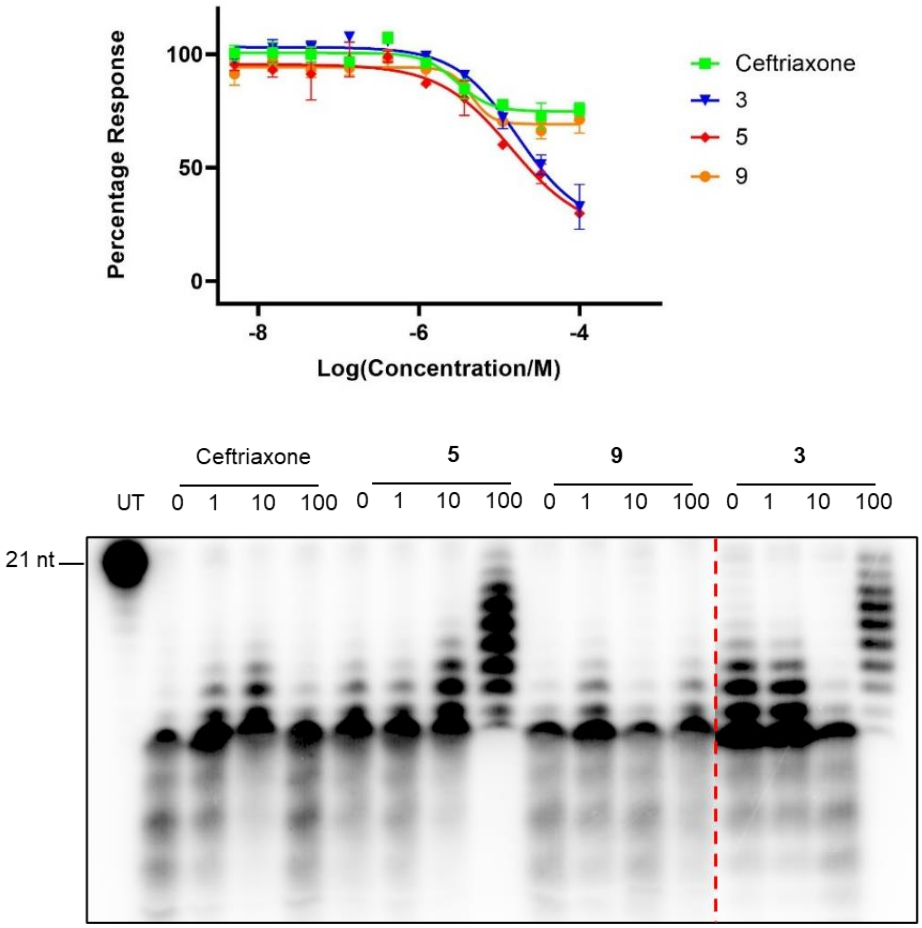

Figure 2.5: *Assays run with SNM1A that was not purified using IMAC.* ***Top:*** *Dose-response curve plotted using the data from the real-time fluorescence assay. Concentrations used [SNM1A] = 1.25 nM and [DNA 21 mer] = 25 nM.* ***Bottom****: Representing gel image from radioactive gel-based assay against SNM1A. Concentrations used [SNM1A] = 0.8 nM, and [DNA (21-mer)] = 100 nM. The indicated concentrations are in μM. UT: untreated A red dotted line is used to separate images taken from 2 separate gels.*

Ceftriaxone and **9** showed much lower inhibition against the non-IMAC purified SNM1A construct compared to hits **3** and **5** (**Figure 2.5**). While in the assay against SNM1A purified using a standard procedure with IMAC (**Figure 2.3**), hit compounds **3**, **5**, and **9** showed nearly identical inhibition. Based on the results of the gel-based assay against non-IMAC purified SNM1A, hits **3** and **5** exhibit partial inhibition concentrations of 100 μM. Hits **3** and **5** showed only partial inhibition in the fluorescence-based assay against non-IMAC purified SNM1A, although the inhibition is too low to calculate IC_{50} values accurately. Due to the relatively lower activity of the non-IMAC purified SNM1A construct, a 1.25 nM enzyme

concentration was used for fluorescence-based assay instead of 0.5 nM. When comparing results from assays against both SNM1A constructs, it appears that inhibition of **9** might be more dependent on the metals present in the active site than in the case of **3** and **5**.

Hydroxamates are known zinc binding groups that are reported to inhibit a variety of zinc (II) containing metalloenzymes, including carbonic anhydrase.[10] Therefore *N*-hydroxyimides were chosen for further optimisation and development of SNM1A inhibitors. Similarly, it has been observed that the extent of inhibition of bacterial MBL can vary in a manner depending on the metal ions present in the active site.[11]

2.2. Development of structural analogues of 3 and 5 against SNM1A

While the initial data for hits **3** and **5** was promising, substantial improvements had to be made to obtain more potent inhibitors. Both **3** and **5** have a flat polyaromatic core, which likely leads to their poor solubility and might enable intercalation of DNA. When designing structural analogues of **3** and **5**, one of the aromatic rings was removed, similarly to what has been done when FEN1 inhibitors were optimised from hit ATH-0013974 to inhibitor FEN1-in-1, as discussed in **Section 1.5.1**.[12] Additionally, the bicyclic *N*-hydroxyimde core was considered more suitable for synthesising a library of analogues as it is more easily modified than the initial tricyclic core of either **3** or **5**. The ester functional group and morpholine ring were introduced to improve the solubility.[13] As sulfur atoms are common in bacterial MBL inhibitors and are involved in chelating metals in the active site, thiourea was introduced in one of the derivatives. The structures and synthetic schemes for five new structural analogues **12**, **14**, **15**, **18** and **20** are shown in **Figure 2.6**.[9,14,15,16] The only novel inhibitor from this list above was compound **18**.

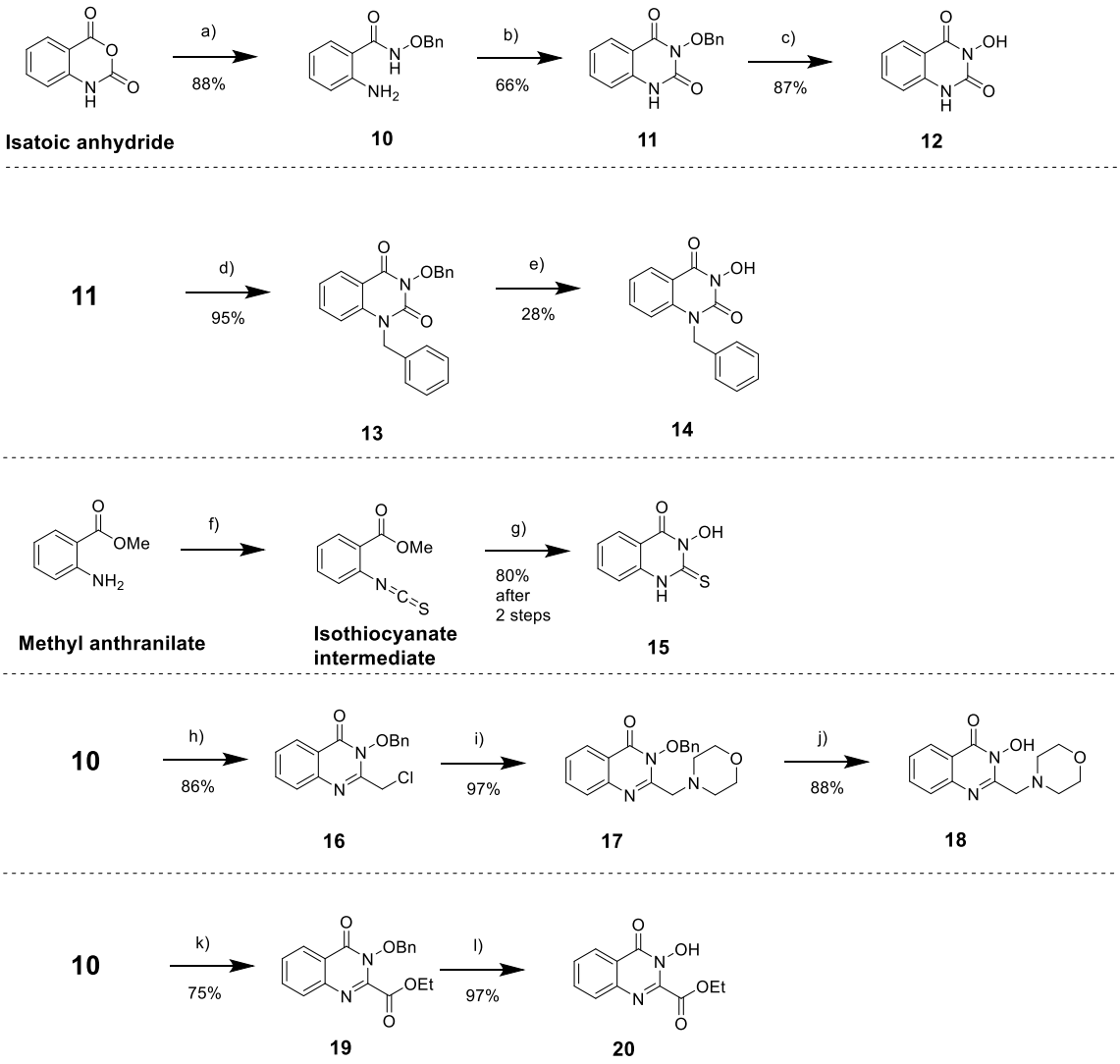

Figure 2.6: *Scheme for synthesis of analogues of* ***3*** *and* ***5****. Conditions for each step:* ***a)*** *$NH_2OBn.HCl$, TEA, THF, reflux, 3 h;* ***b)*** *triphosgene, TEA, THF, 0 °C, 2 h;* ***c)*** *Pd/C, H_2, DMF, RT, 2 h;* ***d)*** *BnBr, Cs_2CO_3, DMF, 80 °C, 2 h;* ***e)*** *conc. $HBr_{(aq)}$, AcOH, reflux, 1 h;* ***f)*** *thiophosgene, H_2O, DCM, RT, 12 h;* ***g)*** *$NH_2OH.HCl$, NaOH, H_2O, $CHCl_3$ RT, 2h;* ***h)*** *2-chloroacetyl chloride, DMF, RT, 2 h;* ***i)*** *morpholine, DMF, 60 °C, 1 h;* ***j)*** *Pd/C, H_2, MeOH, RT, 2 h;* ***k)*** *ethyl chlorooxoacetate, pyridine, DCM, RT, 12 h; then p-toluenesulfonic acid, toluene, reflux, 2 h;* ***l)*** *Pd/C, H_2, EtOAc, RT, 15 min.*

Inhibitor **12** was synthesised from the commercially available isatoic anhydride in an overall yield of 51% over 3 steps. In step **a)**, isatoic anhydride was reacted with *O*-benzylhydroxylamine to form an amide bond and produce compound **10**. Compound **10** was purified using column chromatography and was produced at a very good yield of 88%. Next, in step **b)**, triphosgene was used to convert compound **10** into **11** via carbonylation-

cyclisation. Compound **11** was purified using column chromatography and was produced at a yield of 66%. Finally, in step **c)**, compound **11** was converted into inhibitor **12** through deprotection of the *O*-benzyl group using a hydrogenation reaction. Hydrogenation reaction in step **c)** was performed using standard conditions: hydrogen gas and palladium on carbon as a catalyst, and produced inhibitor **12** at a very good yield of 87%.

Inhibitor **14** was synthesised from compound **11** in an overall yield of 27% over 2 steps. First, in step **d)**, **11** was alkylated using benzyl bromide to produce compound **13**. After alkylation, **13** was purified using filtration and step **d)** resulted in an excellent yield of 95%. Next, in step **e)**, the *O*-benzyl group in **13** was removed to produce inhibitor **14**. A hydrogenation reaction was not used because there were two benzyl groups in compound **13**. Instead, the *O*-benzyl group was selectively removed under strongly acidic conditions using concentrated hydrobromic acid and acetic acid. Inhibitor **14** was purified by filtration. The yield of step **e)** was very poor, resulting in only 28% yield after isolation.

Inhibitor **15** was synthesised from the commercially available methyl anthranilate with a very good overall yield of 80% over two steps. First, in step **f)**, the amine group from methyl anthranilate was converted into isothiocyanate using thiophosgene to form **isothiocyanate intermediate**. The **isothiocyanate intermediate** was purified using extraction and was then directly used in the next step. In step **g)**, **isothiocyanate intermediate** was reacted with hydroxylamine, and the second ring was cyclised to form inhibitor **15**. Inhibitor **15** was then purified using filtration.

Inhibitor **18** was synthesised from compound **10** with a good overall yield of 73% over 3 steps. First, in step **h)**, **10** was reacted with 2-chloroacetyl chloride via a cyclocondensation

reaction to produce compound **16**. Compound **16** was produced in step **h)** at a very good yield of 86% and was purified using extraction. Next, in step **i)**, compound **16** was converted into **17** through nucleophilic substitution of chloride with morpholine. **17** was purified using column chromatography and extraction. Compound **17** was produced in an excellent yield of 97%. Finally, in step **j)**, the benzyl protecting group in **17** was removed to produce inhibitor **18**. The hydrogenation reaction procedure used in step **j)** were similar to those used in step **c)**. Step **j)** produced **18** in a very good yield of 88%.

Inhibitor **20** was synthesised from compound **10** in a good overall yield of 73% over 2 steps. First, in step **k)**, compound **10** was reacted with ethyl chlorooxoacetate to form an amide bond; this was followed by a cyclisation reaction, using p-toluenesulfonic acid as a catalyst, to produce **19**, which was purified using column chromatography, and giving **19** in a good yield (75%). Next, in step **l)**, the benzyl protecting group was removed to convert **19** into inhibitor **20** using hydrogenation. Similarly to steps **c)** and **j)**, palladium on carbon as a catalyst and hydrogen gas were used for the hydrogenation reaction. The yield of step **l)** was excellent (97%), and inhibitor **20** was purified using filtration.

Following the synthesis, analogues **12**, **14**, **15**, **18**, and **20** were tested using the real-time fluorescence assay against SNM1A (**Figure 2.7**).

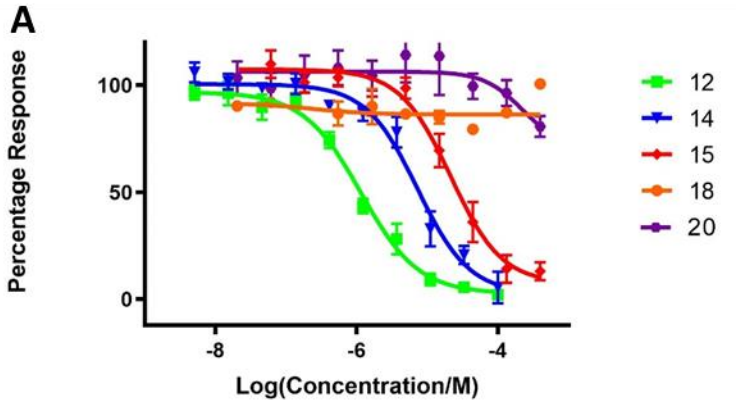

B

Compound	IC_{50}/μM
12	1.2
14	7.3
15	22
18	>250
20	>250

Figure 2.7: A: *Dose-response curve plotted using the data from real-time fluorescence assay against SNM1A. Concentrations used [SNM1A] = 0.5 nM and [DNA] = 25 nM.* ***B:*** *Table of IC_{50} calculated for each inhibitor.*

Out of the five synthesised compounds, only inhibitor **12** showed slightly better inhibition than hits **3** and **5** in the fluorescence-based assay against SNM1A. Compound **12** had an IC_{50} of 1.2 μM. The inhibition of compound **12** against SNM1A is poor compared to its inhibition against FEN1 and XPG, which has IC_{50} of 0.079 μM and 0.16 μM, respectively.[9] This substantial difference in the IC_{50} between SNM1A, FEN1 and XPG might indicate structural differences, which may allow for the development of selective inhibitors against these enzymes.

Unfortunately, **18** and **20** showed no inhibition against SNM1A, whilst **14** had an IC_{50} of 7.3 μM. Such a potency decrease might be caused by a steric clash between the bulky benzyl group of **14** and a residue in the SNM1A active site. Therefore, it was considered that it might be more favourable to investigate modifications further away from the hydroxamate pharmacophore involved in chelating the metals ions. Replacing the urea with a thiourea functional group also lowered the potency; inhibitor **15** had an IC_{50} of 22 μM. Hence, it was decided to focus on metal binders containing oxygen-based functional groups.

Before designing another set of inhibitors, commercially available analogues of cyclic hydroxamic acids were tested against SNM1A in an attempt to gain more data on a structure-activity relationship (SAR).

2.3. Hydroxypyrimidinone and FEN1 inhibitors against SNM1A

As mentioned in **Section 1.5.1,** FEN1 and ERCC1-XPF nucleases are inhibited by *N*-hydroxyimides and their structural analogue, hydroxypyrimidinones.[17] Similarly, both *N*-hydroxyimides and hydroxypyrimidinones inhibit HIV integrase.[11] Due to a high degree of structural and metal-binding similarity between these two pharmacophores, it was considered possible that hydroxypyrimidinones might inhibit SNM1A. Therefore, commercially available hydroxypyrimidinones (**HP-1**, **HP-2**, **HP-3**, and **HP-4**) were tested against SNM1A. Additionally, N-hydroxyimide based FEN1 inhibitors, including cellularly active FEN1-in-1, were tested against SNM1A to determine whether these inhibitors also exhibit the off-target inhibition (**Figure 2.8**).[18]

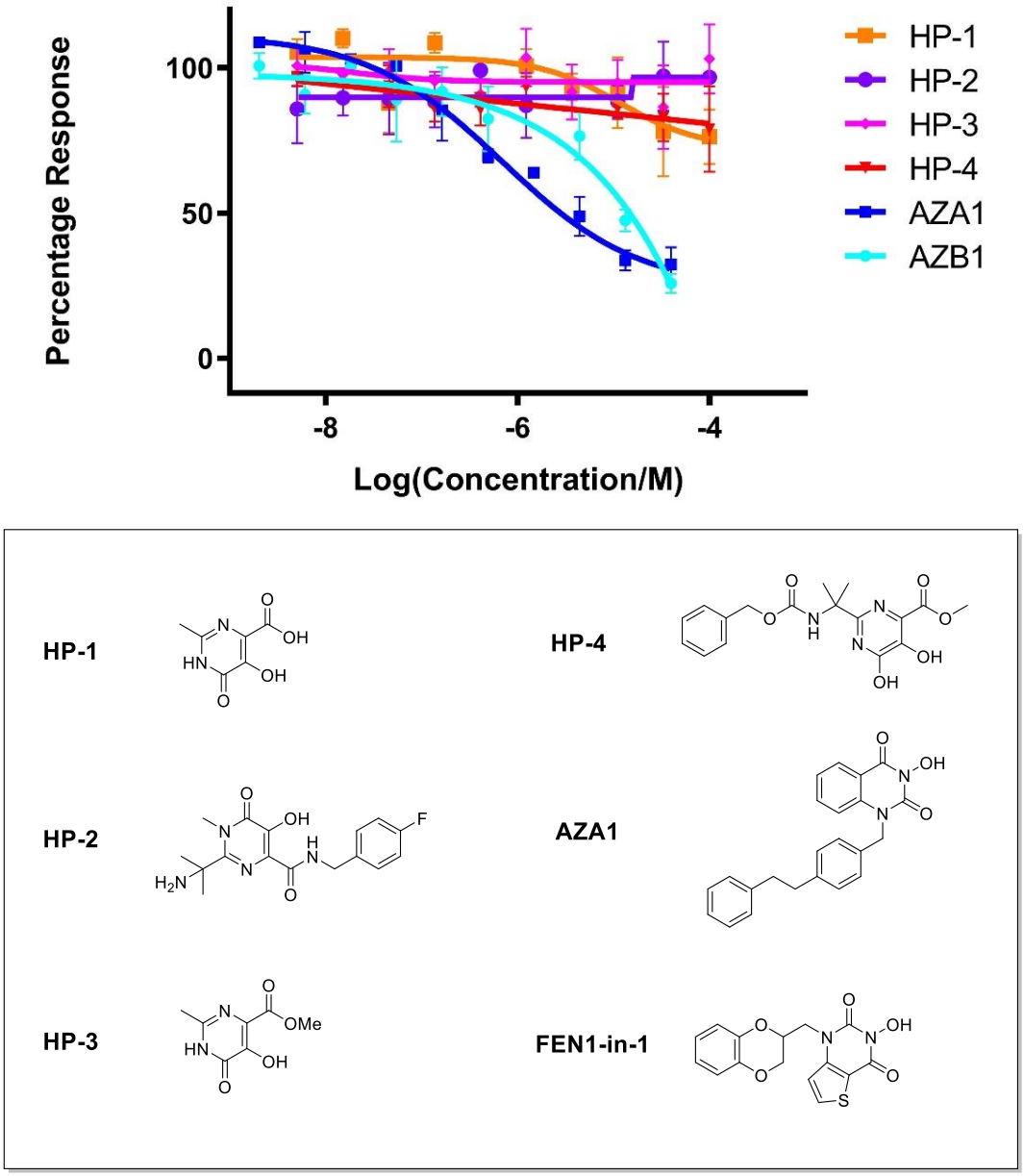

Figure 2.8: Top: *Dose-response curve plotted using the data from real-time fluorescence assay. Concentrations used [SNM1A] = 0.5 nM and [DNA] = 25 nM.* ***Bottom:*** *Structures of tested compounds.*

Quite unexpectedly, none of the commercial hydroxypyrimidinones (**HP-1**, **HP-2**, **HP-3**, and **HP-4**) inhibitors showed inhibition against SNM1A. While both FEN1 inhibitors inhibited SNM1A—with **AZA1** (also known as AZ1353160) being the more potent one—the inhibition was too low to calculate IC_{50} accurately. As **FEN1-in-1** has an IC_{50} of 11 nM

against FEN1, it is doubtful that it would have off-target interaction with SNM1A. **FEN1-in-1** was successfully soaked into crystals of SNM1A and yielded a crystal structure.

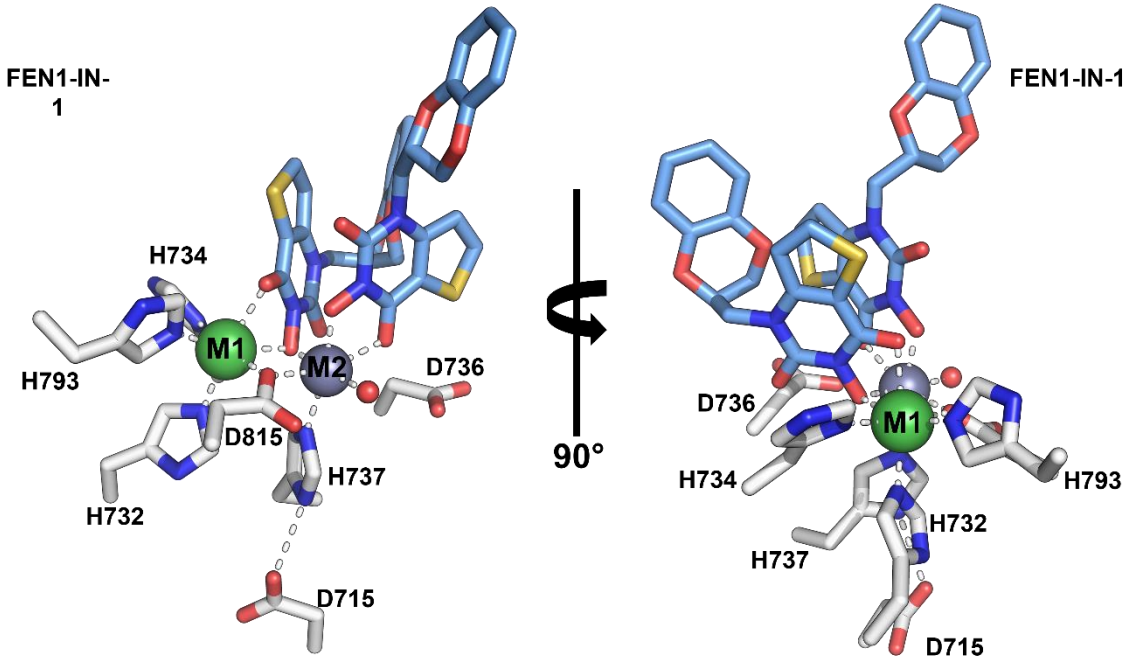

Figure 2.9: *Structure of two* ***FEN1-in-1*** *inhibitors bound to the active site of SNM1A.* ***M1:*** *Nickel.* ***M2:*** *Zinc*

The crystal structure of **FEN1-in-1** and SNM1A complex (**Figure 2.9**) has a very similar binding mode to the one observed in the structure of hit **3** bound to SNM1A (**Figure 2.1A**), with oxygen atoms from *N*-hydroxyl and carbonyl functional groups involved in metal chelating. Again, it can be observed that the *N*-hydroxyl group can displace the catalytic water bridged between metal ions. Similarly, in the two structures of SNM1A with **FEN1-in-1** and **3**, two inhibitor molecules were observed bound at the active site. In the structure of **FEN1-in-1** bound to SNM1A, the two molecules are apparently less well-stacked to each other than in the structure of hit **3** bound to SNM1A (**Figure 2.1**). The apparently reduced stacking between two **FEN1-in-1 molecules** might be caused by a steric clash from the benzodioxan side chain. If the inhibition of SNM1A by either **FEN1-in-1** or **3** depends on the binding of two molecules of the inhibitor, the additional steric clash from the side chain

could explain why **FEN1-in-1** has a lower potency than **3**. By contrast, in the structure of **FEN1-in-1** bound to the actives site of the FEN1, only one molecule of the inhibitor is present.[19]

Undertaken attempts to improve the *N*-hydroxyimide hits **3** and **5** proved relatively unsuccessful, whilst the intriguing presence of two molecules bound to the active site made the structure-based design of inhibitors difficult. Consequently, the further development of cyclic *N*-hydroxyimide inhibitors was halted. Although no lead was directly developed based on hit **3**, the information obtained from these compounds became useful in the later stages of the project described in **Chapters 3** and **4**. Validation of hydroxamate as a pharmacophore against SNM1A was helpful in designing a library of compounds based on hit **25** (**Chapter 3**). Owing to its very consistent inhibition, **3** was subsequently used as a positive control in assays against SNM1A.

2.4. Cyclic N-hydroxyimide hit 3 against SNM1B and SNM1C

When enzymes SNM1B and SNM1C became available for testing, hit **3** was tested against both these nucleases (**Figure 2.10**). As SNM1B exhibits similar exonuclease activity to SNM1A, the same substrates and conditions were used to test inhibitors against both enzymes. Similar conditions were used for testing with SNM1C. However, due to the difference in the catalytic activity, SNM1C is an endonuclease, a slightly different substrate was used for assays with it. For the real-time fluorescence assay for SNM1C, a 20-nucleotide ssDNA substrate labelled with FITC and BHQ was used, similar to the substrate for assays with SNM1A and SNM1B. Whereas, for SNM1C, fluorophore and quencher were 20 nucleotides apart, with a FITC at the 5′ end and a BHQ at the 3′ end. Typically for the radioactive gel-based assay against SNM1A, a 21 nucleotide long oligonucleotide is used,

in this case, a 51-mer radiolabeled substrate was used instead. This 51-mer oligonucleotide substrate was the standard substrate used for gel-based assays against SNM1C; at the same time, this substrate was also utilised for SNM1A and SNM1B to make the gels more consistent.[20]

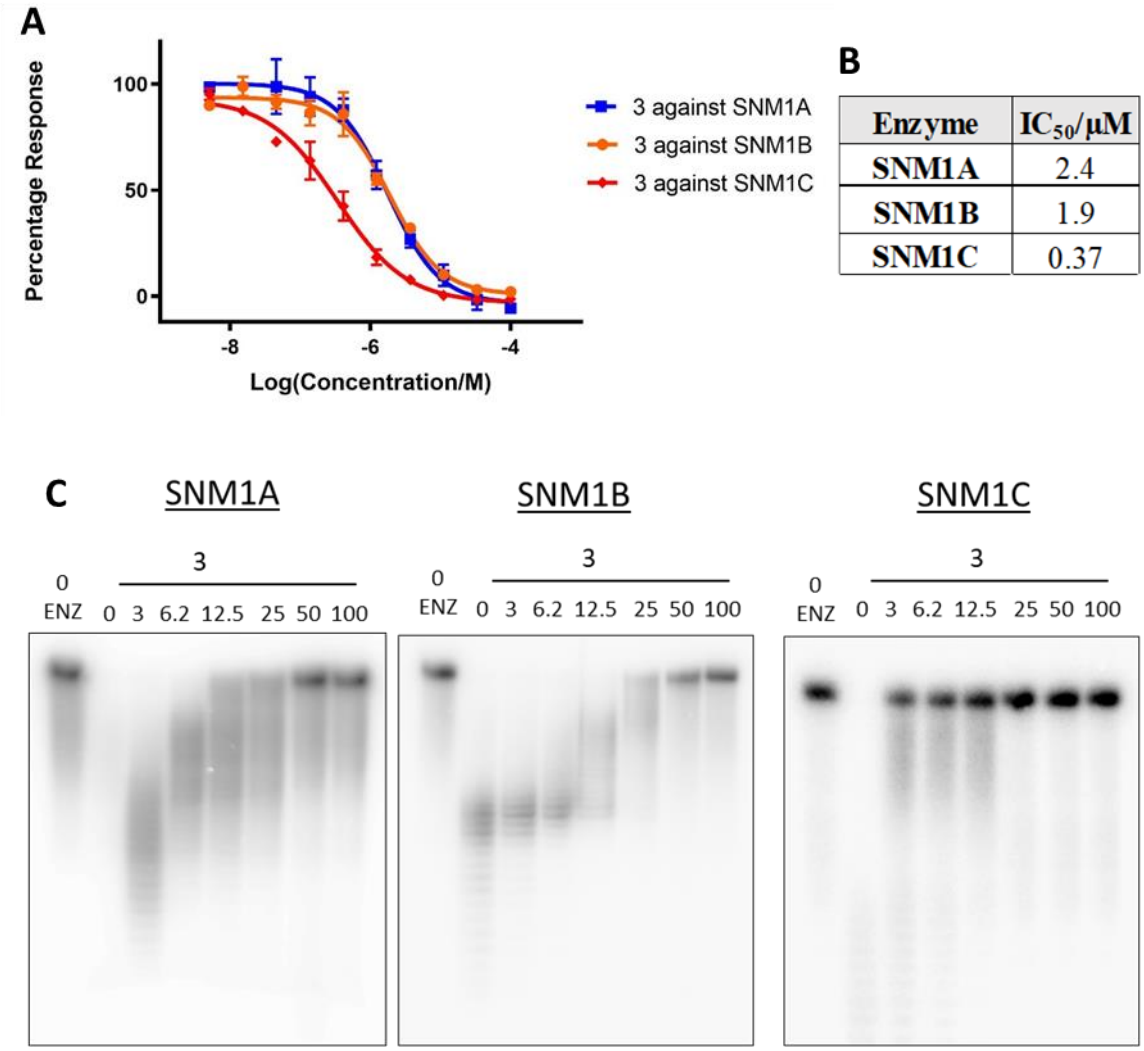

Figure 2. 10: A: *Dose-response curve plotted using the data from real-time fluorescence assay. Concentrations used [SNM1A] = 0.5 nM, [SNM1B] = 0.25 nM, [SNM1C]= 50 nm and [DNA] = 25 nM.* ***B:*** *Table of* IC_{50} *calculated for inhibitor* ***3*** *against SNM1A/B/C.* ***C:*** *Gel images from radioactive gel-based assays against SNM1A/B/C. Concentrations used [SNM1A] = 0.5 nM, [SNM1B] = 2 nM [SNM1C] = 2nM and [DNA (51-mer)] = 10 nM. The indicated concentrations are in µM.*

In both fluorescence-based and gel-based assays, hit **3** inhibits all three enzymes: SNM1A, B, and C, and shows the best potency against SNM1C. Based on the fluorescence assay, inhibition of SNM1A and SNM1B by **3** is nearly identical, but in the gel-based assay, it appears that **3** is slightly more potent against SNM1A. Slight variations observed while comparing results from fluorescence-based and gel-based assays should not be surprising, as there is a difference in the final readout from both assays. Additionally, the difference between enzyme concentrations in the assays might affect the observed inhibition, *e.g.* a higher concentration of SNM1B than SNM1A is used in the gel-based assay. In contrast, a higher concentration of SNM1A than SNM1B is used in the fluorescence-based assay. Overall, these results further validate cyclic *N*-hydroxyimides as inhibitors of a broad range of nucleases.

2.5. Inhibition of SARS-CoV-2 nsp14-nsp10 complex

Although the primary focus of this project was the development of hMBL nuclease inhibitors, since the start of the COVID-19 pandemic in 2019, there arose an urgent need to develop therapeutics to treat SARS-CoV-2. The nsp14-nsp10 complex has been identified as an attractive target owing to its role in maintaining genome stability.[21] The nsp14-nsp10 complex comprises two non-structural proteins, where nsp14 (also known as ExoN) exhibits 3′ to 5′ exoribonuclease activity.[22] Nsp10, while not having its own nuclease activity, once complexed with nsp14, substantially enhances nsp14 nuclease activity. In an attempt to find a nsp14-nsp10 complex inhibitor, N-hydroxyimides and hydroxypyrimidinones were tested against it. Unfortunately, it was only possible to test inhibitors against nsp14-nsp10 complex using a radioactive gel-based assay. The digestion of oligonucleotides labelled with a FITC and BHQ, commonly used for fluorescence-based assays, by nsp14-nsp10 was found to be

highly inefficient due to a prolonged reaction time. Because the nsp14-nsp10 complex has ribonuclease activity, a 20-mer RNA substrate was used instead of a DNA substrate for the assays. As no other more precise assays were available, the IC_{50} was estimated from a gel-based assay by quantifying the gel digestion products and using it to determine the dose-response curves.

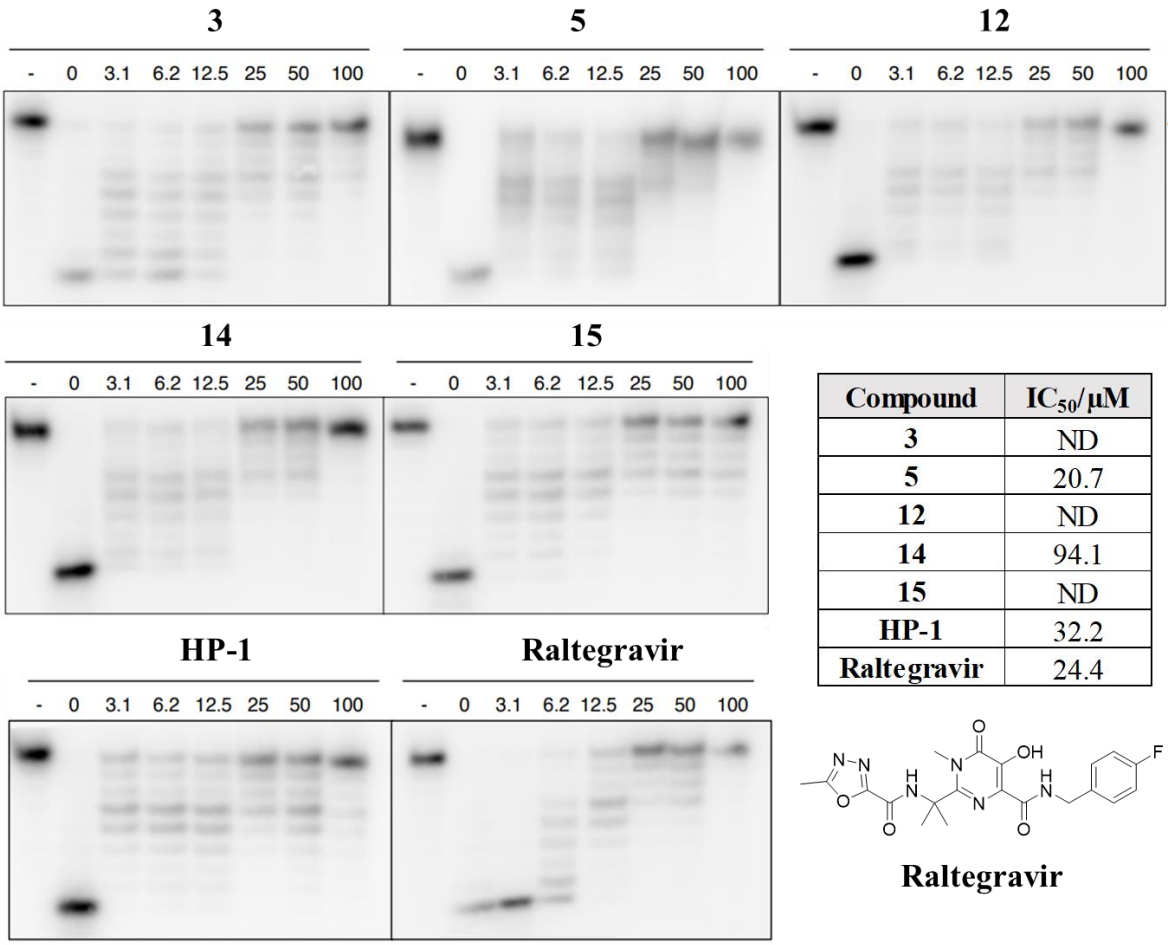

Compound	IC_{50}/μM
3	ND
5	20.7
12	ND
14	94.1
15	ND
HP-1	32.2
Raltegravir	24.4

Figure 2.11: *Gel images from radioactive gel-based assays against nsp14-nsp10 complex. The indicated concentrations are in μM. Concentrations used [nsp14-nsp10] = 100 nM and [RNA (20-mer)] = 10 nM. The table shows IC_{50} estimated from the gel-based assay. The structure of raltegravir is shown.*

All the compounds tested in **Figure 2.11** showed at least partial inhibition of the nsp14-nsp10 complex nuclease activity. An IC_{50} was calculated only for four (**5**, **14**, **HP1**, and **raltegravir**) out of seven tested inhibitors, with **5** and **raltegravir** being most potent

based on the IC_{50}. Inhibitor **5** had an IC_{50} = 20.7 μM, while **raltegravir** had an IC_{50} = 24.4 μM. Due to incomplete or inconsistent inhibition, the IC50 was not determined for three compounds: **3**, **12**, and **15**. Because the gel-based assay is not a quantitative assay, the calculated IC_{50} should only be treated as a rough estimate of potency. Still, for compounds **5**, **12**, **14**, **HP-1** and **raltegravir**, full inhibition was observed at 100 μM inhibitor concentration.

In comparison to SNM1A, which was only inhibited by *N*-hydroxyimides, nsp14-nsp10 is inhibited by both *N*-hydroxyimides and hydroxypyrimidinones. Raltegravir, having a hydroxypyrimidinone core, was tested against the nsp14-nsp10 complex because of high interest in drug repurposing to find a treatment against COVID-19.[23] Raltegravir is a clinically approved drug that inhibits HIV integrase and is used in the treatment of HIV.[24]

The described studies on Sars-CoV-2 nsp14-nsp10 have already been published.[25]

2.6. References

[1] B. Sengerová, C. K. Allerston, M. Abu, S. Y. Lee, J. Hartley, K. Kiakos, C. J. Schofield, J. A. Hartley, O. Gileadi and P. J. McHugh, *Journal of Biological Chemistry*, 2012, **287**, 26254-26267.

[2] C. K. Allerston, S. Y. Lee, J. A. Newman, C. J. Schofield, P. J. Mchugh and O. Gileadi, *Nucleic Acids Research*, 2015, **43**, 11047–11060

[3] J. Brem, S. S. van Berkel, D. Zollman, S. Y. Lee, O. Gileadi, P. J. McHugh, T. R. Walsh, M. A. McDonough and C. J. Schofield, *Antimicrob Agents Chemother*, 2016, **60**, 142-150.

[4] A. J. M. Farley, Y. Ermolovich, K. Calvopiña, P. Rabe, T. Panduwawala, J. Brem, F. Björkling and C. J. Schofield, *ACS Infectious Diseases*, 2021, **7**, 1809-1817.

[5] WO9819648A2.

[6] A. J. Birch, M. Salahud-Din and D. C. C. Smith, *J. Chem. Soc.* 1966, **5**, 523-7.

[7] D. Xie, Y. Wang, J. Xie, J. Lu, J. Cui, M. Zhang, L. Fu and Y. Wang, *Medicinal Chemistry Research*, 2014, **23**, 4977-4989.

[8] S. Y. Lee, J. Brem, I. Pettinati, T. D. W. Claridge, O. Gileadi, C. J. Schofield and P. J. McHugh, *Chemical Communications*, 2016, **52**, 6727-6730.
[9] C. M. Au - Swaim, T. J. Au - Brittain, D. R. Au - Marzolf and O. Au - Kokhan, *JoVE*, 2020, DOI: doi:10.3791/60690, e60690.
[10] A. Di Fiore, A. Maresca, C. T. Supuran and G. De Simone, *Chemical Communications*, 2012, **48**, 8838-8840.
[11] S. T. Cahill, H. Tarhonskaya, A. M. Rydzik, E. Flashman, M. A. McDonough, C. J. Schofield and J. Brem, *Journal of Inorganic Biochemistry*, 2016, **163**, 185-193.
[12] L. N. Tumey, D. Bom, B. Huck, E. Gleason, J. Wang, D. Silver, K. Brunden, S. Boozer, S. Rundlett, B. Sherf, S. Murphy, T. Dent, C. Leventhal, A. Bailey, J. Harrington and Y. L. Bennani, *Bioorganic & Medicinal Chemistry Letters*, 2005, **15**, 277-281.
[13] A. P. Kourounakis, D. Xanthopoulos and A. Tzara, *Medicinal Research Reviews*, 2020, **40**, 709-752.
[14] J. Tang, K. Maddali, M. Metifiot, Y. Y. Sham, R. Vince, Y. Pommier and Z. Wang, *Journal of Medicinal Chemistry*, 2011, **54**, 2282-2292.
[15] R. R. Deore, G. S. Chen, P.-T. Chang, T.-R. Chern, S.-Y. Lai, M.-H. Chuang, J.-H. Lin, F.-L. Kung, C.-S. Chen, C.-T. Chiou and J.-W. Chern, *ChemMedChem*, 2012, **7**, 850-860.
[16] P. S. Khokhlov, V. N. Osipov and A. V. Roshchin, *Russian Chemical Bulletin*, 2011, **60**, 153-156.
[17] T. M. Chapman, C. Wallace, K. J. Gillen, P. Bakrania, P. Khurana, P. J. Coombs, S. Fox, E. A. Bureau, J. Brownlees, D. W. Melton and B. Saxty, 2015, **25**, 4104-4108.
[18] T. A. Ward, P. J. Mchugh and S. T. Durant, *PLOS ONE*, 2017, **12**, e0179278.
[19] J. C. Exell, M. J. Thompson, L. D. Finger, S. J. Shaw, J. Debreczeni, T. A. Ward, C. McWhirter, C. L. B. Siöberg, D. M. Molina, W. M. Abbott, C. D. Jones, J. W. M. Nissink, S. T. Durant and J. A. Grasby, 2016, 815-821. ISSN 1552-4450.
[20] Y. Yosaatmadja, H.T Baddock, J. A. Newman, M. Bielinski, A. E. Gavard, S. M. M. Mukhopadhyay, A. A. Dannerfjord, C. J. Schofield, P. J. McHugh and O. Gileadi, *Nucleic Acids Research*, 2021, **49**, 9310-9326.
[21] E. C. Smith, H. Blanc, M. Vignuzzi and M. R. Denison, *PLoS Pathogens*, 2013, **9**, e1003565.
[22] M. Bouvet, I. Imbert, L. Subissi, L. Gluais, B. Canard and E. Decroly, *Proceedings of the National Academy of Sciences*, 2012, **109**, 9372-9377.
[23] Y. L. Ng, C. K. Salim and J. J. H. Chu, *Pharmacology & Therapeutics*, 2021, **228**, 107930.
[24] Z. Temesgen, *Therapeutics and Clinical Risk Management*, 2008, **4**, 493-500.
[25] H. T. Baddock, S. Brolih, Y. Yosaatmadja, M. Ratnaweera, M. Bielinski, L. P. Swift, A. Cruz-Migoni, H. Fan, J. R. Keown, A. P. Walker, G. M. Morris, J. M. Grimes, E. Fodor, C. J. Schofield, O. Gileadi and P. J. McHugh, *Nucleic Acids Research*, 2022.

Chapter 3. Development of quinazoline based inhibitors

3.1. Hit validation

In addition to hits **3** and **9**, quinazoline hit **25** was also identified by the ELF in the HTS. Similarly to hits **3** and **9**, hit **25** was soaked into SNM1A crystals, but no inhibitor bound crystal structure with **25** was achieved. While hit **25** did not yield a crystal structure, it has a hetero core that is much more amenable to modifications than **3** or **9** (**Figure 3.1**).

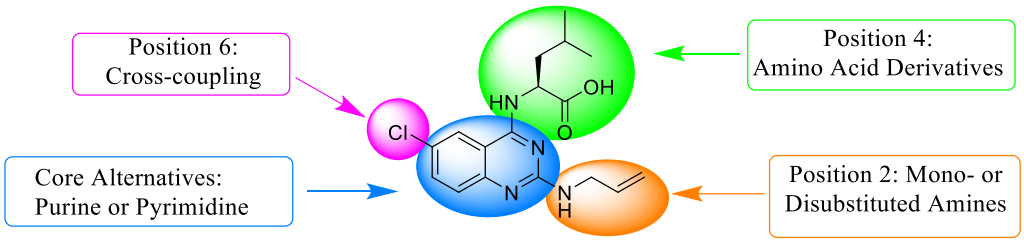

Figure 3.1: *Structure of **25** with potential modification assigned to the core and side chains.*

At position 4 of the quinazoline ring system, there is an *L*-leucine, which can be replaced with various natural and unnatural amino acids. At quinazoline position 2, there is an allylamine, which can be replaced by either mono- or disubstituted amines, as well as other substituted heteroatoms, such as alcohols or thiols. At quinazoline position 6, there is chlorine which could be used for a cross-coupling reaction. The quinazoline core could also be replaced with a variety of cores which would allow to keep amino acid and amine side chains at the same orientation, the examples being purine or pyrimidine. As **25** possessed this advantage, it was further tested using fluorescence-based and gel-based assays against SNM1A, purified with and without IMAC (**Figure 3.2**).

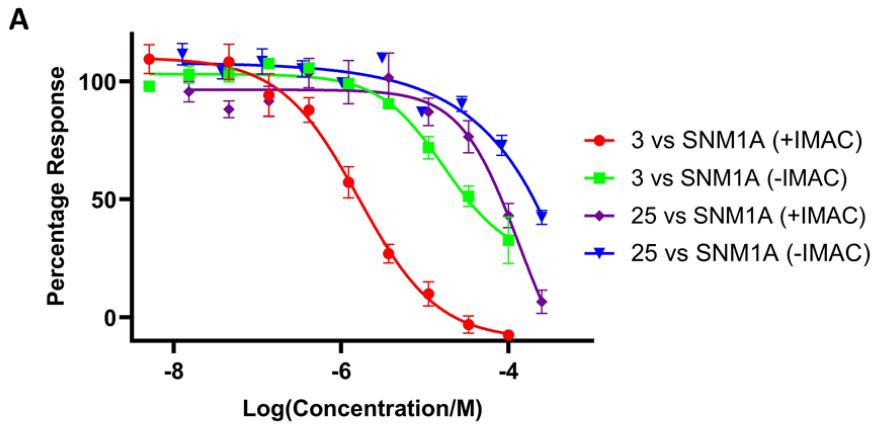

B

SNM1A (+/−IMAC)	Compound	IC_{50}/μM
+	**3**	2.4
−	**3**	ND
+	**25**	129
−	**25**	ND

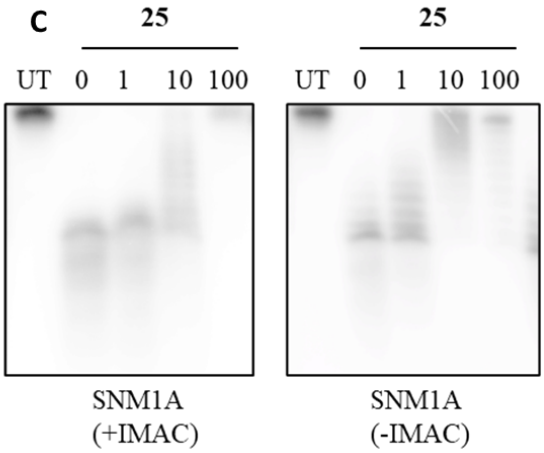

Figure 3.2: A: *Dose-response curve plotted using the data from the real-time fluorescence assay for* ***25*** *with* ***3*** *as control. Concentrations used [SNM1A (IMAC +)] = 0.5 nM, [SNM1A (IMAC −)] = 1.25 nM and [DNA] = 25 nM.* ***B****: Table of calculated* IC_{50}*. ND- Not determined.* ***C****: Gel image from the radioactive gel-based assay with* ***25*** *tested against SNM1A (IMAC +/−). Concentrations used [SNM1A (IMAC +)] = 0.8 nM, [SNM1A (IMAC −)] = 0.8 nM, and [DNA] = 100 nM. The indicated concentrations of the inhibitor are in μM. UT-untreated.*

It can be observed that hit **25** inhibits both constructs of SNM1A in fluorescence-based and gel-based assays. Similarly to **3**, hit **25** is more potent against IMAC purified SNM1A than the enzyme produced without IMAC purification. As **25** is less inhibitory and more soluble than **3**, it was tested up to a higher concentration in the fluorescence-based assay. While the IC_{50} for **3** against SNM1A (−IMAC) was not determined, it probably is more potent than **25** is against both SNM1A (+/−IMAC) enzymes based on the dose-response curves. Although **25** was less inhibitory than **3**, it was still decided that it is worth further optimising hit **25**

since there exist many opportunities for subsequent modifications and creating a library of quinazoline analogues for SAR studies.

3.2. Initial optimisation of hit 25

Hit **25** and its analogues can be synthesised within three steps from a commercially available starting material, 2,4,6-trichloroquinazoline. While 2,4,6-trichloroquinazoline is commercially available(£ 94 for 1 g), it was more cost-effective to synthesise it in two steps from 2-amino-5-chlorobenzoic acid (£ 43 for 100 g) (**Figure 3.3**).[1]

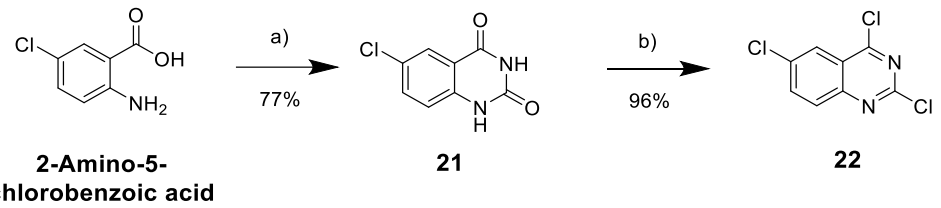

Figure 3.3: a) *Urea, 170 °C, 3 h;* ***b)*** *$POCl_3$, diethylaniline, reflux, 4 h.*

Synthesis of 2,4,6-trichloroquinazoline (**22**) proceeded in a good overall yield of 74% over 2 steps from 2-amino-5-chlorobenzoic acid, at a scale of 10 grams. While step **a)** might seem to be a solid-state reaction, at a temperature of 170 °C urea is molten and acts as both solvent and reactant. Compound **21** was purified using filtration and was produced at a good yield of 77%. Step **b)** was performed using standard $POCl_3$ chlorination. Compound **22** was purified using extraction and filtration through a silica plug. Step **b)** proceeded in an excellent yield of 96%. Subsequently, **22** was used to synthesise **25** and its analogues.

When designing analogues of **25**, it was hypothesised that carboxylic acid chelates the metal ions in the active site and may therefore be important for inhibition. To test this hypothesis, analogues of **25** with the carboxylic acid replaced by an amide (**34**), ester (**24**), or alcohol (**36**) were synthesised. Additionally, analogues with inverted stereochemistry and

methylated allylamine side chain were synthesised. The synthesis of mentioned analogues was based on previously published synthetic schemes for similar compounds (**Figure 3.4**).[2]

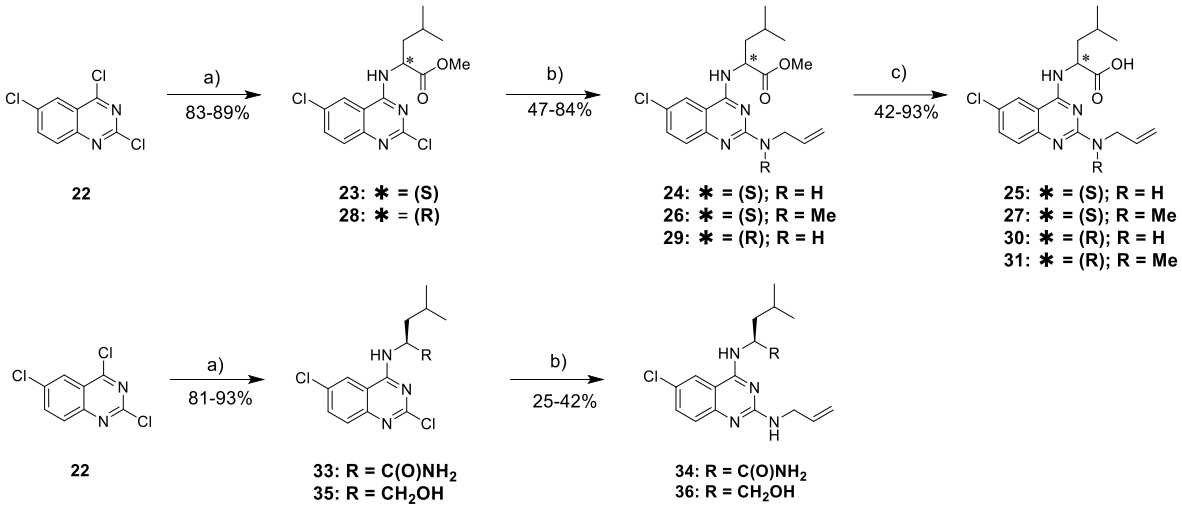

Figure 3.4: *Synthetic route for analogues of **25**. Reaction conditions: **a)** Amino acid derivative, DIPEA, DMF, RT, 16 h; **b)** Allylamine or N-allylmethylamine, MeOH, 120 °C, 20 min; **c)** LiOH, MeOH, THF, H_2O, 100 °C, 10 min. In the synthesis of **31**, reactions **b)** and **c)** were done without purification after step **b)** and resulted in an overall yield of 89% after two steps.*

The synthesis of **25** and its analogues was relatively straightforward. Step **a)** of the synthesis was aromatic nucleophilic substitution reaction at position 4, resulting in very good yields of >80%. Products of step **a)** did not require purification using column chromatography; liquid-liquid extraction was sufficient to purify the products of step **a)** (**23**, **28**, **33**, and **35**). It was found that precipitating the product by water dilution of the reaction mixture, and collecting the product using filtration, offer a more efficient process.

Similarly to step **a)**, the reaction in step **b)** was a nucleophilic aromatic substitution; however, as position 2 is a lot less reactive, the reaction in step **b)** required a much higher temperature. While in step **a)** the reaction occurred at room temperature, step **b)** required raising the temperature to over 100°C. Due to a higher temperature, step **b)** resulted in lower yield, which resulted from side reactions, particularly the formation of an amide bond

through a reaction of a nucleophilic amine with a methyl ester. It was found that the optimal condition for this reaction was the temperature of 120°C for 20 minutes in a microwave reactor. Performing the reaction in a sealed vial and a microwave reactor allowed for the use of a solvent with a lower boiling point (*e.g.* methanol), rapid heating and controlled reaction time.[3] It was observed that step **b)** was much more efficient when *N*-allylmethylamine was used instead of allylamine. Reactions with allylamine, a monosubstituted amine, resulted in an average yield of 49%, while reactions with *N*-allylmethylamine, a disubstituted amine, resulted in a yield greater than 80%. This difference in yield is probably caused by monosubstituted amine being more reactive toward methyl ester, as it is less bulky than a disubstituted amine. In most cases, purification using column chromatography was required after step **b)**. When synthesising **31**, the reaction in step **b)** resulted in a conversion close to 100% and the reaction mixture was evaporated and used in the next step (step **c)**) without any further purification.

Step **c)** was initially attempted using standard conditions for methyl ester hydrolysis, using 5 equivalents of LiOH in a mixture of methanol and water stirred at room temperature for two hours, which was the time required for the reaction to go to completion.[4] Unfortunately, while the starting material was completely consumed after two hours, most of the product decomposed. It was then attempted to perform the hydrolysis in a microwave under heating to shorten the reaction time.[5] It was predicted that heat might increase the rate of hydrolysis more than the decomposition rate and, over a short duration, would cause the hydrolysis reaction to outperform the decomposition. Hydrolysis conditions using 5 equivalents of LiOH in a mixture of water, tetrahydrofuran and methanol heated for 10 minutes at 100°C

in a microwave reactor with subsequent neutralisation with hydrochloric acid worked satisfactorily. Ester hydrolysis in a microwave reactor was performed at a yield above 40%.

Interestingly, the hydrolysis of methyl ester in the synthesis of **27** and **31** resulted in higher yields than in the synthesis of **25** and **30**. For comparison, hydrolysis of **26** to form **27** resulted in a 93% yield, while hydrolysis of **24** to form **25** resulted in a 59% yield. Therefore, it can be implicated that analogues with a disubstituted amine sidechain at position 2 were more stable in basic conditions than with monosubstituted. Still, each compound was purified using column chromatography after hydrolysis in step **c)**. Following synthesis, all compounds were tested against SNM1A using the fluorescence-based assay. Additionally, compounds **27** and **30,** which showed promising results in the fluorescence-based assay, were further tested using the gel-based assay. (**Figure 3.6**)

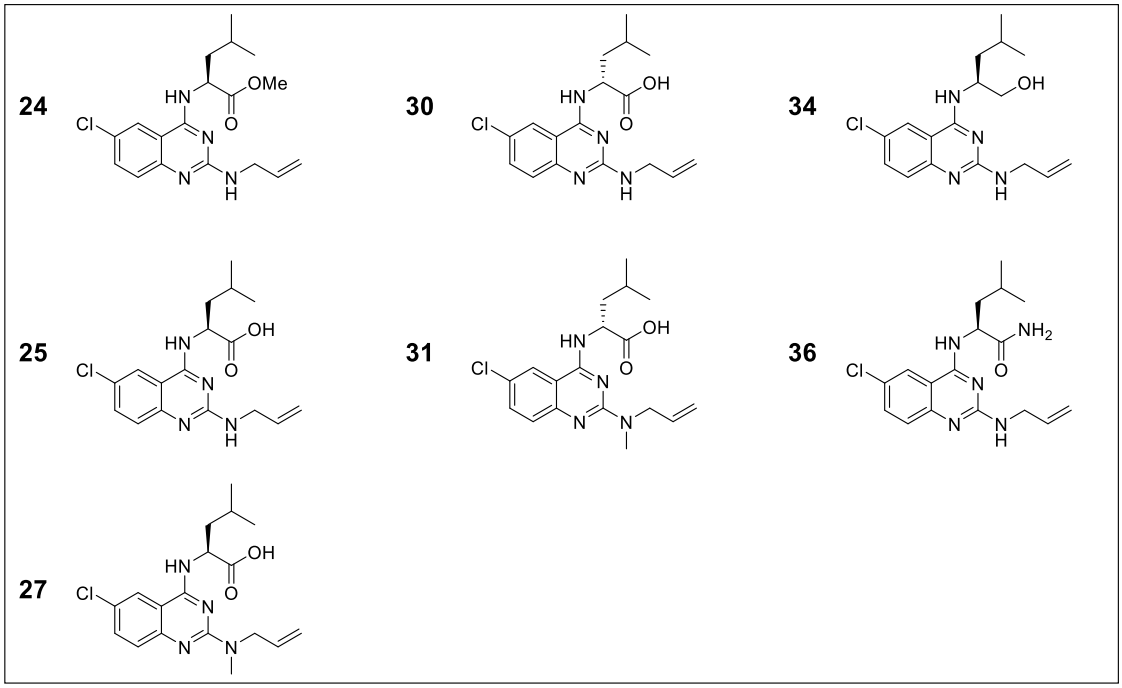

Figure 3.5: *Structure of hit **25** and its analogues.*

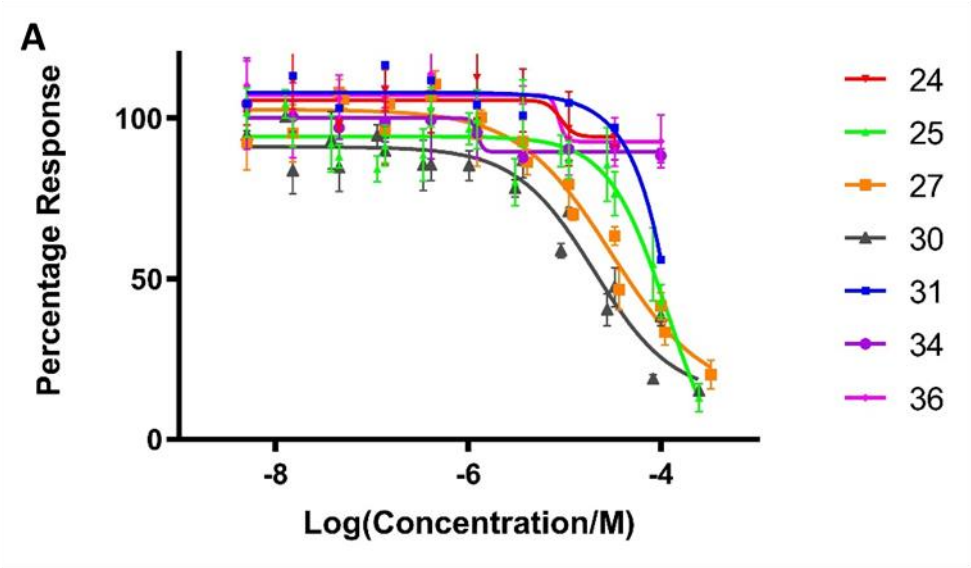

B

Compound	IC_{50}/μM
24	ND
25	129
27	31
30	20
31	ND
34	ND
36	ND

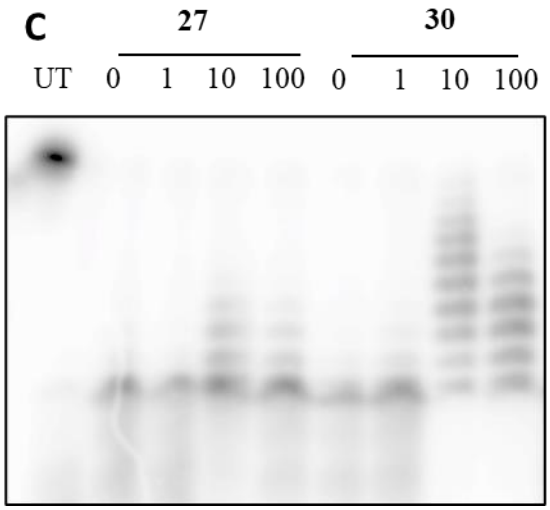

Figure 3.6 A: *Dose-response curve plotted using the data from real-time fluorescence assay. Concentrations used [SNM1A] = 0.5 nM and [DNA] = 25 nM.* ***B:*** *Table of IC_{50} calculated for each inhibitor. ND- Not determined.* ***C:*** *Gel image from radioactive gel-based assay for **27** and **30** against SNM1A. Concentrations used [SNM1A] = 0.8 nM, and [DNA] = 100 nM. The indicated concentrations are in μM. UT- Untreated.*

Results obtained from the fluorescence-based assay support the thesis that the carboxylic acid is important for inhibition since compounds **24**, **34** and **36**, in which carboxylic acid was replaced with other functional groups, showed no inhibition. Based on the fluorescence-based assay, both inversions of the stereocenter (**30**, IC_{50} = 20 μM) and methylation allylamine side chain (**27**, IC_{50} = 31 μM) resulted in a substantial increase in potency compared to the original hit **25** (IC_{50} = 129 μM). Surprisingly when both modifications were

combined (**31**, IC_{50} not determined), there was a decrease in potency. The gel-based assay shows that SNM1A is partially inhibited by **30** at concentrations of 10 and 100 μM, whilst **27** at the same concentration, inhibits SNM1A very weakly. The fluorescence-based assay delivered promising results with minor modifications resulting in a more than four-fold increase in potency (compounds **30** and **27**). Because of that, the decision was made to develop this series of inhibitors further. Next, the decision was to focus on alterations of the amino acid side chain, primarily replacing leucine with other amino acids.

3.3. Introduction of hydroxamate functional group

3.3.1. Identification of acyclic hydroxamate inhibitor through screening

Alongside the development of novel nuclease inhibitors, both in-house and commercially available compounds were tested using the fluorescence-based assay against SNM1A (**Figure 3.8**). Tested in-house compounds included a series of amino acid-derived hydroxamates (**HA1−5**, **Figure 3.7**), which were previously shown to be weakly inhibitory against bacterial MBLs.[6]

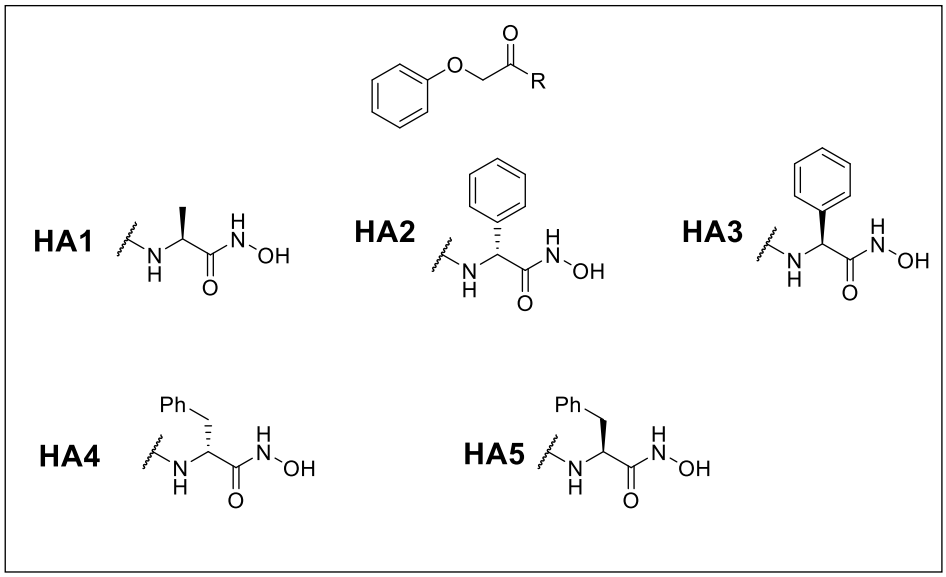

Figure 3.7: *Structure of amino acid-derived hydroxamic acids.*

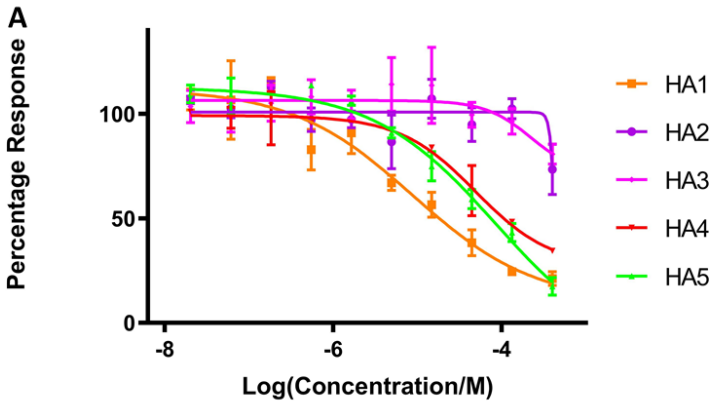

B

Compound	IC_{50}/μM
HA1	12
HA2	ND
HA3	ND
HA4	136
HA5	85

Figure 3.8: *Dose-response curve plotted using the data from real-time fluorescence assay. Concentrations used [SNM1A] = 0.5 nM and [DNA] = 25 nM.* ***B:*** *Table of IC_{50} calculated for inhibitors. ND- Not determined.*

Out of the **HA** series, compound **HA1** exhibited the highest potency, having an IC_{50} = 12 μM. Compounds with bulkier side chains, particularly **HA2** and **HA3**, showed a substantially lower inhibition than **HA1**. This result has further validated hydroxamates as effective pharmacophores against SNM1A. While in **Chapter 2**, cyclic hydroxamates were shown to inhibit SNM1A, in **Figure 3.8**, acyclic hydroxamates were shown to inhibit SNM1A. Promising results from testing **HA1**, together with results demonstrated in

Chapter 2, influenced alteration in the design of analogues of hit **25**, primarily by replacing carboxylic acid with hydroxamic acid.

3.3.2. Hydroxamate analogues of hit 25

A hydroxamic acid group was introduced to further improve the series of inhibitors based on hit **25**. Additionally, because of the observed lower potency in inhibitors with bulky side chains in **Figure 3.8**, it was decided to focus on amino acids with smaller side chains such as alanine. The amino acids chosen to synthesise hydroxamate-based analogues of **25** included glycine, alanine, β-alanine, serine, valine, and leucine. A β-alanine side chain was introduced to observe the effect of a longer linker between the metal chelating functional group and the quinazoline core. Serine was introduced to observe the impact of a polar side chain on the inhibition. Leucine was used because this has been the amino acid side chain in previously developed inhibitors, while valine was introduced since it is structurally similar to leucine. While both enantiomers of alanine were used, inhibitors containing other amino acids were synthesised as a racemic mixture. Alanine was the only one synthesised as two enantiomers as based on the data from **Section 3.3.1**, inhibitors with smaller side-chain (**HA1**) performed significantly better than those with more bulky side-chain (**HA2-5**). It was initially planned that if any of the inhibitors synthesised as racemic mixtures showed high enough potency, it would be synthesised as separate enantiomers too.

The hydroxamate-based analogues of **25** were synthesised (**Figure 3.9**) using a similar scheme to the one described in **Section 3.2.**

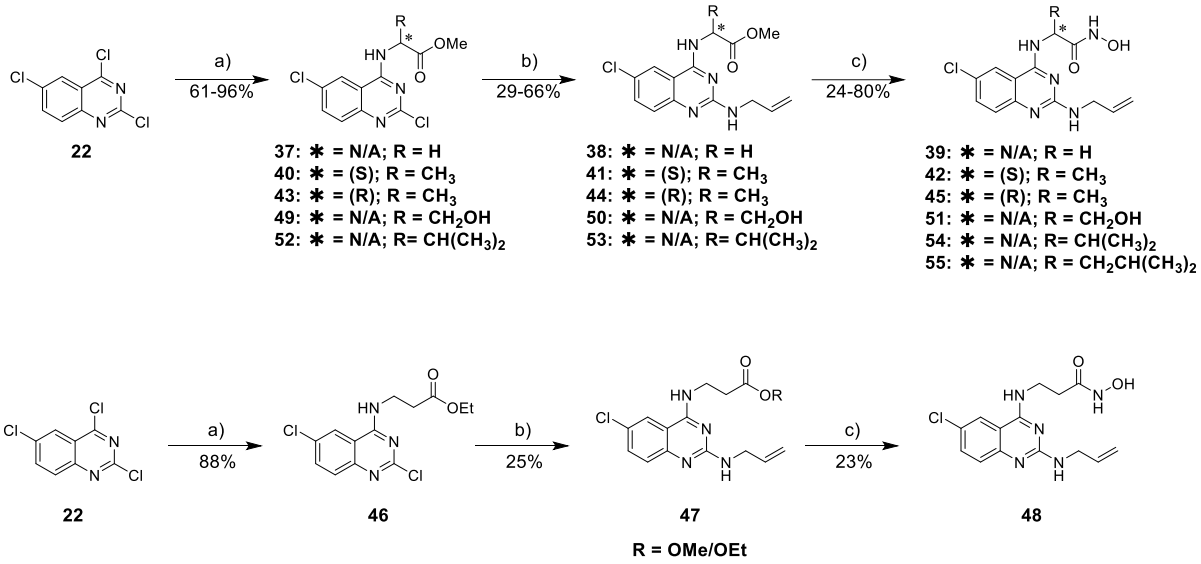

Figure 3.9: *Synthetic route for hydroxamate analogues of **25**. Reaction conditions: **a)** Amino acid derivative, DIPEA, DMF, RT, 16 h; **b)** Allylamine, MeOH, 120 °C, 20 min; **c)** $NH_2OH{\cdot}HCl$, NaOMe, MeOH, RT, 2-24 h.*

The first two steps, **a)** and **b)**, were performed in the same conditions as used to synthesise **25** and its analogues, as described in **Section 3.2**. Similarly to results from **Section 3.2**, step **a)** proved very efficient, with the majority of reactions resulting in yields exceeding 80%, while step **b)** resulted in more variable and poorer yields, mainly below 50%. Compound **47,** a product of the reaction in step **b)**, was obtained as a methyl and ethyl ester mixture (**Figure 3.10**).

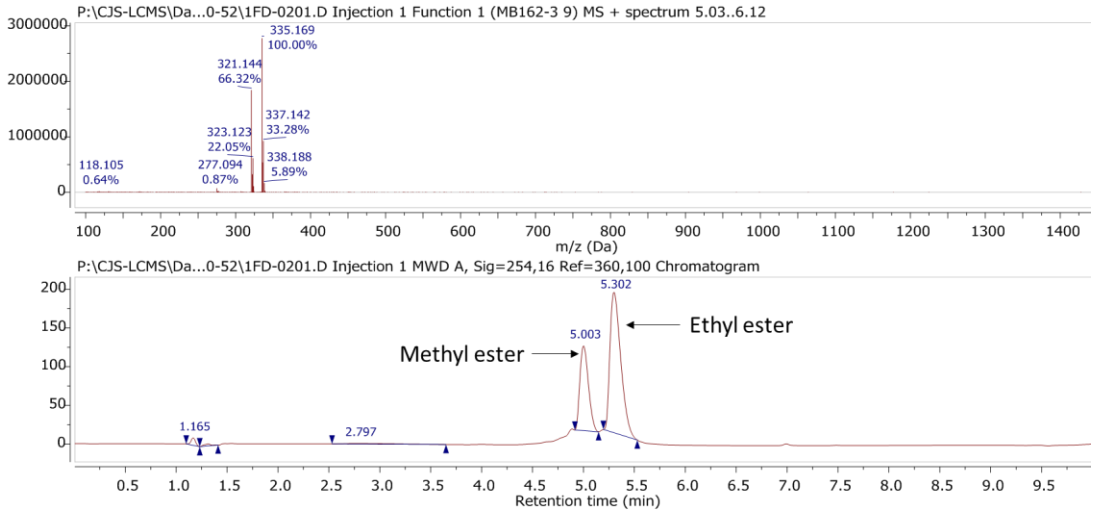

Figure 3.10*: UV trace and mass spectrum for compound **47**.*

The ethyl ester from the starting material **46** was partially converted into the methyl ester by methanol, the solvent of the reaction. The mixture of esters could not be separated using column chromatography and was used for the next step together. The presence of both esters was confirmed using LC-MS and NMR analysis. In **Figure 3.10**, the masses of both esters can be observed, and in the UV trace, two major peaks are shown and assigned.

In step **c)**, an aminolysis reaction with hydroxylamine was performed to convert ester into a hydroxamic acid. Initially, the aminolysis was attempted using commercially available hydroxylamine (50% solution in water) solution, but unfortunately, the presence of water resulted in hydrolysis as a side reaction. To avoid hydrolysis, a hydroxylamine solution in methanol was prepared by mixing hydroxylamine hydrochloride and sodium methoxide. Generally, the aminolysis was completed within 2 hours. However, for the synthesis of **54,** the reaction time had to be extended to 24 hours as the rate was slower, possibly due to the steric hindrance caused by the isopropyl side chain in the valine. The aminolysis reaction resulted in a varying range of yields without a rational pattern. The best yield in step **c)** was observed for both *L* and *D*-alanine analogues (**42** and **45**), with 72% and 80% yields, respectively, whilst analogues with both more and less bulky sidechains (**39**, **51**, **54**, and **55**) had substantially lower yields. After synthesis, specific rotation was measured for both enantiomers, **42** ($[\alpha]_D^{25}$ = +3.1 (c = 0.5 in MeOH)) and **45** ($[\alpha]_D^{25}$ = −2.1 (c = 0.5 in MeOH)). While the results prove that there is enantiomeric excess in a sample of each compound, both values do not have the same magnitude, and therefore it is not sure if each sample consists of a pure enantiomer. Due to basic conditions used in step **c)**, chiral scrambling is possible. Chiral HPLC could be done to further investigate enantiomeric excess in inhibitors **42** and

45. All analogues were tested using the fluorescence-based assay against SNM1A (**Figure 3.11**).

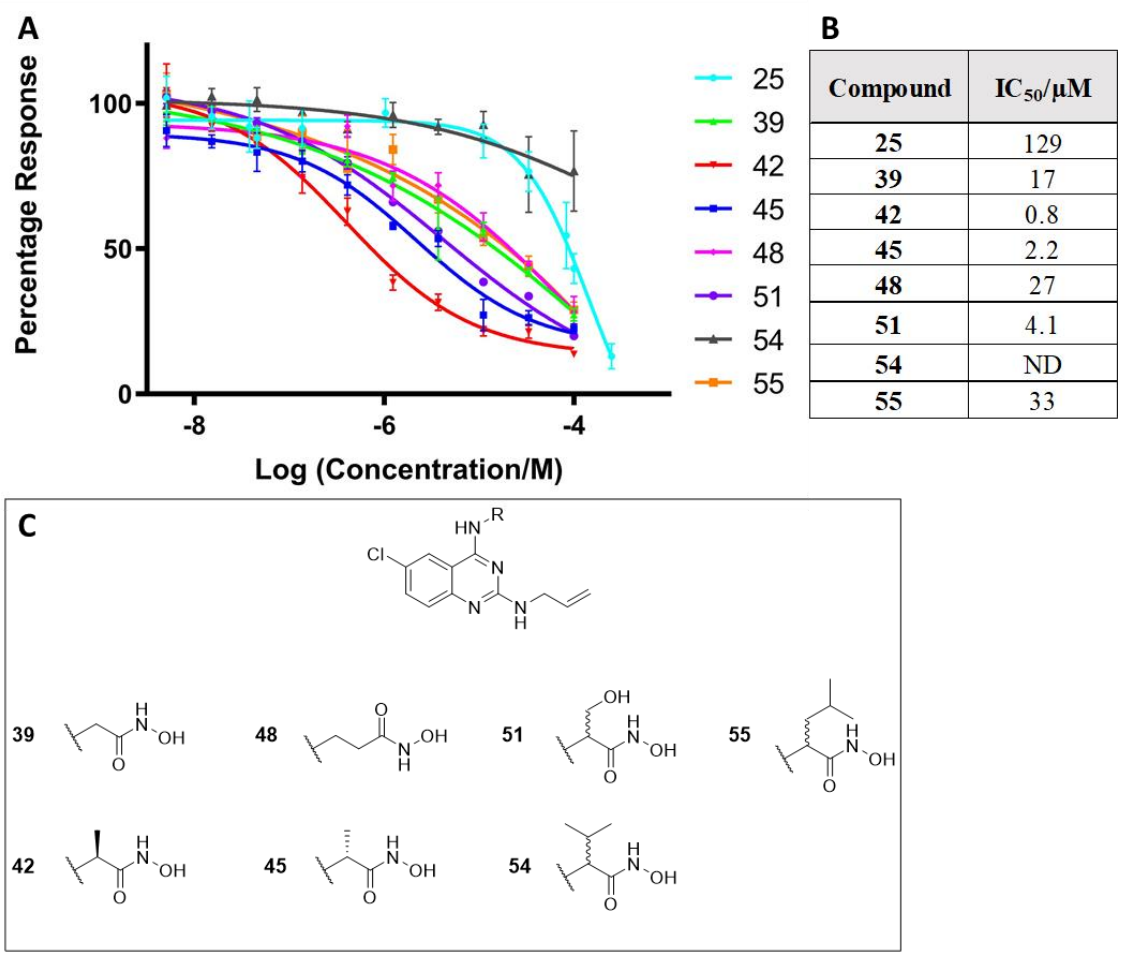

Compound	IC_{50}/μM
25	129
39	17
42	0.8
45	2.2
48	27
51	4.1
54	ND
55	33

Figure 3.11: *Dose-response curve plotted using the data from the real-time fluorescence assay. Concentrations used [SNM1A] = 0.5 nM and [DNA] = 25 nM.* ***B:*** *Table of IC_{50} calculated for inhibitors. ND-Not determined.* ***C:*** *Structure of hydroxamate-based analogues of* ***25****.*

Based on the results shown in **Figure 3.11**, all inhibitors except for **54** were more potent than the initial hit **25**. Particularly good potency was observed for compounds **42** (IC_{50} = 0.8 μM), **45** (IC_{50} = 2.2 μM), and **51** (IC_{50} = 4.1 μM), with inhibitor **42** being the first inhibitor to have IC_{50} in the submicromolar range. Based on the fluorescence-based assay result, it can be observed that analogues with less bulky amino acid side chains are overall more potent inhibitors. A leucine-based analogue (**55**, IC_{50} = 33 μM) showed substantially lower

inhibition than alanine-based analogues (**42** and **45**), while a valine-based analogue (**54**) can be considered non-inhibitory. Although less bulky sidechains are preferred, a glycine-based analogue (**39**, IC_{50} = 17 μM), which only has hydrogen atoms in its amino acid side chain, exhibited lower inhibition than inhibitors alanine-based analogues, **42** and **45**. An increase of linker length by the introduction of β-alanine (**48**, IC_{50} = 27 μM) also decreased inhibition, compared to **42** and **45**. Owing to the encouraging results of inhibitor **42**, it was decided to entirely focus on the acyclic hydroxamate functional group as the primary pharmacophore against SNM1A and keep *L*-alanine as an amino acid side chain in the future analogues. As it appeared that the amino acid side chain had been—at least partially—optimised, it was decided to next focus on optimising position 2, where the allylamine was present.

3.3.3. Testing hydroxamate-based HDAC inhibitors against SNM1A

Following the promising results with the hydroxamate-based analogues of **25**, commercially available hydroxamate-based histone deacetylase (HDAC) inhibitors (**Figure 3.13**), including clinically used drug Panobinosat, were tested against SNM1A by using fluorescence-based assay (**Figure 3.12**).[7,8] HDAC inhibitors were tested to determine whether these compounds might have off-target interactions with SNM1A.

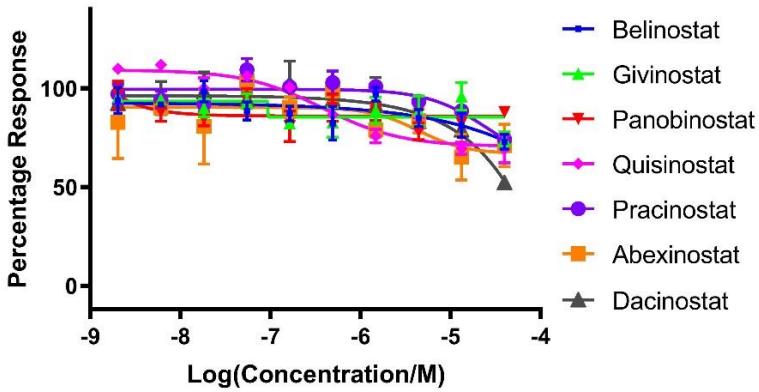

Figure 3.12: *Dose-response curve plotted using the data from real-time fluorescence assay. Concentrations used [SNM1A] = 0.5 nM and [DNA] = 25 nM.*

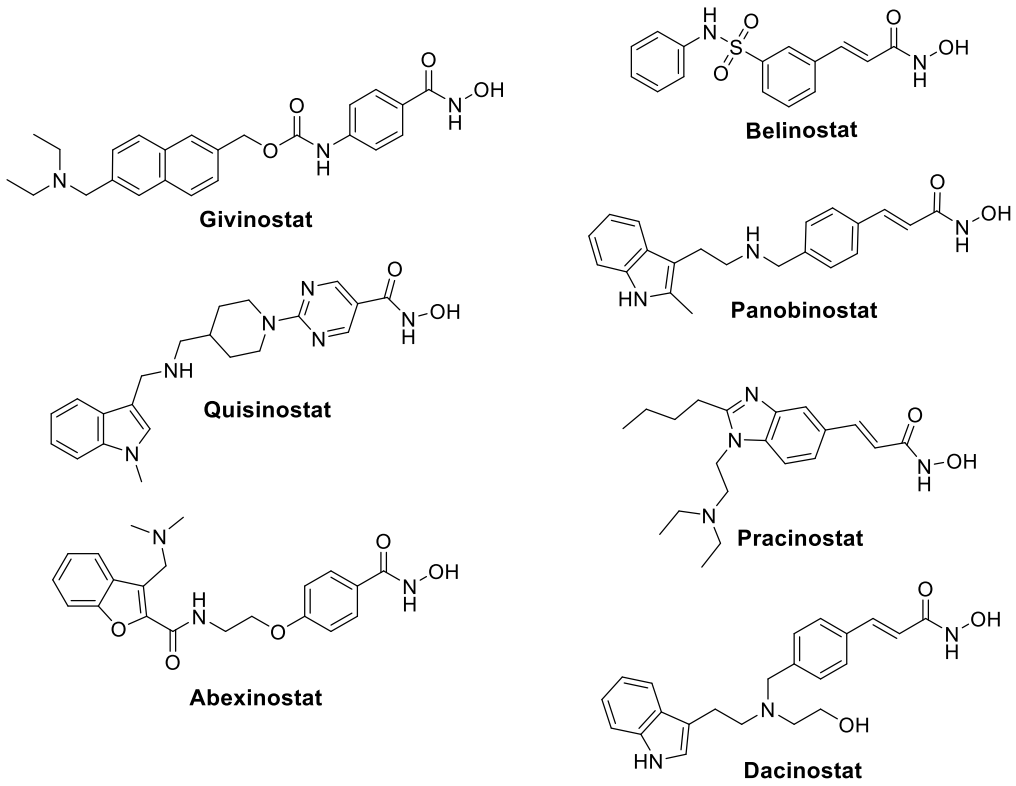

Figure 3.13: *Structures of hydroxamate-based HDAC inhibitors tested against SNM1A.*

Both hydroxymate-based analogues of **25** and the HDAC inhibitors (**Figure 3.12**) have the same metal-chelating functional group. All tested HDAC inhibitors inhibited SNM1A substantially less than most of the hydroxymate-based analogues of **25** from **Section 3.3.2**. The inhibition of SNM1A by HDAC inhibitors tested in **Figure 3.12** was too low to calculate IC_{50}s. The hydroxamic acid group in HDAC inhibitors is positioned on an aryl ring or alkene conjugated with an aryl ring, likely restricting bond rotations around the hydroxamate group. By contrast, the analogues of **25** have hydroxamic acids as part of the amino acid side chain, which is much more flexible. This difference in flexibility of side chains containing hydroxamic acid might explain the variation in potency between hydroxymate-based analogues of **25** and HDAC inhibitors.

3.4. Modifications at position 2 of the quinazoline ring

3.4.1. Introduction of the carbonyl group at position 2

After completing optimisation at position 4, modifications at position 2 were pursued. Alterations at position 2 included the introduction of a carbonyl group (**Figure 3.14**).

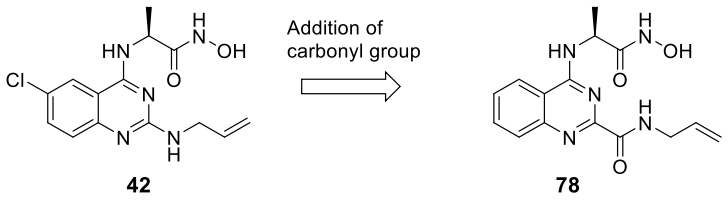

Figure 3.14: *Introduction of the carbonyl group at position 2 of inhibitor **42**.*

To introduce the carbonyl group, a new intermediate (**72**) with an acyl chloride at position 2 was synthesised (**Figure 3.15**). For the synthesis of **72**, a previously published synthetic route was used.[9] In the synthesis of **72** and preparation of new analogues of **25**, the chlorine at position 6 was removed because starting material, anthranilamide, was available in the group.

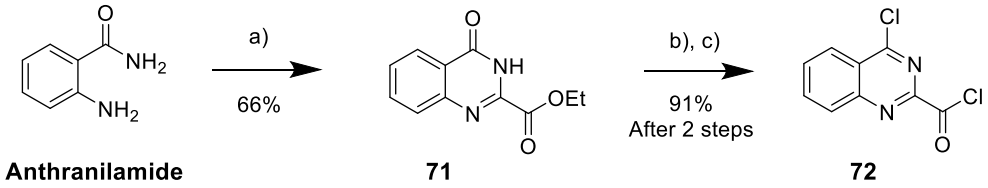

Figure 3.15: *Synthesis of intermediate **72**. Reaction conditions: **a)** Diethyl oxalate, reflux, 24 h; **b)** NaOH, EtOH, H_2O, reflux, 1 h; **c)** $SOCl_2$, DMF, $CHCl_3$, reflux, 3 h.*

The intermediate **72** was synthesised in 3 steps from anthranilamide, in an overall yield of 60%. In step **a)**, compound **71** was synthesized using a cyclocondensation reaction between anthranilamide and diethyl oxalate. Compound **71** was purified using recrystallisation in ethanol and was produced in 66% yield. Next, in step **b)**, ethyl ester from compound **71** was hydrolysed under basic conditions, using sodium hydroxide as the base. After hydrolysis,

the newly formed carboxylic acid was allowed to crystalise under cooling in acidified solution, and then it was filtered out. The carboxylic acid was then directly converted into compound **72** using thionyl chloride as a chlorinating agent and dimethylformamide as a catalyst. After the chlorination reaction, the thionyl chloride and solvent were evaporated under reduced pressure, and since compound **72** was very reactive, it was used directly in the next step without any further purification. The two step synthesis of **72** from **71** was very efficient, proceeding in a 91% yield.

While in the 2,4,6-trichloroquinazoline (**22**), position 4 was more reactive than position 2, the opposite is observed in the intermediate **72**. Due to a highly reactive acyl chloride at position 2, this position became more reactive than position 4. Therefore, the decision was made to synthesise an analogue with an allylamine group, with the amino acid side chain switched around (**Figure 3.16**). Analogues of **25** with the carbonyl modification were synthesised as both carboxylic acids and hydroxamic acids. The synthesis of analogues of **25** (**74**, **75**, **77**, and **78**) was based on a previously published synthetic route and synthetic routes used in this project.[9]

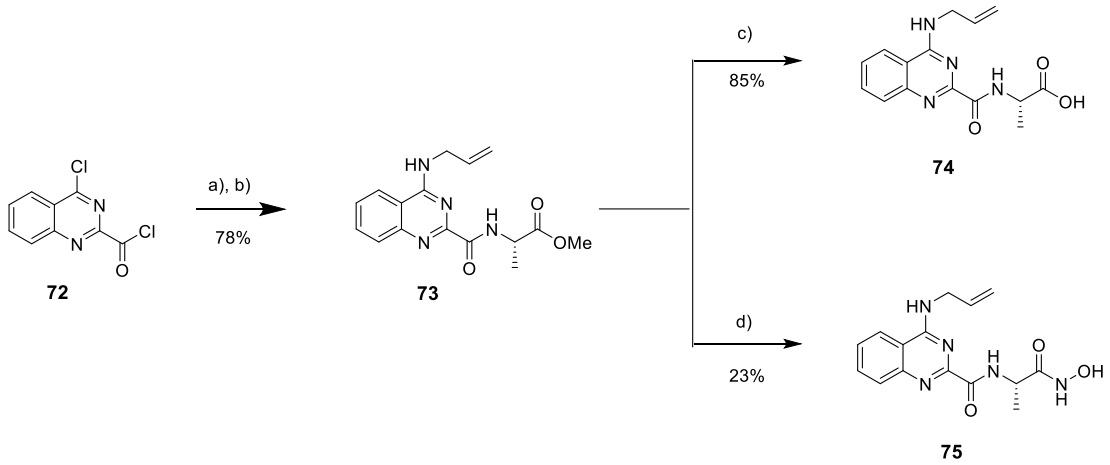

Figure 3.16: *Synthesis of **74** and **75**. Reaction conditions: **a)** L-alanine methyl ester hydrochloride, DIPEA, DCM, -40 °C, 1 h; **b)** Allylamine, RT, 12 h; **c)** LiOH, MeOH, THF, H_2O, 100 °C, 10 min; **d)** $NH_2OH{\cdot}HCl$, NaOMe, MeOH, RT, 2 h.*

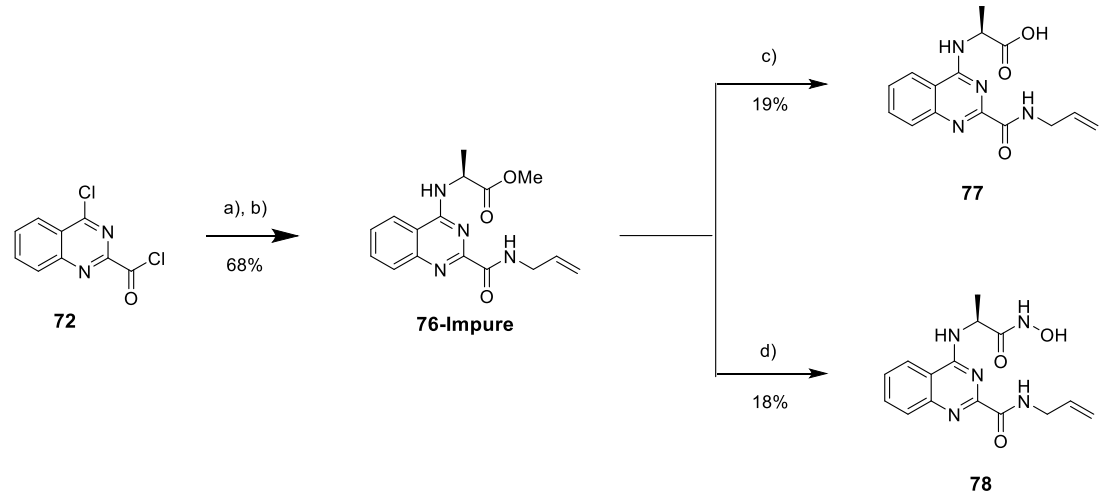

Figure 3.17: *Synthesis of **77** and **78**. Reaction conditions: **a)** Allylamine, DIPEA, DCM, -40 °C, 1 h; **b)** L-alanine methyl ester hydrochloride, RT, 12 h; c) LiOH, MeOH, THF, H_2O, 100 °C, 10 min; **d)** $NH_2OH{\cdot}HCl$, NaOMe, MeOH, RT, 2 h.*

The synthesis of analogues **25** started with a stepwise substitution at acyl chloride and position 4. For the synthesis of **73**, *L*-alanine methyl ester (1.3 equivalent) was added first, followed by the addition of excess allylamine (2 equivalent). **73** was synthesised at a good yield of 78% and was easily purified using column chromatography.

For the synthesis of **76**, allylamine (1.3 equivalent) was first added, followed by addition of excess *L*-alanine methyl ester (2 equivalent). In the synthesis of **76**, a substantial amount of

a side product caused by the double addition of allylamine was observed. By contrast, no double addition of any reactant was observed in the synthesis of **73**. The reason why double addition was only observed in the synthesis of **76** might be because allylamine is more reactive than *L*-alanine methyl ester and the fact that allylamine was added first. Attempts to separate the product and the side product using column chromatography proved unsuccessful, and the impure **76** was used in the next step. The UV trace from LCMS analysis of crude **76** is shown in **Figure 3.18**; based on it, approximately a 1:1 ratio of the product to the side product can be observed on the UV trace. Repeating the reaction and using allylamine as a limiting agent should reduce the extent of double addition at both positions 2 and 4.

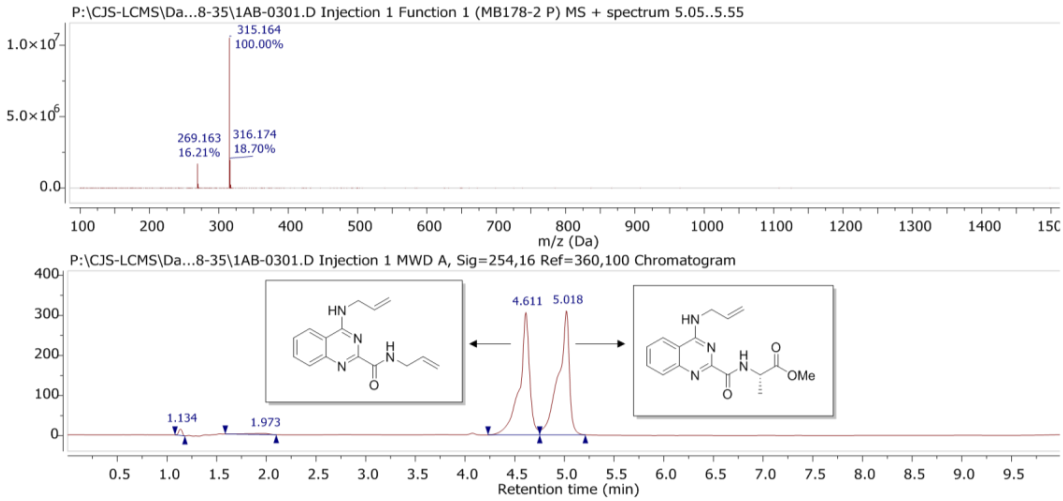

Figure 3.18: *UV trace and MS spectrum from LCMS using the sample from impure **76**. With structures of product and side product. Mass corresponding to each peak in UV trace was used to identify compounds corresponding to each peak.*

Intermediates **73** and **76** were then used to synthesise corresponding carboxylic acids (**74** and **77**) and hydroxamic acids (**75** and **78**) using hydrolysis and aminolysis reactions, respectively. Conditions used for hydrolysis (step **c)**) and aminolysis (step **d)**) were the same as those used to synthesise previous analogues of **25** in **Section 3.2** and **3.3.2**. Synthesis of

inhibitor **74** was the most efficient, resulting in very good yield and requiring only column chromatography for purification. However, the synthesis of inhibitors **75**, **77**, and **78** was more troublesome, with a substantial amount of side products being observed. Therefore, reversed-phase high-performance liquid chromatography (RP HPLC) was used to purify these derivatives (**75**, **77**, and **78**). Following the synthesis, all the derivatives of **25** containing a carbonyl modification at position 2 were tested against SNM1A using a fluorescence-based assay (**Figure 3.19**).

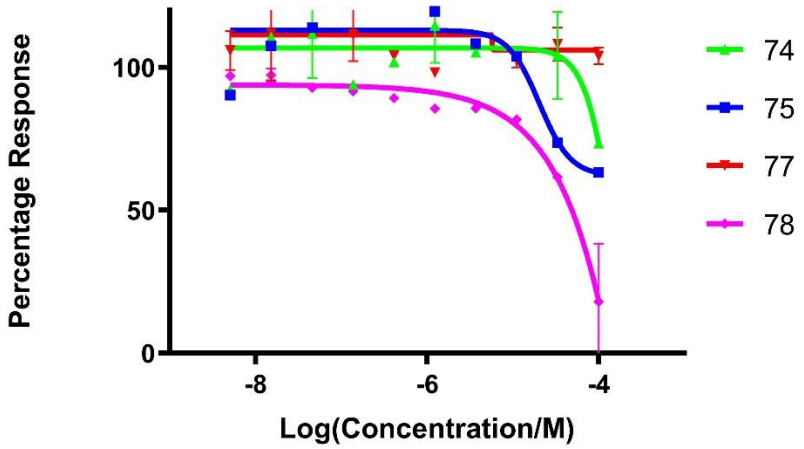

Figure 3.19: *Dose-response curve plotted using the data from the real-time fluorescence assay. Concentrations used [SNM1A] = 0.5 nM and [DNA] = 25 nM.*

All the inhibitors (**74**, **75**, **77**, and **78**) with the carbonyl functional group at position 2 showed substantially lower inhibition than **42**, which at this time was the best identified inhibitor of SNM1A. Calculation of IC_{50} was only possible for inhibitor **78**, which had an IC_{50} of 14 μM. Compound **77** showed no inhibition, while **74** and **75** showed partial inhibition. Compounds with a hydroxamic acid pharmacophore (**75** and **78**) showed better inhibition than the ones with a carboxylic acid functional group (**74** and **77**). Moving the amino acid side chain to position 2 (**74** and **75**) resulted in a decrease in potency compared to either **78** or **42**, which

have an amino acid side chain at position 4. Therefore, for the rest of the project, the amino acid side chain will be kept at position 4.

3.4.2. Replacement of allylamine at position 2 of the quinazoline ring

Further modifications at position 2 of the quinazoline ring focused primarily on replacing allylamine with other amines. Analogues of **42** with a variety of amines at position 2 were synthesised, including monosubstituted amines, disubstituted amine, cyclic amines, amines with aromatic sidechains, or amines with basic side chains (**Figure 3.20**). Conditions for synthesising these analogues were based on synthetic routes shown in **Section 3.3.2**.

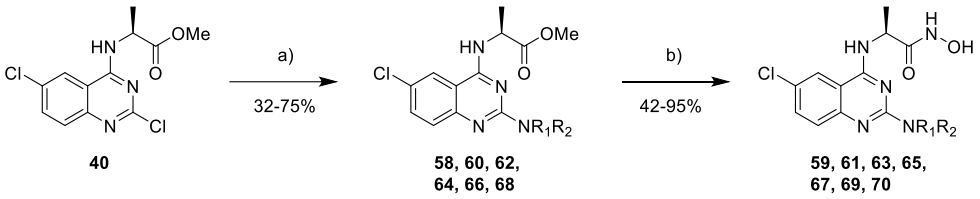

Compound	NR_1R_2	Compound	NR_1R_2
58, 59	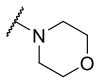	66, 67	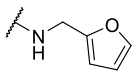
60, 61		68, 69	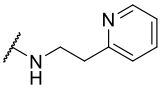
62, 63	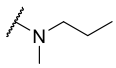	70	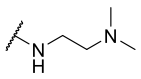
64, 65	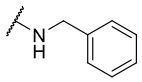		

Figure 3.20: *Synthesis of analogues of* ***42****. Reaction conditions:* ***a)*** *NHR_1R_2, MeOH, 100-120 °C, 20-40 min;* ***b)*** *$NH_2OH{\cdot}HCl$, NaOMe, MeOH, RT, 2 h.*

The synthesis of these analogues was based on that of other inhibitors in this chapter and used common starting material **40**. Similarly to the observations described in **Section 3.2**, nucleophilic substitution at position 2 was more efficient when using the disubstituted amine once compared to monosubstituted amines. In the synthesis of all analogues except **70**,

purification using column chromatography was performed. In the synthesis of **70,** no purification was performed after step **a)**, and the crude intermediate was used for the aminolysis reaction. After aminolysis, **70** was purified using RP HPLC because it was very polar due to the dimethylamine side chain. The overall yield of the aminolysis (step **b)**) was good, with most aminolysis reactions resulting in a yield above 80%.

The use of alcohol and thiol nucleophiles for a substitution reaction at position 2 was also tried. Sodium ethoxide and sodium ethanethiolate were used, and conditions similar to those used for amines were attempted; 100−120°C in a microwave reactor and ethanol was used as the solvent (**Figure 3.21**). Unfortunately, there was no product formation under these conditions and a substantial amount of decomposition for reaction with thiol.

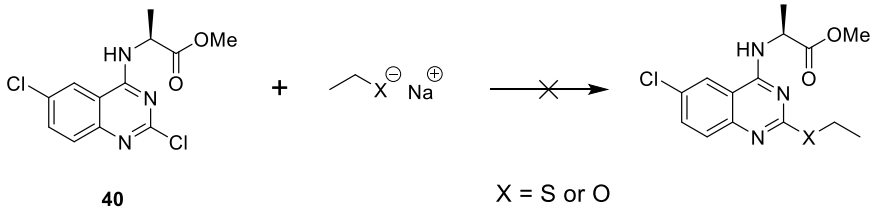

Figure 3.21: *Attempted synthesis of analogues of **42**. Reaction conditions: EtOH, 100-120 °C, 20 min.*

Next, it was attempted to use acidic conditions instead of basic for reaction with alcohol, based on reaction published in a patent.[10] For this reaction, ethanol and hydrochloric acid in dioxane were used (**Figure 3.22**). This nucleophilic substitution under acidic conditions was successful, and its product (**56**) was further used to synthesise hydroxamate-based inhibitor (**57**) under standard aminolysis conditions. Synthesis of **57** was very efficient, with high yields above 80% in both steps, as shown in **Figure 3.22**, with each being purified with column chromatography. No other alternative reactions were found in literature or attempted with thiol as a nucleophile.

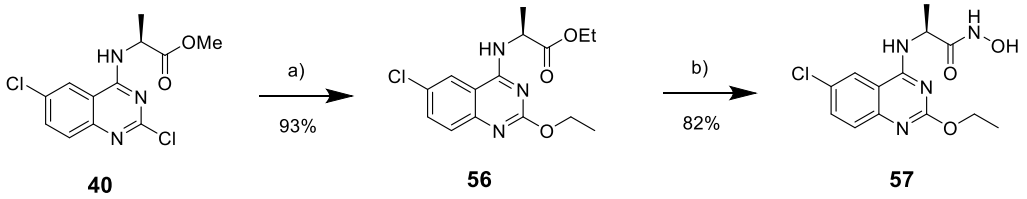

40 **56** **57**

Figure 3.22: *Synthesis of **57**. Reaction conditions: **a)** 4 M HCl in dioxane, EtOH, 50 °C; **b)** $NH_2OH{\cdot}HCl$, NaOMe, MeOH, RT, 2 h.*

3.4.3. Testing hydroxamate-base analogues of 25 against SNM1A, SNM1B and SNM1C

Following the synthesis of **57**, **59**, **61**, **63**, **65**, **67**, **69**, and **70**, these compounds were tested against SNM1A and SNM1B. Additionally, compounds **42**, **45**, **51**, and **78** from **Section 3.3.2** and **3.4.1**, which showed good inhibition against SNM1A, were tested against SNM1B. From the inhibitors tested against both SNM1A and B, compounds were selected to be then tested against SNM1C. Only a limited number of inhibitors was tested against SNM1C since the current fluorescence-based assay against SNM1C uses substantially more enzymes than assays using SNM1A or B. Fluorescence-based assays against SNM1A, SNM1B, and SNM1C used 0.5 nM, 0.25 nM and 50 nM enzyme concentrations, respectively. Additionally, only a limited quantity of SNM1C was available for testing. Compounds chosen to be tested against SNM1C were **42**, **45**, **51, 57, 67**, **78**. Inhibitors **42**, **45** and **51** were selected because these compounds were the best three inhibitors against SNM1A, whilst **67** was chosen because it was most inhibitory against SNM1B. **67** and **78** were selected because of the alcohol and carbonyl modifications and relatively good inhibition against SNM1B. **Figure 3.23** presents a table summarising the IC_{50} values for inhibitors tested against SNM1A, B, and C using a fluorescence-based assay. **Figure 3.24** shows dose-response curves of selected compounds tested against SNM1A, B and C using the fluorescence-based assay.

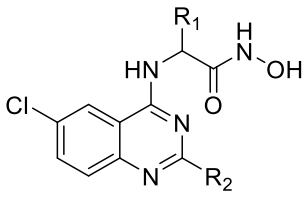

Compound	R_1	R_2	SNM1A (IC_{50}/μM)	SNM1B (IC_{50}/μM)	SNM1C (IC_{50}/μM)
42			0.8	19	12
45			2.2	96	49
51			4.1	24	17
57			67	13	13
59			42	40	NT
61			ND	ND	NT
63			20	18	NT
65		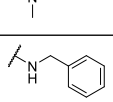	34	11	NT
67		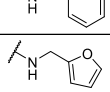	44	2.5	3.7
69		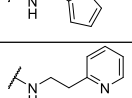	56	32	NT
70		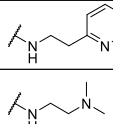	ND	ND	NT
78		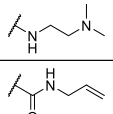	84	22	8.1

Figure 3.23: *Activities of hydroxamate-based analogues of* ***25*** *against SNM1A, SNM1B and SNM1C.* IC_{50} *values were calculated using results from fluorescence-based assays. Concentrations used [SNM1A] = 0.5 nM, [SNM1B] = 0.25 nM, [SNM1C] = 50 nM and [DNA] = 25 nM. ND- Not determined. NT- Not tested.*

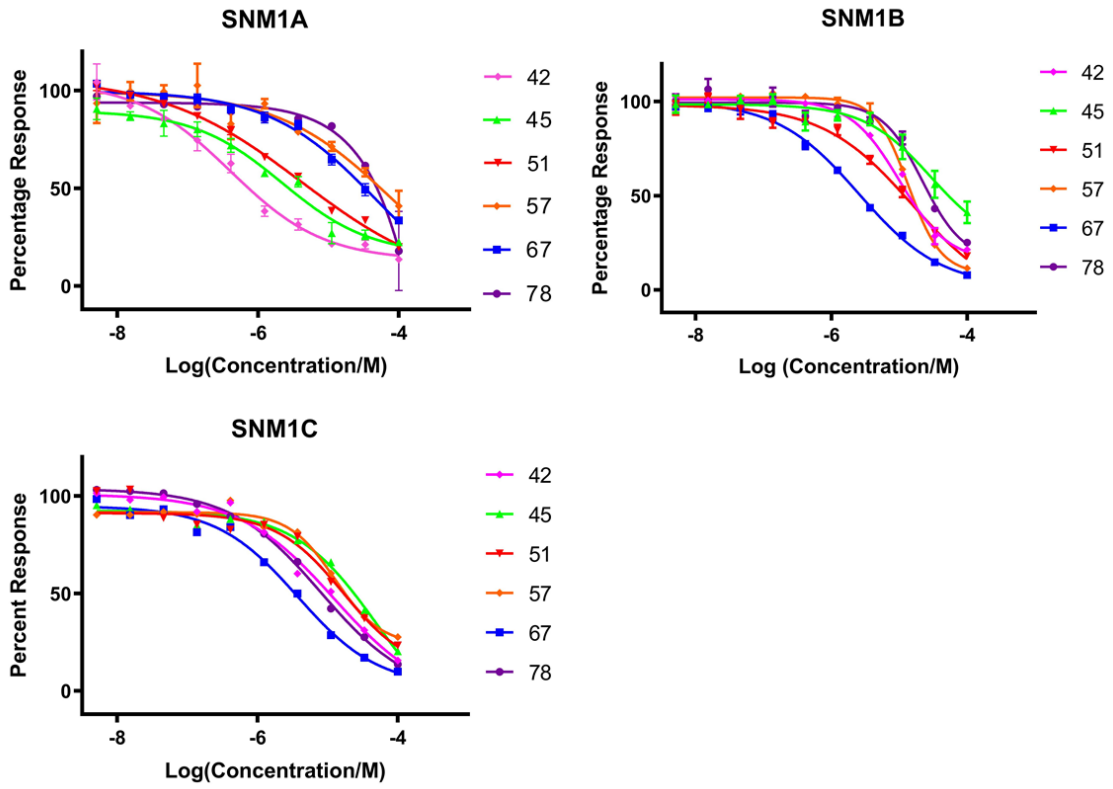

Figure 3.24: *Dose-response curve for selected inhibitors plotted using the data from the real-time fluorescence assay. Concentrations used [SNM1A] = 0.5 nM, [SNM1B] = 0.25 nM, [SNM1C]= 50 nM and [DNA] = 25 nM.*

Based on results from **Figure 3.23**, it may be concluded that hydroxamate-based inhibitors inhibit all three nucleases, SNM1A, B, and C. Some trends can be observed from the obtained data, although the assays cannot be fully compared to one another, especially with assays against SNM1C using a higher enzyme concentration and different substrate than those against the other two enzymes (SNM1A/B). After testing all the above compounds, **42** (IC_{50} = 0.8 μM against SNM1A) was still the most potent inhibitor against SNM1A, while **67** (IC_{50} = 2.5 μM and 3.7 μM against SNM1B and SNM1C, respectively) was the most potent inhibitor against SNM1B and SNM1C. Against all 3 three enzymes, **42** was more potent than **45** or **51**, making *L*-alanine the preferred amino acid side chain modification (of

the derivatives made). IC_{50} values were not determined for compounds **61** and **70**, as these compounds showed weak and incomplete inhibition in the initial assay screen.

Overall, inhibitors with a monosubstituted amine modification (*i.e.* **42**, **45**, **51**, and **67**) at position 2 were more potent than inhibitors with a disubstituted amine (*i.e.* **59**, **61**, and **63**) at position 2. For inhibitors tested against SNM1A, smaller side chains at position 2 are apparently preferred, such as allylamine (**42**, **45**, and **51**) rather than bulky ones like benzylamine (**56**). For comparison for SNM1B, smaller differences in inhibition can be observed between bulky and smaller amine modifications at position 2. Inhibitors with an amine side chain at position 2 (*i.e.* **42**, **45**, and **51**) were generally more inhibitory against SNM1A than inhibitors with either alcohol (**57**) or amide (**78**). By contrast, inhibitors with amine (*i.e.* **42**, **45**, and **51**), alcohol (**57**), or amide (**78**) modifications at position 2 showed very similar levels of inhibitions against both SNM1B and SNM1C. Compounds **42**, **45**, **57**, **67**, and **78** were then tested using the radioactive gel-based assay against all three enzymes (**Figure 3.25**, **3.26**, and **3.27**).

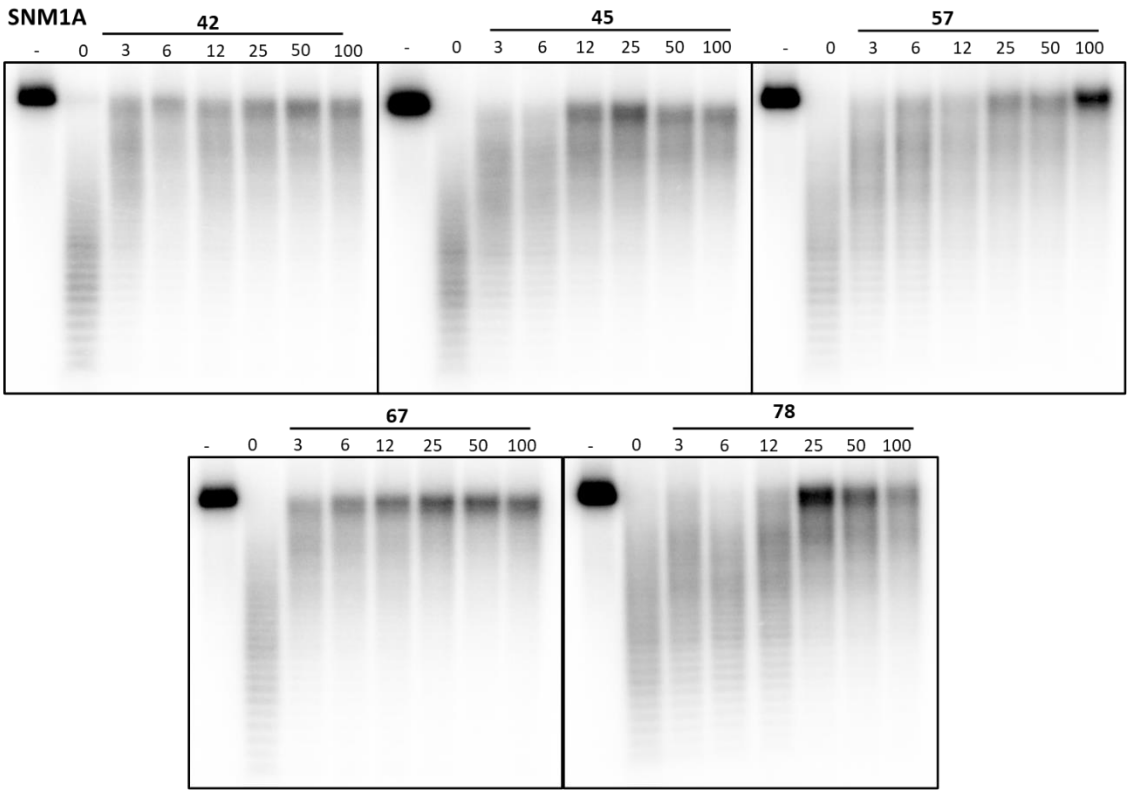

Figure 3.25: *Gel image from radioactive gel-based assays with SNM1A. Concentrations used [SNM1A] = 0.5 nM, and [DNA 50-mer] = 10 nM. The indicated concentrations are in μM.*

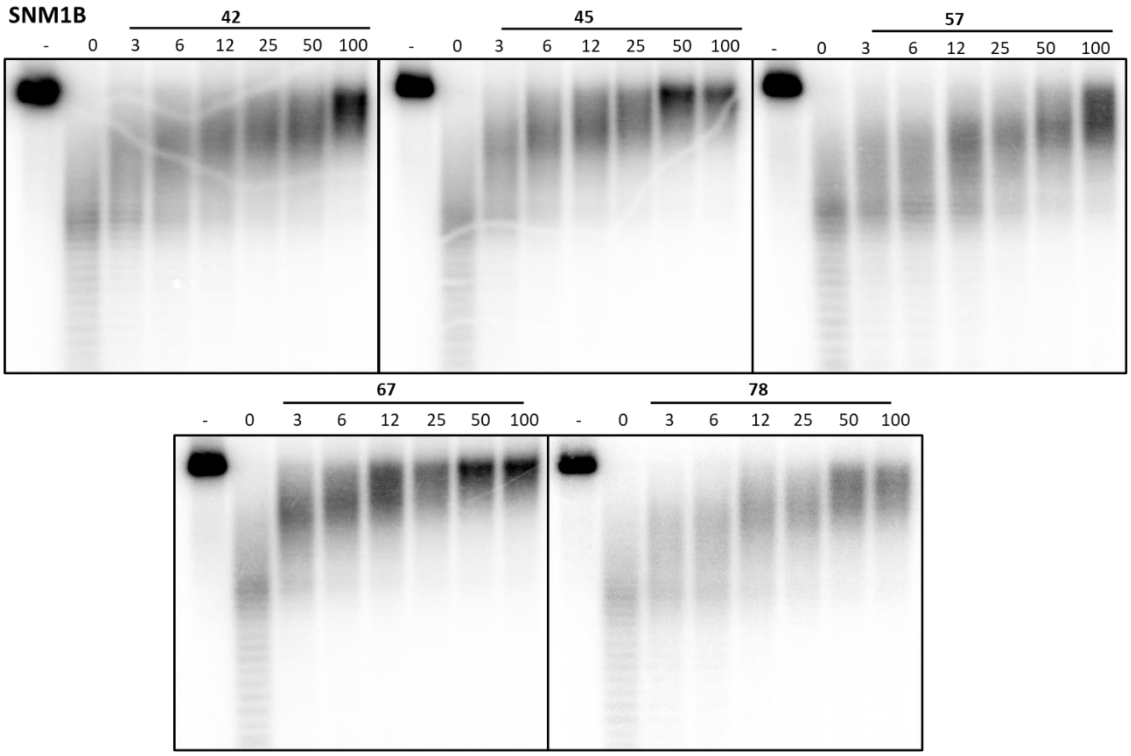

Figure 3.26: *Gel image from radioactive gel-based assays with SNM1B. Concentrations used [SNM1B] = 2.5 nM, and [DNA 50-mer] = 10 nM. The indicated concentrations are in μM.*

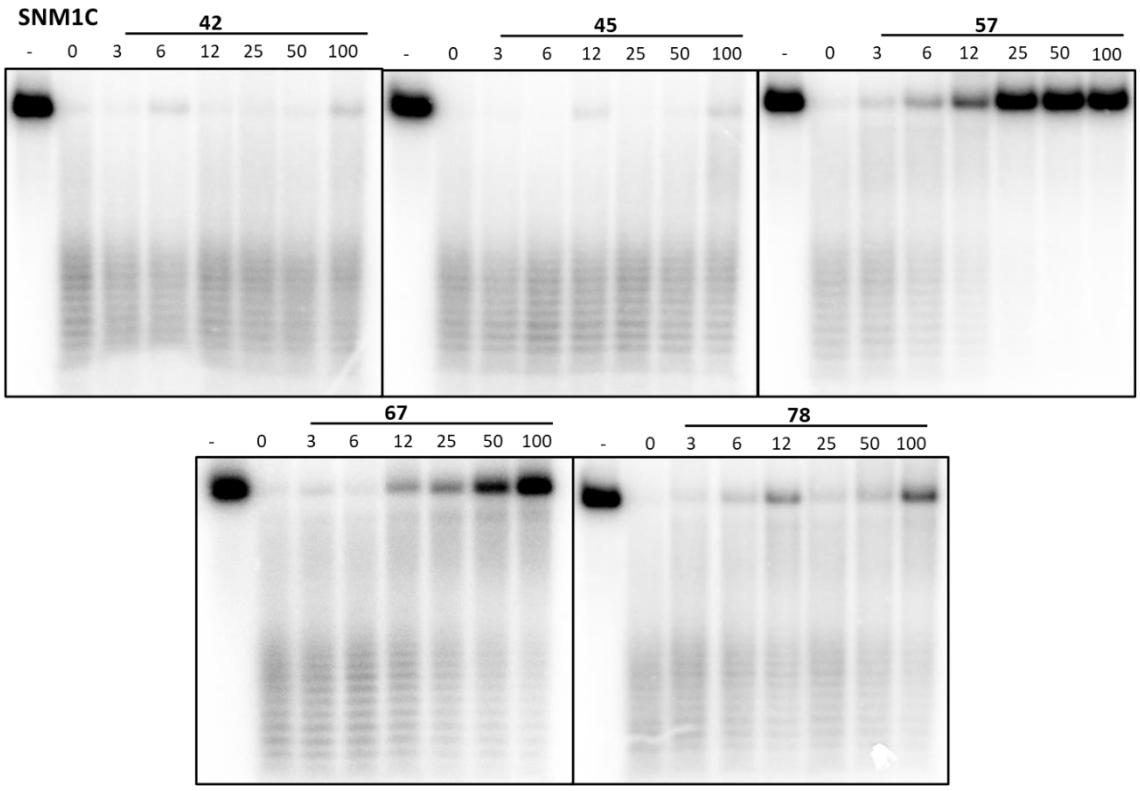

Figure 3.27: *Gel image from radioactive gel-based assays with SNM1C. Concentrations used [SNM1C] = 2.5 nM, and [DNA 50-mer] = 10 nM. The indicated concentrations are in μM.*

The gel-based assay further validates inhibition of all three enzymes by this series of inhibitors, although these results are not entirely consistent with the results from the fluorescence-based assays. From the inhibitors tested against SNM1A and SNM1B, all the tested compounds were shown to be inhibitory, while for SNM1C, only **57** and **67** showed consistent inhibition. From the gel-based assay results with SNM1A, **42** and **67** seem to be most inhibitory, with similar levels of DNA digestion, while based on the fluorescence-based assay, **42** has a substantially lower IC_{50} than **67**. For SNM1B, **67** is the most inhibitory in the gel-based assay, which corresponds to the results from **Figure 3.23**. At the same time, **45** seems to inhibit SNM1B more than **42**, which contradicts the fluorescence-based assay results. Overall, this series of hydroxamate-based inhibitors might be best described as non-selective inhibitors of SNM1A/B/C nucleases.

3.5. Crystal structures of SNM1A with hydroxamate-based inhibitors

Throughout the project, attempts were made to soak selected analogues of **25** into the crystal of SNM1A. Out of the compounds soaked, structures of inhibitors **42**, **51**, **67**, and **78** bound to the active site of SNM1A were achieved (**Figure 3.28**, **3.29**, **3.30**, and **3.31**).

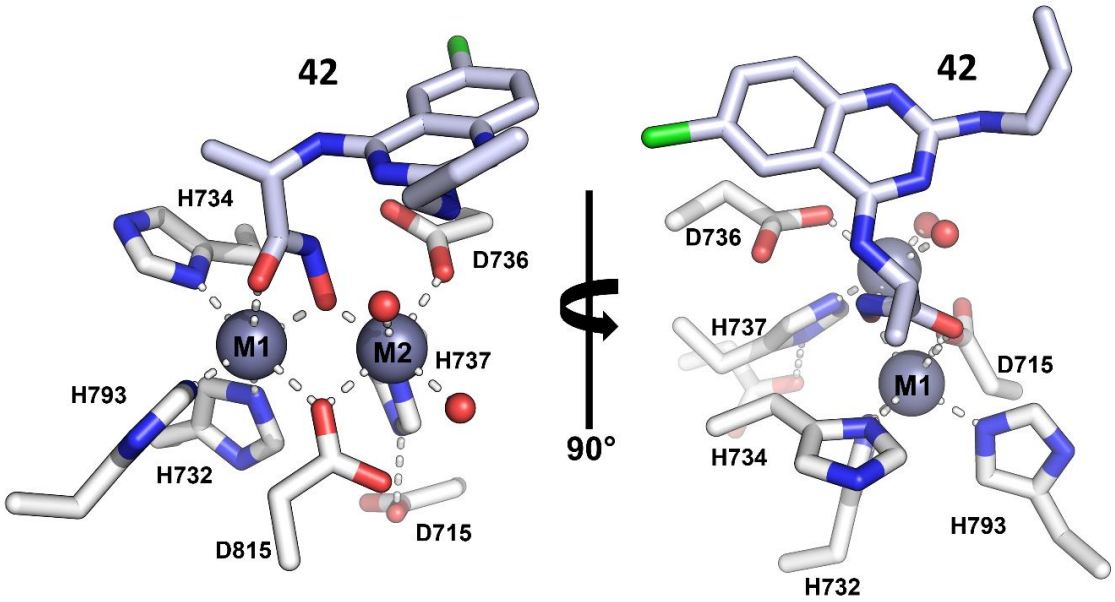

Figure 3.28: *View from a structure of inhibitor **42** bound to the active site of SNM1A. **M1**: Zinc. **M2**: Zinc*

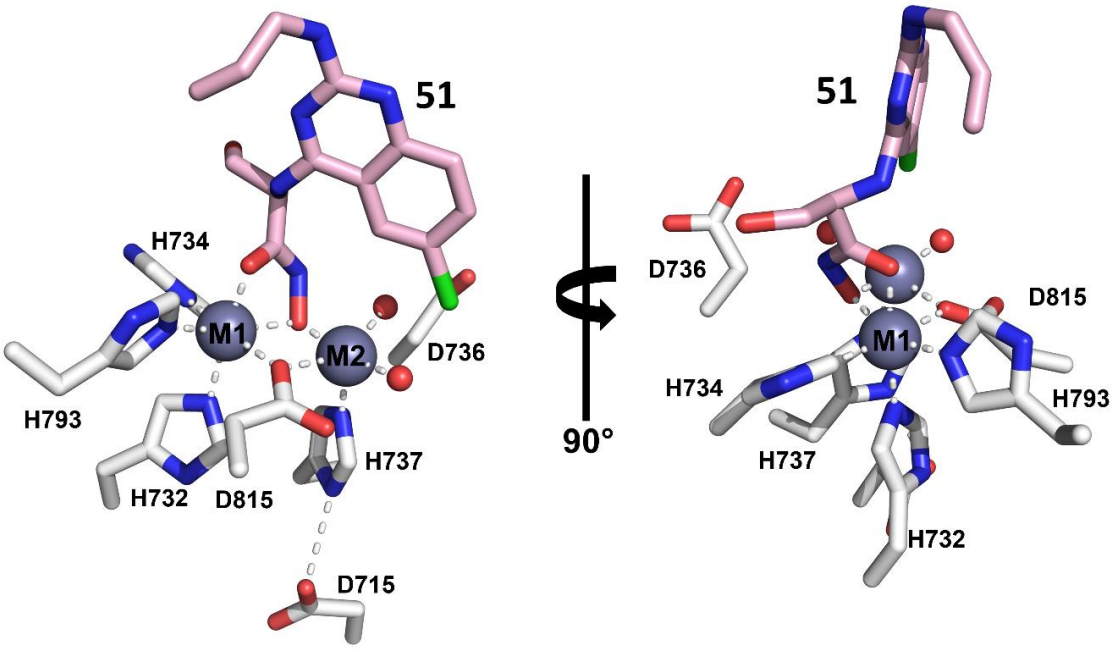

Figure 3.29: *View from a structure of inhibitor* ***51*** *bound to the active site of SNM1A.* ***M1****: Zinc.* ***M2****: Zinc*

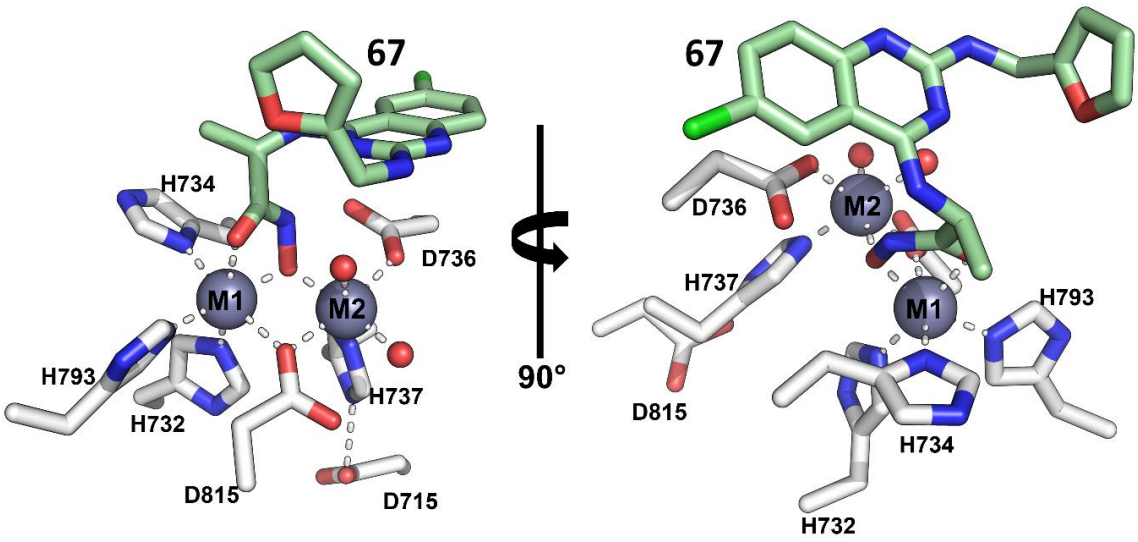

Figure 3.30: *View from a structure of inhibitor* ***67*** *bound to the active site of SNM1A.* ***M1****: Zinc.* ***M2****: Zinc*

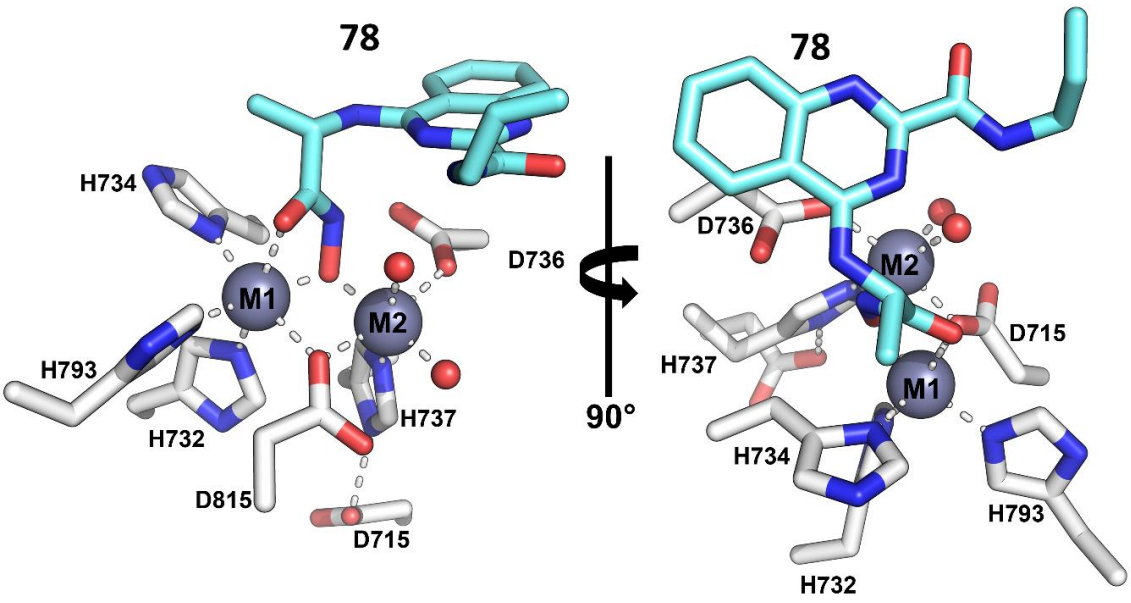

Figure 3.31: *View from a structure of inhibitor **78** bound to the active site of SNM1A. **M1**: Zinc. **M2**: Zinc*

Clear similarities are observed in the structures of inhibitors **42**, **51**, **67**, and **78** bound to SNM1A. In all four structures, a nearly identical binding of the hydroxamate pharmacophore to the metals in the active site is observed. Both oxygens from the carbonyl and hydroxyl groups are involved in the metal chelation. The carbonyl oxygen is chelating metal ion **M1**, while the hydroxyl group is bridged between metals and displaces catalytic water. Both active site metal ions present in structures of **42**, **51**, **67**, and **78** bound to SNM1A were zinc (II) ions. Two zinc (II) ions are considered to be the physiologically relevant metals.[11]

Structures of SNM1A with **42**, **67**, and **78** (**Figure 3.28**, **3.29**, and **3.30**) are very similar, with the similar positioning of the core and *L*-alanine amino acid side chain. In the structures with these 3 inhibitors, both metal ions have an octahedral coordination. This orientation of the core might be preferred due to π-interaction between the aromatic ring in the quinazoline and the Asp736, as shown in **Figure 3.32**. Additionally, as apparent in **Figure 3.32**, a possible interaction exists between the chloride at position 6 and Ser735. No further direct

interactions were observed, especially between the side chain at position **2** and the protein, with this side chain pointing away from the active site.

In the structure of **51** bound to SNM1A (**Figure 3.31**), the position of the quinazoline core is in a different orientation to that observed in the other structures. This shift in orientation of the inhibitor core apparently results in a displacement of Asp736, causing it to no longer chelate the metal ion **M2**. Due to the lack of chelation by Asp736, metal ion **M2** no longer has the octahedral coordination geometry.

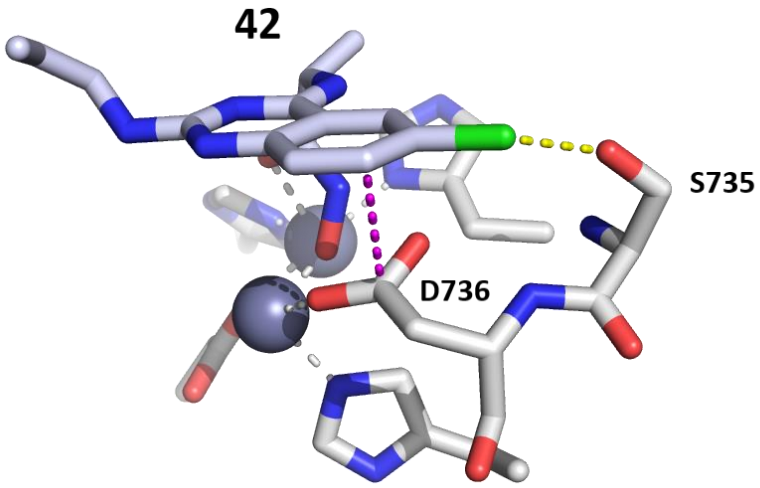

Figure 3.32: *View from a structure of inhibitor **42** bound to the active site of SNM1A, showing possible interaction between **42** and side chains of the SNM1A. Yellow dotted line: interaction between chlorine and Ser735. Magenta dotted line- π-interaction between quinazoline and Asp736.*

These crystal structures of inhibitors bound to the active site of SNM1A were found to be useful for the rational structure-based design of new inhibitors as pursued in the remaining part of the project.

3.6. Modifications at position 6 of the quinazoline ring

Following modifications at positions 2 and 4, the next to be modified was position 6 where chloride was present. Due to the potential interaction with Ser735 shown in **Figure 3.32**, it

was decided to substitute chloride with fluoride and methoxy groups, which might form a hydrogen bond with the hydroxyl group from the serine side chain. Additionally, a phenyl group was introduced at position 6 to investigate the effects of a bulkier group on inhibition. Since the Suzuki coupling procedure, used for cross-coupling usually requires basic conditions, a dimethylamine modification was used at position 2 for synthesis inhibitors, as shown in **Figure 3.33**. Previously, as described in **Section 3.2**, it was observed that analogues of **25** with disubstituted amines at position 2 were more stable toward basic conditions; therefore, dimethylamine, which is the smallest disubstituted amine, was used. For cross-coupling, a starting material with bromide instead of chloride was used as bromide is normally more reactive.

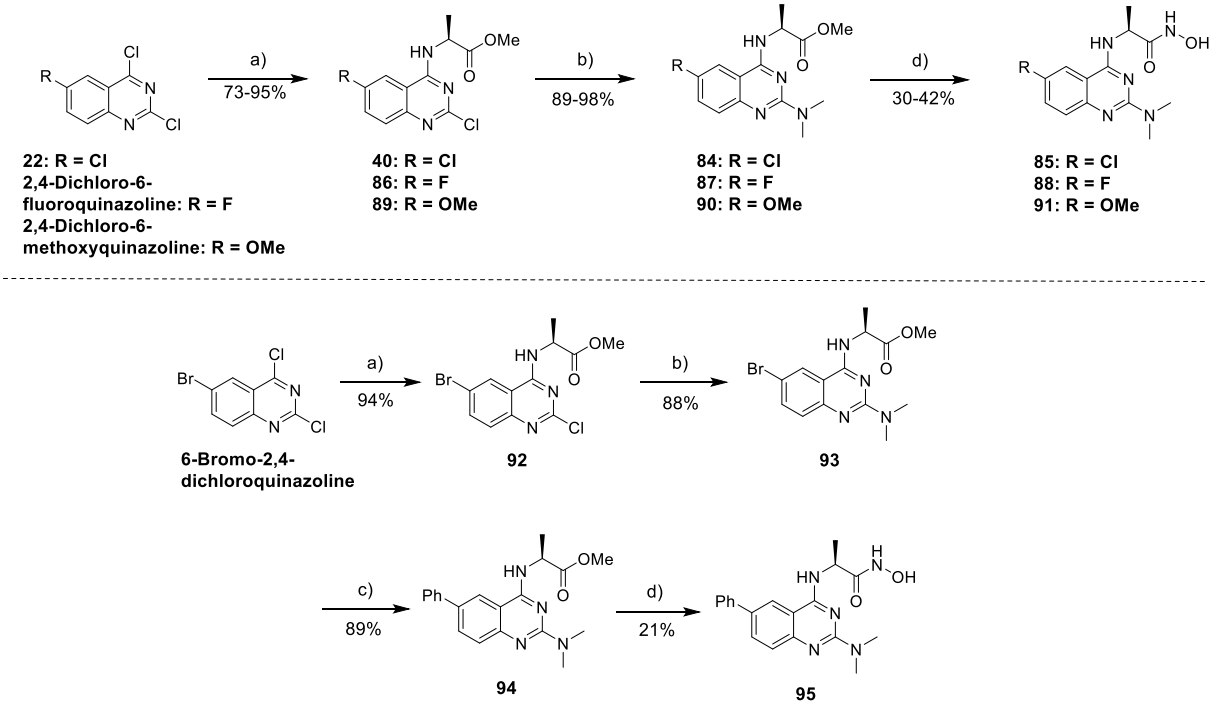

Figure 3.33: *Synthesis of analogues of **42**. Reaction conditions: **a)** L-Alanie methyl ester hydrochloride, DIPEA, DMF, RT, 16 h; **b)** 2 M $NHMe_2$ in THF, DMF, 100 °C, 4 h; **c)** $PhB(OH)_2$, $NaHCO_3$, $Pd(dppf)Cl_2$, 1,4-dioxane, H_2O, 100 °C, 1 h; **d)** $NH_2OH{\cdot}HCl$, NaOMe, MeOH, RT, 2 h.*

Steps **a)** and **d)** were performed using conditions previously described in **Section 3.3.2**. For step **b)** new conditions for the aromatic nucleophilic substitution were used. Instead of using microwave and methanol as solvent, the reaction was performed using a hot plate and dimethylformamide as a solvent. Dimethylformamide can also be substituted with other solvents with a higher boiling point like dioxane. This change resulted in excellent yields (above 88%). However, this condition was not checked in a reaction using monosubstituted amines. In step **c)**, there was an initial problem with decomposition due to the hydrolysis. It was found that the reason for hydrolysis was the use of K_3PO_4 as a base; thus, replacing it with the less basic $NaHCO_3$ resulted in a very efficient conversion giving **94** in a yield of 89%. Following step **c)**, compound **94** was purified using extraction and column chromatography. After aminolysis in step **d),** all the compounds had to be purified using RP HPLC due to the presence of an unknown contaminating material, which could not be removed by standard column chromatography. Following the synthesis, compounds **85**, **88**, **91**, and **95** were tested against SNM1A and SNM1B using the fluorescence-based assay (**Figure 3.34**).

Compound	R	SNM1A (IC_{50}/μM)	SNM1B (IC_{50}/μM)
85	Cl	11	9.8
88	F	13	23
91	OMe	74	ND
95	Ph	ND	ND

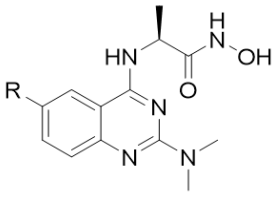

Figure 3.34: *Activity of hydroxamate-based analogues against SNM1A and SNM1B. IC_{50} values were calculated using results from fluorescence-based assays. Concentrations used [SNM1A] = 0.5 nM, [SNM1B] = 0.25 nM, and [DNA] = 25 nM. ND: Not determined.*

The introduction of phenyl (**95**), fluoride (**88**), or methoxide (**91**) groups did not improve the inhibition potency compared to inhibitors **42** or **67**. IC_{50} values for the inhibition of compounds **95** against both SNM1A/B, and **91** against SNM1B was not determined due to an incomplete inhibition at the highest used concentration (100 μM). While the inhibition by analogues with chloride (**85**) and fluoride (**88**) groups was similar, the methoxy (**91**) and phenyl (**95**) derivatives showed lower potency. These results, therefore, indicate that the introduction of a functional group larger than chloride at position 6 might decrease inhibition. Modifications at position 6 did not increase potency. It was decided to further investigate modifications at position 2 using the structural data described in **Section 3.5**.

3.7. References

[1] R. A. Smits, I. J. P. de Esch, O. P. Zuiderveld, J. Broeker, K. Sansuk, E. Guaita, G. Coruzzi, M. Adami, E. Haaksma and R. Leurs, *Journal of Medicinal Chemistry*, 2008, **51**, 7855-7865.
[2] L. Zhu, J. Jin, C. Liu, C. Zhang, Y. Sun, Y. Guo, D. Fu, X. Chen and B. Xu, *Bioorganic & Medicinal Chemistry*, 2011, **19**, 2797–2807.
[3] C. O. Kappe, *Angewandte Chemie International Edition*, 2004, **43**, 6250-6284.
[4] B. Dayal, G. Salen, B. Toome, G. S. Tint, S. Shefer and J. Padia, *Steroids*, 1990, **55**, 233-237.
[5] B. Dayal, G. Salen and V. Dayal, *Chemistry and Physics of Lipids*, 1991, **59**, 97-103.
[6] M. W. Walter, M. H. Valladares, R. M. Adlington, G. Amicosante, J. E. Baldwin, J.-M. Frère, M. Galleni, G. M. Rossolini and C. J. Schofield, *Bioorganic Chemistry*, 1999, **27**, 35–40.
[7] A. Grassadonia, P. Cioffi, F. Simiele, L. Iezzi, M. Zilli and C. Natoli, *Cancers*, 2013, **5**, 919-942.
[8] J.-D. Liu, C.-Y. Sun, L. Tang, Y.-Y. Wu, Q.-Y. Wang, B. Hu and Y. Hu, *Scientific Reports*, 2016, **6**, 27361.
[9] C. Hao, F. Zhao, H. Song, J. Guo, X. Li, X. Jiang, R. Huan, S. Song, Q. Zhang, R. Wang, K. Wang, Y. Pang, T. Liu, T. Lu, W. Huang, J. Wang, B. Lin, Z. He, H. Li, F. Li, D. Zhao and M. Cheng, *Journal of Medicinal Chemistry*, 2018, **61**, 265-285.
[10] US20100069383

[11] B. Sengerová, C. K. Allerston, M. Abu, S. Y. Lee, J. Hartley, K. Kiakos, C. J. Schofield, J. A. Hartley, O. Gileadi and P. J. McHugh, *Journal of Biological Chemistry*, 2012, **287**, 26254-26267.

Chapter 4. Development of selective SNM1B inhibitor

4.1. Identification of phosphate-binding pocket as a target

Obtained crystal structures of **42** bound to the active site of SNM1A revealed that the allylamine side chain, while not directly interacting with any part of the protein, was in close proximity to the phosphate-binding pocket (**Figure 4.1**). The allylamine side chain was observed to be ~7.3−8.3 Å away from the phosphate-binding pocket residues, **Lys883**, **Ser992**, and **Glu993**.

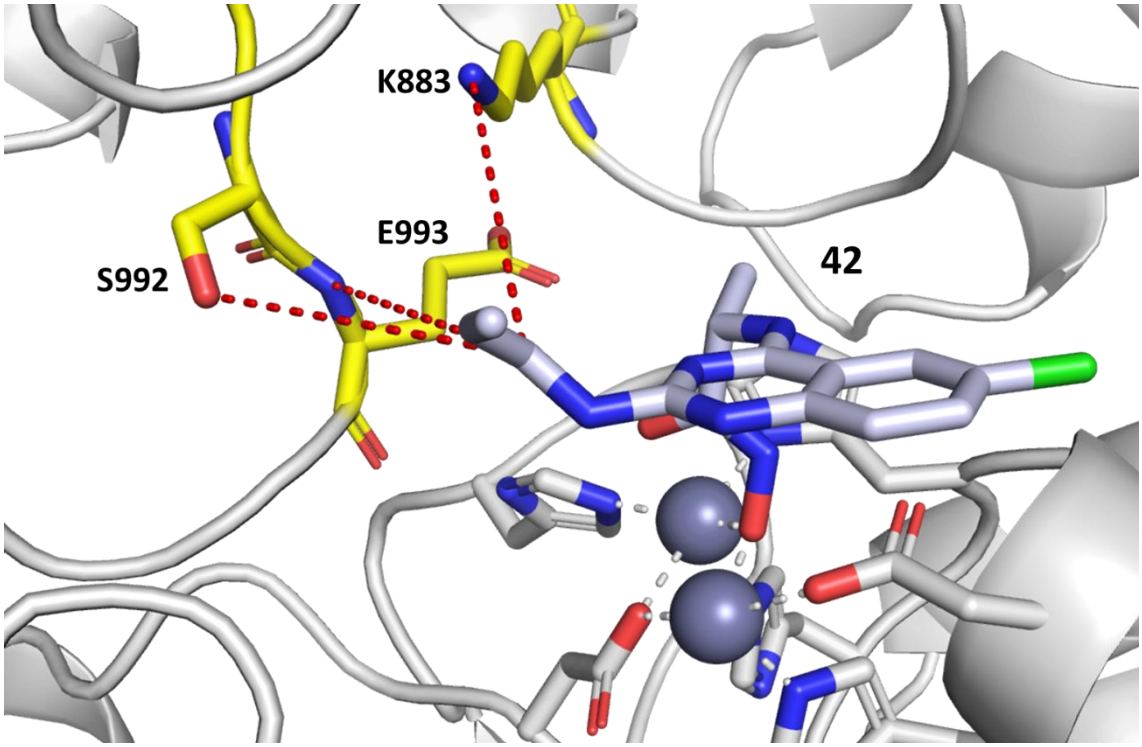

Figure 4.1: *Structure of **42** bound to the active site of SNM1A showing close proximity between the allylamine side chain at position 2 of the quinazoline ring and the phosphate-binding pocket residues (**Lys883**, **Ser992**, and **Glu993**).*

An active site phosphate-binding pocket is present in both SNM1A and SNM1B and is apparently not present in SNM1C. This pocket is proposed to be essential for exonuclease activity as it interacts with the 5'-phosphate group in DNA.[1] The conserved phosphate-binding pocket residues are highlighted in **Figure 4.2**.

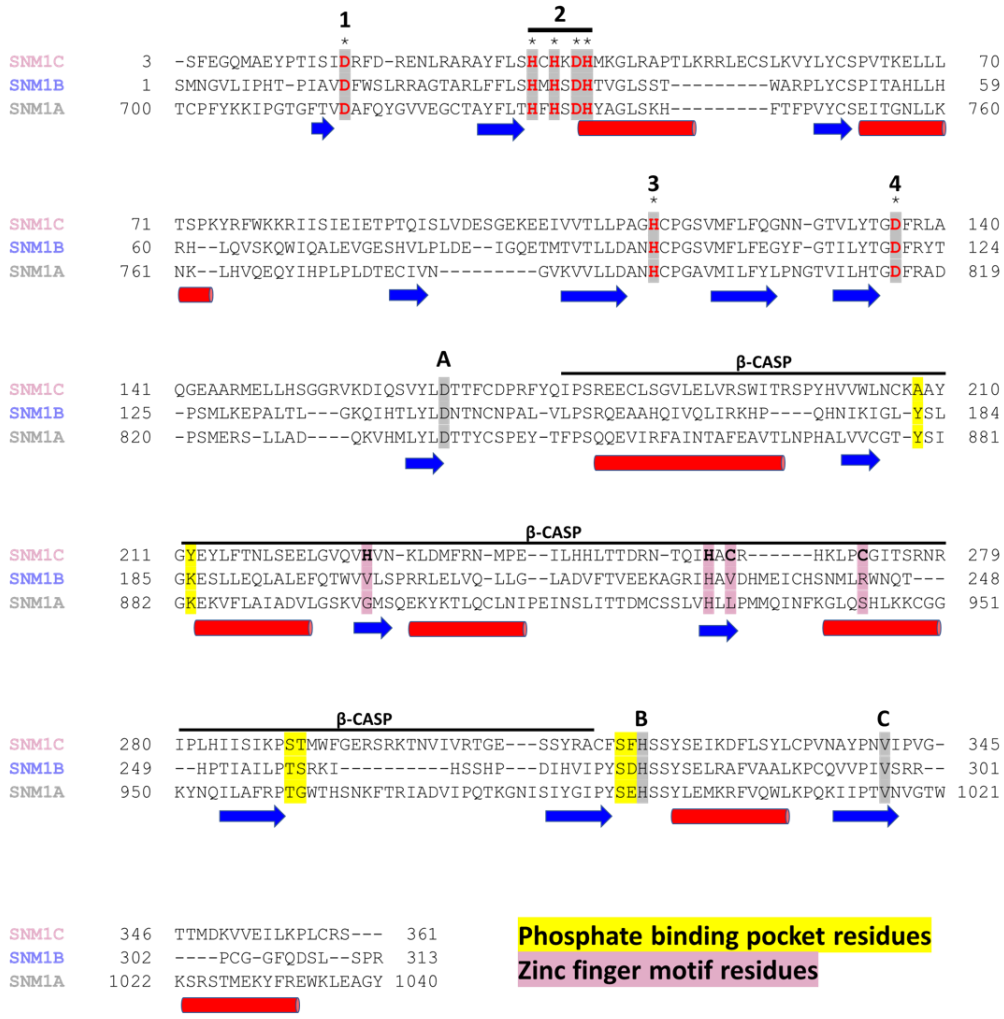

Figure 4.2: *Structural sequence alignments of the human SNM1 nuclease family enzymes. The structural alignment was carried out using PROMALS3D.*[2] *α-Helices are drawn as red cylinders and the β-strands as blue arrows. The conserved MBL family motifs are labelled as 1–4, and the canonical β-CASP motifs are labelled A–C. The conserved phosphate binding residues in SNM1A and SNM1B are highlighted in yellow. The residues that made up the zinc finger-like structure in SNM1C are highlighted in pink.*

The majority of SNM1 nuclease inhibitors developed up to this point have been non-specific and inhibit all three SNM1 enzymes at relatively similar concentration ranges. As the phosphate-binding pocket is seemingly only present in SNM1A and SNM1B, designing an inhibitor that would interact with both the active site and the phosphate-binding pocket might increase selectivity towards these enzymes. Developing an inhibitor that would selectively inhibit SNM1A and SNM1B, while not inhibiting SNM1C, might be beneficial, especially

since SNM1A and SNM1B are both involved in the interstrand-cross link repair, and they might exhibit some redundancy in this pathway.[3]

4.1.1. Testing bacterial MBL inhibitors containing a phosphonate group against SNM1A and SNM1B

In the search for compounds that might potentially interact with both metal ions in the active site and the phosphate-binding pocket, bacterial MBL inhibitors containing a phosphonate group were chosen since this functional group is a phosphate bioisostere. Compounds **81** and **83** were synthesised using reported synthetic routes (**Figure 4.3**).[4,5]

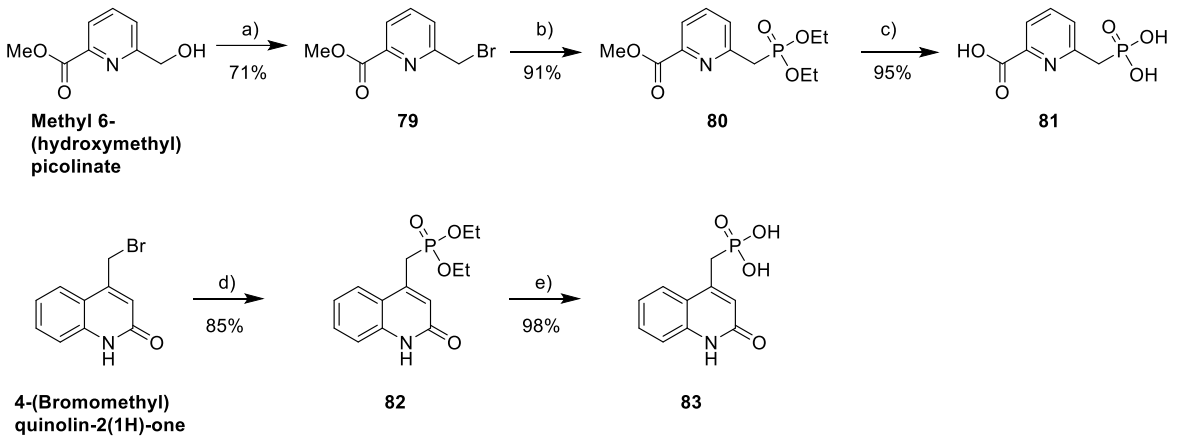

Figure 4.3: *Synthesis scheme for **81** and **83**. Reaction conditions: **a)** PBr_3, $CHCl_3$, 0 °C, 4 h; **b)** $P(OEt)_3$, toluene, reflux, 2 h; **c)** 6 M $HCL_{(aq)}$, reflux, 16 h; **d)** $P(OEt)_3$, 1,4-dioxane, reflux, 2 h; **e)** 4 M HCL in 1,4-dioxane, reflux, 24 h.*

Compound **81** was synthesised from methyl 6-(hydroxymethyl) picolinate in an overall yield of 61% over 3 steps. In step **a)**, methyl 6-(hydroxymethyl) picolinate was converted into **79** via bromination reaction using phosphorus tribromide. **79** was produced in a good yield of 71% and was purified using column chromatography. Next, in step **b)**, **79** was converted into **80** using nucleophilic substitution reaction using triethyl phosphite as the nucleophile. **80** was produced at an excellent yield of 91% and was purified using column chromatography. Finally, in step **c)**, **80** was converted into **81** via simultaneous deprotection

of methyl ester and two ethyl phosphate esters under heat and acidic conditions. **81** did not require any purification and was produced at an excellent yield of 95%.

Compound **83** was synthesised from 4-(bromomethyl)quinolin-2(1H)-one in a very good yield of 83% over steps. In the synthesis of **83**, steps **d**) and **e**) were performed in similar conditions to those used for steps **b**) and **c**). Purification using column chromatography was only required after step **d)**, while no purification was necessary after the deprotection of the ethyl phosphate esters in step **e**). The yield of steps **d**) and **e**) was 85% and 98%, respectively.

Following synthesis, **81** and **83** were tested against SNM1A and SNM1B. Neither of these compounds inhibited SNM1A or SNM1B, although unexpectedly, **81** was observed to apparently enhance the activity of SNM1A. When SNM1A was treated with at least 10 μM of **81**, the rate of digestion of the DNA substrate increased, as shown in **Figure 4.4**. No similar effect was observed for SNM1B.

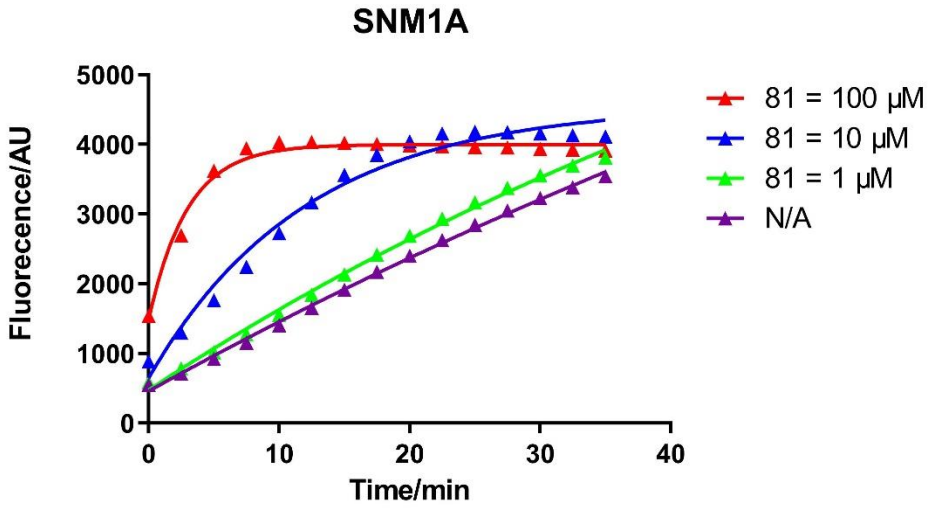

Figure 4.4: *Enzyme activity assay with SNM1A. Measurement of fluorescence emission released upon digestion of modified DNA by SNM1A. The fluorescence emission is proportional to the extent of digestion of DNA substrate. [SNM1A] = 0.5 nM and [DNA] = 25 nM.*

4.1.2. Crystal structure of 81 bound to SNM1A

Although neither **81** nor **83** displayed inhibition of SNM1A, they were still soaked into crystals of SNM1A. Consequently, a structure of **81** bound to the active site of the SNM1A was obtained (**Figure 4.5**).

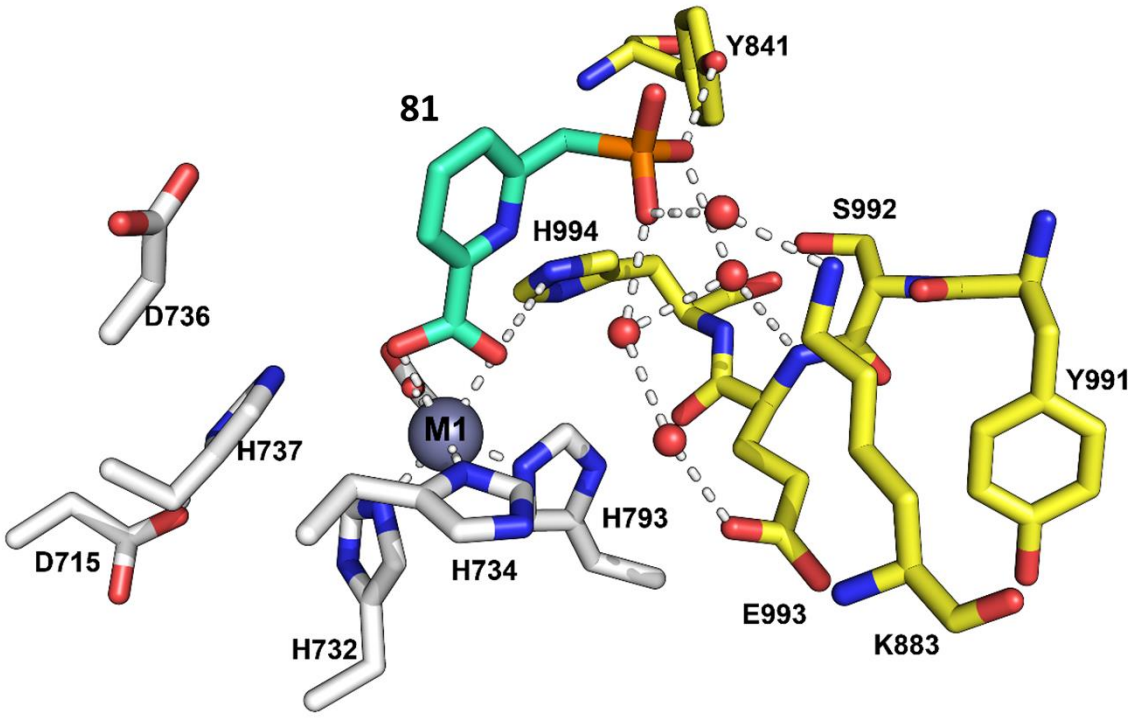

Figure 4.5: *View from a crystal structure of **81** bound to SNM1A. The carboxylic acid in **81** chelates to the metal in the active site and phosphonate group interacts with phosphate-binding pocket residues. Amino acids involved in chelating metals in the active site are in white. Amino acids that are part of the phosphate-binding pocket are in yellow. **M1**: Zinc.*

In the crystal structure of **83** with SNM1A, **83** is observed to interact with the metal **M1** in the active site and the phosphate-binding pocket. Compound **83** chelates metal ion **M1** using both oxygens in its carboxylic acid. The second metal is missing from the active site, which is common for structures of SNM1A, as mentioned in **Section 2.1**. The phosphonate site chain interacts directly and indirectly with the phosphate-binding pocket. One oxygen in the phosphonate hydrogen bonds with the hydroxyl group from **Tyr841**. At the same time, two

oxygens from the phosphonate group indirectly interact with amino acids **Lys883**, **Glu993** and **Ser993** via hydrogen bond interactions with water molecules. This structure validates the strategy of simultaneously targeting the active site and phosphate-binding pocket. Based on these encouraging results from the new crystal structure, it was decided to introduce phosphate bioisostere modifications, including a phosphonate, into the hydroxamate-based inhibitor series developed in **Chapter 3**.

4.2. Introduction of phosphate bioisostere to analogues of 25

4.2.1. Synthesis of analogues of 42 containing phosphate bioisostere

A phosphonate group was chosen as the phosphate bioisostere since this was the functional group found in **83,** and it is commonly found in clinically used drugs. It was decided to introduce this functional group into the side chain at position 2 of the quinazoline ring found in analogues of **42**.[6]

Initially, the intention was to synthesise analogues of **42** containing a phosphonate group using the reaction between intermediate **40** or **72** and amino phosphonic acid, as shown in **Figure 4.6**. The use of amino phosphonic acid in an aromatic nucleophilic substitution was unsuccessful as the amine's nucleophilicity is probably decreased by the adjacent phosphonic acid. Next, it was attempted to react the more reactive acyl chloride in **72** with amino phosphonic acid, however this reaction also failed since the amino phosphonic acid was only soluble in a basic solution of methanol or water.

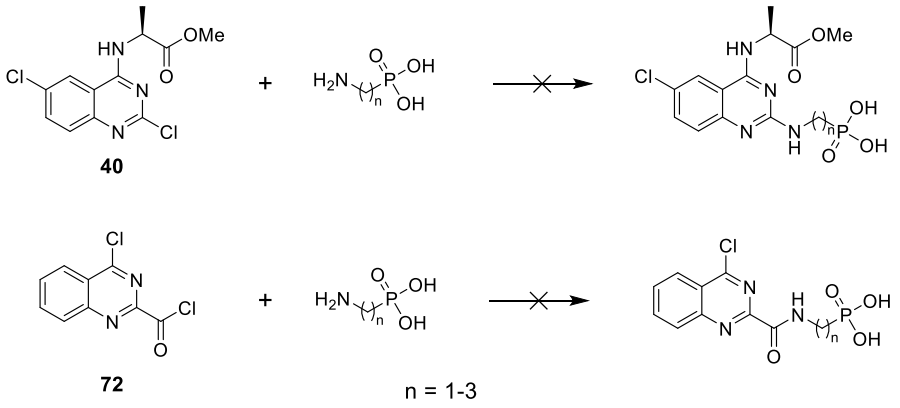

Figure 4.6: *Initial strategy to introduce a phosphonate functional group.*

After the failed attempts to synthesise an analogue of **42** containing a phosphonate group, an extensive literature search for reactions with amino phosphonic acid was carried out. A promising amide coupling reaction between amino phosphonic acid and an *N*-hydroxysuccinimide (NHS) ester in a mixture of water, dimethylformamide and base was found.[7] Following this finding, a new intermediate **100**, containing a benzyl protected *L*-alanine hydroxamic acid side chain at position 4 and an NHS ester at position 2, was synthesised (**Figure 4.7**). Benzyl protected hydroxamic acid was used since it allows for the introduction of the hydroxamic acid functional group earlier in the synthesis, whilst protecting the hydroxamic acid makes it much more stable and compatible with other steps within the synthetic route. The benzyl protection can easily be removed at any stage of the synthesis using a simple hydrogenation reaction. Due to the introduction of the benzyl protection, the chloride on position 6 was removed from the compound. Previously, while synthesising compound **9** (**Section 2.1**), unintended reduction of the aromatic chloride was observed as a side reaction of hydrogenation.

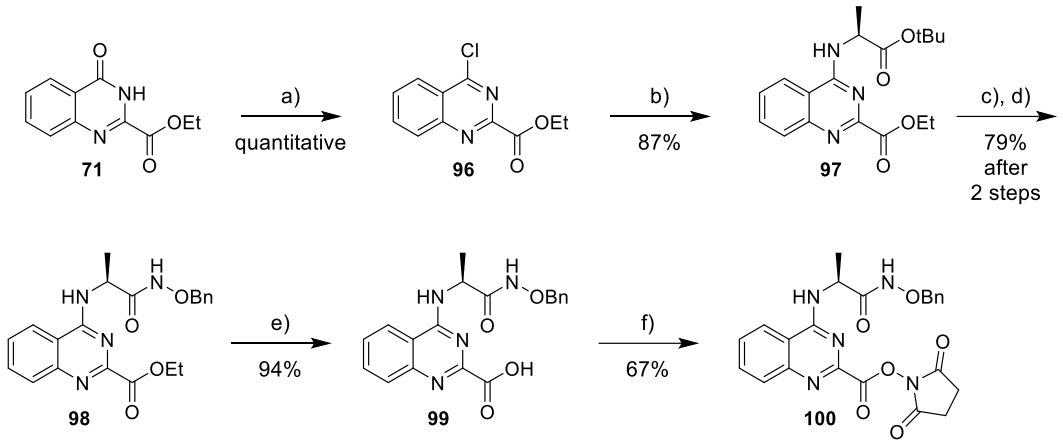

Figure 4.7: *Synthesis scheme for active ester **100**. Reaction conditions: **a)** $SOCl_2$, DMF, $CHCl_3$, reflux, 3 h; **b)** L-alanine tert-butyl ester hydrochloride, TEA, DCM, RT, 72 h; **c)** 4 M HCL in 1,4-dioxane, DCM, RT, 16 h; **d)** $NH_2OBn{\cdot}HCl$, HATU, DIPEA, DCM , RT, 16 h; **e)** 2 M $KOH_{(aq)}$, THF, 0 °C, 2 h; **f)** NHS, DCC, DMF, RT, 16 h.*

The synthesis of active ester **100** from starting material **71** was relatively efficient, with an overall yield of 43% after 6 steps and was done on a multi-grams scale. The synthesis route began with step **a**), chlorination of **71** using thionyl chloride to produce **96** in quantitative yield. Compound **96** did not require any purification. Next, in step **b**), the chloride of **96** was replaced by *L*-alanine tert-butyl ester via a nucleophilic aromatic substitution to give **97**. The substitution reaction to produce **97** resulted in a very good yield of 87% and required column chromatography for purification. Using both ethyl ester and tert-butyl ester simultaneously allowed for two selective deprotections at different points in the synthetic route. First, the tert-butyl ester **97** was selectively removed in step **c**) under acidic conditions and, without any purification, to produce intermediate carboxylic acid. The newly formed intermediate carboxylic acid was used, in step **d**), in amide coupling with *O*-benzylhydroxylamine and HATU, as the coupling reagent, to give **98**. After amide coupling, the intermediate **98** was purified using column chromatography, and the overall yield after ester hydrolysis and amide coupling was 79%. Following the coupling reaction, ester hydrolysis of **98**, step **e**), was performed under basic conditions using potassium hydroxide. The hydrolysis of **98**

resulted in an excellent yield of 94% of **99**, which was obtained by extraction. Finally, the NHS ester was synthesised using carboxylic acid **99**, with NHS and DCC as coupling agents. The NHS ester **100** was purified first by filtration to remove dicyclohexylurea precipitate and then using column chromatography. The NHS ester **100** was obtained in a yield of 67%. The active ester **100** was then used for an amide coupling reaction with amino phosphonic acids (**Figure 4.8**).

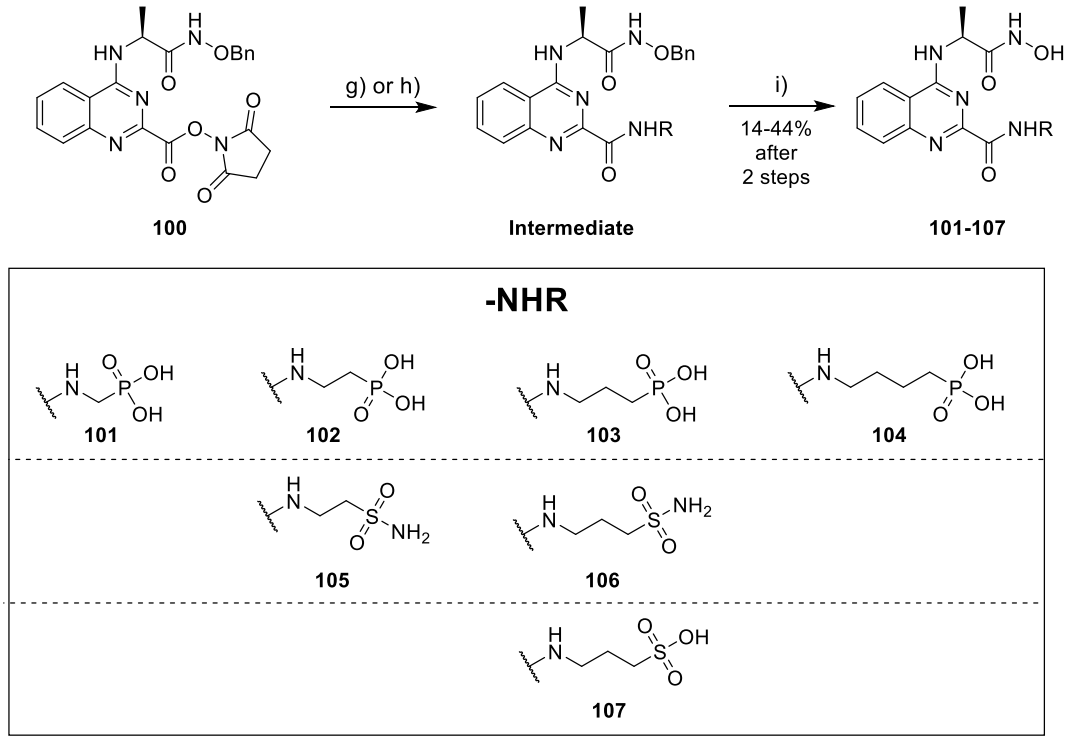

Figure 4.8: *Synthesis of analogues of **25** containing a phosphate bioisostere. Reaction conditions:* ***g)*** *Amino phosphonic acid or amino sulfonic acid, 0.4 M $NaHCO_{3(aq)}$, DMF, RT 3 h;* ***h)*** *Amino sulfonamide, TEA, DMF, RT, 3 h;* ***i)*** *$H_{2(g)}$, Pd/C, MeOH or H_2O/DMF mixture, 3 h.*

2-Aminoethylphosphonic acid was initially used for the reaction with NHS ester **100**. Successful amide coupling and benzyl deprotection produced inhibitor **102.** It was then decided to synthesise inhibitors with 4 different chain lengths to the phosphonate group to find the optimal linker length. For reactions with amino phosphonic acids, the reaction was

initially attempted with triethylamine as a base, but it was later discovered that an aqueous sodium bicarbonate solution resulted in better solubility.

For step **g)**, NHS ester **100** was dissolved in DMF, and amino phosphonic acid in an aqueous sodium bicarbonate solution was added dropwise. This reaction was monitored using LC-MS and reached completion within 3 hours. No purification was done after the amide coupling, although the solution needed to be acidified before the hydrogenation step. When the hydrogenation was performed under basic conditions, the N-O bond in the hydroxamate was hydrogenated, and amide was produced as a side product. In contrast, no N-O bond cleavage was observed under neutral or acidic conditions. Hydrogenation was performed under a hydrogen atmosphere, and palladium on carbon was used as the catalyst. After deprotection of the benzyl group, the catalyst was removed using filtration through celite. Due to the high polarity and poor solubility in organic solvents, inhibitors **101**−**104** were purified using RP HPLC.

Following the successful synthesis of analogues of **25** containing a phosphonate group, it was decided to introduce different phosphate bioisosteres. From a list of potential bioisosteres, sulfonate and sulfonamide were chosen due to their simplicity and the commercial availability of amino sulfonic acid and amino sulfonamide starting materials.[8] For reaction with amino sulfonic acid, the same reaction conditions were used as for the reaction with phosphonic acids. However, for reactions with the amino sulfonamides, the aqueous solution was no longer required as these compounds were much more soluble in organic solvents, and the use of DMF or MeOH as a solvent was possible. The products **105**−**107** were purified using RP HPLC.

The synthesis of inhibitors **101−107** from NHS ester **100** resulted in relatively poor yields of between 14−44% after 2 steps, with the highest yields for the reactions with amino sulfonamides.

4.2.2. Testing of analogues of 25 containing phosphate bioisostere

After synthesising inhibitors in **Section 4.2.1**, the compounds in question were tested against SNM1A and SNM1B using a fluorescence-based assay (**Figure 4.9**).

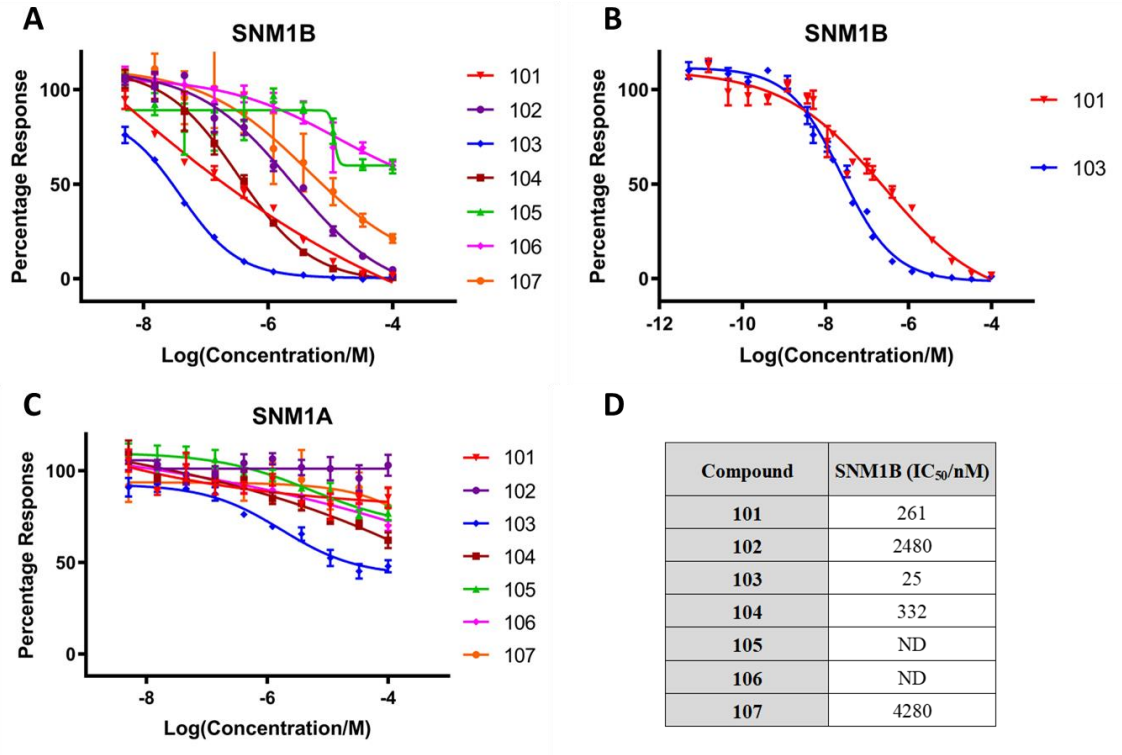

Compound	SNM1B (IC_{50}/nM)
101	261
102	2480
103	25
104	332
105	ND
106	ND
107	4280

Figure 4.9: A: *Dose-response curves for inhibitors* ***101-107*** *tested against SNM1B plotted using a real-time fluorescence assay.* ***B:*** *Dose-response curve for inhibitors* ***101*** *and* ***103*** *tested against SNM1B plotted the data from real-time fluorescence assay. The graph shows a curve over a wider range of concentrations of inhibitors.* ***C:*** *Dose-response curve for inhibitors* ***101−107*** *tested against SNM1A plotted the data from real-time fluorescence assay.* ***D:*** *Table of IC_{50} values calculated for inhibitors tested against SNM1B. Concentrations used [SNM1A] = 0.5 nM, [SNM1B] = 0.25 nM, and [DNA] = 25 nM. ND: Not determined.*

Initially, all inhibitors (**101−107**) were tested at concentrations ranging from 0.5 nM to 100 μM against both SNM1A and SNM1B; however, at 0.5 nM, inhibitors **101** and **103** still showed partial inhibition against SNM1B. Therefore, inhibitors **101** and **103** were tested at

a much wider range of concentrations, including at 5 pM. These experiments demonstrated that inhibitors containing the phosphonate functional group are exceptionally potent inhibitors of SNM1B, with compounds **101** (IC_{50} = 261 nM against SNM1B), **103** (IC_{50} = 25 nM against SNM1B), and **104** (IC_{50} = 332 nM against SNM1B) having IC_{50} values in the subnanomolar range. Compound **103** was the best inhibitor of this series with an IC_{50} of 25 nM, suggesting that it has its phosphonate group at the optimal linker length. **103** is the most potent inhibitor developed in this project overall. Sulfonate **107** (IC_{50} = 4280 nM against SNM1B) also showed inhibition against SNM1B, although it was lower than the comparable phosphonate, **103**. Inhibitors **105** and **106**, which contain the sulfonamide functional group, did not inhibit either SNM1A or SNM1B.

This series of compounds (**101**−**107**) was substantially more potent against SNM1B than SNM1A. None of the inhibitors tested against SNM1A showed complete inhibition, even at 100 μM. Inhibitor **103** was the most potent against SNM1A, but only displayed about 50% inhibition at 100 μM. Next, the phosphonate-based inhibitors (**101**−**104**) were tested against SNM1A and SNM1B using the gel-based assay (**Figure 4.10**).

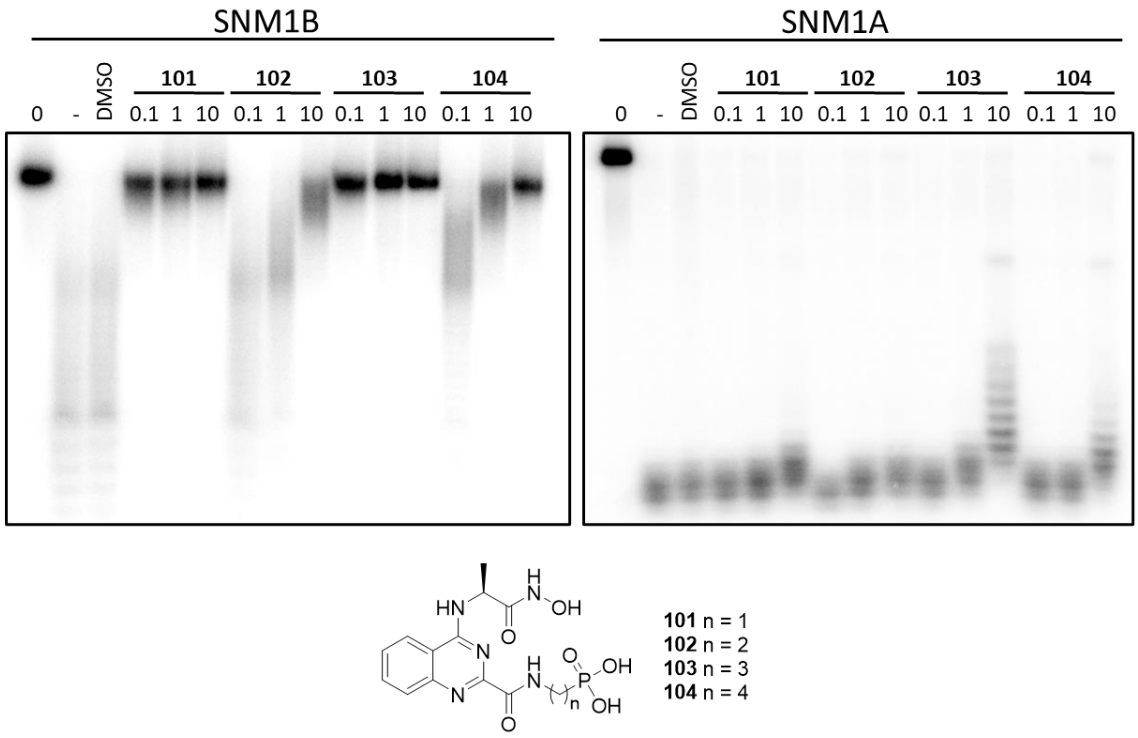

Figure 4.10: *Gel image from radioactive gel-based assays testing inhibitors* ***101-104*** *against SNM1A and SNM1B. The structure of tested inhibitors is shown below gels. Concentrations used [SNM1A] = 0.5 nM, [SNM1B] = 1.0 nM and [DNA 50-mer] = 10 nM. 2% DMSO was used as a control. The indicated inhibitor concentrations are in μM.*

Results from the gel-based assays with inhibitors containing a phosphonate group were reasonably consistent with the fluorescence-based assay. In both assays, these inhibitors were very potent against SNM1B, while showing insignificant inhibition of SNM1A. In the gel-based assay, it was observed that **101** showed substantially better inhibition than **104**, while in the fluorescence-based assay, these inhibitors had IC_{50} values of a similar magnitude. Similarly to the result obtained from the fluorescence-based assay, inhibitors **101** and **103** were the most potent compounds and showed almost complete inhibition at 0.1 μM in the gel-based assay with SNM1B. Therefore, it was decided to test these two inhibitors (**101** and **103**) in a gel-based assay with a wider concentration range (**Figure 4.11**).

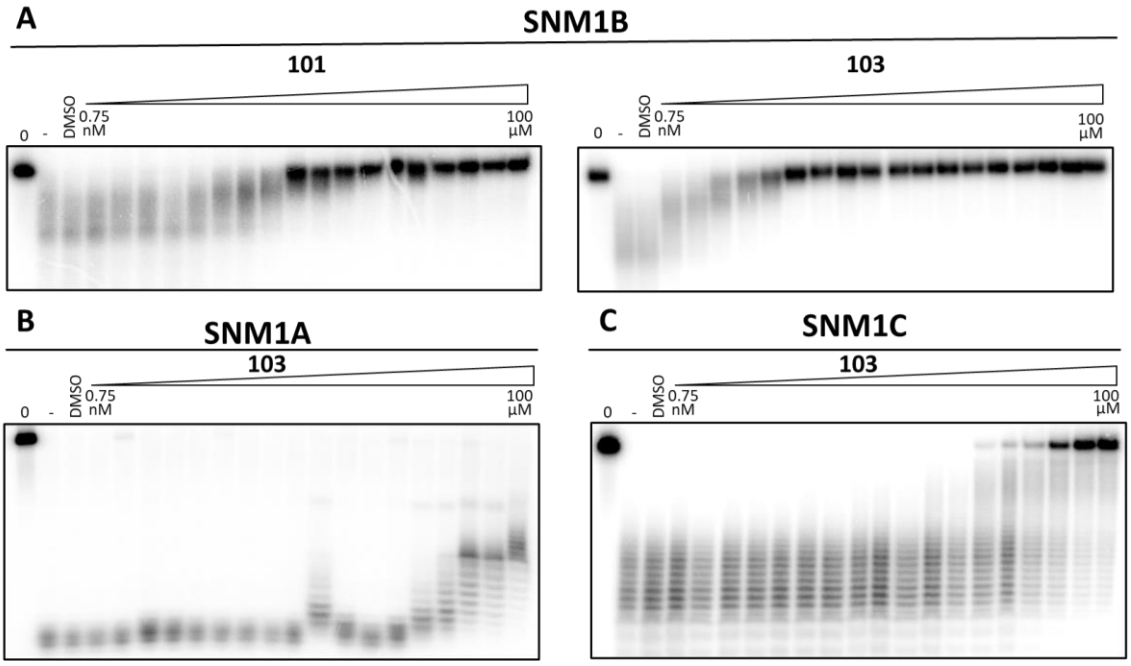

Figure 4.11: A: *Gel image from radioactive gel-based assays testing inhibitors* ***101*** *and* ***103*** *against SNM1B.* ***B:*** *Gel image from radioactive gel-based assays testing inhibitors* ***103*** *against SNM1A.* ***C:*** *Gel image from radioactive gel-based assays testing inhibitors* ***103*** *against SNM1C. Concentration used [Inhbitor] = two-fold dilutions (from 100 µM to 0.75 nM), [SNM1A] = 0.5 nM, [SNM1B] = 1.0 nM, [SNM1C] = 2.5nM and [DNA 50-mer] = 10 nM. 2% DMSO was used as a control.*

Further gel-based assays confirmed that inhibitor **103** is more potent than **101** against SNM1B. After **103** showed such an outstanding inhibition against SNM1B, it was decided to additionally test it against SNM1A and SNM1C at the wider concentration range using a gel-based assay. Unexpectedly, **103** was more potent against SNM1C than SNM1A, although SNM1C has no assigned phosphate-binding pocket. Still, **103** was a substantially better inhibitor of SNM1B than the remaining two enzymes. In the gel-based assays in **Figures 4.11A** and **4.11C**, inhibitors were tested at a wide range of concentrations, and a range of digestion products between no digestion and full digestion was observed; however, this was not the case for SNM1A. Therefore, it was decided to use the data from these gel-based assays to estimate IC_{50} values for SNM1B and SNM1C (**Figure 4.12B**).

Additionally, **103** was tested against SNM1C using a fluorescence-based assay **(Figure 4.12A**).

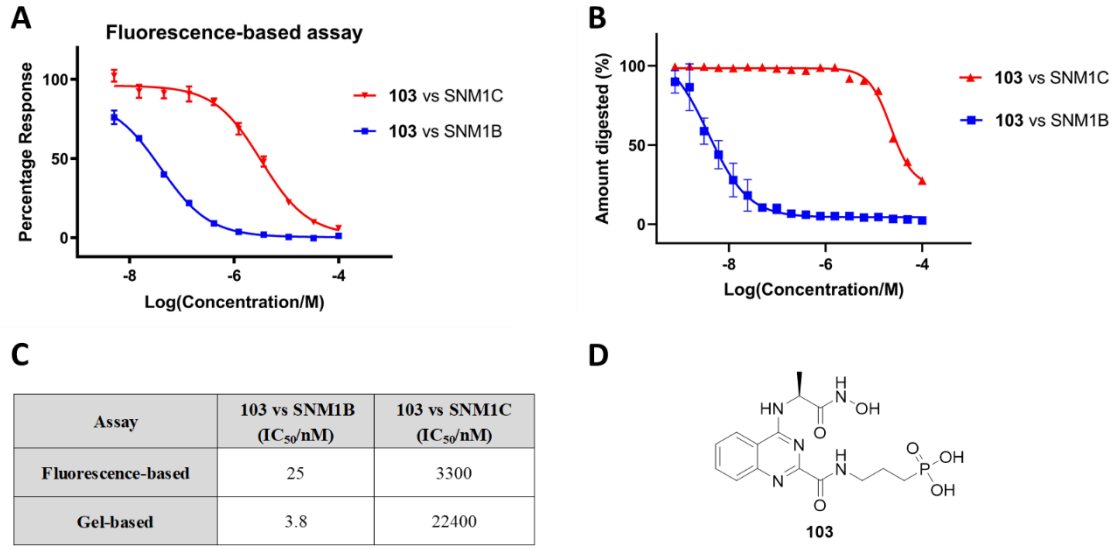

Assay	103 vs SNM1B (IC_{50}/nM)	103 vs SNM1C (IC_{50}/nM)
Fluorescence-based	25	3300
Gel-based	3.8	22400

Figure 4.12: A: *Dose-response curves for inhibitors **103** tested against SNM1B and SNM1C plotted using a real-time fluorescence assay. Concentrations used [SNM1B] = 0.25 nM, [SNM1C] = 5 nM, and [DNA] = 25 nM.* ***B:*** *Inhibition profile curves generated from gel-based assays with **103** against SNM1B and SNM1C in **Figure 4.11**. Digestion products from the gel-based assays were quantified and fitted to a dose-response curve using non-linear regression.* ***C:*** *IC_{50} values calculated using data from both fluorescence-based and gel-based assays.* ***D:*** *Structure of **103**.*

In both fluorescence-based and gel-based assays, **103** was more potent against SNM1B than SNM1C. Against SNM1B, the IC_{50} values for **103** were 3.8 nM and 25 nM in the gel-based and fluorescence-based assay, respectively, whilst against SNM1C, the IC_{50} values were 22400 nM and 3300 nM. Based on a gel-based assay, the estimated IC_{50} value for inhibitor **103** against SNM1C was more than 5000-fold higher than SNM1B. While, based on a fluorescence-based assay, the estimated IC_{50} value for inhibitor **103** against SNM1C was 130-fold higher than the value for SNM1B. Based on these IC_{50} values and lack of substantial inhibition of SNM1A, inhibitor **103** may be considered a selective inhibitor of SNM1B. Since inhibitor **103** was potent and selective against SNM1B in *in vitro* studies, it

was chosen as a candidate for a further round of testing to determine whether the obtained result would translate to cells.

The current data for the analogues of **25**, especially the structural data, suggested that **103** is a competitive inhibitor of SNM1B. To test this prediction, inhibitor **103** was tested at a range of different concentrations of DNA substrate. Data in **Figure 4.13** suggests that IC_{50} values for **103** increase as the concentration of substrate increases, thus confirming that **103** is indeed a substrate competitive inhibitor of SNM1B.

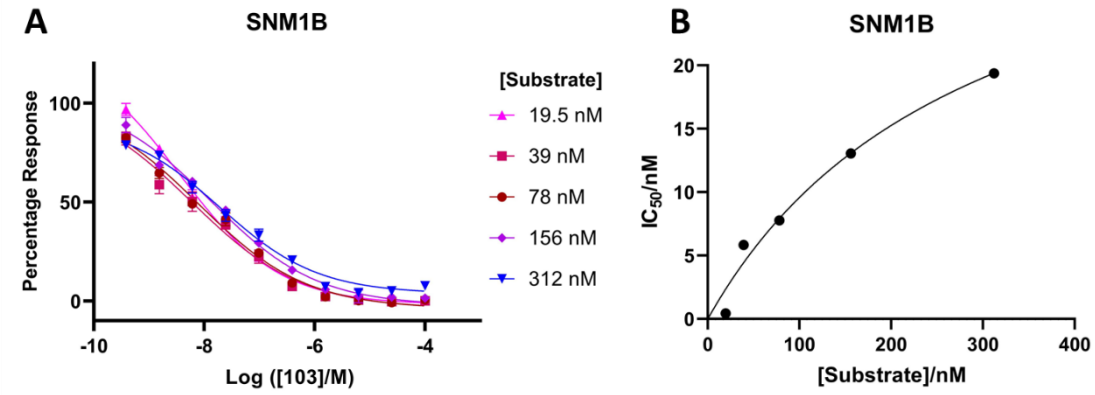

Figure 4.13: A: *Dose-response curves calculated for **103**, tested at different concentrations of DNA substrate against SNM1B. Tested using a fluorescence-based assay.* ***B:*** *IC_{50} values for **103** plotted against the substrate concentration. IC_{50} values were calculated using date from curves in **A**. [SNM1B] = 0.5 nM.*

4.2.3. Crystal structure of inhibitor 103 bound to SNM1B

A crystal structure of **103** bound to the active site of SNM1B was obtained by the co-crystallisation of SNM1B with **103** (**Figures 4.14** and **4.15**). As anticipated, the hydroxamic acid side chain interacts with the metals in the active site, while the phosphonate group interacts with the phosphate-binding pocket through hydrogen bonding. This occupation of the active site is also what would be anticipated for a substrate competitive inhibitor.

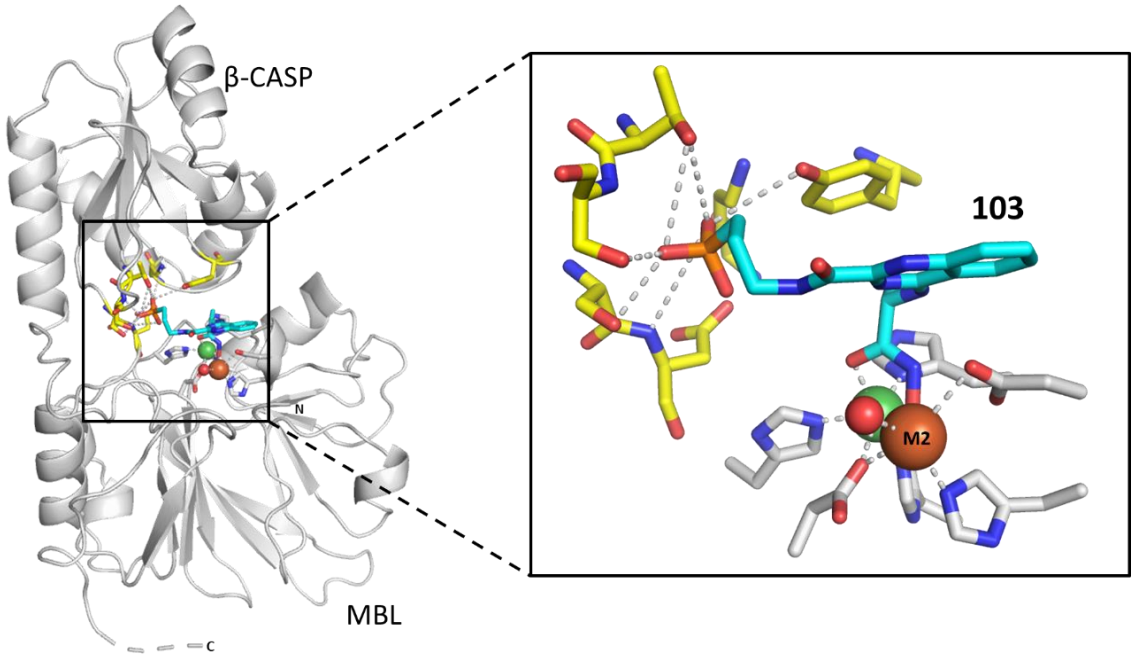

Figure 4.14: *Image from a structure of* ***103*** *bound to the active site of SNM1B. SNM1B depicted as a cartoon; and only amino acids involved in metal chelation and phosphate binding pocket are highlighted. Two domains, β-CASP and MBL domains are labelled. White amino acid side chains = amino acids involved in metal chelation. Yellow amino acids = phosphate-binding pocket.* ***C*** *= carboxyl terminus. N = amino terminus.* ***M1****: Nickel.* ***M2****: Iron.*

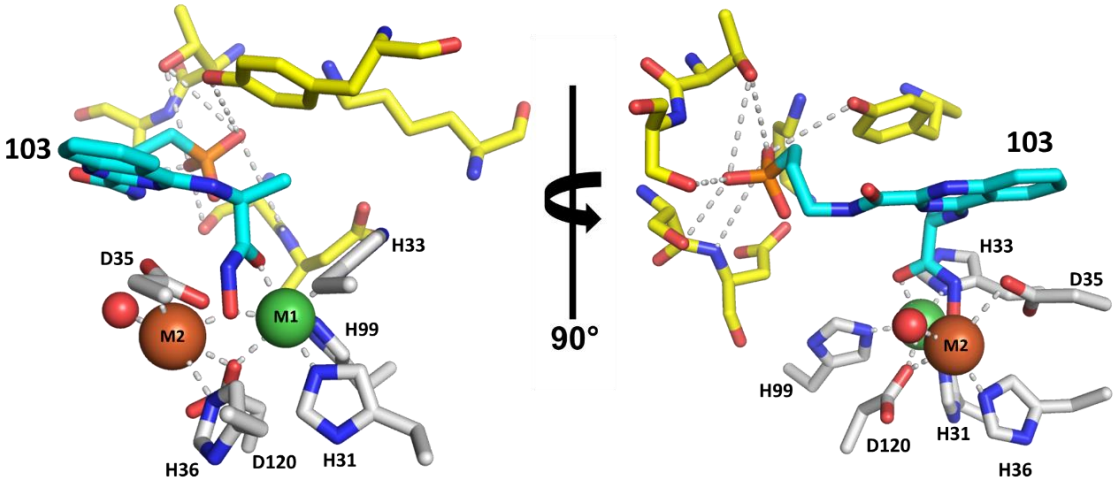

Figure 4.15: *Image from a structure of* ***103*** *bound to the active site of SNM1B with a focus on the metal chelation by* ***103****. Amino acids involved in metal chelation and phosphate binding pocket are high lighted. Amino acids involved in the metal chelation are labelled. White amino acid side chains = amino acids involved in metal chelation. Yellow amino acids = phosphate-binding pocket.* ***M1****: Nickel.* ***M2****: Iron*

The binding mode of the hydroxamic acid to the metals in the SNM1B active site is very similar to the binding observed in the crystal structures of hydroxamate-based inhibitors

bound to SNM1A in **Section 3.5**. Like with the crystal structures described in **Section 3.5**, the hydroxamic acid chelates the metals in the active site using both of its oxygen atoms. The hydroxyl group binds both metals and displaces the 'catalytic' water, whilst the carbonyl group chelates the metal **M1**. Metal **M1** has octahedral coordination, while metal **M2** square pyramidal coordination. Metal ions present in the active site of SNM1B inhibitor complex were assigned as a nickel for **M1** and iron for **M2**.

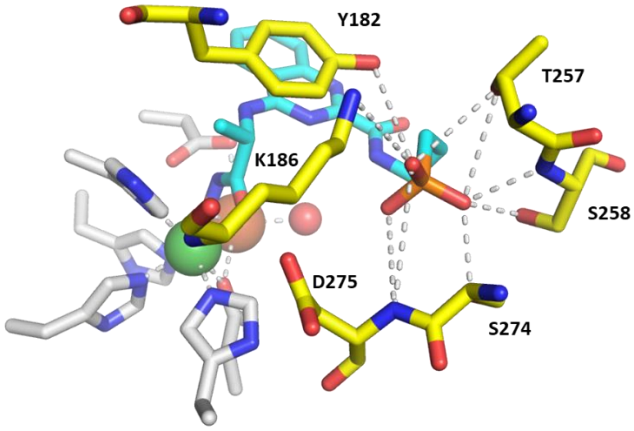

Figure 4.16: *Image of the structure of **103** bound to the active site of SNM1B with a focus on interactions between **103** and the phosphate-binding pocket. Amino acids involved in metal chelation and phosphate binding pocket are high lighted. Amino acids involved in the metal chelation are assigned. White amino acid side chains = amino acids involved in metal chelation. Yellow amino acids = phosphate-binding pocket*

As designed, the structure reveals the phosphonate side chain binding in the phosphate-binding pocket (**Figure 4.16**). The closest atoms of **Tyr182**, **Lys186**, **Thr257**, **Ser258**, **Ser274**, and **Asp275** are at a distance of 2.6−4.5 Å from the oxygen atoms of the phosphonate group. The phosphonate is positioned to form hydrogen bonds with hydroxyl groups in the side chains of **Tyr182**, **Thr257**, **Ser258** and **Ser278**; the amine from the **Lys186** side chain; and the nitrogen atom from the backbone amide bonds of **Ser258** and **Asp275**. As **103** appears to form hydrogen bonds with a large number of residues (which are also likely involved in a substrate binding), it is proposed that it may be challenging for

resistance to evolve, as this might require mutations to multiple amino acids, some of which are known to have a detrimental effect on the nuclease activity.[1] The crystal structure of **103** bound to SNM1B thus confirms that the inhibitor binds in the designed manner.

Before introducing the phosphonate group, the best inhibitor of SNM1B was **67**, with an IC_{50} value of 2.5 μM in the fluorescence-based assay. After introducing the phosphonate group, **103** became the best inhibitor with an IC_{50} value of 25 nM in the fluorescence-based assay, which represents a 100-fold increase in potency ones compared to **67**. The additional interactions with the phosphate-binding pocket likely explain the considerable increase in potency of **103** compared to inhibitors without the phosphonate group developed in **Chapter 3**.

Additionally, structural studies for inhibitor **103** and SNM1A were attempted to try and explain the selectivity of inhibitor **103**. In these studies, inhibitor **103** was soaked into the crystal of SNM1A, but no crystal structure with inhibitor bound was obtained. But by analysing the structures of SNM1A and SNM1B, the selectivity of inhibitors could be explained by slightly different positioning of the phosphate binding pocket in both enzymes. In SNM1A, the phosphate binding pocket is ~2 Å further away from the active site than in SNM1B. As well, based on structural studies, it is considered that the phosphate binding pocket in SNM1B is a higher affinity pocket.[1]

4.3. Development of prodrug of 103 and testing in cell-based assays

While inhibitor **103** showed promising results in the fluorescent-based and gel-based assays, concerns quickly arose about problems the phosphonate group may cause in a cell-based context. As phosphonate groups have a highly negative charge at physiological pH, diffusion

across the cell membrane by **103** might be very limited.[9] Therefore, it was planned to convert inhibitor **103** into a prodrug, which would have an improved bioavailability and could be easily metabolised back into **103** once inside the cell.

4.3.1. Synthesis of the prodrug

After a thorough review of phosphonate prodrugs, two prodrug modifications were chosen; pivaloyloxymethyl (POM) and isopropyloxycarbonyloxymethyl (POC).[10] These modifications can be found in the clinically used drugs, adefovir dipivoxil and tenofovir disoproxil, which are used to treat hepatitis B and HIV.[11,12] Both prodrug modifications are converted to their corresponding active drugs by esterases (**Figure 4.17**), particularly human carboxylesterase 2 (hCES2), which is expressed in a broad range of tissues and cell types.[13]

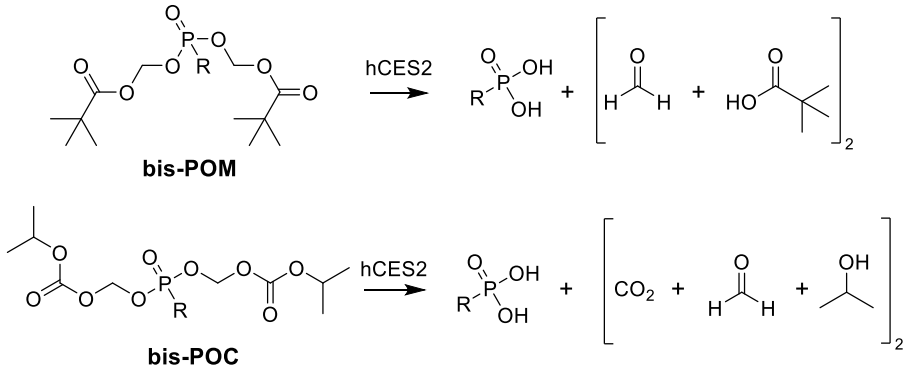

Figure 4.17: *Structure of bis-POM and bis-POC prodrugs, together with the products of prodrug cleavage.*

Two approaches for synthesising a prodrug of **103** were considered, as shown in **Figure 4.18**. The first approach was the conversion of a benzyl protected intermediate of **103** into its prodrug version through reaction with chloromethyl POC or POM. The second approach was to synthesise the POC/POM protected amino phosphonate and couple it with the active ester **100**. After both steps, benzyl deprotection would be required to produce the prodrug. Although the second approach has more steps than the first one, it was considered to be safer

since the risk of side reactions seemed lower. Additionally, it was thought that the phosphonic acid in the intermediate of **103** might cause solubility issues, and it might be challenging to purify larger quantities of it.

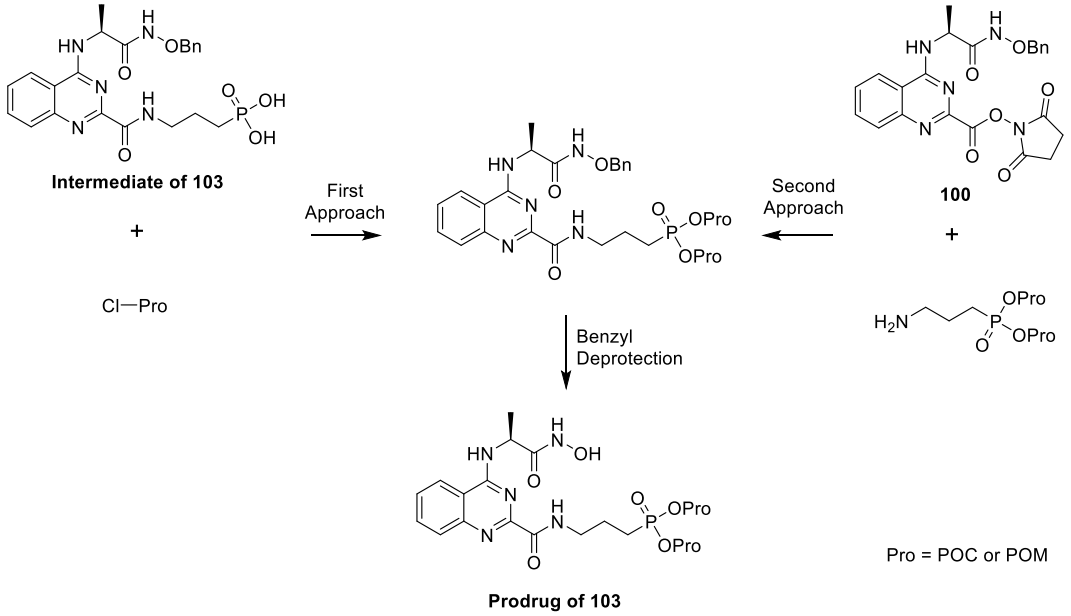

Figure 4.18: *Approaches considered for the synthesis of a prodrug of* ***103****.*

In the initial attempts to synthesise a POC and POM protected amino phosphonate, the POC modification appeared to be less stable and more prone to decomposition than POM. Therefore, it was decided to primarily focus on POM prodrug modification. The synthesis of POM protected amino phosphonate was partially based on a patent procedure, in which the synthesis of this compound is provided.[14] The primary difference between the patent route and that reported here was that in the patent, a CBZ group was used to protect the amine in synthesis, while in my route, an azide was used as a "masked amine". The final two steps of the prodrug synthesis, amide coupling and benzyl deprotection, were based on conditions previously used in the synthesis of inhibitors **101-107** described in **Section 4.2.1**.

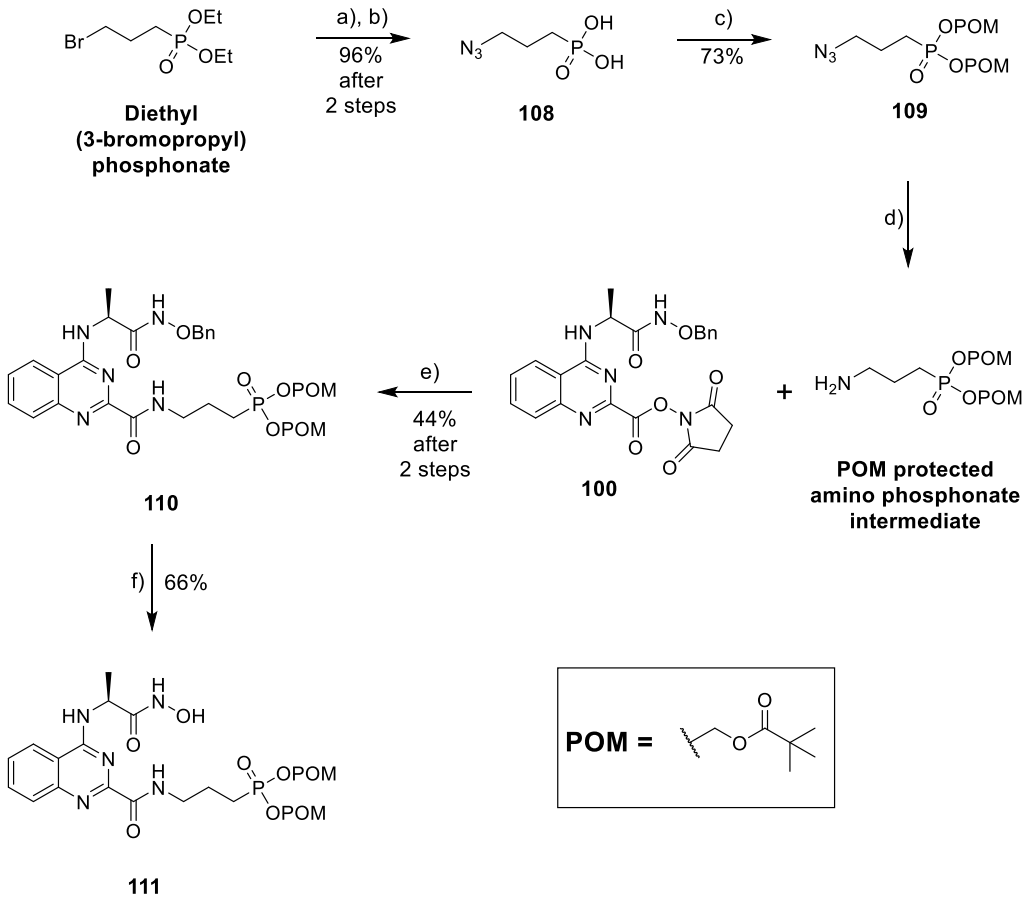

Figure 4.19: *Synthesis of prodrug* ***111****. Reaction conditions:* ***a)*** *NaN_3, acetone, reflux, 24 h;* ***b)*** *TMBS, MeCN, RT, 24 h, then MeOH/H_2O (9:1), RT, 16 h;* ***c)*** *Chloromethyl pivalate, MeCN, 60 °C, 40 h;* ***d)*** *PPh_3. H_2O, THF, RT, 12 h;* ***e)*** *TEA, DMF, −20 °C, 5 h;* ***f)*** *Pd/C, $H_{2(g)}$, MeOH, RT, 3 h.*

Synthesis of **108** from diethyl (3-bromopropyl)phosphonate was based on the literature procedure.[15] First, in step **a)**, nucleophilic substitution of bromide with azide was performed. Next, in step **b)**, dealkylation of the diethyl phosphonate using trimethylbromosilane (TMBS) was performed to produce **108**. Both steps **a)** and **b)** were very efficient and resulted in an excellent overall yield of 96% after 2 steps, and the only purification required was filtration after step **a)** to remove the salt precipitate. Protection of phosphonate in step **c)** was performed using previously reported conditions.[14] **108** was reacted under heating with chloromethyl pivalate to produce **109**. Compound **109** was purified using column chromatography and was produced at a good yield of 73%. To monitor reaction **c)**, a special

thin-layer chromatography (TLC) stain based on propargyl alcohol and copper (I) bromide had to be used.[16]

Initially, reduction of azide via hydrogenation using palladium on carbon as a catalyst was attempted. Unfortunately, partial decomposition was observed in the hydrogenation reaction, possibly caused by the free amine reacting with pivalate ester. It was then attempted to use the Staudinger reaction to reduce the azide, which resulted in substantially less decomposition being observed. However, the POM protected amino phosphate was relatively unstable and decomposed on the column chromatography or rotary evaporation. Therefore, the intermediate amine was not purified after the Staudinger reaction, but instead was dried under a nitrogen flow and then using a Schlenk line. The crude amine was then directly used for amide coupling with **100**. Amide coupling, step **e)**, had to be performed at −20 °C to prevent decomposition, resulting in an acceptable yield of 44% over 2 steps. As no purification was performed after the azide reduction (step **d)**), the triphenylphosphine oxide byproduct in the reaction mixture had to be removed after the amide coupling (step **e)**). Due to the difficulty of removing triphenylphosphine oxide and other side products, compound **110** required two consecutive column chromatography purifications. Finally, the benzyl group was removed under standard hydrogenation conditions using palladium on carbon as a catalyst, and resulting in a 66% yield. Again, two consecutive column chromatographies were required to purify prodrug **111** completely.

4.3.2. Testing of prodrug 111

Before testing the prodrug in a cell-based assay, it was first tested against SNM1B using the fluorescence-based and gel-based assays to determine how potent it was with the phosphonate group protected by POM esters (**Figure 4.20**). As predicted, in both assays,

prodrug **111** showed substantially lower inhibition than the corresponding inhibitor **103**. At the highest tested concentration of 100 μM, **111** showed only partial inhibition of SNM1B.

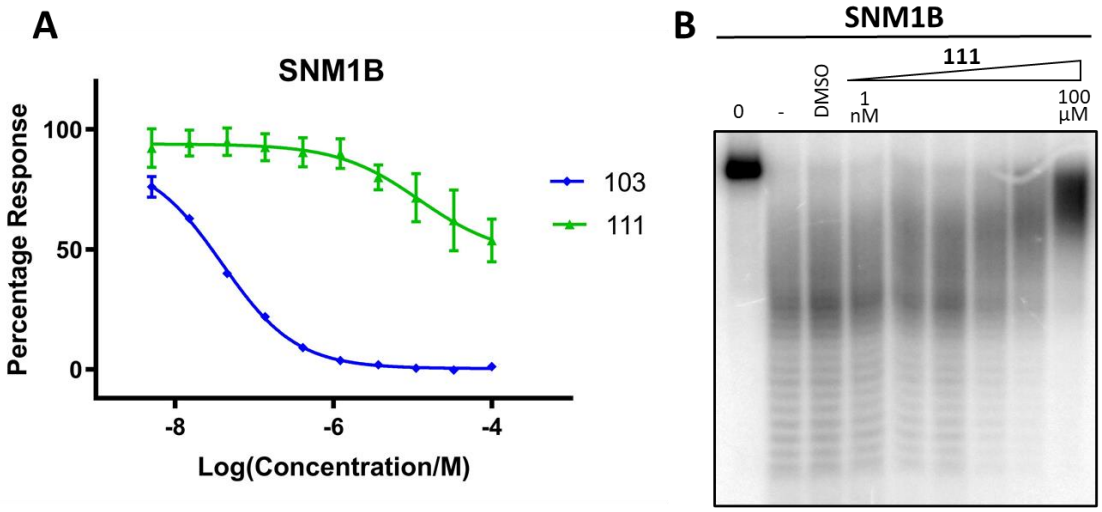

Figure 4.20: A: *Dose-response curves calculated for **103** and **111** tested against SNM1B. Concentrations used: [SNM1B] = 0.5 nM and [DNA] = 10 nM.* ***B:*** *Gel image from radioactive gel-based assays testing prodrug **111** against SNM1B. Concentration used [Inhbitor] = ten-fold dilutions (from 100 μM to 1 nM), [SNM1B] = 1.0 nM and [DNA 50-mer] = 10 nM. 2% DMSO was used as a control.*

Next, it was decided to investigate whether the prodrug is cleaved to release the active drug. Non-heat treated equine serum was used as a source of esterases to demonstrate the prodrug could be hydrolysed under biological conditions. The product of incubating the prodrug with equine serum was tested against SNM1B using a gel-based assay (**Figure 4.21**). The prodrug alone only showed partial inhibition at 100 μM, while the product of the incubation with equine serum showed much more potent inhibition. The potency of the metabolised prodrug increased with the incubation time, with the product after 4 hours nearly fully inhibiting SNM1B at 1, 10, 100 μM of the incubation product. Based on this result, it can be inferred that it is very probable that under the tested conditions, prodrug **111** is converted into SNM1B inhibitor **103**.

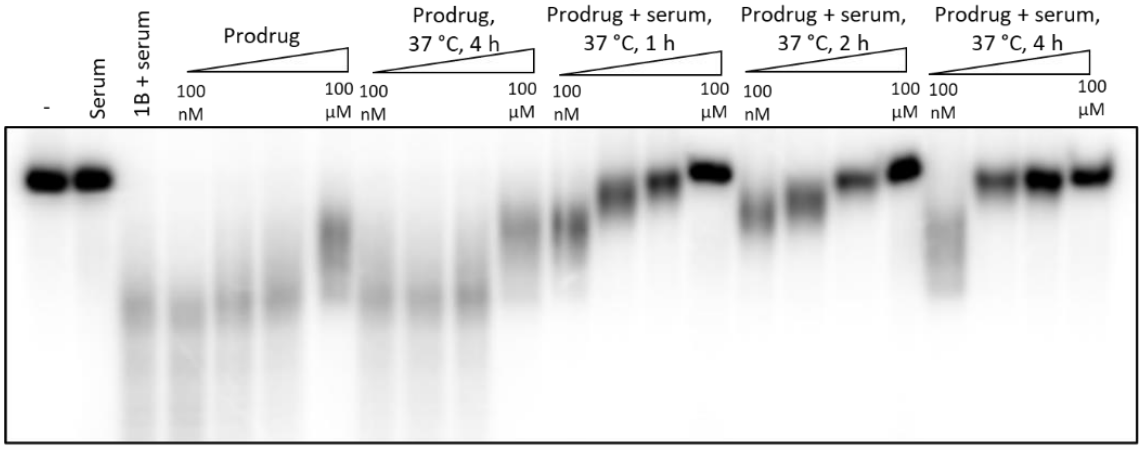

Figure 4.21: *Gel image from radioactive gel-based assays testing prodrug **111** and product of prodrug metabolism against SNM1B. Prodrug **111** was treated with and without equine serum. In the experiment where prodrug was treated with serum, 99% serum concentration was used. Concentrations used [Inhbitor] = ten-fold dilutions (from 100 µM to 100 nM), [SNM1B] = 1.0 nM and [DNA 50-mer] = 10 nM. Serum by itself was tested against SNM1B as a control.*

Next, the prodrug **111** was tested in cell survival assays. U2OS and HeLa cell lines were chosen for initial short-term cellular survival studies as they both have previously been used to study the role of SNM1B. [17] HeLa cells were used to produce SNM1B knockdown cells using siRNA, which were used for studies indicating the sensitivity of these cells towards ICL-inducing agents (MMC and cisplatin).[18] U2OS cell lines were used in studies investigating links between SNM1B and the Fanconi anaemia repair pathway. Initial testing focused on testing the effects of prodrug **111** compared to active inhibitor **103** (**Figures 4.22** and **4.23**).

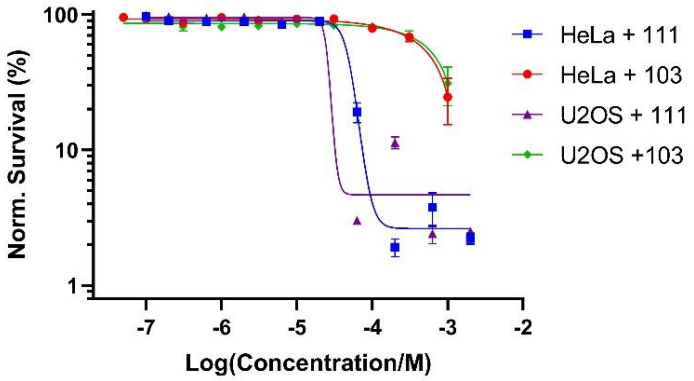

Figure 4.22: *HeLa and U2OS cells were treated with the indicated compound dosages, and 48 hour later, their cellular viability was assessed with a resazurin assay. Relative survival was normalized to untreated cells and fitted to a dose-response curve, plotted showing mean ± SEM of four technical replicates.*

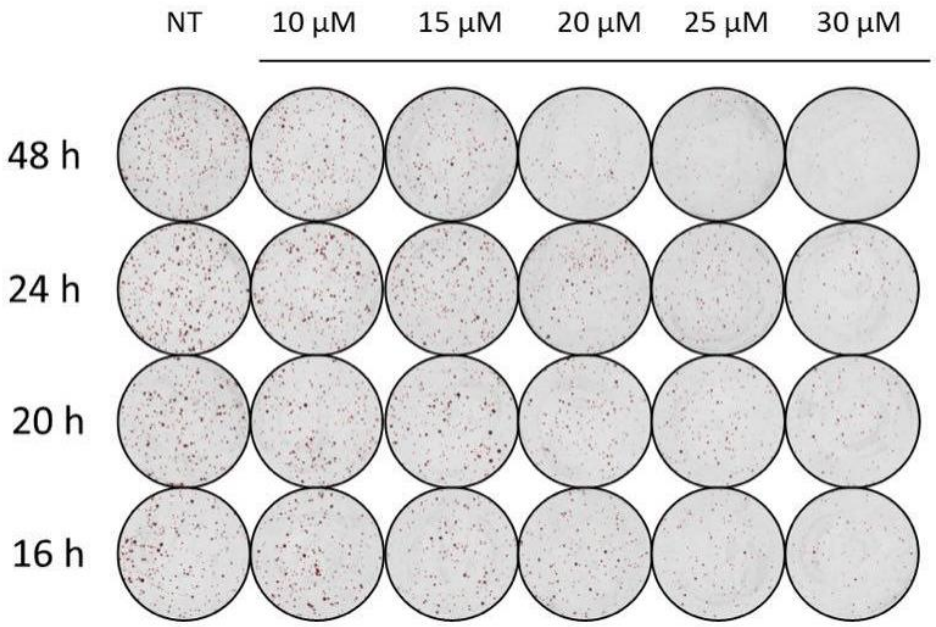

Figure 4.23: *Images of HeLa cells samples treated with the indicated compound dosages of prodrug* ***111****. Images were taken at time points 16 h, 20 h, 24 h and 48 h. Their cellular viability was assessed with a resazurin assay.*

The initial cellular survival study showed that prodrug **111** caused higher cellular toxicity than the corresponding active inhibitor **103**, in both U2OS and HeLa cell lines. Based on the images in **Figure 4.23**, it can be observed that there is a significant decrease in cell survivability at time point 48 hours and concentrations above 20 µM. Due to the increase in

the toxicity of the prodrug when compared to the **103**, it can be inferred that the prodrug is probably much more easily absorbed into the cell. As indicated in previous studies, the lack of SNM1B function in cells can cause genome instability and telomere dysfunction, which might explain the toxicity of the prodrug **111**.[19]

After seeing the encouraging result in this preliminary assay, it was decided to test whether the prodrug **111** sensitises cells towards DNA damaging agents via inhibition of SNM1B. The chosen genotoxic agents were cisplatin and zeocin, which induce interstrand crosslinks and double strand breaks, respectively, and to which SNM1B depleted cells have previously been shown to be sensitive. First, sublethal doses of cisplatin or zeocin were tested with a range of prodrug concentrations. Next, the sublethal dose of prodrug was tested with variable concentrations of cisplatin or zeocin. Cellular survival was again tested using U2OS and HeLa cell lines.

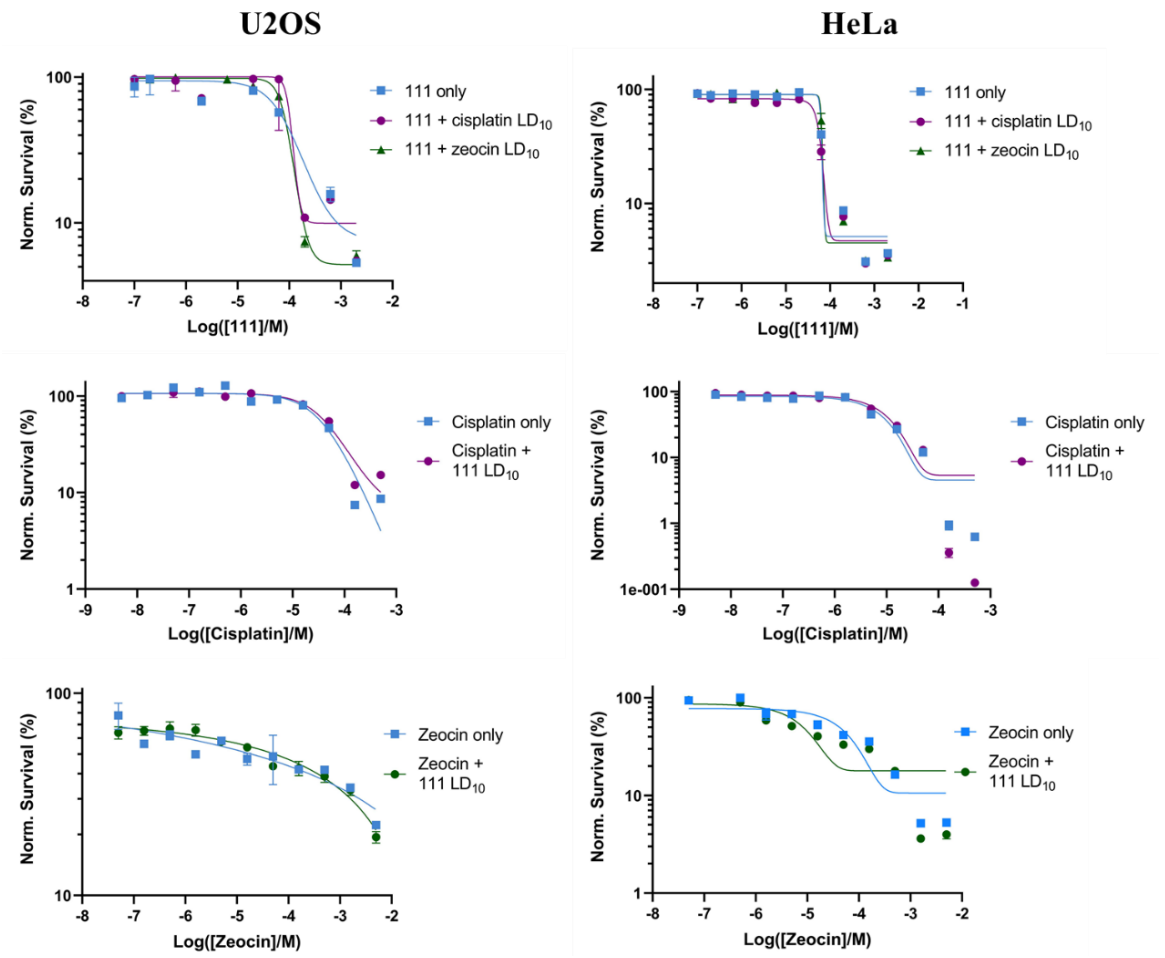

Figure 4.24: *Dose-response curves for testing synergy between prodrug **111** and genotoxic agents (cisplatin and zeocin). Cell survival was measured as in **Figure 4.22**. LD_{10}: lethal dose which kills 10% of cells.*

No synergistic effect between the genotoxic agents and prodrug **111** was observed in either of the cell lines used. While, a lack of synergy between prodrug **111** and zeocin might have been expected as the zeocin induces double strand breaks, and SNM1B is not involved in repairing this type of lesion. The synergy between prodrug **111** and cisplatin was anticipated, as cisplatin is ICL inducing drug.

The reasons why no sensitization of cells towards DNA damaging agents was observed can be connected to both issues with the prodrug or the target protein, SNM1B. Potential problems connected to prodrug **111** include prodrug not being properly cleaved to produce the active drug or the prodrug is being metabolised inside the cells.

As the role of SNM1B in DNA damage repair is not fully understood, it is difficult to precisely predict what biological effect inhibition of SNM1B would have on these cell lines and if it would be enough to sensitize the cells towards DNA damaging agents. Previous studies on interstrand crosslink repair have shown some genetic redundancy between SNM1B and SNM1A, which might cause that inhibition of SNM1B by itself might not be enough to sensitize the cell towards cisplatin.[3]

4.3.3. Problems with the decomposition of prodrug 111

Throughout the testing of prodrug **111**, stability issues were encountered, primarily the decomposition of the hydroxamic acid group. Different decomposition products were identified while testing the stability of prodrug **111** and investigating the products of its ester hydrolysis by hCES2. The prodrug was treated with and without hCES2 esterase, and LC-MS was used to analyse the sample after 30 minutes and 24 hours. Identified masses and their predicted corresponding decomposition and ester hydrolysis products are shown in **Figure 4.24**.

A

Condition	Mass Observed	Corresponds to
30 min, HEPES only	596.23 (99%)	**Intermediate 1**: Loss of formaldehyde
24 h, HEPES only	425.14 (99%)	**Decompositon product 1**: Cleavage of one POM and loss of hydroxamic acid.
30 min, hCES2	512.18 (74%)	**Intermediate 2**: Cleavage of one POM
	596.23 (26%)	**Intermediate 1**: Loss of formaldehyde
24 h, hCES2	398.12 (major peak)	**103**: active drug
	311.08 (major peak)	**Decomposition product 2**: Cleavage of two POMs and loss of hydroxamic acid

B

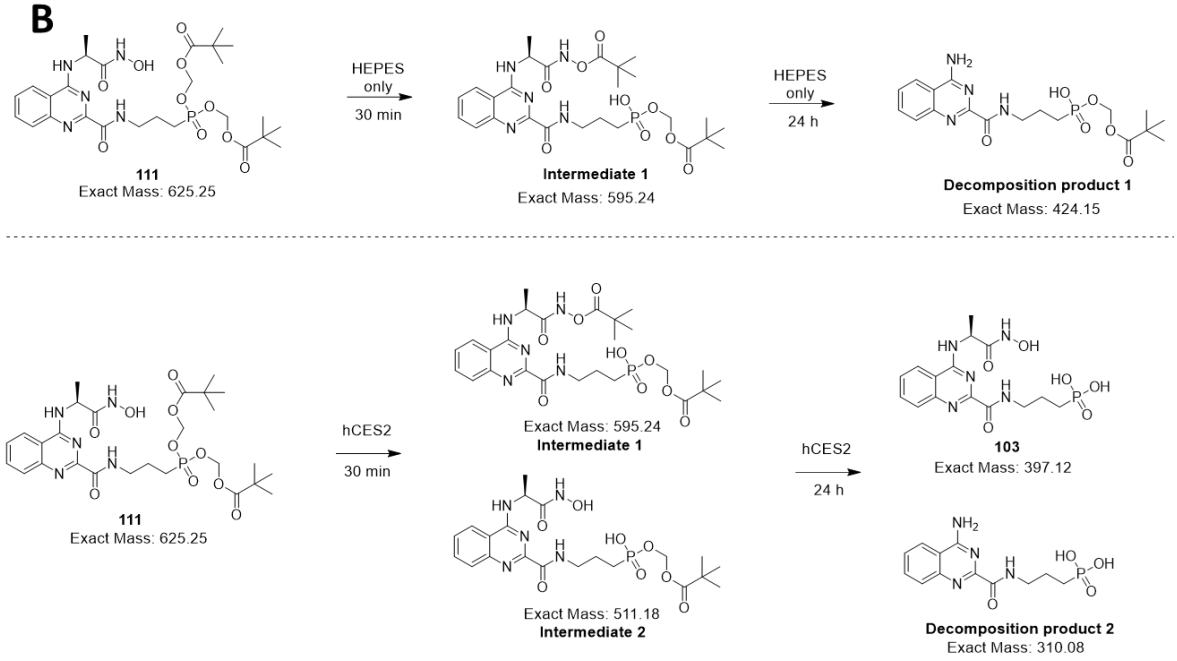

Figure 4.25: A: *Table with masses observed after treatment of prodrug* ***111*** *with ± hCES2 in 50 mM HEPES-KOH (pH 7.5) and incubated for either 30 min or 24 h at 37°C. The masses were found using positive ion mode MS analysis.* ***B:*** *Predicted structures of products formed after treatment of prodrug* ***111*** *with ± hCES2. The mass corresponding to each proposed structure is given.*

When prodrug **111** was treated only with HEPES-KOH (pH 7.5) buffer at 37°C, two different mass species were observed: 596.23 and 425.14, which were detected after 30 minutes and 24 hours, respectively. The mass 596.23 species corresponds to a loss of formaldehyde from **111**, identifying the potential structure of this **intermediate 1** was more challenging. Similarly, determining the structure of **decomposition product 1** was difficult, but decomposition of the hydroxamic acid was recognized as a potential source of the mass loss. Decomposition via Lossen rearrangement has been implicated for hydroxamate-based

HDAC inhibitors and is considered the reason for hydroxamate mutagenicity.[20] Subsequently, it was identified that mass 425.14 corresponds to the decomposition of the hydroxamic acid via Lossen rearrangement and the loss of one POM protecting group.

Additionally, after considering Lossen rearrangement as the decomposition source, it was identified that the loss of formaldehyde observed in the **intermediate I** is most probably caused by a reaction between the hydroxamic acid with the POM protecting group. Formation of the pivalate ester with a hydroxyl group from the hydroxamic acid would make the hydroxyl group a better leaving group and thus promote decomposition.[21] A potential mechanism of decomposition of the hydroxamic acid via Lossen rearrangement is shown in **Figure 4.25**.

At the same time, when active inhibitor **103** was treated with HEPES-KOH (pH 7.5) buffer at 37°C for 24 hours, no noticeable decomposition was observed. The higher stability of **103** compared to prodrug **111** implies the involvement of the POM modification via Lossen rearrangement causing overall decomposition of the prodrug.

As expected, after treating prodrug **111** with hCES2 for 24 hours, a mass of 398.12, which corresponds to the active drug **103**, was observed. A second mass of 311.08 was also found in the major peak, which probably corresponds to **decomposition product 2** (**103** after loss of its hydroxamic acid). Unfortunately, the exact ratio between the two products could not be determined, as they were observed in a single overlapping peak. After 30 minutes of treatment with hCES2, in addition to finding a mass corresponding to **intermediate 1**, a mass of 512.18 was observed. The species with a mass of 512.18 was proposed to be

intermediate 2, a product of cleavage of the first POM protecting group. After 30 minutes the species with the mass of **intermediate 2** was observed as the major product.

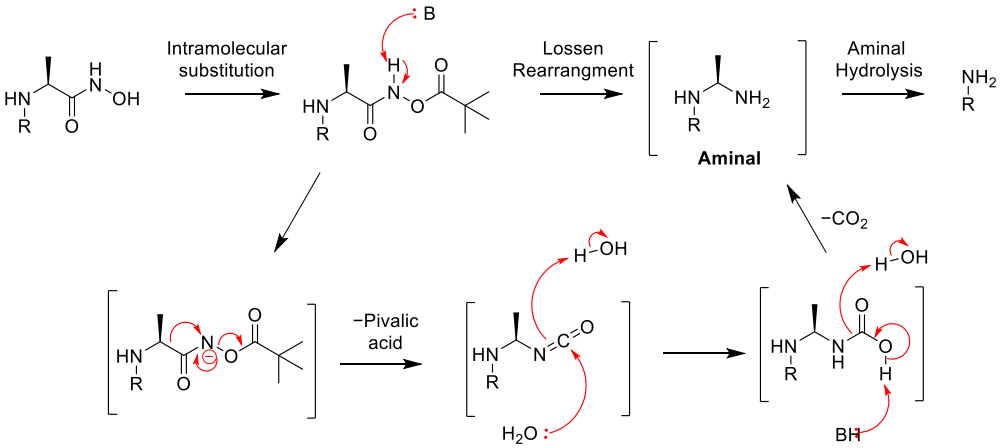

Figure 4.26: *Proposed mechanism of decomposition of hydroxamic acid via Lossen rearrangement. As the rearrangement transforms the hydroxamic acid into an amine, an aminal is produced by the rearrangement. In the final proposed step of decomposition, the aminal is hydrolysed. B: Base.*

While this experiment confirmed that hCES2 is capable of cleaving the POM protecting group in prodrug **111** to release active inhibitor **103**, the overall stability of the prodrug, especially of the hydroxamic acid functional group, is a concern. Further experiments are required to characterise the stability of this prodrug. As the intermediates and decomposition products were identified by mass spectrometric studies, additional spectroscopic techniques, such as NMR, could be used to confirm the corresponding structures.

4.4. References

[1] H. T. Baddock, J. A. Newman, Y. Yosaatmadja, M. Bielinski, C. J. Schofield, O. Gileadi and P. J. McHugh, *Nucleic Acids Research*, 2021, **49**, 9294–9309.
[2] J. M. Pei, B. H. Kim and N. V. Grishin, *Nucleic Acids Res*, 2008, **36**, 2295-2300.
[3] B. Sengerová, C. K. Allerston, M. Abu, S. Y. Lee, J. Hartley, K. Kiakos, C. J. Schofield, J. A. Hartley, O. Gileadi and P. J. Mchugh, *Journal of Biological Chemistry*, 2012, **287**, 26254–26267.

[4] A. Y. Chen, P. W. Thomas, Z. Cheng, N. Y. Xu, D. L. Tierney, M. W. Crowder, W. Fast and S. M. Cohen, *ChemMedChem*, 2019, **14**, 1271–1282.
[5] O. A. Pemberton, P. Jaishankar, A. Akhtar, J. L. Adams, L. N. Shaw, A. R. Renslo and Y. Chen, *Journal of Medicinal Chemistry*, 2019, **62**, 8480–8496.
[6] H. Yu, H. Yang, E. Shi and W. Tang, *Med Drug Discov*, 2020, **8**, 100063.
[7] J.-T. Wang, T.-C. Lin, Y.-H. Chen, C.-H. Lin and J.-M. Fang, *MedChemComm*, 2013, **4**, 783.
[8] T. S. Elliott, A. Slowey, Y. Ye and S. J. Conway, *MedChemComm*, 2012, **3**, 735.
[9] A. J. Wiemer and D. F. Wiemer, *Top Curr Chem*, 2015, **360**, 115-160.
[10] K. M. Heidel and C. S. Dowd, *Future Med Chem*, 2019, **11**, 1625-1643.
[11] T. M. Dando and G. L. Plosker, *Drugs*, 2003, **63**, 2215–2234.
[12] K. A. Lyseng-Williamson, N. A. Reynolds and G. L. Plosker, *Drugs*, 2005, **65**, 413–432.
[13] S. Casey Laizure, V. Herring, Z. Hu, K. Witbrodt and R. B. Parker, *Pharmacotherapy: The Journal of Human Pharmacology and Drug Therapy*, 2013, **33**, 210–222.
[14] WO 2012150866
[15] A. K. Tucker-Schwartz and R. L. Garrell, *Chemistry – A European Journal*, 2010, **16**, 12718–12726.
[16] T. Schröder, M. Gartner, T. Grab and S. Bräse, *Organic & Biomolecular Chemistry*, 2007, **5**, 2767.
[17] I. Demuth, P. S. Bradshaw, A. Lindner, M. Anders, S. Heinrich, J. Kallenbach, K. Schmelz, M. Digweed, M. S. Meyn and P. Concannon, *DNA Repair*, 2008, **7**, 1192–1201.
[18] I. Demuth, M. Digweed and P. Concannon, *Oncogene*, 2004, **23**, 8611-8618.
[19] Y. C. Lam, S. Akhter, P. Gu, J. Ye, A. Poulet, M.-J. Giraud-Panis, S. M. Bailey, E. Gilson, R. J. Legerski and S. Chang, *The EMBO Journal*, 2010, **29**, 2230-2241.
[20] S. Shen and A. P. Kozikowski, *ChemMedChem*, 2016, **11**, 15–21.
[21] M. Thomas, J. Alsarraf, N. Araji, I. Tranoy-Opalinski, B. Renoux and S. Papot, *Organic & Biomolecular Chemistry*, 2019, **17**, 5420–5427.

Chapter 5. Conclusions

In summary, in this project a novel series of hydroxamate-based inhibitors that inhibit SNM1A, SNM1B and SNM1C nucleases was successfully developed using hits from a high-throughput screen. The most potent and promising inhibitor from this series was **103**, which manifests selective inhibition of SNM1B.

The studies described in **Chapter 2** primarily focused on the cyclic hydroxamate inhibitors. The initial cyclic hydroxamate hit **3** was chosen because of its very promising potency, with IC_{50} values of 2.4 μM (for SNM1A), 1.9 μM (for SNM1B) and 0.37 μM (for SNM1C). Attempts to optimize hit **3** resulted in only a small potency increase, as shown for inhibitor **12**, which had an IC_{50} of 1.2 μM against SNM1A. Due to a minimal improvement in potency and accompanying issues with drug-like properties, such as solubility, the further development of cyclic hydroxamate inhibitors was halted. While the development of cyclic hydroxamates inhibitors was unfruitful, it helped identify the hydroxamate group as an interesting pharmacophore for targeting SNM1A, SNM1B and SNM1C.

As described in **Chapter 3**, subsequent studies focused on optimization of hit **25**, which had an IC_{50} of 129 μM. Although hit **25** was ~50-fold less potent than hit **3**, compound **25** was much easier to modify, which allowed for an efficient synthesis of a set of analogues of **25**. Hit **25** was based on 2,4,6-trisubstituted quinazoline, and positions 2, 4 and 6 of quinazoline core were optimised. As described in **Chapter 3**, 31 analogues of **25** were developed and tested. Out of all modifications of **25**, the most important and resulting with the highest potency increase was the introduction of hydroxamic acid, inspired by cyclic hydroxamate inhibitors from **Chapter 2**. The optimisations of hit **25** resulted in inhibitor **42**, which had

IC_{50} of 0.8 μM, and which is, therefore, ~160-fold more potent than **25**. Inhibitors developed in **Chapter 3** were also inhibitory against SNM1B and SNM1C. Inhibitor **67** was the most potent against SNM1B and SNM1C, with an IC_{50} value of 2.5 μM and 3.5 μM, respectively. While poor selectivity of these inhibitors was a big concern, the successful determination of crystal structures of inhibitors **42**, **51**, **67**, and **78** bound to the active site of SNM1A provided important structural information that could be utilised to optimise these inhibitors further through the structure-based design.

In **Chapter 4,** further optimization of the quinazoline inhibitors, initially explored in **Chapter 3**, was described. The use of structural information and identification of the phosphate-binding pocket as a potential target was crucial for the optimisation of the quinazoline inhibitors. The inhibitors targeting phosphate-binding pockets, **101-107**, were designed against SNM1A and SNM1B. Inhibitors **101-107** showed only substantial potency against SNM1B, with **103** being the most potent inhibitor developed in this project. Inhibitor **103** had IC_{50} of 25 nM and 3.8 nM in fluorescence-based and gel-based assays against SNM1B, respectively. At the same time, inhibitor **103** showed a very low and incomplete inhibition against SNM1A, and **103** was 130−5000-fold less potent against SNM1C compared to SNM1B**.** While inhibitor **103** was potent and selective against SNM1B using assays that relied on purified, recombinant enzymes, the attempt to achieve a similar result in a biological system, namely human cell lines, was more challenging and proved unsuccessful.

Inhibitor **103** had to be modified into a prodrug form for cellular studies due to potential issues with its cell permeability. The synthesis of prodrug **111** was successful, and a noticeable biological effect was observed when tested in a cell survival assay. Unfortunately,

prodrug **111** was not observed to sensitise cells towards genotoxic agents, therefore making inhibition of SNM1B and ICL repair by **111** doubtful in cells. Additional issues arose when prodrug **111** was treated with ±hCES2 esterase to examine the release of the active inhibitor **103**. In addition to the release of the active inhibitor **103**, different decomposition products were observed. The apparent instability of prodrug **111** might explain why the anticipated synergy between the SNM1B inhibitor and genotoxic agents was not detected. As decomposition was only observed in prodrug **111** and not in the corresponding active drug **103**, the instability of the prodrug is most likely caused by the presence of pivaloyloxymethyl (POM) modification. Therefore, the primary goal of future work should be finding a prodrug modification that would be more stable and less likely to cause undesired decomposition of the prodrug. Fortunately, various phosphonate modifications have been developed over the years and are now commonly used in prodrugs. Potential phosphonate prodrug modifications which could be introduced include CycloSal, ProTide or HepDirect.[1] Each of the modifications has its specific mechanism of cleavage, which usually requires a specific enzyme to release the active drug. The ProTide motif seems to be the most promising out of the prodrug approaches as it is known for good *in vivo* stability and is commonly used in clinically used nucleotide-based drugs, such as remdesivir.

Additionally, instead of converting inhibitor **103** into a prodrug to overcome issues with cell permeability, a drug delivery system such as Lipofectamine, commonly for transfection of nucleic acids, could be used. Drug delivery systems like Lipofectamine forms liposomes that can encapsulate non-cell permeable molecules (*e.g* RNA). The liposomes are then able to transport the load across the cell membrane and release it inside the cell.[2]

Further more use of hydroxamic acid pharmacophore might have to be reconsidered. Although hydroxamic acids are present in clinically used drugs, notably in hydroxamate-based histone deacetylase inhibitors, there is substantial concern about the mutagenicity linked to the decomposition of the hydroxamic acid inside cells.[3] Therefore, substituting hydroxamic acid with some other metal-chelating pharmacophore might be required to improve the stability. Needless to say, the stability of the prodrug is only one of many properties that might need to be improved before any drug candidate against SNM1A, SNM1B, or SNM1C can be developed.[4]

---

[1] K. M. Heidel and C. S. Dowd, *Future Med Chem*, 2019, **11**, 1625-1643.
[2] X. Pan, H. Veroniaina, N. Su, K. Sha, F. Jiang, Z. Wu and X. Qi, *Asian Journal of Pharmaceutical Sciences*, 2021, **16**, 687-703.
[3] S. Shen and A. P. Kozikowski, *ChemMedChem*, 2016, **11**, 15–21.
[4] L. Di, E. H. Kerns and G. T. Carter, *Curr Pharm Des*, 2009, **15**, 2184-2194.

Chapter 6. Materials and Methods

6.1. Procedures biochemistry

Protein purification – standard procedure (using IMAC)

SNM1A, SNM1B, and SNM1C proteins were purified from insect cells using previously reported protocols by Dr Hannah Baddock (Weatherall Institute of Molecular Medicine (WIMM), University of Oxford), Dr Joseph Newman (SGC) and Dr Yuliana Yosaatmadja (SGC) in the Structural Genomics Consortium (SGC), University of Oxford.[1,2]

Protein purification – non-IMAC purified SNM1A

Cloning and expression are the same as for **Protein purification – standard procedure (using IMAC)** but different in the purification procedure.

Thawed cell aliquots were lysed by sonication in lysis buffer (50 mM HEPES, pH 7.5, 5% glycerol (v/v), 500 mM NaCl, 1 mM TCEP, supplemented with protease inhibitors) before the lysates were cleared by centrifugation (40 000 x g, 30 min). The supernatant was concentrated, passed through a 0.45 um membrane (Millipore) and then diluted to obtain a buffer concentration of 100 mM NaCl before passing through an ion exchange column (HiTrap SP FF GE Healthcare Life Sciences) pre-equilibrated in the SP buffer A (50 mM HEPES, 100 mM NaCl, 5% glycerol, and 1 mM TCEP. Protein was eluted using a linear gradient to SP buffer B (SP buffer A with 1 M NaCl) and fractions containing the SNM1A protein were identified by SDS-PAGE. Protein-containing fractions were pooled, concentrated, and diluted in SP buffer A before being loaded onto a HiTrap-Heparin HP column (GE Healthcare Life Sciences). Protein containing fractions (as determined by

absorbance at 280 nm and SDS-PAGE) were again pooled, and the histidine tag was cleaved by incubation with TEV protease (at a 20:1 SNM1A:TEV mass ratio) overnight, at 4oC, whilst being dialysed using a 3.5 kDa molecular weight cut-off snakeskin membrane (ThermoFisher Scientific) into a buffer containing 50 mM HEPES, 500 mM NaCl, 5% glycerol, 1 mM TCEP. SNM1A proteins were further purified by size exclusion chromatography using an AKTA Express S75 Superdex column (GE, LifeSciences) in a buffer containing 50 mM HEPES, pH 7.5, 500 mM NaCl, 5% glycerol, 1 mM TCEP.

X-ray crystallography: SNM1A

Protein crystallization was performed by vapour diffusion in sitting drops at 4°. A protein solution at 9-10 mg/mL was mixed 100 nL of protein (10mg/mL) and 50nL of reservoir solution containing 30% PEG 1000, 0.1M MIB pH 6.0 (MIB is sodium malonate dibasic monohydrate, imidazole, boric acid buffer). The crystals contained malonate bound to the active site. For soaking compound into the active site, the crystals were first incubated overnight in malonate-free liquor (30% (v/v) PEG, 0.1 M HEPES, pH 7.0) to remove the malonate at the active site; compounds were subsequently soaked overnight at a final concentration of approximately 20 mM before harvesting and cryo-cooling. Crystals were harvested by loop mounting, and directly plunging into liquid nitrogen X-ray crystallographic was performed at the Diamond Light Source. This work was done by Dr Joseph Newman and Dr Yuliana Yosaatmadja.

X-ray crystallography: SNM1B with 103

Crystallisation of SNM1B in complex with **103** was achieved by sitting drop vapour diffusion, at 4°C, in conditions containing 6% PEG6K -- 0.1M MES pH 6.5. SNM1B was incubated at 10 mg/mL with 1 mM of **103** for 10 min on ice for 10 minutes before crystallization. Crystals were cryoprotected in the reservoir solution supplemented with 20% ethylene glycol, and plunged into liquid nitrogen. X-ray crystallography was performed in Diamond. This work was done by Dr Joseph Newman.

Real-time fluorescence assays

The protocol was carried out according to the previously reported procedure.[3] Briefly, reactions were carried out in black 384-well microplates (Corning, USA) in a total volume of 25 μL per well. An ssDNA substrate (**DNA1** for SNM1A and SNM1B or **DNA2** for SNM1C) containing a 5' FITC-conjugated T and an internal BHQ-conjugated T was used. The reaction comprised 25 nM DNA substrate, indicated amounts of protein (SNM1A, SNM1B or SNM1C), and reaction buffer: 20 mM HEPES-KOH (pH 7.5), 10 mM $MgCl_2$, 50 mM KCl, 0.5 mM TCEP, 0.05% Triton X-100, and 5% (v/v) glycerol. Inhibitors were solubilised in DMSO and serially diluted to desired inhibitor concentration with DMSO concentration kept at a constant 1% (v/v) in the final reaction mixture. Proteins were incubated for 10 min at RT with the stated compound where applicable, before the reaction was started with the addition of DNA substrate. The fluorescence spectra were measured every 150 s, for 35 min, at 37 °C with a PHERAstar FSX (BMG Labtech) (excitation 495 nm, emission 525 nm).

The real-time fluorescence assays were carried out together with Dr Hannah Baddock and Lucy Henderson.

Calculation of IC_{50}s

The enzymatic activity of the appropriate enzyme was determined using the real-time fluorescence assay in the presence of 0−100 μM or 0−250 μM of each compound. The fluorescence intensity for each reaction was plotted against time, and the rate of increase in fluorescence was determined. This was normalised to the untreated enzyme control and plotted against compound concentration. The resulting values were fitted to an inhibitor–response curve to determine IC50 values using Prism software (GraphPad Software, Inc., La Jolla, CA, USA.

Generation of 3′ radiolabelled DNA substrates

10 pmol of ssDNA (**DNA3** (20-mer) or **DNA4** (51-mer) was labelled with 3.3 pmol α32P-dATP by incubation with terminal deoxynucleotidyl transferase (20 U TdT, ThermoFisher Scientific) for 1 h at 37 °C. The solution was then passed through a P6 Micro Bio-Spin column (BioRad), before diluting as appropriate for radioactive gel-based assays.

Gel-based nuclease activity assays

The protocol was carried out according to the previously reported procedure.[3] Nuclease reactions were carried out in 10 μL volumes containing 20 mM HEPES-KOH (pH 7.5), 10 mM $MgCl_2$, 50 mM KCl, 0.5 mM TCEP, 0.05% Triton X-100, 5% glycerol and indicated amounts of protein (SNM1A, SNM1B or SNM1C). Inhibitors were solubilised in DMSO and serially diluted to desired inhibitor concentration with DMSO concentration kept at a

constant 0.2% in the final reaction. Inhibitors were pre-incubated for 10 min at RT with the protein of interest, before reactions were started with the addition of 10 nM DNA substrate and allowed to react at 37 °C for 40 min. Reactions were then quenched with 10 μL of stop solution (95% formamide, 10 mM EDTA, 0.25% (v/v) bromophenol blue, 0.25% xylene cyanol) and boiled at 100 °C for 5 min.

Reactions were analysed by 20% denaturing polyacrylamide gel electrophoresis (40% 19:1 acrylamide:bis-acrylamide, BioRad) and 7 M urea in 1 x Tris-Borate-EDTA buffer. Electrophoresis was carried out at 525 V for 1 h 15 min, before gels were fixed for 1 h in a 50% methanol, 10% acetic acid solution and dried for 2 h at 80 °C under vacuum. Dried gels were exposed to a Kodak phosphorimager screen and scanned with a Typhoon 9400 instrument (GE).

Dr Hannah Baddock and Lucy Henderson carried out the radioactive gel-based assays.

Gel quantification

Where applicable, gel-based assays were quantified in FIJI/ImageJ to determine the amount of substrate left undigested compared to the amount digested. This was reported as a percentage and plotted against compound concentration before fitting to a non-linear regression to generate IC50 values.

Oligonucleotides used in assays

All the oligonucleotides were purchased from Eurofins Genomics.

Name	Sequence	Description
DNA1	5′ P-A[FITC]TA ATT TGA [BHQ]TCA TCT ATT AT- OH 3′	The substrate used for real-time fluorescence assays against SNM1A and SNM1B.
DNA2	5′ HO-[FITC]TAA TTA ATA ATA GAT CAC CT[BHQ]-OH 3′	The substrate used for real-time fluorescence assays against SNM1C.
DNA3	5′ P-ATA ATT TGA TCA TCT ATT AT- OH 3′	The substrate that is 3′ radiolabelled and used for radioactive gel-based assays against SNM1A and SNM1B
DNA4	5′ P-ATA AAT ATT TTT TAT TAA TAA TAG ATC ACC TTT CTT TCT CTT CTC CCC TT - OH 3′	The substrate that is 3′ radiolabelled and used for DNA substrates radioactive gel-based assays against SNM1A, SNM1B, and SNM1C

DNA1:

DNA2:

Both FITC (fluorescein isothiocyanate) and BHQ (black hole quencher 1) are conjugated to a thymidine nucleotide.

Determining mode of inhibition

Reactions were carried out using conditions for the real-time fluorescence assays, but with concentrations of the DNA substrate varying between 19.5 and 312 nM. A similar analysis was carried out to generate IC_{50} values.

Cell lines and culture conditions

U2OS and HeLa cell lines were cultured in high glucose Dulbecco's modified Eagle medium (DMEM) supplemented with 10% foetal calf serum. Cells were cultured under standard conditions in 5% CO_2 at 37 °C.

Resazurin viability assays

Assays were carried out in transparent, flat-bottomed 96-well plates. 3000 cells/well were seeded and allowed to adhere overnight before adding drugs at indicated concentrations. Cells treated with cisplatin were left for 3 h, before the media was removed, the wells were washed with PBS and replaced with fresh DMEM. All other drugs were left in place for the duration of the assays. 48 h later, 20 μL of 0.15 mg/mL resazurin (suspended in PBS) was added per well, then incubated for 4 h at 37°C. Resorufin was quantified by fluorescence

(560 nm excitation, 590nm emission) using a SpectraMax M2E plate reader (Molecular Devices). Cell survival was normalised against untreated cells for each cell line, plotted as a percentage against compound concentration and fitted to a dose-response curve.

Testing of esterase cleavage products

1 mM (final concentration) of the pro drug **111** was incubated with ± equine sera (Gibco, 16050130) at 37°C for the indicated times. The incubation products were then serially diluted and used for a standard radioactive gel-based assay against SNM1B.

Esterase cleavage reactions using hCES2

Esterase cleavage reactions were carried out in 450 μL volumes in 50 mM HEPES-KOH (pH 7.5), containing 10 μM of the pro-drug **111** ± 30 U hCES2 (Sigma-Aldrich, E0412-1VL) or 10 μM of the active inhibitor **103** with buffer only. These were incubated for either 30 min or 24 h at 37 °C, at which point 30 kDa spin columns were used to remove hCES2, and LC-MS was used to analyse the reaction products.

6.2. Chemical Synthesis

General Methods

All reagents were purchased from Sigma-Aldrich, Acros Organics, Fluka, Fluorochem, Abcr, and Fisher Scientific and used without purification. Microwave reactions were performed using an Initiator 2 microwave reactor (Biotage). Flash column chromatography was performed on a Biotage Isolera automated flash column chromatography platform using Biotage Sfär or Biotage SNAP Ultra columns. Semi-preparative RP HPLC was performed

on a Shimadzu LC-20AR machine using an ACE 5 AQ (250 × 21.2mm) HPLC column utilising the following solvents: MilliQ H_2O + 0.1% (v/v, solvent A) TFA, MeCN + 0.1% (v/v, solvent B) TFA.

IR spectra were recorded using a Bruker Tensor 27 FT-IR spectrometer as a solid or thin film. Selected characteristic peaks are reported in cm^{-1}. NMR spectra were recorded using Bruker Avance spectrometers in the deuterated solvent stated. Assignments given correspond with the numbering system as drawn; where assignments are not provided, it was not possible to assign the resonances due to overlapping signals. Low-resolution mass spectra were recorded on an Agilent Technologies 1260 Infinity LC-MS system fitted with a 6120 Quadrupole mass spectrometer. High-resolution mass spectra (HRMS) were recorded in HPLC grade methanol using electrospray ionisation (ESI+/-) on a Bruker APEX III FT-ICR mass spectrometer. Optical rotations were measured using a Perkin-Elmer polarimeter at 25 °C and $[\alpha]_D^{25}$ values are given in 10^{-1} deg cm^2 g^{-1}. LC-MS was performed on the same system utilising a Merc Chromolith C18 (100 x 4.2 mm) column. MilliQ H2O + 0.1% formic acid (v/v, solvent A), MeCN + 0.1% formic acid (v/v, solvent B). Method used for LCMS; flow = 1.5 mL/min, gradient:

Time/min	Solvent A/%	Solvent B/%
0.0	98.0	2.0
0.5	98.0	2.0
7.5	25.0	75.0
8.5	0.0	100.0
9.0	0.0	100.0
9.25	98.0	2.0
10.0	98.0	2.0

Procedures and Characterisation

General procedure A

To a solution of **22** (1 equiv.) and amino acid derivative (1.2−2 equiv.) in anhydrous DMF (5 mL) at 0 °C, anhydrous DIPEA (2 equiv.) was added dropwise. The reaction mixture was stirred for 16 h at RT under an inert atmosphere and then diluted with cold H_2O (75 mL). The resultant precipitate was collected by filtration and dried under a vacuum.

General procedure B

To a solution of 2-chloroquinazoline derivative in MeOH (4 mL), allylamine (1 mL) was added. The reaction mixture was stirred for 20 min at 120 °C in a microwave reactor, then concentrated *in vacuo*.

General procedure C

To a solution of ester (1 equiv.) in a mixture of THF/MeOH (1:1, 3 ml), 2.5 M $LiOH_{(aq)}$ (5 equiv.) was added. The reaction mixture was stirred for 10 min at 100 °C in a microwave

reactor. The reaction was then neutralised using 1 M $HCl_{(aq)}$ (5 equiv.) and then concentrated *in vacuo*.

General procedure D

To a solution of ester (1 equiv.) and $NH_2OH{\cdot}HCl$ (3 equiv.) in MeOH (5 mL), a solution of NaOMe 25 wt. % in MeOH (10 equiv.) was added dropwise. The reaction mixture was stirred for 2 h. If the reaction was not completed after 2 h: additional NaOMe (2 equiv.) was added dropwise, and the reaction was stirred for a further 1h; this was repeated until the reaction was complete. The reaction was monitored using TLC. The reaction mixture was acidified to pH 2 with 4 M HCl in 1,4-dioxane and concentrated *in vacuo*.

2-Benzyloxy-6-bromo-benzo[de]isoquinoline-1,3-dione (1)[4]

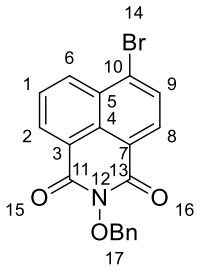

The compound was synthesised using a literature procedure.[4] To a solution of 6-bromo-benzo[de]isochromene-1,3-dione (300 mg, 1.08 mmol, 1 equiv.) in anhydrous pyridine (10 ml), *O*-benzylhydroxylamine hydrochloride (346 mg, 2.16 mmol, 2 equiv.) was added. The reaction mixture was stirred under reflux for 2 h under an inert atmosphere, then cooled to RT, concentrated *in vacuo,* and EtOH (20 mL) was added to a solid residue. The precipitate was collected by filtration, washed with cold EtOH, and dried to give 2-benzyloxy-6-bromo-benzo[de]isoquinoline-1,3-dione (395 mg, 1.03 mmol, 96%) as an orange solid.

IR ν_{max}/cm^{-1} (solid): 1719 and 1677 (C=O);

^{1}H NMR (400 MHz, $CDCl_3$) δ 8.63 (dd, *J* = 7.3, 1.2 Hz, 1H, C(6)H), 8.55 (dd, *J* = 8.5, 1.2 Hz, 1H, C(2)H), 8.38 (d, *J* = 7.9 Hz, 1H, C(9)H, 8.00 (d, *J* = 7.9 Hz, 1H, C(8)H), 7.81 (dd, *J* = 8.5, 7.3 Hz, 1H. C(1)H), 7.66 – 7.57 (m, 2H, OBn(17) ArH_2), 7.39 – 7.28 (m, 3H, OBn(17) ArH_3), 5.20 (s, 2H, OBn(17) -CH_2-); ^{13}C NMR (101 MHz, $CDCl_3$) δ 160.53, 133.99, 133.94, 132.51, 131.60, 131.35, 131.12, 130.90, 130.02, 129.21, 128.54, 128.32, 128.30, 123.31, 122.42, 78.70;

LRMS: *m/z*(%)= 382.2 (100), 384.2 (98) $[M + H]^+$; HRMS: calcd. $C_{19}H_{13}O_3N^{79}Br$ $[M + H]^+$: 382.0073; found: 382.0070.

2-Benzyloxy-6-methoxy-benzo[de]isoquinoline-1,3-dione (2)[4]

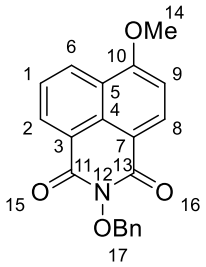

The compound was synthesised using a modified version of a literature procedure.[4] To a solution of 1 (360 mg, 0.94 mmol, 1 equiv.) and $CuSO_4$ (10 mg, 0.06 mmol, 0.06 equiv) in anhydrous MeOH (8 mL), NaOMe 25 wt. % in MeOH (0.27 mL, 1.43mmol, 1.5 equiv.) was added. The reaction mixture was stirred under reflux for 12 h under an inert atmosphere, then cooled to RT. The precipitate was collected by filtration, washed with H_2O, and dried to give 2-benzyloxy-6-methoxy-benzo[de]isoquinoline-1,3-dione (286 mg, 0.86 mmol, 90%) as a yellow solid.

IR ν_{max}/cm^{-1}(solid): 1770 and 1743 (C=O);

^{1}H NMR (400 MHz, $CDCl_3$) δ 8.64 (dd, *J* = 7.3, 1.3 Hz, 1H, C(6)H), δ 8.60 (dd, *J* = 8.4, 1.2 Hz, 1H, C(2)H), 8.59 (d, *J* = 8.3 Hz, 1H, C(8)H), 7.72 (dd, *J* = 8.4, 7.3 Hz, 1H, C(1)H), 7.69 (dd, *J* = 7.8, 1.7 Hz, 2H, OBn(17) ArH_2), 7.46 – 7.33 (m, 3H, OBn(17) ArH_3), 7.07 (d, *J* = 8.3 Hz, 1H, C(9)H), 5.26 (s, 2H, OBn(17) -CH_2-), 4.14 (s, 3H, OMe(14) -CH_3). ^{13}C NMR (101 MHz, $CDCl_3$) δ 161.49, 161.47, 161.00, 134.40, 134.09, 132.09, 130.12, 129.42, 129.16, 128.82, 128.61, 126.24, 123.91, 122.70, 115.19, 105.58, 78.64, 56.48;

LRMS: *m/z*(%)= 334.2 (100) $[M + H]^+$; HRMS: calcd. $C_{20}H_{16}O_4N$ $[M + H]^+$: 334.1074; found: 334.1075.

2-Hydroxy-6-methoxy-benzo[de]isoquinoline-1,3-dione (3)[4]

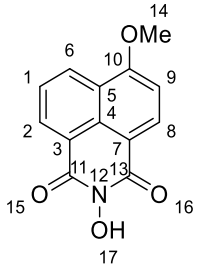

The compound was synthesised using a literature procedure.[4] To a solution of **2** (275 mg, 0.83 mmol, 1 equiv.) in DMA (10 mL), palladium on carbon (35 mg, 10 wt. %) was added. The reaction mixture was stirred for 4 h at RT under a hydrogen atmosphere. The reaction was filtered through Celite, washed with DMA, then concentrated *in vacuo*. The solid residue was then washed with MeOH and dried to give 2-hydroxy-6-methoxy-benzo[de]isoquinoline-1,3-dione (194 mg, 0.80 mmol, 96%) as a yellow solid.

Melting point (recrystallised from EtOH): 259−261°C; Lit.: 267−269°C;[4]

IR ν_{max}/cm^{-1}(solid): 1703 and 1650 (C=O);

^{1}H NMR (400 MHz, DMSO-d_6) δ 10.63 (brs, 1H, O(17)H), 8.51 (app. ddd, J = 8.5, 7.8, 1.2 Hz, 2H, C(6)H, C(2)H), 8.46 (d, J = 8.3 Hz, 1H, C(8)H), 7.81 (dd, J = 8.4, 7.3 Hz, 1H, C(1)H), 7.32 (d, J = 8.4 Hz, 1H, C(9)H), 4.13 (s, 3H, OMe(14) -CH_3). ^{13}C NMR (101 MHz, DMSO-d_6) δ 160.91, 160.55, 160.48, 133.42, 131.13, 128.47, 127.44, 126.51, 122.90, 122.20, 114.40, 106.43, 56.70;

LRMS: m/z(%)= 244.1 (100) $[M + H]^+$; HRMS: calcd. $C_{13}H_9O_4N^{23}Na$ $[M + Na]^+$: 266.04238; found: 266.04261.

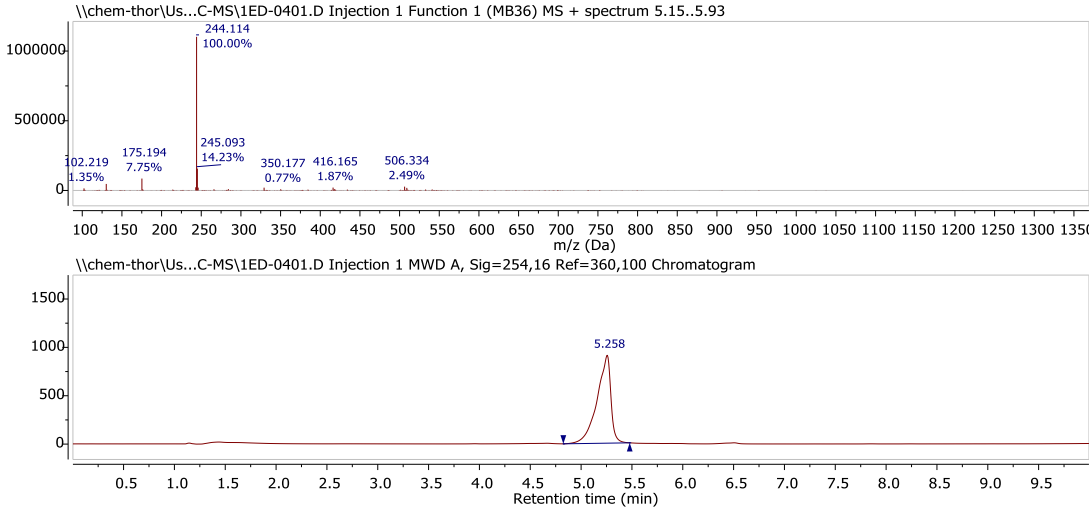

Analytical data (^{1}H NMR) were in accord with those previously reported.[4]

5-Methoxy-benzo[de]isochromene-1,3-dione (4)[5]

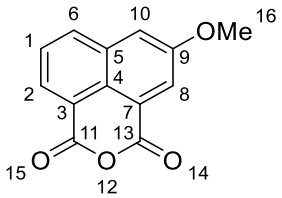

The compound was synthesised using a literature procedure.[5] To a solution 3-hydroxy-1,8-naphthalic anhydride (100 mg. 0.46 mmol, 1 equiv.) in anhydrous acetone (5 mL), SO_4Me_2

(0.8 mL, 0.93 mmol, 2 equiv.) and K_2CO_3 (200 mg, 1.45 mmol, 3 equiv.) were added. The reaction mixture was stirred under reflux for 3 h under an inert atmosphere, then concentrated *in vacuo*. Then 1 M $HCl_{(aq)}$ (20 mL) was added, the precipitate was filtered, washed with H_2O and dried to give 5-methoxy-benzo[de]isochromene-1,3-dione (78 mg, 0.34 mmol, 74%) as a cream solid.

Melting point: 242−244°C; Lit.: 245−247°C;[5]

IR ν_{max}/cm^{-1}(solid): 1774 and 1739 (C=O);

^{1}H NMR (400 MHz, DMSO-d_6) δ 8.42 (dd, *J* = 8.3, 1.1 Hz, 1H, C(2)H), 8.35 (dd, *J* = 7.3, 1.1 Hz, 1H, C(6)H), 8.06 (d, *J* = 2.5 Hz, 1H, C(8)H), 8.02 (d, *J* = 2.6 Hz, 1H, C(10)H), 7.86 (dd, *J* = 8.3, 7.3 Hz, 1H, C(1)H), 4.01 (s, 3H, OMe(16) -CH_3); ^{13}C NMR (101 MHz, DMSO-d_6) δ 161.1, 160.8, 158.3, 134.5, 133.7, 130.2, 128.5, 125.6, 123.7, 121.0, 119.4, 114.8, 56.6;

LRMS: *m/z*(%)= 229.1 (100) $[M + H]^+$; HRMS: calcd. $C_{13}H_9O_4$ $[M + H]^+$: 229.0495; found: 229.0498;

Analytical data (melting point) were in accord with those previously reported.[5]

4,6-Dichloro-3-nitroquinoline (6)[6]

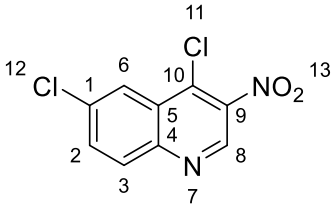

The compound was synthesised using a literature procedure.[6] To a solution of 6-chloro-3-nitroquinolin-4-ol (100 mg, 0.45 mmol, 1 equiv.) in anhydrous DCM (2 mL) and anhydrous

DMF (3 drops), $SOCl_2$ (80 µL, 1.1 mmol, 2.4 equiv.) were added. The reaction mixture was stirred under reflux for 2 h under an inert atmosphere. It was then cooled, quenched with sat. $NaHCO_{3(aq)}$ (10 mL) and extracted with DCM (2 × 10 mL). The combined organic layer was washed with brine (20 mL), dried over $MgSO_4$, then concentrated *in vacuo*. The product was purified using flash column chromatography (2−10% EtOAc in cyclohexane) to give 4,6-dichloro-3-nitroquinoline (86mg, 0.35 mmol, 78%) as a yellow solid.

IR ν_{max}/cm^{-1}(thin film): 1528 and 1334 (N=O)

^{1}H NMR (400 MHz, chloroform-*d*) δ 9.23 (s, 1H, C(8)H), 8.40 (dd, *J* = 2.3, 0.5 Hz, 1H, C(6)H), 8.16 (dd, *J* = 8.9, 0.5 Hz, 1H, C(3)H), 7.88 (dd, *J* = 9.0, 2.3 Hz, 1H, C(2)H); ^{13}C NMR (101 MHz, chloroform-*d*) δ 147.8, 144.7, 136.5, 135.5, 134.2, 132.0, 126.6, 124.9;

LRMS: *m/z*(%)= 243.0 (100), 245 (62) $[M + H]^+$;

4-Azido-6-chloro-3-nitroquinoline (7)

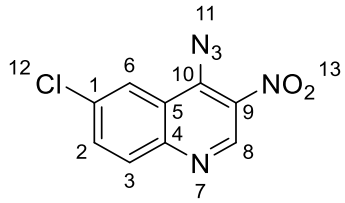

To a solution of **6** (86 mg, 0.35 mmol, 1 equiv.) in anhydrous DMF (2 mL), NaN_3 (46 mg, 1.1 mmol, 3 equiv.) was added. The reaction mixture was stirred for 2 h at RT and concentrated *in vacuo*. The solid residue was redissolved in DCM (10 mL), washed with both H_2O (10 mL) brine (2 × 10 mL), then dried over $MgSO_4$ and concentrated *in vacuo* to give 4-Azido-6-chloro-3-nitroquinoline (75 mg, 0.30 mmol, 86%) as a brown solid.

IR ν_{max}/cm^{-1}(thin film): 2125 (N=N=N), 1566 (N=O) and 1360 (N=O)

^{1}H NMR (400 MHz, chloroform-*d*) δ 9.31 (s, 1H. C(8)H), 8.38 (dd, *J* = 2.3, 0.5 Hz, 1H, C(6)H), 8.07 – 8.01 (m, 1H, C(3)H), 7.82 (dd, *J* = 9.0, 2.3 Hz, 1H, C(2)H); ^{13}C NMR (101 MHz, chloroform-*d*) δ 148.08, 145.85, 139.66, 134.98, 134.22, 131.23, 123.57, 122.71;

LRMS: *m/z*(%)= 250.0 (100), 252.0 (31) $[M + H]^+$;

6-Chloroquinoline-3,4-diamine (8)[6]

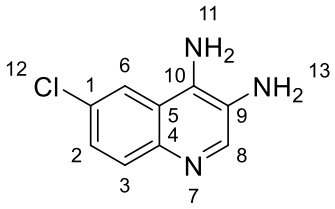

The compound was synthesised using a modified version of a literature procedure.**6** To a degassed solution of 7 (40 mg, 0.16 mmol, 1 equiv.) in MeOH (5 mL), Raney nickel 50% slurry in H_2O (10 mg) was added. The reaction mixture was stirred at RT under an H_2 atmosphere for 1 h. The reaction mixture was then filtered through Celite, then concentrated *in vacuo*. 6-chloroquinoline-3,4-diamine (31 mg, 0.16 mmol, 99%) was obtained as a brown oil.

^{1}H NMR (400 MHz, methanol-d4) δ 8.19 (s, 1H, C(8)H), 8.01 (d, J = 2.2 Hz, 1H, C(6)H), 7.66 (d, J = 8.9 Hz, 1H, C(3)H), 7.33 (dd, J = 9.0, 2.2 Hz, 1H, C(2)H); ^{13}C NMR (101 MHz, methanol-d4) δ 141.46, 141.13, 136.46, 129.79, 129.11, 126.30, 124.81, 119.74, 119.22;

LRMS: *m/z*(%)= 194.1 (100), 196.1 (34) $[M + H]^+$; HRMS: calcd. C9H9N335Cl $[M + H]^+$: 194.0480; found: 194.0481.

9-Chloro-1,4-dihydropyrazino[2,3-c]quinoline-2,3-dione (9)

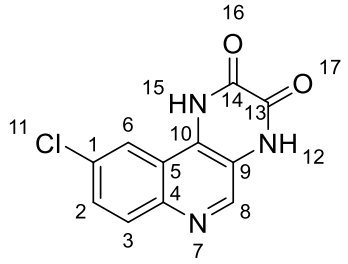

A mixture of **8** (30 mg, 0.15 mmol, 1 equiv.) in diethyl oxalate (1.5 mL, excess) was stirred under reflux for 2 h. The reaction mixture was then cooled to 0 °C. The precipitate was collected by filtration, washed with MeOH and DCM, and dried under vacuum. 9-Chloro-1,4-dihydropyrazino[2,3-c]quinoline-2,3-dione (14 mg, 0.06 mmol, 36%) was obtained as a brown solid.

Melting point (recrystallised from EtOH): >300°C;

IR ν_{max}/cm^{-1}(solid): 1687 and 1659 (C=O);

^{1}H NMR (400 MHz, DMSO-d_6) δ 12.44 (brs, 2H, N(12)H, N(15)H), 8.73 (d, J = 2.2 Hz, 1H, C(6)H), 7.97 (d, J = 8.9 Hz, 1H, C(3)H), 7.67 (dd, J = 8.9, 2.2 Hz, 1H, C(2)H); ^{13}C NMR (101 MHz, DMSO-d_6) δ 157.44, 155.41, 142.95, 140.86, 132.04, 131.88, 128.86, 126.24, 120.94, 119.54, 118.40;

LRMS: *m/z*(%)= 248.0 (100), 250.0 (32) $[M + H]^+$; HRMS: calcd. $C_{11}H_7O_2N_3{}^{35}Cl$ $[M + H]^+$: 248.02216; found: 248.02213.

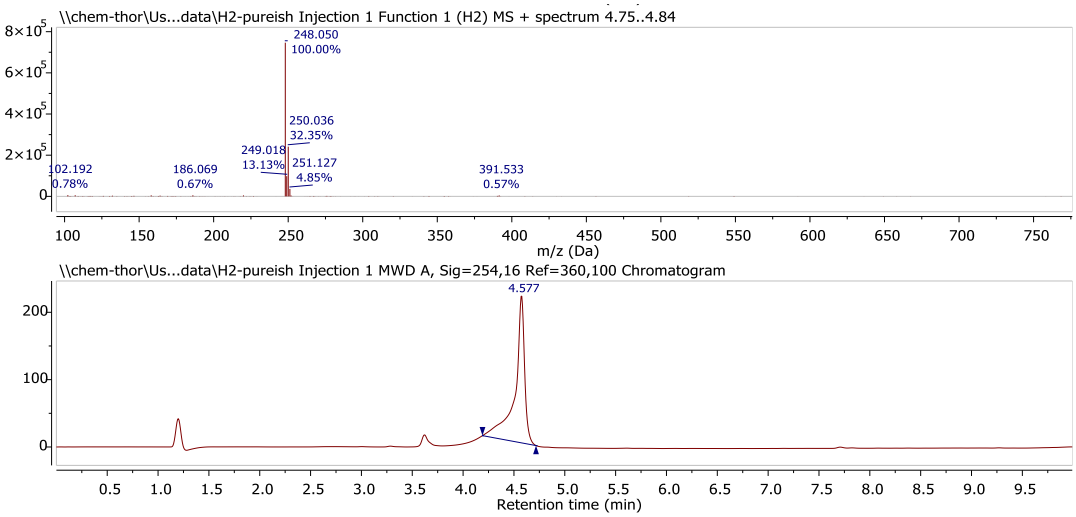

2-Amino-*N*-(benzyloxy)benzamide (10)[7]

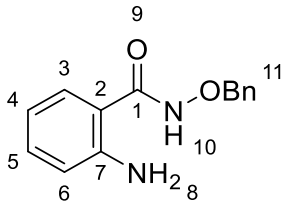

The compound was synthesised using a literature procedure.[7] To a solution of isatoic anhydride (6 g, 36.8 mmol, 1 equiv.) and *O*-benzylhydroxylamine hydrochloride (8.6 g, 54.0 mmol, 1.5 equiv.) in anhydrous THF (50 mL), TEA (7.5 mL, 54.0 mmol, 1.5 equiv.) was added. The reaction mixture was stirred under reflux for 3 h under an inert atmosphere and then concentrated *in vacuo*. The product was purified using flash column chromatography (10−30% EtOAc in cyclohexane) to give 2-amino-*N*-(benzyloxy)benzamide (7.8g, 32.2 mmol, 88%) as a white solid.

Melting point: 101−104°C; Lit: 104−106°C;[7]

IR ν_{max}/cm^{-1}(solid): 1626 (C=O);

^{1}H NMR (400 MHz, DMSO-d_6) δ 11.65 (s, 1H, N(10)H), 7.96 (dd, *J* = 7.9, 1.5 Hz, 1H, C(3)H), 7.68 (ddd, *J* = 8.5, 7.2, 1.6 Hz, 1H, C(5)H), 7.60 – 7.53 (m, 2H, OBn(11) ArH_2), 7.48 – 7.34 (m, 3H, OBn(11) ArH_3), 7.30 – 7.19 (m, 2H, C(6)H, C(4)H) 5.10 (s, 2H, OBn(11) -CH_2-); ^{13}C NMR (101 MHz, DMSO-d_6) δ 159.50, 148.53, 139.18, 135.56, 134.95, 129.93, 129.32, 128.84, 127.72, 123.17, 115.93, 114.91. 77.95;

LRMS: *m/z*(%)= 243.1 (100) $[M + H]^+$; HRMS: calcd. $C_{14}H_{15}O_2N_2$ $[M + H]^+$: 243.1128; found: 243.1127;

Analytical data (melting point and ^{1}H NMR) were in accord with those previously reported.[7]

3-Benzyloxyquinazoline-2,4-dione (11)[8]

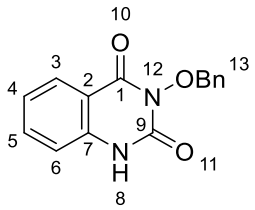

The compound was synthesised using a literature procedure.[8] To a solution of **10** (1 g, 4,1 mmol, 1 equiv.) and triphosgene (1.35 g, 4.5 mmol, 1.1 equiv.) in anhydrous THF (40 mL) at 0 °C, TEA (1.26 mL, 9.0 mmol, 2.2 equiv.) was added dropwise. The reaction mixture was stirred for 2 h at RT under an inert atmosphere and then concentrated *in vacuo*. The product was purified using flash column chromatography (10−60% EtOAc in cyclohexane) to give 3-benzyloxyquinazoline-2,4-dione (726 mg, 2.71 mmol, 66%) as a white solid.

Melting point(recrystallised from EtOH): 201−203°C; Lit: 207−209°C;[8]

IR ν_{max}/cm^{-1}(solid): 1733 and 1664 (C=O);

^{1}H NMR (400 MHz, DMSO-d_6) δ 11.44 (s, 1H, N(8)H), 7.59 – 7.35 (m, 5H, OBn(13) ArH_5), 7.29 (dd, *J* = 8.0, 1.6 Hz, 1H, C(3)H), 7.15 (ddd, *J* = 8.6, 7.0, 1.6 Hz, 1H, C(5)H), 6.71 (d, *J* = 8.2 Hz, 1H, C(6)H), 6.49 (t, *J* = 7.5 Hz, 1H C(4)H), 4.90 (s, 2H, OBn(13) -CH_2-); ^{13}C NMR (101 MHz, DMSO-d_6) δ 167.68, 150.01, 136.52, 132.57, 129.33, 128.76, 128.71, 128.21, 116.79, 115.11, 112.81, 77.41;

LRMS: *m/z*(%)= 269.1 (100) $[M + H]^+$; HRMS: calcd. $C_{15}H_{11}O_2N_3$ $[M - H]^-$: 267.0776; found: 267.0775;

Analytical data (^{1}H NMR) were in accord with those previously reported.[8]

3-Hydroxyquinazoline-2,4-dione (12)[8]

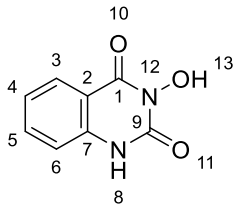

To a degassed solution of **11** (50 mg, 0.19 mmol, 1 equiv.) in DMF (2 mL), palladium on carbon (10 mg, 10 wt. %) was added. The reaction mixture was stirred under an H_2 atmosphere for 2 h. The reaction mixture was filtered through Celite, then concentrated *in vacuo*. 3-Hydroxyquinazoline-2,4-dione (28 mg, 0.16 mmol, 87%) was obained as a white solid.

Melting point (recrystalised from *i*-PrOH): >300°C; Lit: >300°C;[8]

IR ν_{max}/cm^{-1}(solid): 1714 and 1654 (C=O);

^{1}H NMR (400 MHz, DMSO-d_6) δ 11.05 (brs, 2H, N(8)H, O(13)H), 7.94 (d, J = 8.1 Hz, 1H, C(3) H), 7.66 (t, J = 7.7 Hz, 1H, C(5)H), 7.35 – 7.13 (m, 2H, C(4)H, C(5)H); ^{13}C NMR (101 MHz, DMSO-d_6) δ 159.87, 149.23, 138.84, 135.14, 127.53, 122.98, 115.75, 114.61;

LRMS: *m/z*(%)= 179.1 (100) $[M + H]^+$; HRMS: calcd. $C_8H_5O_3N_2$ $[M - H]^-$: 177.0306; found: 177.0298;

Analytical data (^{1}H NMR) were in accord with those previously reported.[8]

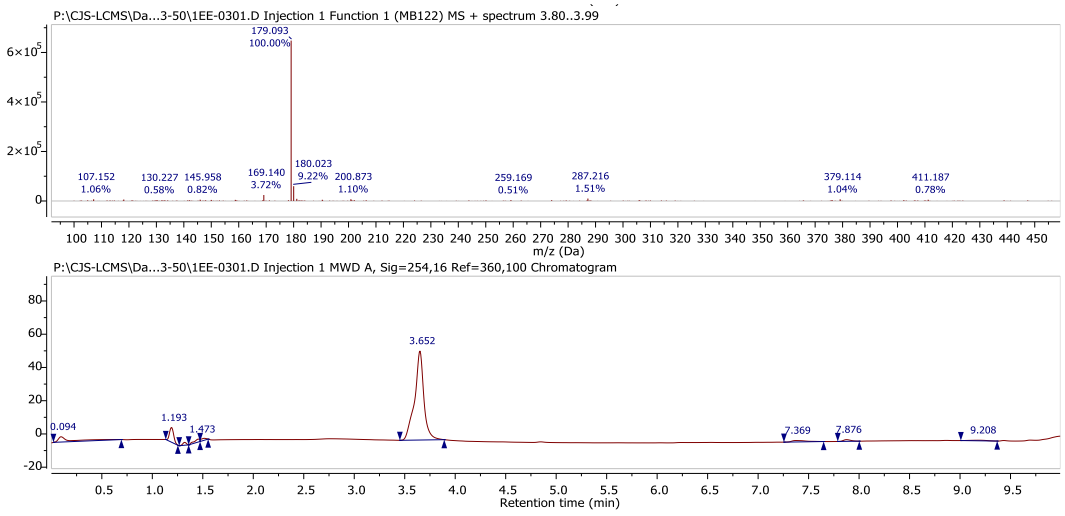

1-Benzyl-3-benzyloxyquinazoline-2,4-dione (13)[9]

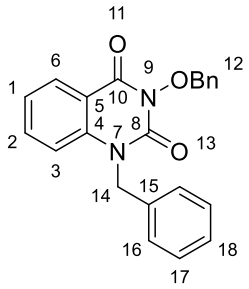

The compound was synthesised using a literature procedure.[9] To a solution of **11** (200 mg, 0.75 mmol, 1 equiv.) and Cs_2CO_3 (485 mg, 1.5 mmol, 2 equiv.) in anhydrous DMF (3 mL), benzyl bromide (106 µL, 0.89 mmol, 1.2 equiv.) was added. The reaction mixture was stirred

at 80 °C for 2 h, then quenched with cold H_2O (75 mL). The precipitate was collected by filtration, washed with H_2O, then dried under a vacuum. 1-Benzyl-3-benzyloxyquinazoline-2,4-dione (256 mg, 0.72 mmol, 95%) was obtained as a white solid.

IR ν_{max}/cm^{-1}(solid): 1720 and 1684 (C=O);

^{1}H NMR (400 MHz, chloroform-*d*) δ 8.26 (dd, *J* = 7.9, 1.7 Hz, 1H, C(6)H), 7.64 (dd, *J* = 6.5, 2.9 Hz, 2H, C(2)H), 7.55 (ddd, *J* = 8.8, 7.3, 1.7 Hz, 1H, C(1)H), 7.45 – 7.16 (m, 10H, OBn(12) ArH_5, $(C(16)H)_2$, $(C(17)H)_2$, (C(18)H)), 7.11 (d, *J* = 8.5 Hz, 1H, C(3)H), 5.37 (s, 2H, $(C(14)H_2)$, 5.29 (s, 2H, OBn(12) -CH_2-). ^{13}C NMR (101 MHz, chloroform-*d*) δ 158.70, 149.68, 139.20, 135.24, 135.22,130.24, 129.18, 129.03, 128.99, 128.49, 127.82, 126.50, 123.42, 114.72, 78.43, 47.47;

LRMS: *m/z*(%)= 359.2 (100) $[M + H]^+$, HRMS: calcd. $C_{22}H_{19}O_3N_2$ $[M + H]^+$: 359.1390; found: 359.1392;

Analytical data (^{1}H NMR and LRMS) were in accord with those previously reported.[9]

1-Benzyl-3-hydroxyquinazoline-2,4-dione (14)[9]

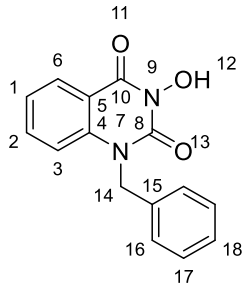

The compound was synthesised using a modified version of a literature procedure.[9] A mixture of **13** (240 mg, 0.67 mmol, 1 equiv.) in conc. HBr (48% in H_2O, 2 mL) and AcOH (2 mL) was stirred under reflux for 1 h. The reaction mixture was then concentrated

in vacuo, dissolved in DMF (0.5 mL) and poured into cold H_2O (50 mL). The resulting precipitate was then collected by filtration, washed with a minimal amount of cold DCM, and dried under vacuum. 1-Benzyl-3-hydroxyquinazoline-2,4-dione (51 mg, 0.19 mmol, 28%) was obtained as a white-off solid.

IR ν_{max}/cm^{-1}(solid): 1712 and 1666 (C=O);

^{1}H NMR (400 MHz, DMSO-d_6) δ 10.86 (s, 1H, O(12)H), 8.09 (dd, *J* = 7.8, 1.6 Hz, 1H, C6)H), 7.67 (ddd, *J* = 8.7, 7.2, 1.7 Hz, 1H, C(2)H), 7.39 – 7.22 (m, 7H, C(3)H, C(1)H, $(C(16)H)_2$, $(C(17)H)_2$, (C(18)H), 5.40 (s, 2H $C(14)H_2$); ^{13}C NMR (101 MHz, DMSO-d_6) δ 158.96, 150.27, 139.13, 136.60, 135.44, 129.19, 128.23, 127.79, 126.91, 123.55, 115.70, 115.61, 46.87;

LRMS: *m/z*(%)= 269.2 (100) $[M + H]^+$; HRMS: calcd. $C_{15}H_{13}O_3N_2$ $[M + H]^+$: 269.0921; found: 269.0922;

Analytical data (^{1}H NMR and HRMS) were in accord with those previously reported.[9]

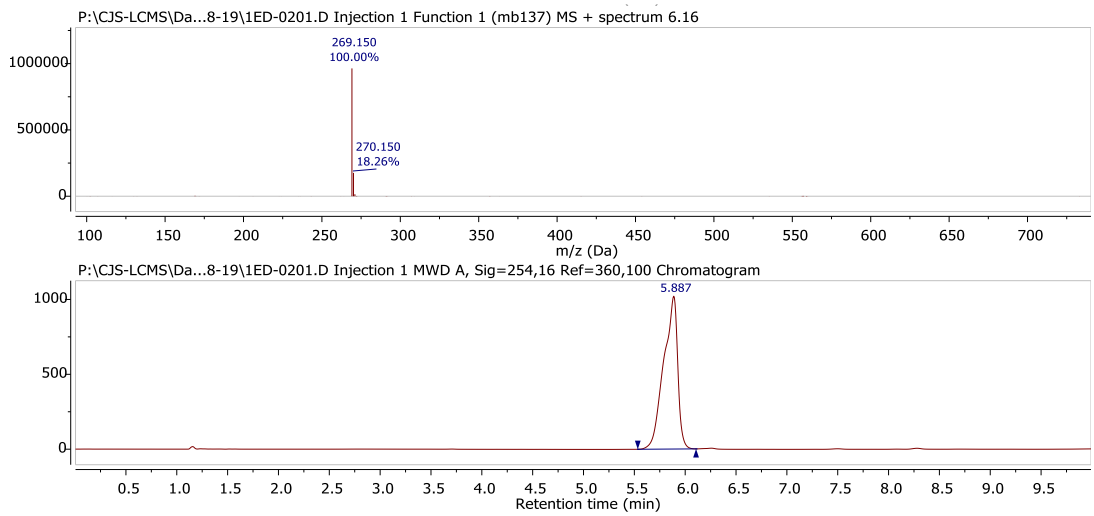

3-Hydroxy-2-thioxo-2,3-dihydroquinazolin-4-one (15)[10]

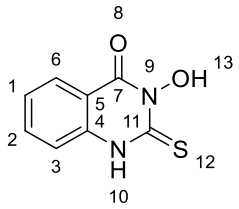

The compound was synthesised using a literature procedure.[10] To a solution of methyl anthranilate (150 µL, 1.16 mmol, 1 equiv.) in H_2O (3 mL) and DCM (10 mL), thiophosgene (100 µL, 1.30 mmol, 1.1 equiv.) was added dropwise. The reaction mixture was stirred at RT for 16 h. It was then diluted with H_2O (15 mL) and extracted with DCM (3 × 15 mL). The combined organic layer was washed with brine (20 mL), dried over Na_2SO_4, then concentrated *in vacuo*. Intermediate methyl 2-isothiocyanatobenzoate was then added to a solution of $NH_2OH{\cdot}HCl$ (82 mg, 1.18 mmol, 1 equiv.) and sodium hydroxide (47 mg, 1.20 mmol, 1 equiv.) in a mixture of chloroform/H_2O (1:1, 10 mL). The reaction mixture was stirred for 2 h at RT. The precipitate was collected by filtration, washed with DCM, and dried under vacuum. 3-Hydroxy-2-thioxo-2,3-dihydroquinazolin-4-one (179 mg, 0.92 mmol, 80%) was obtained as a white solid.

Melting point (recrystalised from EtOH): 247−249°C; Lit: 252−254°C;[10]

IR ν_{max}/cm^{-1}(solid): 1701 (C=O) and 1619 (C=S);

^{1}H NMR (400 MHz, DMSO-d_6) δ 12.97 (s, 1H, , N(10)H), 11.24 (s, 1H, O(13)H), 7.98 (d, *J* = 8.0 Hz, 1H, C(6)H), 7.75 (t, *J* = 7.9 Hz, 1H C(2)H), 7.40 (d, *J* = 8.4 Hz, 1H, C(3)H), 7.35 (t, *J* = 7.6 Hz, 1H, C(1)H). ^{13}C NMR (101 MHz, DMSO-d_6) δ 173.26, 157.07, 139.07, 135.67, 127.47, 124.78, 116.32, 116.19;

LRMS: *m/z*(%)= 195.1 (100) $[M + H]^+$; HRMS: calcd. $C_8H_5O_2N_2S$ $[M - H]^-$: 193.0077; found: 193.0070;

Analytical data (^{1}H NMR) were in accord with those previously reported.[10]

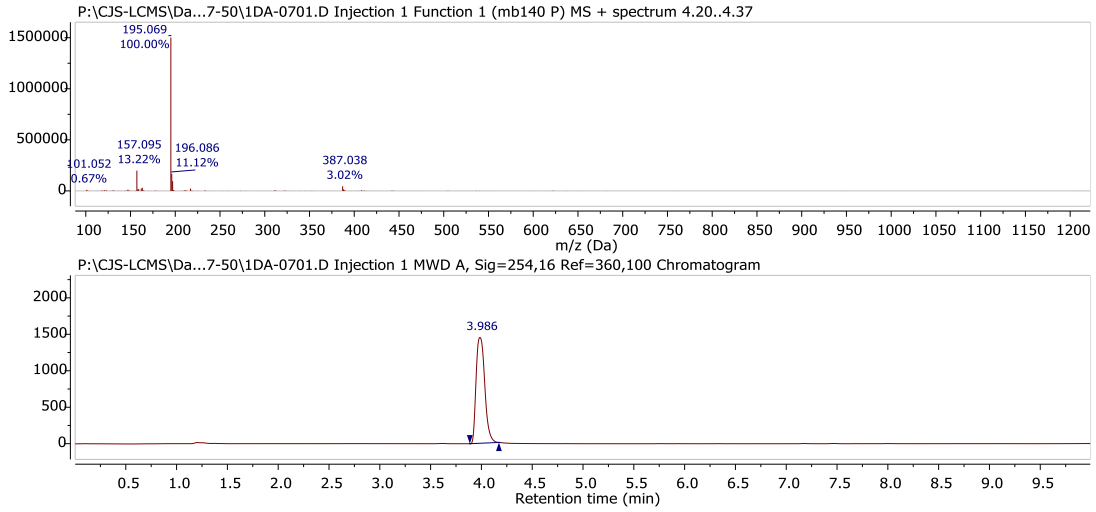

3-Benzyloxy-2-(chloromethyl)quinazolin-4-one (16)

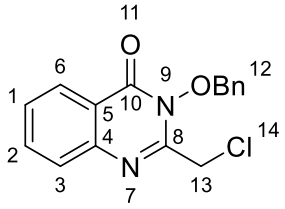

To a solution of **10** (200 mg, 0.82 mmol, 1 equiv.) in anhydrous DMF (3 mL), 2-chloroacetyl chloride (70 µL, 0.88 mmol 1,1 equiv.) was added. The reaction mixture was stirred 16 h at RT and under an inert atmosphere. Then, it was quenched with H_2O (20 mL) and extracted with EtOAc (3 × 20 mL). The combined organic layer was washed with sat. $NaHCO_{3(aq)}$ (20 ml) and brine (20 ml), dried over Na_2SO_4, then concentrated *in vacuo*. 3-Benzyloxy-2-chloromethylquinazolin-4-one (212 mg, 0.71 mmol 86%) was obtained as a white solid.

IR ν_{max}/cm^{-1}(solid): 1739 (C=O);

^{1}H NMR (400 MHz, DMSO-d_6) δ 8.22 (ddd, *J* = 8.0, 1.5, 0.5 Hz, 1H, C(6)H), 7.91 (ddd, *J* = 8.5, 7.1, 1.6 Hz, 1H, C(2)H), 7.76 (dt, *J* = 8.1, 1.0 Hz, 1H, C(3)), 7.69 – 7.57 (m, 3H, OBn(12) ArH_2, C(1)H), 7.54 – 7.41 (m, 3H, OBn(12) ArH_3), 5.39 (s, 2H, OBn(12) -CH_2-), 4.84 (s, 2H, C(13)H_2); ^{13}C NMR (101 MHz, DMSO-d_6) δ 157.55, 151.89, 146.01, 135.36, 134.16, 130.21, 129.81, 129.17, 128.22, 128.08, 126.74, 123.16, 78.67, 42.06;

LRMS: *m/z*(%)= 301.1 (100), 303.1 (32) $[M + H]^+$; HRMS: calcd. $C_{16}H_{14}O_2N_2{}^{35}Cl$ $[M + H]^+$: 301.0738; found: 301.0739;

3-Benzyloxy-2-(morpholinomethyl)quinazolin-4-one hydrochloride (17)

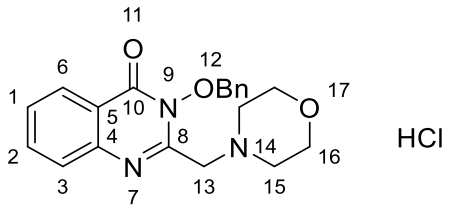

To a solution of **16** (190 mg, 0.63 mmol, 1 equiv.) in anhydrous DMF (1 mL), morpholine (70 µL, 0.81 mmol, 1 equiv.) was added dropwise. The reaction mixture was stirred under an inert atmosphere at 60 °C for 1 h. Then, it was diluted with H_2O (15 mL) and extracted with EtOAc (3 × 15 mL). The combined organic layer was washed with brine (2 × 20 mL), dried over Na_2SO_4, then concentrated *in vacuo*. The product was then purified using flash column chromatography (0−5% MeOH with 1% NH_2Me in DCM). The product was then converted to hydrochloride salt. 3-Benzyloxy-2-(morpholinomethyl)quinazolin-4-one hydrochloride (238 mg, 97%) was obtained as a white solid.

IR ν_{max}/cm^{-1}(solid): 1698 (C=O);

^{1}H NMR (400 MHz, chloroform-*d*) δ 8.27 (ddd, *J* = 8.0, 1.5, 0.6 Hz, 1H C(6)H), 7.75 (ddd, *J* = 8.5, 7.1, 1.5 Hz, 1H, C(2)H), 7.68 (ddd, *J* = 8.2, 1.3, 0.6 Hz, 1H, C(3)H), 7.52 (ddd, *J* =

8.2, 7.1, 1.3 Hz, 1H, C(1)H), 7.45 – 7.34 (m, 5H, OBn(12) ArH_5), 5.35 (s, 2H, OBn(12) -CH_2-), 5.23 (s, 2H, C(13)H_2), 4.01 (s, 4H C(16)H_4), 3.31 (s, 4H, C(15)H_4); ^{13}C NMR (101 MHz, chloroform-*d*) δ 157.47, 144.90, 134.98, 132.72, 130.64, 130.21, 129.34, 128.23, 127.96, 126.90, 122.81, 78.99, 77.36, 77.04, 76.73, 63.99, 53.44, 51.53;

LRMS: *m/z*(%)= 352.2 (100) $[M + H]^+$; HRMS: calcd. $C_{20}H_{22}O_3N_3$ $[M + H]^+$: 352.1656; found: 352.1657;

3-Hydroxy-2-(morpholinomethyl)quinazolin-4-one (18)

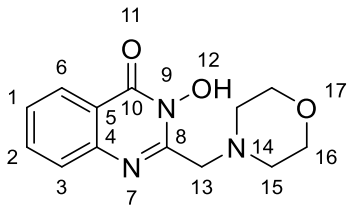

To a degassed solution of **17** (210 mg, 0.54 mmol, 1 equiv.) in MeOH (5 mL), palladium on carbon (30 mg, 10 wt.%) was added. The reaction mixture was stirred for 2 h under an H_2 atmosphere. Then, it was filtered through Celite, then concentrated *in vacuo*. 3-Hydroxy-2-(morpholinomethyl)quinazolin-4-one (124 mg, 0.47 mmol, 88%) was obtained as a white solid.

IR ν_{max}/cm^{-1}(solid): 1679 (C=O);

^{1}H NMR (400 MHz, DMSO-d_6) δ 8.20 (ddd, *J* = 8.0, 1.5, 0.6 Hz, 1H, C(6)H), 7.90 (ddd, *J* = 8.5, 7.1, 1.6 Hz, 1H C(2)H), 7.78 (ddd, *J* = 8.2, 1.2, 0.6 Hz, 1H, C(3)H), 7.62 (ddd, *J* = 8.2, 7.1, 1.2 Hz, 1H, C(1)H), 4.78 (s, 2H, C(13)H_2), 3.99-3.94 (m, 4H, C(16)H_4), 3.81 – 3.46 (m, 4H C(15)H_4); ^{13}C NMR (101 MHz, DMSO-d_6) δ 157.85, 148.16, 145.47, 134.91, 127.83, 127.61, 126.54, 122.29, 63.59, 54.61, 52.86;

LRMS: *m/z*(%)= 262.2 (100) $[M + H]^+$; HRMS: calcd. $C_{13}H_{16}O_3N_3$ $[M + H]^+$: 262.11862; found: 262.11871;

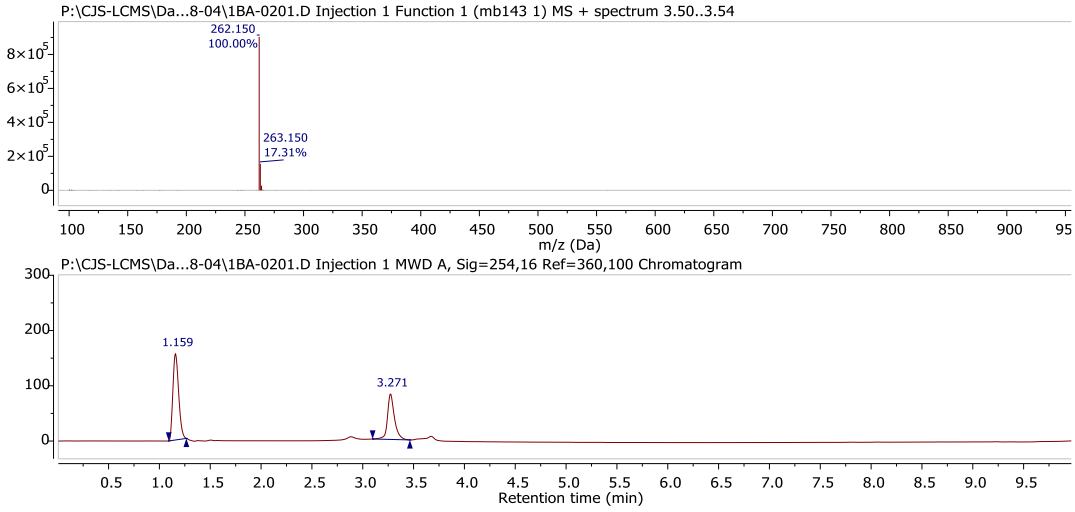

Ethyl 3-benzyloxy-4-oxo-3,4-dihydroquinazoline-2-carboxylate (19)[7]

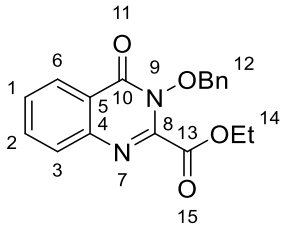

The compound was synthesised using a modified version of a literature procedure.[7] To a solution of **10** (500 mg, 1.9 mmol, 1 equiv.) and ethyl chlorooxoacetate (225 µL, 2.3 mmol, 1.2 equiv.) in anhydrous DCM (10 mL), anhydrous pyridine (180 µL, 2.3 mmol, 1.2 equiv.) was added dropwise. The reaction mixture was stirred at RT under an inert atmosphere for 16 h. Then, it was concentrated *in vacuo,* and p-toluenesulfonic acid monohydrate (360 mg, 1.9 mmol, 1 equiv.) in toluene (10 mL) was added. The reaction mixture was stirred under reflux for 2 h, quenched with sat. $NaHCO_{3(aq)}$, and extracted with EtOAc (3 × 15 mL). The combined organic layer was washed with brine (40 mL), dried over Na_2SO_4, then

concentrated *in vacuo*. The product was purified using flash column chromatography (10−20% EtOAc in cyclohexane) to Ethyl 3-benzyloxy-4-oxo-3,4-dihydroquinazoline-2-carboxylate (462 mg, 1.4 mmol, 75%) was obtained as a white solid.

Melting point: 122−125°C; Lit: 123−124°C;[7]

IR ν_{max}/cm^{-1}(solid): 1745 and 1699 (C=O);

^{1}H NMR (400 MHz, chloroform-*d*) δ 8.37 (dt, *J* = 8.0, 1.2 Hz, 1H, C(6)H), 7.88 – 7.76 (m, 2H, C(2)H, C(3)H), 7.65 – 7.52 (m, 3H, C(1)H, OBn(12) ArH_2), 7.48 – 7.37 (m, 3H OBn(12) ArH_3), 5.43 (s, 2H, OBn(12) -CH_2-), 4.47 (q, *J* = 7.1 Hz, 2H OEt(14), -CH_2-), 1.39 (t, *J* = 7.1 Hz, 3H, OEt(14), -CH_3); ^{13}C NMR (101 MHz, chloroform-*d*) δ 160.04, 157.46, 145.99, 145.72, 134.76, 133.22, 130.10, 129.51, 128.71, 128.38, 128.29, 126.86, 123.70, 79.86, 63.46, 13.95;

LRMS: *m/z*(%)= 325.2 (100) $[M + H]^+$; HRMS: calcd. $C_{18}H_{17}O_4N_2$ $[M + H]^+$: 325.1183; found: 325.1184;

Analytical data (^{1}H NMR and ^{13}C NMR) were in accord with those previously reported.[7]

Ethyl 3-hydroxy-4-oxo-3,4-dihydroquinazoline-2-carboxylate (20)

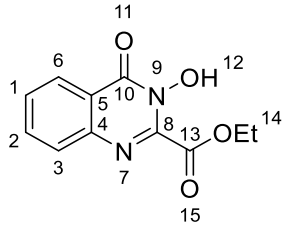

The compound was synthesised using a literature procedure.[7] To a degassed solution of **19** (60 mg, 0.19 mmol, 1 equiv.) in EtOAc (5 mL), palladium on carbon (10 mg, 10 wt. %) was

added. The reaction mixture was stirred under an H_2 atmosphere for 15 min. The reaction mixture was filtered through Celite and then concentrated *in vacuo* to give ethyl 3-hydroxy-4-oxo-3,4-dihydroquinazoline-2-carboxylate (42 mg, 0.18 mmol, 97%) as a white solid.

Melting point (recrystalised from EtOH): 134−136°C; Lit: 149−151°C;[7]

IR ν_{max}/cm^{-1}(solid): 1669 and 1610 (C=O);

^{1}H NMR (400 MHz, DMSO-d_6) δ 12.42 (s, 1H, O(12)H), 8.21 (d, *J* = 7.8 Hz, 1H, C(6)H), 7.90 (t, *J* = 7.2 Hz, 1H, C(2)H), 7.77 (d, *J* = 8.1 Hz, 1H, C(3)H), 7.65 (t, *J* = 7.5 Hz, 1H, C(1)H), 4.44 (q, *J* = 7.1 Hz, 2H, OEt(14), -CH_2-), 1.34 (t, *J* = 7.1 Hz, 3H, OEt(14), CH_3);

^{13}C NMR (101 MHz, DMSO-d_6) δ 160.24, 157.58, 146.83, 145.92, 135.14, 128.55, 128.13, 126.60, 122.98, 63.30, 14.29;

LRMS: *m/z*(%)= 235.1 (100) $[M + H]^+$; HRMS: calcd. $C_{11}H_9O_4N_2$ $[M - H]^-$: 233.0568; found: 233.0563;

Analytical data (^{1}H NMR and ^{13}C NMR) were in accord with those previously reported, but a substantial difference in melting points was observed.[7]

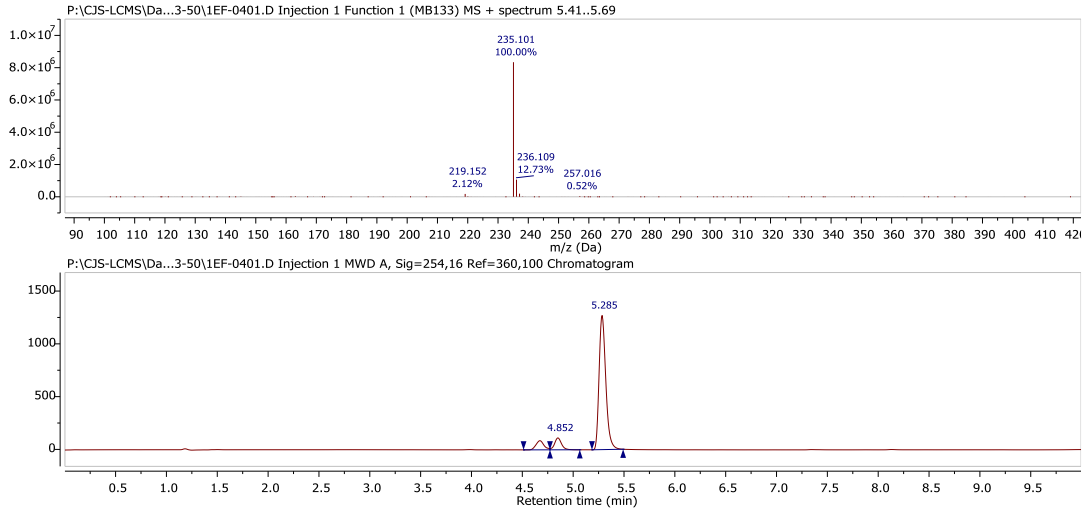

6-Chloroquinazoline-2,4-dione (21)[11]

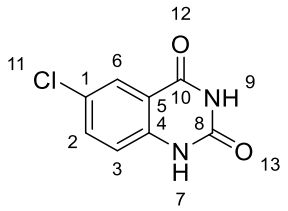

The compound was synthesised using a literature procedure.[11] A mixture of 2-Amino-5-chlorobenzoic acid (10 g, 58 mmol, 1 equiv.) and urea (35 g, 580 mmol, 10 equiv.) were stirred for 3 h at 170 °C. Then the reaction mixture was cooled to 100 °C, and H_2O (50 mL) was added. It was stirred for a further 10 min and cooled to 0 °C. The precipitate was collected by filtration and washed with cold H_2O. The precipitate was added to 0.5 M $NaOH_{(aq)}$ (100 mL) and stirred under reflux for 10 min. Then, it was cooled at 0 °C for 1 h, and the precipitate was collected by filtration. The precipitate was washed with cold H_2O and dried under a vacuum. 6-Chloroquinazoline-2,4-dione (8.9 g, 45 mmol, 77%) was obtained as a white solid.

^{1}H NMR (400 MHz, DMSO-d_6) δ 11.45 (s, 1H, N(9)H), 11.28 (s, 1H, N(7)H), 7.82 (d, J = 2.5 Hz, 1H, C(6)H), 7.69 (dd, J = 8.7, 2.5 Hz, 1H, C(2)H), 7.19 (d, J = 8.8 Hz, 1H, C(3)H); ^{13}C NMR (101 MHz, DMSO-d_6) δ 162.30, 150.50, 140.20, 135.30, 126.77, 126.39, 118.00, 116.26;

LRMS: m/z(%)= 197.0 (100), 199.0 (35) $[M + H]^+$

Analytical data (^{1}H NMR) were in accord with those previously reported.[11]

2,4,6-Trichloroquinazoline (22)

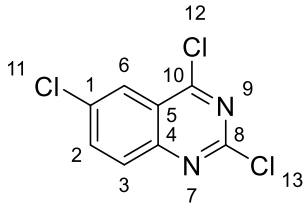

The compound was synthesised using a literature procedure.[11] To a solution of **21** (8.9 g, 45 mmol, 1 equiv.) in $POCl_3$ (26 mL, 270 mmol, 6 equiv.), diethylaniline (13.5 mL, 90 mmol, 2 equiv.) was slowly added. The reaction mixture was stirred under reflux for 4 h. It was then diluted with Et_2O (200 mL), poured slowly to cold H_2O (200 mL) and extracted with Et_2O (3 × 200 mL). The combined organic layer was washed with brine and dried over $NaSO_4$. The product was filtered through a pad of silica in DCM and then concentrated *in vacuo* to give 2,4,6-Trichloroquinazoline (10.1 g, 43 mmol, 96%) as a yellow solid.

^{1}H NMR (400 MHz, chloroform-*d*) δ 8.24 (dd, *J* = 2.2, 0.7 Hz, 1H, C(6)H), 7.96 (dd, *J* = 9.0, 0.7 Hz, 1H, C(2)H), 7.92 (dd, *J* = 9.0, 2.1 Hz, 1H, C(3)H). ^{13}C NMR (101 MHz, chloroform-*d*) δ 162.96, 155.45, 150.85, 137.15, 135.29, 129.68, 124.90, 123.03.

LRMS: *m/z*(%)= 233.0 (100), 235.0 (86), 237.0 (26) $[M + H]^+$.

Analytical data (^{1}H NMR) were in accord with those previously reported.[11]

Methyl (2,6-dichloroquinazolin-4-yl)-*L*-leucinate (23)

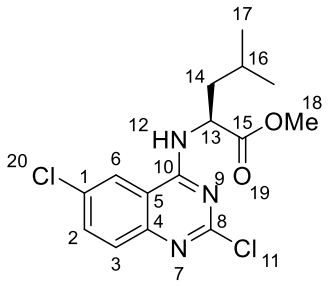

General procedure A using **22** (300 mg, 1.28 mmol, 1 equiv.) and *L*-leucine methyl ester hydrochloride (320 mg, 1.76 mmol, 1.4 equiv.). Methyl (2,6-dichloroquinazolin-4-yl)-*L*-leucinate (391 mg, 1.14 mmol, 89%) was obtained as a pale yellow solid.

IR ν_{max}/cm^{-1}(thin film): 1724 (C=O);

^{1}H NMR (400 MHz, chloroform-*d*) δ 7.63 (d, *J* = 2.2 Hz, 1H, C(6)H), 7.56 (dd, *J* = 8.9, 2.1 Hz, 1H, C(2)H), 7.51 (d, *J* = 8.9 Hz, 1H, C(3)H), 6.93 (d, *J* = 7.7 Hz, 1H, N(12)H), 5.04 (ddd, *J* = 9.9, 7.6, 3.9 Hz, 1H, C(13)H), 3.89 (s, 3H, OMe(18) -CH_3), 1.90 – 1.72 (m, 3H, C(14)H, C(16)H_2), 1.00 (dd, *J* = 7.6, 6.1 Hz, 6, (C(17)H_3)$_2$); ^{13}C NMR (101 MHz, chloroform-*d*) δ 175.37, 159.88, 157.54, 149.15, 134.27, 131.84, 129.16, 120.63, 113.61, 53.02, 52.85, 41.20, 25.21, 23.08, 22.00;

LRMS: *m/z*(%)= 342.1 (100), 344.1 (64) $[M + H]^+$; HRMS: calcd. $C_{15}H_{18}O_2N_3{}^{35}Cl_2$ $[M + H]^+$: 342.0771; found: 342.0770;

Methyl (2-allylamino-6-chloroquinazolin-4-yl)-*L*-leucinate (24)

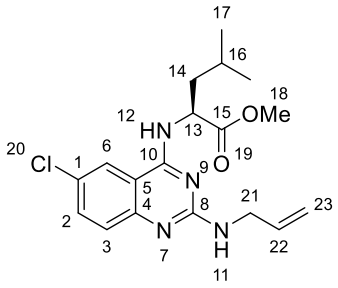

General procedure B using **23** (290 mg, 0.87 mmol, 1 equiv.). The product was purified using flash column chromatography (10−50% EtOAc in cyclohexane) to give methyl (2-allylamino-6-chloroquinazolin-4-yl)-*L*-leucinate (146 mg, 0.40 mmol 47 %) as a yellow solid.

IR ν_{max}/cm^{-1}(thin film): 1726 (C=O);

^{1}H NMR (400 MHz, chloroform-*d*) δ 7.50 (d, *J* = 2.3 Hz, 1H, C(6)H), 7.41 (dd, *J* = 8.9, 2.2 Hz, 1H, C(3)H), 7.30 (d, *J* = 8.9 Hz, 1H, C(2)H), 6.07 (s, 1H, N(12)H), 5.97 (ddt, *J* = 17.2, 10.6, 5.5 Hz, 1H, C(22)H), 5.25 (dd, *J* = 17.2, 1.7 Hz, 1H, C(23)H), 5.12 (dd, *J* = 10.2, 1.5 Hz, 1H, C(23)H), 4.97 – 4.87 (m, 1H, C(6)H), 4.10 (app. ddt, *J* = 5.7, 4.1, 1.6 Hz, 2H, C(21)H$_2$), 3.78 (s, 3H, OMe(18) -CH$_3$), 1.98 – 1.71 (m, 3H, C(14)H$_2$, C(16)H), 1.00 (d, *J* = 6.1 Hz, 3H, C(17)H$_3$), 0.97 (d, *J* = 5.9 Hz, 3H, C(17)H$_3$). ^{13}C NMR (101 MHz, chloroform-*d*) δ 174.56, 159.15, 158.97, 150.73, 135.69, 133.24, 127.07, 125.90, 120.46, 115.49, 52.40, 52.33, 43.94, 41.36, 25.00, 22.86, 22.10;

LRMS: *m/z*(%)= 363.2 (100), 365.2 (36) [M + H]$^{+}$; HRMS: calcd. $C_{18}H_{24}O_2N_4{}^{35}Cl$ [M + H]$^{+}$: 363.15823; found 363.15891;

$[\alpha]_D^{25}$ = −8.1 (c = 1 in $CHCl_3$);

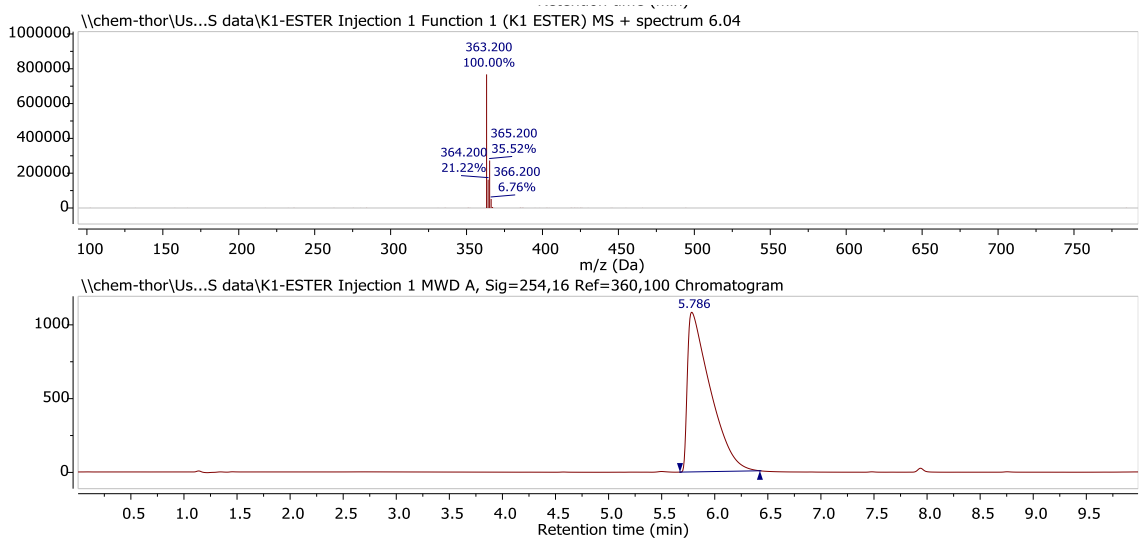

(2-Allylamino-6-chloroquinazolin-4-yl)-*L*-leucine (25)

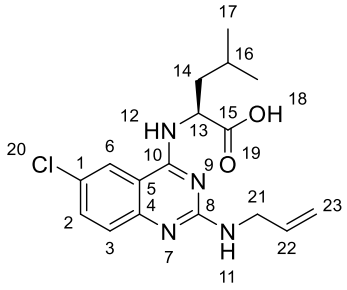

General procedure C using **24** (60 mg, 0.17 mmol, 1 equiv.). Purified using flash column chromatography (0−10% MeOH with 1% Formic acid in EtOAc) to give (2-allylamino-6-chloroquinazolin-4-yl)-*L*-leucine (34 mg, 0.10 mmol, 59%) as a white solid.

IR ν_{max}/cm^{-1}(solid): 3038 (O-H) and 1666 (C=O);

^{1}H NMR (500 MHz, DMSO-d_6 + Hydrochloric acid-*d* solution) δ 8.76 (d, *J* = 2.2 Hz, 1H, C(6)H), 7.80 (dd, *J* = 8.9, 2.3 Hz, 1H, C(2)H), 7.49 (d, *J* = 8.9 Hz, 1H, C(3)H), 5.80 (ddt, *J* = 15.9, 10.3, 5.3 Hz, 1H, C(22)H), 5.18 (d, *J* = 17.2 Hz, 1H C(23)H), 5.06 (d, *J* = 10.4 Hz, 1H, C(23)H), 4.64 (dd, *J* = 10.9, 4.1 Hz, 1H, C(13)H), 3.96 (d, *J* = 5.4 Hz, 2H, C(21)H_2),

1.99 – 1.92 (m, 1H, C(14)H), 1.72 – 1.53 (m, 2H, C(14)H, C(16)H), 0.86 (d, J = 6.2 Hz, 3H, C(17)H_3), 0.81 (d, J = 6.1 Hz, 3H, C(17)H_3); ^{13}C NMR (126 MHz, DMSO-d_6 + Hydrochloric acid-d solution) δ 173.05, 163.42, 159.65, 138.10, 135.98, 134.19, 128.82, 124.62, 119.14, 116.92, 110.69, 53.67, 43.28, 24.95, 23.23, 21.49;

LRMS: *m/z*(%)= 349.2 (100), 351.2 (33) $[M + H]^+$; HRMS: calcd. $C_{17}H_{22}O_2N_4{}^{35}Cl$ $[M + H]^+$: 349.14267; found: 349.14258

$[\alpha]_D^{25} = -7.3$ (c = 0.3 in MeOH:1M $HCl_{(aq)}$ (9:1));

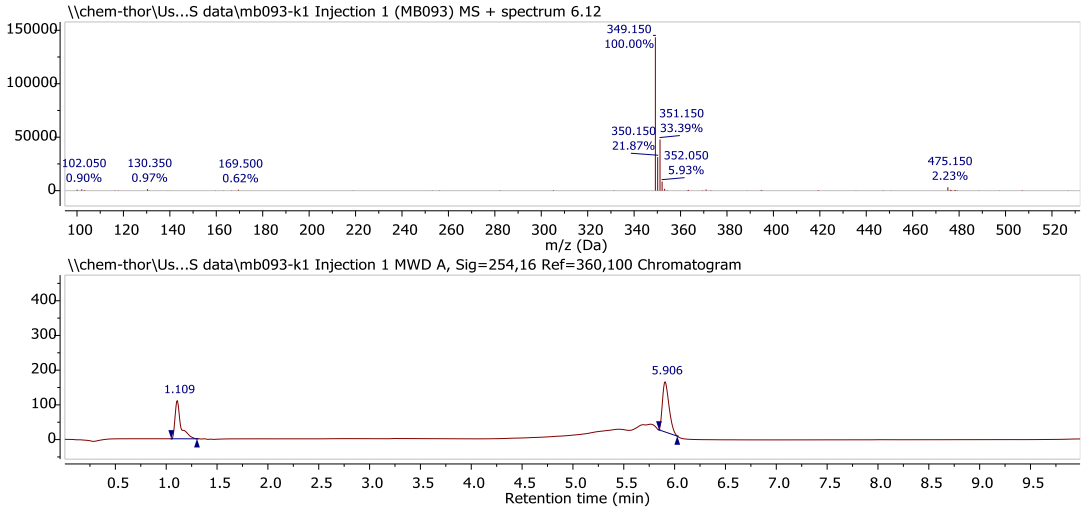

Methyl (2-allyl(methyl)amino-6-chloroquinazolin-4-yl)-*L*-leucinate (26)

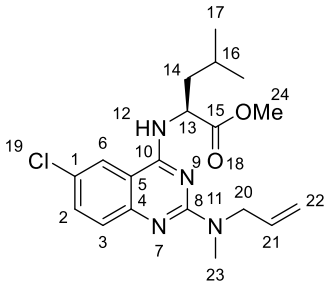

To a solution of **23** (350 mg, 1.02 mmol, 1 equiv.) in MeOH (4 mL), *N*-methylallylamine (0.5 mL, 5.20 mmol, 5.1 equiv.) was added. The reaction was stirred at 120 °C for 20 min in a microwave reactor and concentrated *in vacuo*. Purified using flash column chromatography (10−50% EtOAc in cyclohexane) to give Methyl 2-allyl(methyl)amino-6-chloroquinazolin-4-yl-*L*-leucinate (325 mg, 0.86 mmol, 84%) as yellow solid.

IR ν_{max}/cm^{-1}(solid): 1727 (C=O);

^{1}H NMR (400 MHz, chloroform-*d*) δ 7.46 (d, *J* = 2.2 Hz, 1H, C(6)H), 7.38 (dd, *J* = 9.0, 2.3 Hz, 1H, C(2)H), 7.32 (d, *J* = 8.9 Hz, 1H, C(3)H), 5.91 (d, *J* = 7.4 Hz, 1H, N(12)H), 5.89 – 5.80 (m, 1H, C(21)H), 5.18 – 5.05 (m, 2H, C(22)H_2), 4.82 (app. q, *J* = 7.2 Hz, 1H, C(13)H), 4.28 (app. td, *J* = 4.0, 2.0 Hz, 2H, C(20)H_2), 3.76 (s, 3H, OMe(24) -CH_3), 3.14 (s, 3H, NMe(23) -CH_3), 1.87 – 1.72 (m, 3H, C(14)H. C(16)H_2), 1.01 (d, *J* = 6.2 Hz, 3H, C(17)H_3), 0.96 (d, *J* = 6.1 Hz, 3H, C(17)H_3). ^{13}C NMR (101 MHz, chloroform-*d*) δ 174.61, 158.86, 158.43, 151.17, 134.64, 133.02, 127.41, 125.23, 120.32, 115.94, 110.43, 52.58, 52.28, 51.57, 41.18, 34.40, 25.01, 22.84, 22.11;

LRMS: *m/z*(%)= 377.2 (100), 379.2 (34) [M + H]$^{+}$; HRMS: calcd. $C_{19}H_{26}O_2N_4{}^{35}Cl$ [M + H]$^{+}$: 377.1739; found: 377.1740;

(2-Allyl(methyl)amino-6-chloroquinazolin-4-yl)-*L*-leucine (27)

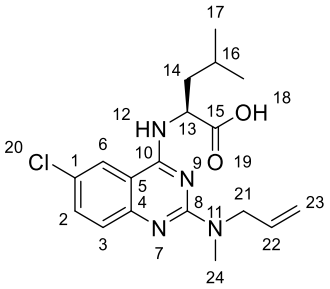

General procedure C using **26** (300 mg, 0.80 mmol, 1 equiv.). Purified using flash column chromatography (0−10% MeOH with 1% Formic acid in EtOAc) to give (2-Allyl(methyl)amino-6-chloroquinazolin-4-yl)-*L*-leucine (268 mg, 0.74 mmol, 93%) as white solid.

IR ν_{max}/cm^{-1}(solid): 3384 (O-H) and 1719 (C=O);

^{1}H NMR (400 MHz, DMSO-d_6 + Hydrochloric acid-*d* solution) δ 8.73 (d, *J* = 2.3 Hz, 1H, C(6)H), 8.05 (d, *J* = 9.0 Hz, 1H, C(3)H), 7.72 (dd, *J* = 9.0, 2.3 Hz, 1H, C(2)H), 5.74 (d, *J* = 14.2 Hz, 1H, C(22)H), 5.18 – 5.08 (m, 2H, C(23)H_2), 4.53 (app. dd, *J* = 10.6, 4.3 Hz, 1H, C(13)H), 4.26-4.14 (m, 2H, C(21)H_2), 3.19 (s, 3H, C(H)$_3$), 1.96 (app. ddd, *J* = 13.0, 10.5, 4.2 Hz, 1H, C(16)H), 1.59 (app. dtt, *J* = 22.2, 9.1, 3.8 Hz, 2H, C(14)H, C(16)H), 0.81 (d, *J* = 6.3 Hz, 3H, C(17)H_3), 0.76 (d, *J* = 6.2 Hz, 3H, C(17)H_3); ^{13}C NMR (101 MHz, DMSO-d_6) δ 173.08, 163.40, 158.53, 151.82, 138.74, 135.40, 131.99, 129.21, 124.26, 119.98, 118.32, 110.64, 53.79, 52.87, 36.72, 24.93, 23.11, 21.49;

LRMS: *m/z*(%)= 363.2 (100), 365.2 (34) $[M + H]^+$; HRMS: calcd. $C_{18}H_{22}O_2N_4{}^{35}Cl$ $[M + H]^+$: 363.15796; found: 363.15823

$[\alpha]_D^{25}$ = −11.6 (c = 1 in MeOH:1M $HCl_{(aq)}$ (9:1));

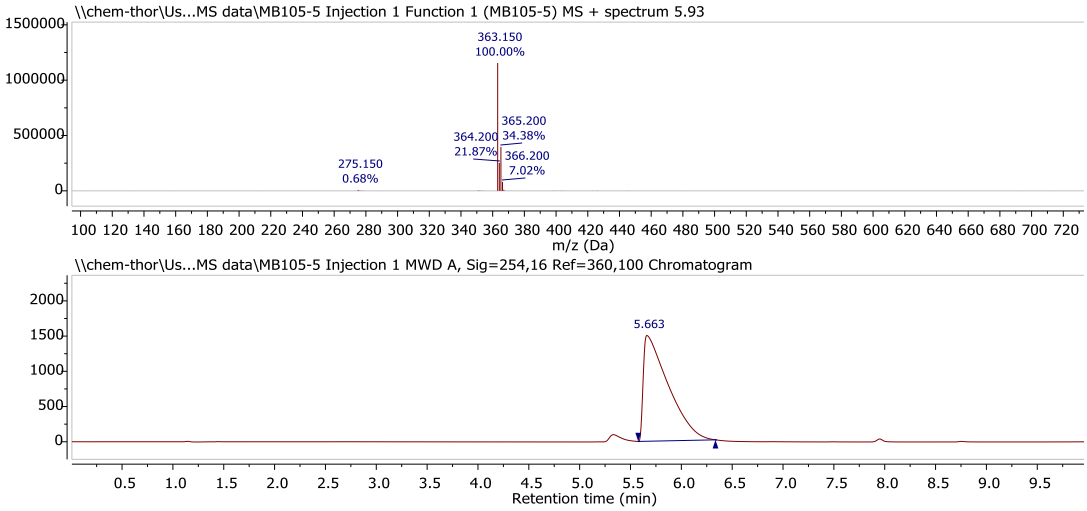

Methyl (2,6-dichloroquinazolin-4-yl)-*D*-leucinate (28)

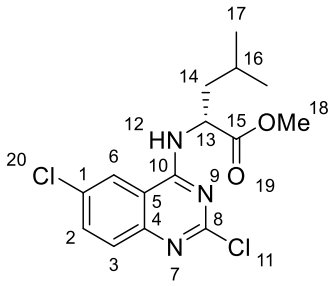

General procedure A using **22** (300 mg, 1.28 mmol, 1 equiv.) and *D*-leucine methyl ester hydrochloride (320, 1.76 mmol, 1.4 equiv.). Methyl (2,6-dichloroquinazolin-4-yl)-*D*-leucinate (366 mg, 1.07 mmol, 83%) was obtained as a pale yellow solid.

IR ν_{max}/cm^{-1}(solid): 1727 (C=O);

^{1}H NMR (400 MHz, chloroform-*d*) δ 7.56 (d, *J* = 1.9 Hz, 1H, C(6)H), 7.47 (dd, *J* = 8.9, 2.2 Hz, 1H, C(2)H), 7.41 (dd, *J* = 8.9, 0.5 Hz, 1H, C(3)H, 7.00 (d, *J* = 7.7 Hz, 1H, N(12)H), 5.01 – 4.90 (m, 1H, C(13)H) 3.83 (s, 3H, OMe(18)-CH_3), 1.73 (dt, *J* = 6.7, 2.0 Hz, 3H, C(14)H_2, C(16)H), 0.94 (d, *J* = 6.2 Hz, 3H, C(17)H_3), 0.91 (d, *J* = 6.3 Hz, 3H, C(17)H_3); ^{13}C NMR

(101 MHz, chloroform-*d*) δ 175.25, 159.73, 157.39, 148.98, 134.13, 131.69, 129.02, 120.49, 113.45, 52.90, 52.70, 41.03, 25.06, 22.95, 21.85;

LRMS: *m/z*(%)= 342.1 (100), 344.1 (62) $[M + H]^+$

Methyl (2-allylamino-6-chloroquinazolin-4-yl)-*D*-leucinate (29)

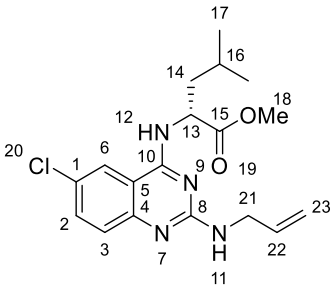

General procedure B using **28** (300 mg, 0.88 mmol, 1 equiv.). The product was purified using flash column chromatography (10−50% EtOAc in cyclohexane) to give methyl (2-allylamino-6-chloroquinazolin-4-yl)-*D*-leucinate (193 mg, 0.55 mmol, 61 %) as a yellow solid.

IR ν_{max}/cm^{-1}(thin film): 1727 (C=O);

^{1}H NMR (400 MHz, chloroform-*d*) δ 7.50 (d, *J* = 2.3 Hz, 1H, C(6)H), 7.41 (dd, *J* = 8.9, 2.3 Hz, 1H, C(2)H), 7.29 (d, *J* = 8.9 Hz, 1H C(3)H, 6.06 (d, *J* = 7.4 Hz, 1H, N(12)H), 6.02 – 5.91 (m, 1H, C(22)H), 5.25 (app. dq, *J* = 17.2, 1.7 Hz, 1H C(23)H), 5.11 (app. dq, *J* = 10.3, 1.5 Hz, 1H, C(23)H), 5.00 (brs, 1H, N(H)11), 4.96 – 4.87 (m, 1H, C(13)H), 4.10 (ddd, *J* = 5.7, 4.0, 1.6 Hz, 2H, C(21)H_2), 3.78 (s, 3H, OMe(18) –CH_3), 1.86 – 1.71 (m, 3H, C(16)H_1, C(14)H_2), 1.00 (d, *J* = 6.1 Hz, 3H, C(17)H_3), 0.97 (d, *J* = 6.1 Hz, 3H, C(17)H_3);

LRMS: *m/z*(%)= 349.2 (100), 351.2 (32) $[M + H]^+$;

(2-Allylamino-6-chloroquinazolin-4-yl)-*D*-leucine (30)

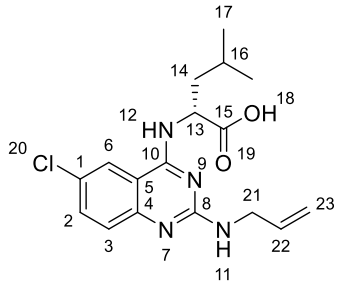

General procedure C using **29** (175 mg, 0.48 mmol, 1 equiv.). The product was purified using flash column chromatography (0−10% MeOH with 1% Formic acid in EtOAc) to give (2-allylamino-6-chloroquinazolin-4-yl)-*D*-leucine (71 mg, 0.20 mmol, 42%) as a white solid.

IR ν_{max}/cm^{-1}(solid): 3252 (O-H) and 1728 (C=O);

^{1}H NMR (400 MHz, DMSO-d_6 + hydrochloride acid-*d* solution) δ 8.71 (d, *J* = 2.2 Hz, 1H, C(6)H), 7.75 (dd, *J* = 8.9, 2.2 Hz, 1H, C(2)H), 7.44 (d, *J* = 8.9 Hz, 1H, C(3)H), 5.77 (app. ddd, *J* = 16.9, 10.6, 5.2 Hz, 1H, C(22)H), 5.13 (dd, *J* = 17.2, 1.7 Hz, 1H, C(23)H), 5.03 (app. d, *J* = 9.5 Hz, 1H C(23)H), 4.66 – 4.56 (m, 1H, C(13)H), 3.92 (app d, *J* = 5.3 Hz, 2H. C(21)H_2), 2.08 – 1.86 (m, 1H, C(16)H), 1.67 – 1.49 (m, 2H, C(14)H, C(16)H), 0.82 (d, *J* = 6.2 Hz, 3H, C(17)H_3), 0.77 (d, *J* = 6.0 Hz, 3H, , C(17)H_3);

LRMS: *m/z*(%)= 349.2 (100), 351.1 (37) $[M + H]^+$

$[\alpha]_D^{25}$ = +5.8 (c = 0.9 in MeOH:1M $HCl_{(aq)}$ (9:1));

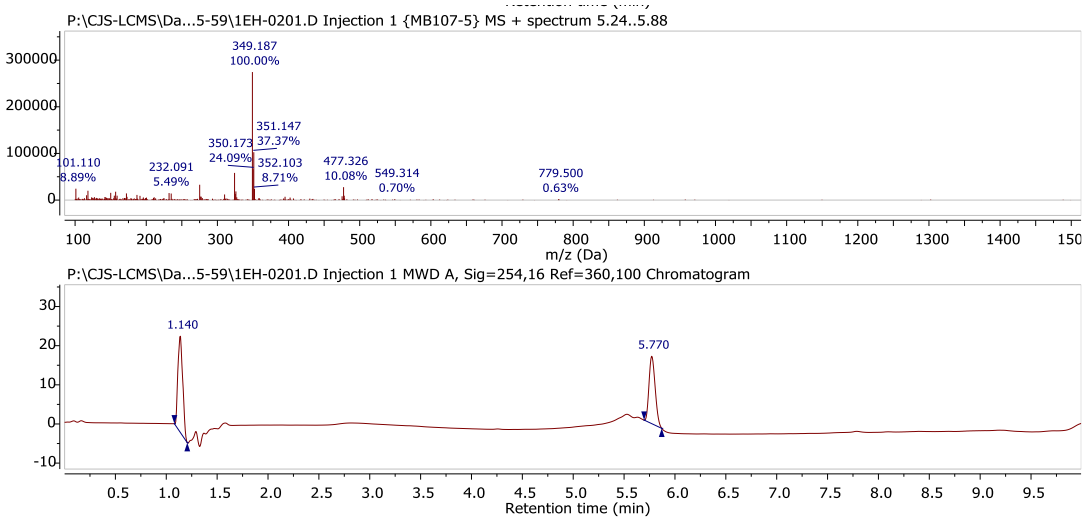

2-Allyl(methyl)amino-6-chloroquinazolin-4-yl-*D*-leucine (31)

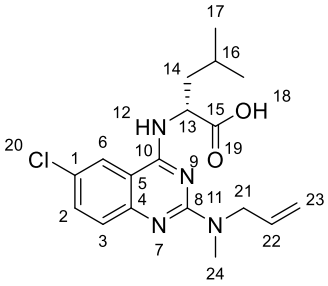

To a solution of **28** (400 mg, 1.17 mmol, 1 equiv.) in MeOH (4 mL), *N*-methylallylamine (0.5 mL, 5.20 mmol, 4.4 equiv.) was added. The reaction was stirred for 20 min at 120 °C in a microwave reactor and then concentrated *in vacuo*. The crude intermediate was used without further purification in the next step using general procedure C. The product was purified using flash column chromatography (0−10% MeOH with 1% formic acid in EtOAc) to give 2-Allyl(methyl)amino-6-chloroquinazolin-4-yl-*D*-leucine (381 mg, 1.05 mmol, 89% after 2 steps) as a white solid.

IR ν_{max}/cm^{-1}(solid): 3335 (O-H) and 1717 (C=O);

^{1}H NMR (400 MHz, DMSO-d_6 + hydrochloride acid-*d* solution) δ 8.73 (d, *J* = 2.0 Hz, 1H, C(6)H), 8.05 (d, *J* = 9.0 Hz, 1H, C(3)H), 7.72 (dd, *J* = 9.0, 2.0 Hz, 1H, C(2)H), 5.73 (app. t, *J* = 11.5 Hz, 1H, C(22)H), 5.32 – 5.00 (m, 2H, C(23)H_2), 4.53 (dd, *J* = 10.6, 4.3 Hz, 1H, C(13)H), 4.20 (s, 2H, C(21)H_2), 3.19 (s, 3H, C(24)H_3), 1.96 (app. ddd, *J* = 13.0, 10.5, 4.2 Hz, 1H, C(14)H), 1.59 (app. ddq, *J* = 19.0, 9.0, 5.0, 4.5 Hz, 2H, C(14)H, C(16)H), 0.81 (d, *J* = 6.0 Hz, 3H, C(17)H_3), 0.76 (d, *J* = 6 Hz, 3H, C(17)H_3); ^{13}C NMR (101 MHz, DMSO-d_6) δ 173.08, 163.40, 158.53, 151.82, 138.74, 135.40, 131.99, 129.21, 124.26, 119.98, 118.32, 110.64, 53.79, 36.72, 24.93, 23.11, 21.49;

LRMS: *m/z*(%)= 363.2 (100), 365.2 (34) $[M + H]^+$

$[\alpha]_D^{25}$ = +11.7 (c = 1 in MeOH:1M $HCl_{(aq)}$ (9:1));

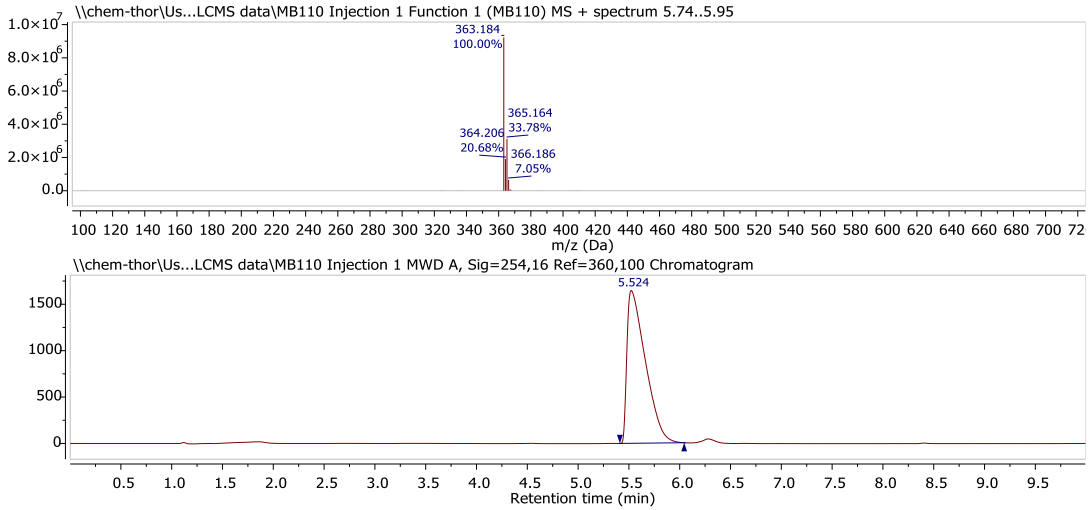

(*S*)-2-Amino-4-methylpentanamide (32)[12]

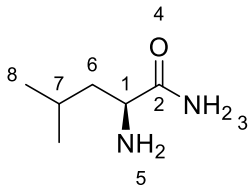

The compound was synthesised using a literature procedure.[12] A mixture of *L*-leucine methyl ester hydrochloride (1 g, 5.4 mmol, 1 equiv.) in MeOH (5 mL) and $NH_{3(aq)}$ (10 mL, excess) was stirred for 48 h at RT and then concentrated *in vacuo.* (*S*)-2-Amino-4-methylpentanamide (710 mg, 5.4 mmol, 100%) was obtained as a white solid.

^{1}H NMR (400 MHz, DMSO-d_6) δ 8.06 (s, 1H, N(3)H), 7.50 (s, 1H, N(3)H), 3.68 (t, J = 7.1 Hz, 1H, C(1)H), 1.67 (td, J = 12.4, 5.8 Hz, 1H, C(7)H), 1.57 (t, J = 7.1 Hz, 2H, C(6)H_2), 0.90 (t, J = 5.5 Hz, 6H, (C(8)H_3)$_2$); ^{13}C NMR (101 MHz, DMSO-d_6) δ 171.32, 51.35, 40.57, 24.16, 22.96, 22.67;

LRMS: *m/z*(%)= 131.2 (100), $[M + H]^+$;

Analytical data (^{1}H NMR, ^{13}C NMR and LRMS) were in accord with those previously reported.[12]

(*S*)-2-(2,6-Dichloroquinazolin-4-yl)amino-4-methylpentanamide (33)

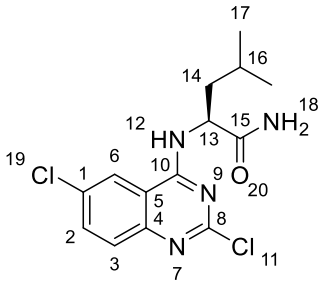

General Procedure A using **22** (300 mg, 1.28 mmol, 1 equiv.) and **32** (320 mg, 2.46 mmol, 1.8 equiv.). (*S*)-2-(2,6-dichloroquinazolin-4-yl)amino-4-methylpentanamide (394 mg, 1.21 mmol, 94%) obtained as a pale yellow solid.

IR ν_{max}/cm^{-1}(solid): 1688 (C=O);

^{1}H NMR (400 MHz, DMSO-d_6) δ 8.69 (d, *J* = 7.9 Hz, 1H, N(12)H), 8.66 (d, *J* = 2.3 Hz, 1H, C(6)H), 7.84 (dd, *J* = 8.9, 2.3 Hz, 1H C(2)H), 7.65 (d, *J* = 8.9 Hz, 1H, C(3)H), 7.62 (s, 1H, N(18)H), 7.09 (s, 1H, N(18)H), 4.71 (ddd, *J* = 11.4, 7.8, 3.8 Hz, 1H, C(13)H), 1.85 (ddd, *J* = 12.7, 11.2, 3.8 Hz, 1H, C(14)H), 1.79 – 1.53 (m, 1H, C(16)H, C(14)H), 0.93 (d, *J* = 6.3 Hz, 3H, C(17)H_3), 0.88 (d, *J* = 6.3 Hz, 3H, C(17)H_3). ^{13}C NMR (101 MHz, DMSO-d_6) δ 174.08, 160.98, 157.50, 149.49, 134.45, 130.59, 129.09, 123.69, 115.01, 53.57, 25.00, 23.66, 21.56;

LRMS: *m/z*(%)= 327.1 (100), 329.1 (66) $[M + H]^+$; HRMS: calcd. $C_{14}H_{17}ON_4{}^{35}Cl_2$ $[M + H]^+$: 327.0774; found: 327.0774;

(*S*)-2-(2-Allylamino-6-chloroquinazolin-4-yl)amino-4-methylpentanamide (34)

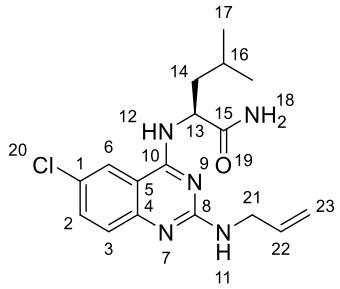

General procedure B using **33** (370 mg, 1.13 mmol, 1 equiv.). Purified using flash column chromatography (0−10% MeOH in DCM) to give (*S*)-2-(2-allylamino-6-chloroquinazolin-4-yl)amino-4-methylpentanamide (97 mg, 0.28 mmol, 25%) as white solid.

IR ν_{max}/cm^{-1}(solid): 1688 (C=O);

^{1}H NMR (400 MHz, DMSO-d_6) δ 8.31 (d, *J* = 2.4 Hz, 1H, C(6)H), 7.81 (d, *J* = 7.8 Hz, 1H, N(12)H), 7.48 (dd, *J* = 8.9, 2.4 Hz, 1H, C(2)H), 7.33 (s, 1H, N(18)H), 7.23 (d, *J* = 8.9 Hz, 1H, C(3)H), 6.96 (s, 1H, N(18)H), 6.76 (s, 1H, N(11)H), 5.91 (ddd, *J* = 15.9, 10.4, 5.1 Hz, 1H, C(22)H), 5.17 (dd, *J* = 17.1, 1.8 Hz, 1H, C(23)H), 5.02 (dd, *J* = 10.2, 1.7 Hz, 1H C(23)H), 4.69 (ddt, *J* = 10.6, 7.7, 4.3 Hz, 1H, C(13)H), 3.95 (dt, *J* = 5.8, 1.6 Hz, 1H, C(21)H), 1.90 – 1.55 (m, 3H, C(14)H_2, C(16)H), 0.93 (d, *J* = 6.3 Hz, 3H, C(17)H_3), 0.87 (d, *J* = 6.3 Hz, 3H, C(17)H_3); ^{13}C NMR (101 MHz, DMSO-d_6) δ 175.08, 159.72, 137.12, 132.89, 123.18, 115.18, 53.02, 43.57, 26.81, 24.99, 23.62, 21.85;

LRMS: *m/z*(%)= 348.2 (100), 348.2 (34) $[M + H]^+$; HRMS: calcd. $C_{18}H_{25}ON_5{}^{35}Cl$ $[M + H]^+$: 348.15875; found: 348.15856;

$[\alpha]_D^{25}$ = +14.5 (c = 1 in MeOH:DMF (9:1));

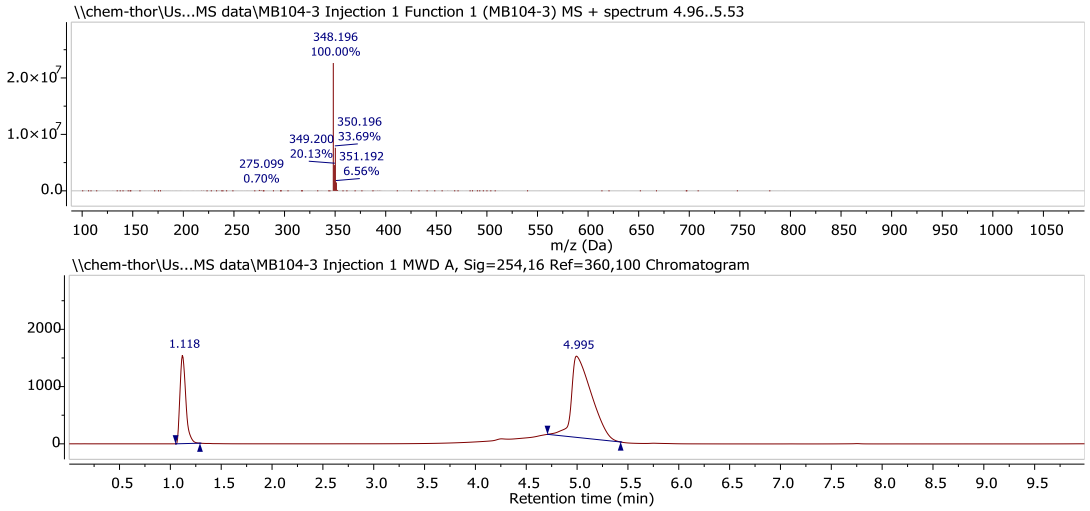

(*S*)-2-(2,6-Dichloroquinazolin-4-yl)amino-4-methylpentan-1-ol (35)

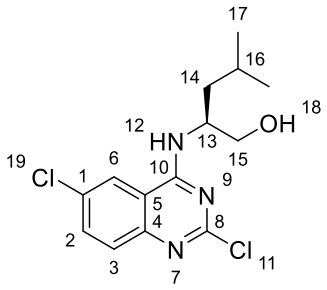

General procedure A using **22** (300 mg, 1.28 mmol, 1 equiv.) and *L*-Leucinol (270 µL, 2.12 mmol, 1.6 equiv.). (*S*)-2-(2,6-dichloroquinazolin-4-yl)amino-4-methylpentan-1-ol (328 mg, 1.05 mmol, 80%) obtained as pale yellow solid.

IR ν_{max}/cm^{-1}(solid): 1733 and 1664 (C=O);

^{1}H NMR (400 MHz, DMSO-d_6) δ 8.55 (d, *J* = 2.3 Hz, 1H, C(6)H), 8.35 (d, *J* = 8.4 Hz, 1H, N(12)H), 7.81 (dd, *J* = 8.9, 2.3 Hz, 1H, C(2)H), 7.62 (d, *J* = 8.9 Hz, 1H, C(3)H), 4.83 (t, *J* = 5.8 Hz, 1H, O(18)H), 4.46 (ddd, *J* = 9.8, 8.2, 4.2 Hz, 1H, C(13)H), 3.49 (td, *J* = 5.8, 3.4 Hz, 2H, C(15)H), 1.76 – 1.52 (m, 2H, C(14)H, C(16)H), 1.44 (tt, *J* = 9.3, 4.6 Hz, 1H, C(14)H),

0.90 (dd, *J* = 6.4, 3.6 Hz, 6H, (C(17)H_3)$_2$); ^{13}C NMR (101 MHz, DMSO-d_6) δ 160.97, 157.90, 149.57, 134.27, 130.42, 129.14, 123.28, 114.99, 63.62, 51.75, 24.88, 23.83, 22.33;

LRMS: *m/z*(%)= 314.1 (100), 316.1 (69) $[M + H]^+$; HRMS: calcd. $C_{14}H_{18}ON_3{}^{35}Cl_2$ $[M + H]^+$: 314.0821; found: 314.0821

(*S*)-2-(2-Allylamino-6-chloroquinazolin-4-yl)amino-4-methylpentan-1-ol (36)

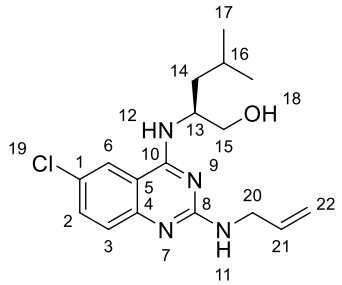

General procedure B using **33** (270 mg, 0.85 mmol, 1 equiv.). Purified using flash column chromatography (0−10% MeOH with 1% formic acid in EtOAc) to give (*S*)-2-(2-allylamino-6-chloroquinazolin-4-yl)amino-4-methylpentan-1-ol (122 mg, 0.36 mmol, 42%) as a white solid.

IR ν_{max}/cm^{-1}(solid): 3650 (O-H)

^{1}H NMR (400 MHz, DMSO-d_6) δ 8.32 (s, 1H, C(6)H), 7.55 (d, *J* = 8.7 Hz, 1H, C(2)H), 7.29 (d, *J* = 8.9 Hz, 1H, C(3)H), 5.92 (ddt, *J* = 17.2, 10.4, 5.3 Hz, 1H, C(21)H), 5.18 (ap. dq, *J* = 17.3, 1.8 Hz, 1H, C(22)H), 5.05 (app. dq, *J* = 10.3, 1.6 Hz, 1H, C(22)H), 4.47 (app. td, *J* = 14.7, 5.4 Hz, 2H, C(20)H_2), 4.07 – 3.92 (m, 1H, C(13)H), 3.48 (dd, *J* = 5.6, 3.8 Hz, 2H, C(15)H_2), 1.83 – 1.54 (m, 2H, C(16)H, C(14)H), 1.45 (app. dd, *J* = 9.7, 5.2 Hz, 1H, C(16)H), 0.91 (d, *J* = 6.5 Hz, 3H, C(15)H_3), 0.88 (d, *J* = 6.5 Hz, 3H, C(15)H_3); 13C NMR (126 MHz, DMSO-d6) δ 163.83, 159.72, 136.60, 133.44, 125.00, 123.15, 115.38, 112.11, 63.76, 51.09, 43.53, 26.82, 24.89, 23.83, 22.52;

LRMS: *m/z*(%)= 335.2 (100), 337.2 (34) $[M + H]^+$; HRMS: calcd. $C_{17}H_{24}ON_4{}^{35}Cl$ $[M + H]^+$: 335.16296 ; found: 335.16332

$[\alpha]_D^{25} = -23.4$ (c = 1 in MeOH:DMF (9:1));

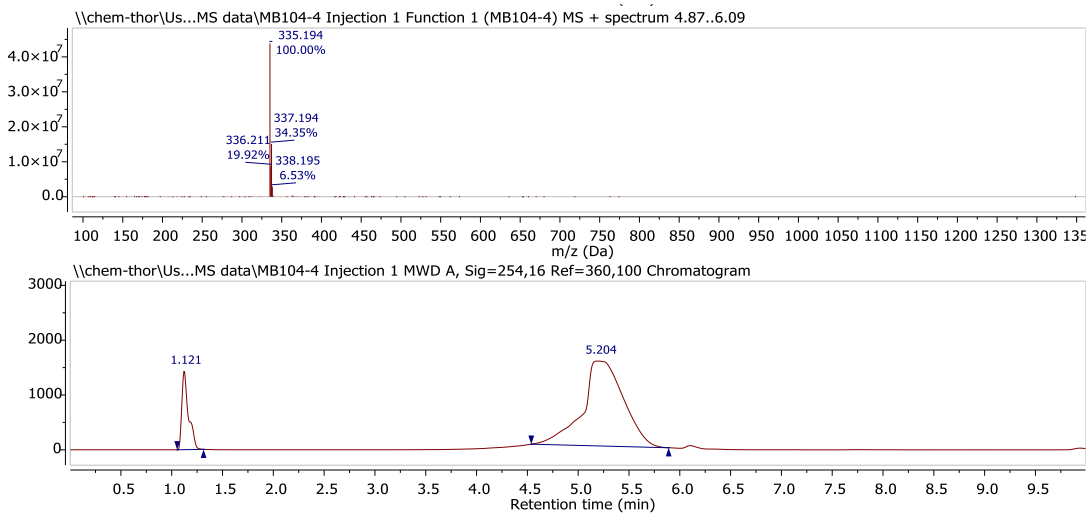

Methyl (2,6-dichloroquinazolin-4-yl-glycinate (37)

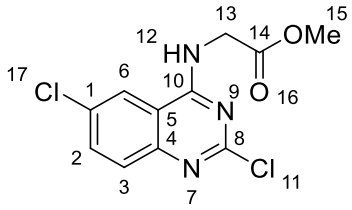

General procedure A using **22** (500 mg, 2.1 mmol, 1 equiv.) and glycine methyl ester hydrochloride (400 mg, 3.2 mmol, 1.5 equiv.). Methyl (2,6-dichloroquinazolin-4-yl)-glycinate (589 mg, 2.0 mmol , 96%) obtained as pink solid.

IR ν_{max}/cm^{-1}(thin film): 1730 (C=O);

^{1}H NMR (400 MHz, DMSO-d_6) δ 9.34 (t, *J* = 5.8 Hz, 1H, N(12)H), 8.46 (d, *J* = 2.3 Hz, 1H, C(6)H), 7.88 (dd, *J* = 8.9, 2.3 Hz, 1H, C(2)H), 7.70 (d, *J* = 8.9 Hz, 1H, C(3)H), 4.29 (d, *J* =

5.8 Hz, 2H, C(13)H), 3.69 (s, 3H. OMe(15) -CH_3); ^{13}C NMR (101 MHz, DMSO-d_6) δ 170.17, 161.05, 157.30, 149.44, 134.75, 130.99, 129.39, 123.00, 114.76, 52.46, 42.91;

LRMS: *m/z*(%)= 286.1 (100), 288.1 (63) $[M + H]^+$; HRMS: calcd. $C_{11}H_{10}O_2N_3{}^{35}Cl_2$ $[M + H]^+$: 286.0145; found: 286.0146;

Methyl (2-allylamino-6-chloroquinazolin-4-yl)-glycinate (38)

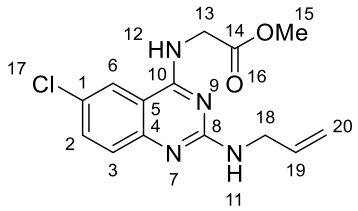

General procedure B using **37** (300 mg, 1.05 mmol, 1 equiv.). The product was purified using flash column chromatography (40−80% EtOAc in cyclohexane) to give methyl (2-allylamino-6-chloroquinazolin-4-yl)-glycinate (93 mg, 0.30 mmol 29%) as a white solid.

IR ν_{max}/cm^{-1}(thin film): 1726 (C=O);

^{1}H NMR (400 MHz, chloroform-*d*) δ 7.48 (d, *J* = 2.3 Hz, C(6)H), 7.38 (dd, *J* = 8.9, 2.3 Hz, 1H, C(2)H), 7.29 (d, *J* = 8.9 Hz, 1H, C(3)H), 6.12 (brs, 1H, N(12)H), 5.90 (ddt, *J* = 17.2, 10.6, 5.5 Hz, 1H, C(19H), 5.19 (dd, *J* = 17.2, 1.6 Hz, 1H, C(20)H), 5.05 (dd, *J* = 10.2, 1.5 Hz, 1H, C(20)H), 5.01 (brs, 1H, N(11)H) 4.25 (d, *J* = 4.9 Hz, 2H. C(13)H), 4.05 (ddd, *J* = 5.7, 4.1, 1.6 Hz, 2H C(18)H), 3.76 (s, 3H, OMe(15) -CH_3); ^{13}C NMR (101 MHz, chloroform-*d*) δ 171.02, 159.12 158.98, 156.02, 135.55, 133.40, 133.16, 126.13, 117.24, 115.61, 52.54, 43.95, 42.87;

LRMS: *m/z*(%)= 307.1 (100), 309.1 (34) $[M + H]^+$; HRMS: calcd. $C_{14}H_{16}O_2N_4{}^{35}Cl$ $[M + H]^+$: 307.0956 ; found: 307.0958;

2-(2-Allylamino-6-chloroquinazolin-4-yl)amino-*N*-hydroxyethanamide (39)

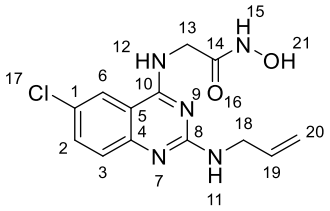

General procedure D using **38** (68 mg, 0.22 mmol, 1 equiv.). The product was purified using flash column chromatography (3−15% MeOH in DCM) to give 2-(2-Allylamino-6-chloroquinazolin-4-yl)amino-*N*-hydroxyethanamide (24 mg, 0.08 mmol 35%) as white solid.

IR ν_{max}/cm^{-1}(solid): 3330 (O-H) and 1640 (C=O);

^{1}H NMR (500 MHz, DMSO-d_6) δ 10.64 (broad s, 1H, O(21)H), 8.22 (s, 1H, C(6)H), 7.58 (s, 1H, C(2)H), 7.34 (d, *J* = 8.9 Hz, 1H, , C(3)H), 5.92 (app. td, *J* = 10.6, 5.0 Hz, 1H, C(19)H), 5.20 (dd, *J* = 17.2, 1.8 Hz, 1H, C(20)H), 5.06 (dd, *J* = 10.3, 1.8 Hz, 1H, C(20)H), 4.03 (d, *J* = 5.2 Hz, 2H, C(13)H), 3.98 (app. td, *J* = 4.8, 4.2, 1.6 Hz, 2H, C(18)H); ^{13}C NMR (126 MHz, DMSO-d_6) δ 172.52, 166.19, 159.88, 136.39, 133.72, 126.50, 125.20, 123.36, 115.68, 112.50, 43.58, 42.41;

LRMS: *m/z*(%)= 308.1 (100), 310.1 (36) $[M + H]^+$; HRMS: calcd. $C_{13}H_{15}O_2N_5{}^{35}Cl$ $[M + H]^+$: 308.0909 ; found: 308.0909;

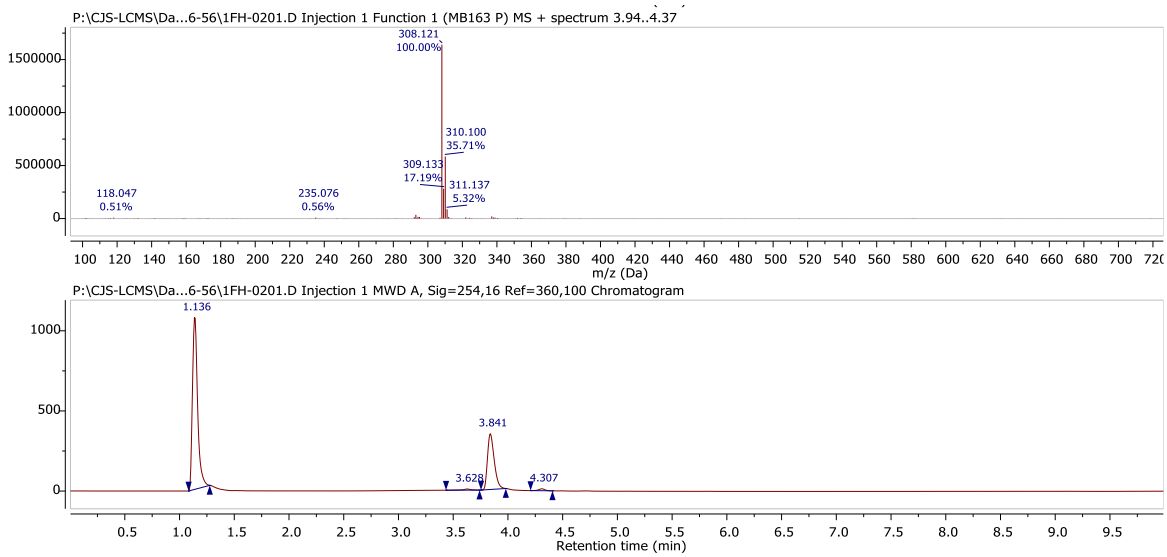

Methyl (2,6-dichloroquinazolin-4-yl-*L*-alaninate) (40)

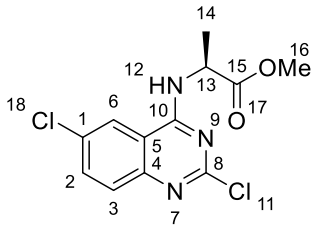

General procedure A using **22** (500 mg, 2.1 mmol, 1 equiv.) and *L*-alanine methyl ester hydrochloride (450 mg, 3.2 mmol, 1.5 equiv.). Methyl (2,6-dichloroquinazolin-4-yl)-*L*-alaninate (605 mg, 2.0 mmol, 95%) was obtained as a yellow solid.

IR ν_{max}/cm^{-1}(thin film): 1719 (C=O);

^{1}H NMR (400 MHz, chloroform-*d*) δ 7.65 (dd, *J* = 2.1, 0.7 Hz, 1H, C(6)H), 7.57 (dd, *J* = 8.9, 2.1 Hz, 1H, C(2)H), 7.53 (dd, *J* = 8.9, 0.6 Hz, 1H, C(3)H), 7.02 (d, *J* = 7.1 Hz, 1H, N(12)H), 5.02 (app. p, *J* = 7.2 Hz, 1H, C(13)H), 3.90 (s, 3H, OMe(16) –CH_3), 1.61 (d, *J* = 7.2 Hz, 3H, C(14)H_3); ^{13}C NMR (101 MHz, chloroform-*d*) δ 174.32, 159.12, 157.48, 149.22, 134.31, 131.84, 129.29, 120.51, 113.67, 53.01, 49.75, 17.97;

LRMS: *m/z*(%)= 300.1 (100), 302.1 (63) $[M + H]^+$; HRMS: calcd. $C_{12}H_{12}O_2N_3{}^{35}Cl_2$ $[M + H]^+$: 300.0301; found: 300.0303;

Methyl (2-allylamino-6-chloroquinazolin-4-yl)-*L*-alaninate (41)

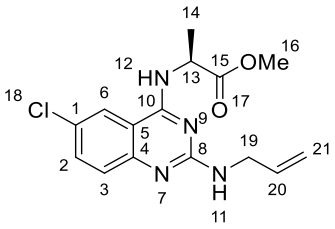

General procedure B using **40** (300 mg, 1.00 mmol, 1 equiv.). The product was purified using flash column chromatography (40−80% EtOAc in cyclohexane) to give methyl (2-allylamino-6-chloroquinazolin-4-yl)-*L*-alaninate (193 mg, 0.60 mmol 60%) as a yellow solid.

IR ν_{max}/cm^{-1}(thin film): 1722 (C=O);

^{1}H NMR (400 MHz, chloroform-*d*) δ 7.53 (d, *J* = 2.3 Hz, 1H, C(6)H), 7.44 (dd, *J* = 8.9, 2.3 Hz, 1H, C(2)H), 7.33 (d, *J* = 8.9 Hz, 1H, C(3)H), 6.14 (d, *J* = 6.7 Hz, 1H, N(12)H), 6.10 – 5.84 (m, 1H, C(20)H), 5.25 (dd, *J* = 17.1, 1.6 Hz, 1H, C(21)H), 5.12 (dd, *J* = 10.3, 1.6 Hz, 1H, C(21)H), 5.06 (brs, 1H, N(11)H), 4.86 (app p, *J* = 7.0 Hz, 1H, C(13)H), 4.10 (app tt, *J* = 5.5, 1.4 Hz, 3H, C(19)H_2), 3.80 (s, 3H, OMe(16) –CH_3), 1.57 (d, *J* = 7.1 Hz, 3H, C(14)H_3);

^{13}C NMR (101 MHz, chloroform-*d*) δ 174.32, 159.15, 158.52, 150.69, 135.66, 133.31, 127.10, 125.99, 120.52, 115.50, 52.58, 49.59, 43.92, 18.09;

LRMS: *m/z*(%)= 321.2 (100), 322.1 (34) $[M + H]^+$; HRMS: calcd. $C_{15}H_{18}O_2N_4{}^{35}Cl$ $[M + H]^+$: 321.1113; found: 321.1113;

(S)-2-(2-Allylamino-6-chloroquinazolin-4-yl)amino-*N*-hydroxypropanamide (42)

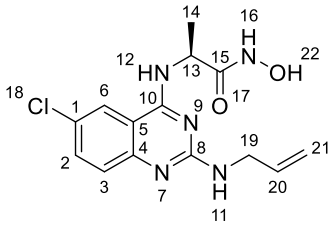

General procedure D using **41** (190 mg, 0.59 mmol, 1 equiv.). The product was purified using flash column chromatography (2−15% MeOH in DCM) to give (*S*)-2-(2-Allylamino-6-chloroquinazolin-4-yl)amino-*N*-hydroxypropanamide (137 mg, 0.43 mmol, 72%) as a white solid.

IR ν_{max}/cm^{-1}(solid): 1656 (C=O);

^{1}H NMR (400 MHz, DMSO-d_6) δ 10.56 (s, 1H, O(22)H), 8.87 (brs, 1H, N(16)H), 8.31 (d, *J* = 2.3 Hz, 1H, C(6)H), 7.98 (s, 1H, N(12)H), 7.49 (dd, *J* = 8.9, 2.4 Hz, 1H, C(2)H), 7.24 (d, *J* = 8.9 Hz, 1H, C(3)H), 6.80 (s, 1H, N(11)H), 5.93 (app. td, *J* = 10.9, 10.4, 5.0 Hz, 1H, C(20)H), 5.19 (dd, *J* = 17.3, 1.9 Hz, 1H, C(21)H), 5.04 (app. d, *J* = 10.8 Hz, 1H, C(21)H) 4.62 (app. p, *J* = 6.6 Hz, 1H, C(13)H), 4.17 – 3.81 (m, 2H, C(19)H), 1.42 (d, *J* = 7.1 Hz, 3H, C(14)H).

LRMS: *m/z*(%)= 322.2 (100), 324.1 (39) $[M + H]^+$; HRMS: calcd. $C_{14}H_{17}O_2N_5{}^{35}Cl$ $[M + H]^+$: 322.1065 ; found: 322.1066;

$[\alpha]_D^{25}$ = +3.1 (c = 0.5 in MeOH);

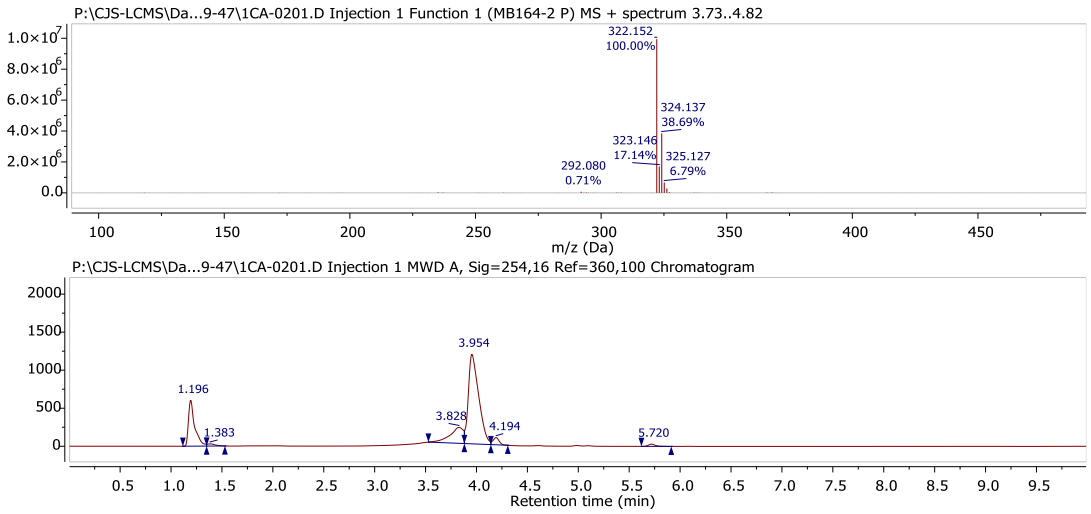

Methyl (2,6-dichloroquinazolin-4-yl)-*D*-alaninate (43)

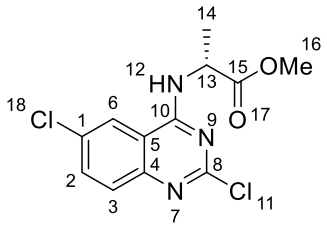

General procedure A using **22** (800 mg, 3.4 mmol, 1 equiv.) and *D*-alanine methyl ester hydrochloride (575 mg, 4.1 mmol, 1.2 equiv.). Methyl (2,6-dichloroquinazolin-4-yl)-*D*-alaninate (624 mg, 2.1 mmol, 61%) was obtained as a yellow solid.

IR ν_{max}/cm^{-1}(thin film): 1718 (C=O);

^{1}H NMR (400 MHz, chloroform-*d*) δ 7.69 (dd, *J* = 1.9, 1.0 Hz, 1H, C(6)H), 7.62-7.60 (m, 2H C(2)H, C(3)H), 6.82 (d, *J* = 7.0 Hz, 1H, N(12)H), 5.03 (app. p, *J* = 7.1 Hz, 1H, C(13)H), 3.88 (s, 3H, OMe(16)-CH_3), 1.61 (d, *J* = 7.1 Hz, 3H, C(14)H_3);

LRMS: *m/z*(%)= 300.1 (100), 302.1 (65) $[M + H]^+$;

Methyl (2-allylamino-6-chloroquinazolin-4-yl)-*D*-alaninate (44)

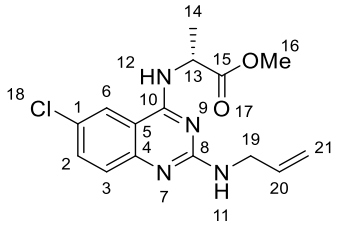

General procedure B using **43** (270 mg, 0.88 mmol, 1 equiv.). The product was purified using flash column chromatography (40−80% EtOAc in cyclohexane) to give methyl (2-allylamino-6-chloroquinazolin-4-yl)-*D*-alaninate (106 mg, 0.33 mmol, 37%) as a yellow solid.

IR ν_{max}/cm^{-1}(thin film): 1727 (C=O);

^{1}H NMR (400 MHz, chloroform-*d*) δ 7.53 (d, *J* = 2.2 Hz, 1H, C(6)H), 7.44 (dd, *J* = 8.9, 2.3 Hz, 1H, C(2)H), 7.33 (d, *J* = 8.9 Hz, 1H, C(3)H, 6.14 (d, *J* = 6.7 Hz, 1H, N(12)H), 6.03 – 5.91 (m, 1H, C(20)H), 5.25 (dd, *J* = 17.1, 1.6 Hz, 1H, C(21)H), 5.12 (dd, *J* = 10.3, 1.6 Hz, 1H, C(21)H), 5.06 (brs, 1H, N(11)H), 4.86 (app. p, *J* = 7.0 Hz, 1H, C(13)H), 4.10 (app. tt, *J* = 5.8, 1.7 Hz, 2H, C(19)H), 3.80 (s, 3H, OMe(16)), 1.57 (d, *J* = 7.1 Hz, 3H, C(14)H); ^{13}C NMR (101 MHz, chloroform-*d*) δ 174.32, 159.15, 158.52, 150.69, 135.66, 133.31, 127.10, 125.99, 120.52, 115.50, 52.58, 49.59, 43.92, 18.09;

LRMS: *m/z*(%)= 321.2 (100), 323.2 (34) $[M + H]^+$;

(*R*)-2-(2-allylamino-6-chloroquinazolin-4-yl)amino-*N*-hydroxypropanamide (45)

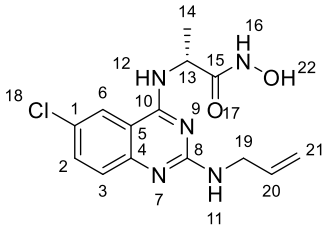

General procedure D using **44** (90 mg, 0.25 mmol, 1 equiv.). The product was purified using flash column chromatography (1−10% MeOH in DCM) to give (*S*)-2-(2-Allylamino-6-chloroquinazolin-4-yl)amino-*N*-hydroxypropanamide (72 mg, 0.22 mmol, 80%) as a white solid.

IR ν_{max}/cm^{-1}(solid): 3383 (O-H) and 1652 (C=O);

^{1}H NMR (400 MHz, DMSO-d_6) δ 10.62 (brs, 1H, O(22)H, 8.34 (brs, 1H, N(16)H), 7.53 (d, *J* = 8.7 Hz, 1H, C(2)H), 7.28 (d, *J* a(dd, *J* = 10.2, 1.9 Hz, 1H, C(21)H), 4.62 (app. p, *J* = 6.2 Hz, 1H, C(21)H), 4.10 – 3.89 (m, 2H, C(19)H$_2$), 1.42 (d, *J* = 7.1 Hz, 3H, C(14)Ha); ^{13}C NMR (101 MHz, DMSO-d_6) δ 170.00, 159.48, 159.28, 152.49, 150.96, 136.98, 132.97, 124.15, 123.30, 115.32, 48.41, 43.54, 18.18;

LRMS: *m/z*(%)= 321.1 (100), 322.1 (36) [M + H]$^{+}$;

$[\alpha]_D^{25}$ = −2.1 (c = 0.5 in MeOH);

A mixture of ethyl/methyl 3-(2-allylamino-6-chloroquinazolin-4-yl)aminopropanoate (47)

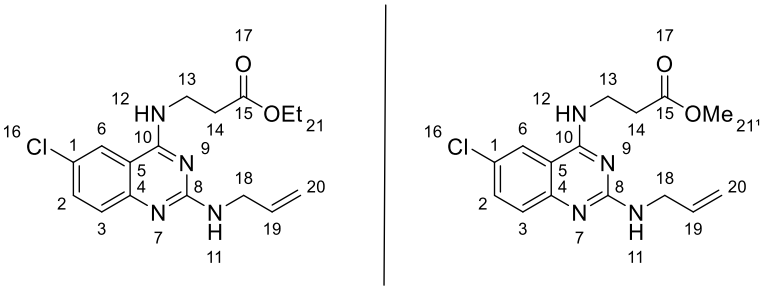

General procedure B using **46** (300 mg, 0.96 mmol, 1 equiv.). The product was purified using flash column chromatography (40−80% EtOAc in cyclohexane) to give a mixture of ethyl/methyl ester of 3-(2-allylamino-6-chloroquinazolin-4-yl)aminopropanoate (80 mg, 0.24 mmol, 25%) as a yellow solid.

IR ν_{max}/cm^{-1}(thin film): 1722 (C=O);

^{1}H NMR (400 MHz, chloroform-*d*) δ 7.47 – 7.41 (m, 2H, C(6)H, C(2)H), 7.35 (d, *J* = 8.8 Hz, 1H, C(2)H), 6.28 – 6.12 (brs, 1H, N(12)H), 5.98 (ddt, *J* = 17.2, 10.6, 5.5 Hz, 1H, C(19)H), 5.25 (dd, *J* = 17.1, 1.7 Hz, 1H, C(20)H), 5.12 (dd, *J* = 10.2, 1.5 Hz, 1H, C(20)H), 4.18 (q, *J* = 7.2 Hz, 1H, OEt(21) -CH_2-)), 4.15 – 4.09 (m, 2H, C(13)H), 3.91 – 3.81 (m, 2H, C(18)H), 3.72 (s, 1.5H, OMe(21') CH_3), 2.71 (m, 2H, C(14)H), 1.27 (t, *J* = 7.2 Hz, 1.5H, OEt(21) -CH_3); ^{13}C NMR (101 MHz, chloroform-*d*) δ 172.95, 159.20, 150.67, 135.69, 133.14, 127.14, 125.91, 120.40, 115.55, 111.75, 60.87(OEt(21) -CH_2-), 51.91((OMe(21') CH_3), 43.99, 36.48, 33.47, 14.19(OEt(21) -CH_3);

LRMS: *m/z*(%)= ethyl ester= 335.2 (100), 337.2 (33); methyl ester= 321.1 (66), 323.1 (22) $[M + H]^+$; HRMS: calcd. $C_{16}H_{20}O_2N_4{}^{35}Cl$ (ethyl ester) $[M + H]^+$: 335.1269; found: 335.1270;

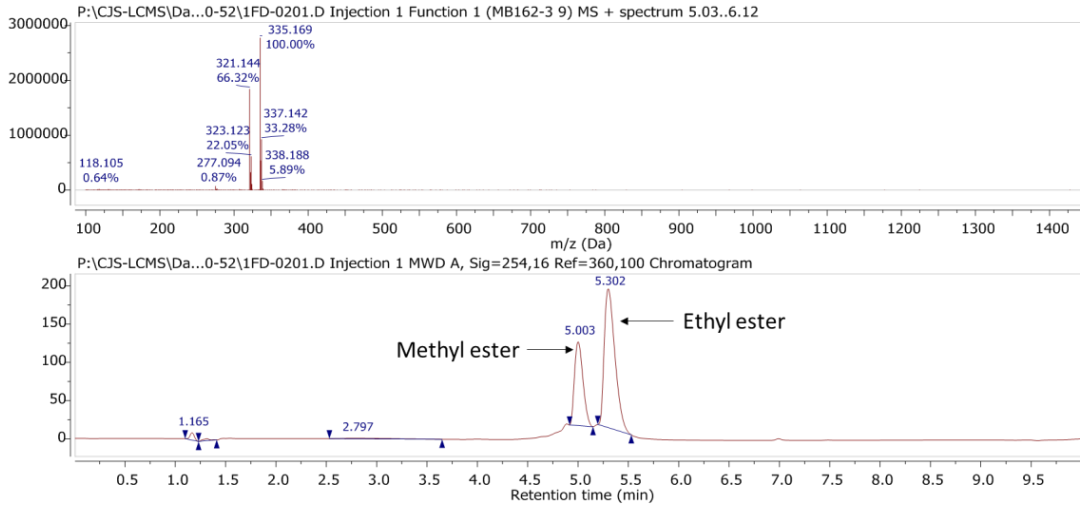

3-(2-Allylamino-6-chloroquinazolin-4-yl)amin)-*N*-hydroxypropanamide (48)

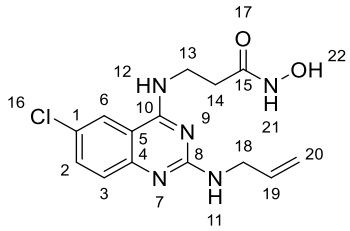

General procedure D using **47** (80 mg, 0.24 mmol, 1 equiv.). Purified using flash column chromatography (2−10% MeOH in DCM) to give 3-(2-allylamino-6-chloroquinazolin-4-yl)amino-*N*-hydroxypropanamide (18 mg, 0.06 mmol 23%) as a colourless film.

IR ν_{max}/cm^{-1}(solid): 3253 (O-H) and 1645 (C=O);

^{1}H NMR (500 MHz, DMSO-d_6) δ 10.49 (brs, 1H, O(22)H), 8.30 – 8.14 (m, 1H, C(6)H), 7.74 – 7.50 (m, 1H, C(2)H,), 7.35 (d, *J* = 8.9 Hz, 1H, C(3)H), 5.94 (ddt, *J* = 17.2, 10.5, 5.3 Hz, 1H, C(19)H), 5.22 (app d, *J* = 17.4 Hz, 1H, C(20)H), 5.08 (app d, *J* = 10.3 Hz, 1H, C(20)H), 4.01 (d, *J* = 6.5 Hz, 2H, C(18)H), 3.72 – 3.66 (m, 2H, C(13)H), 2.40 (t, *J* = 7.1 Hz, 2H, C(14)H); ^{13}C NMR (126 MHz, DMSO) δ 173.41, 167.76, 160.71, 159.48, 134.35, 133.82, 129.19, 125.35, 123.12, 115.06, 111.66, 49.06, 43.61, 31.17;

LRMS: *m/z*(%)= 322.1 (100), 324.1 (33) $[M + H]^+$; HRMS: calcd. $C_{14}H_{17}O_2N_5{}^{35}Cl$ $[M + H]^+$: 322.1065 ; found: 322.1065;

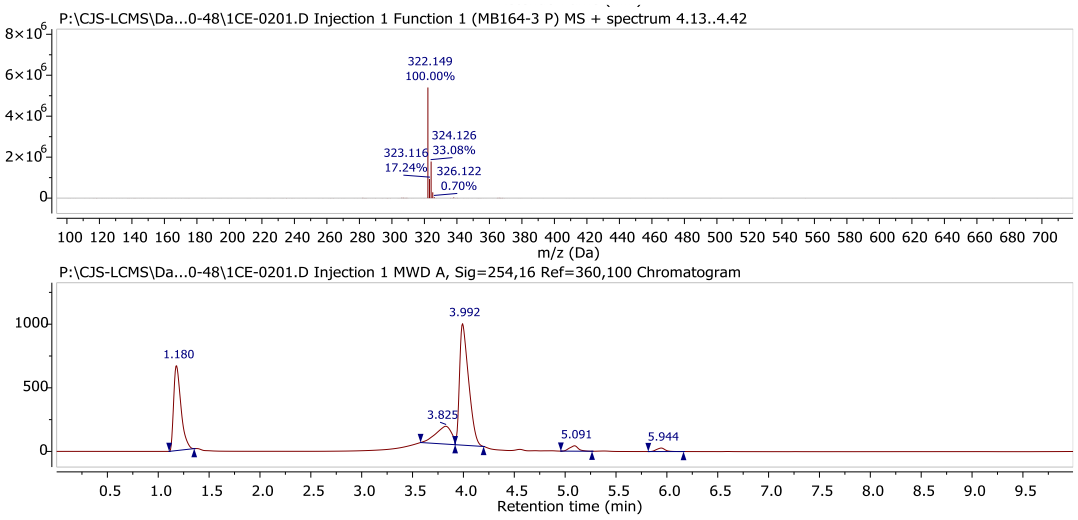

Methyl (2,6-dichloroquinazolin-4-yl)-serinate (49)

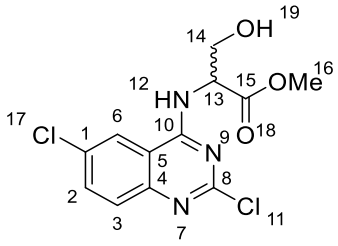

General procedure A using **22** (500 mg, 2.1 mmol, 1 equiv.) and serine methyl ester hydrochloride (500 mg, 3.2 mmol, 1.5 equiv.). Methyl (2,6-dichloroquinazolin-4-yl)-serinate (572 mg, 1.8 mmol, 85%) obtained as white solid.

IR ν_{max}/cm^{-1}(solid): 3230 (O-H) and 1736 (C=O);

^{1}H NMR (400 MHz, DMSO-d_6) δ 8.95 (d, *J* = 7.1 Hz, 1H, N(12)H), 8.66 (d, *J* = 2.3 Hz, 1H, C(6)H), 7.87 (dd, *J* = 8.9, 2.3 Hz, 1H, C(2)H), 7.69 (d, *J* = 8.9 Hz, 1H, C(3)), 5.18 (brs, 1H, O(19)H), 4.84 (dt, *J* = 7.2, 5.7 Hz, 1H C(13)H), 3.90 (d, *J* = 5.7 Hz, 2H, C(14)H_2), 3.67 (s,

3H, OMe(16) -CH_3); ^{13}C NMR (101 MHz, DMSO-d_6) δ 170.34, 160.42, 156.68, 149.07, 134.29, 130.45, 128.83, 122.96, 114.24, 60.56, 57.04, 52.13;

LRMS: *m/z*(%)= 316.1 (100), 318.1 (66) $[M + H]^+$; HRMS: calcd. $C_{12}H_{12}O_3N_3{}^{35}Cl_2$ $[M + H]^+$: 316.0250 ; found: 316.0251;

Methyl (2-allylamino-6-chloroquinazolin-4-yl)-serinate (50)

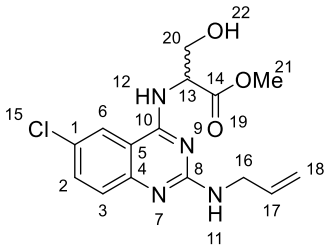

General procedure B using **49** (300 mg, 0.95 mmol, 1 equiv.). Purified using flash column chromatography (0-10% MeOH in DCM) to give product as methyl (2-allylamino-6-chloroquinazolin-4-yl)-serinate (110 mg, 0.33 mmol, 34%) as a white solid.

IR ν_{max}/cm^{-1}(solid): 3356 (O-H) and 1735 (C=O);

^{1}H NMR (400 MHz, chloroform-*d*) δ 7.44 (d, *J* = 2.3 Hz, 1H, C(6)H), 7.40 (dd, *J* = 8.9, 2.2 Hz, 1H, C(2)H), 7.28 (d, *J* = 9.0 Hz, 1H, C(3)H), 6.63 (s, 1H, N(12)H), 5.92 (ddt, *J* = 17.1, 10.5, 5.3 Hz, 1H, C(17)H), 5.22 (dd, *J* = 17.1, 1.6 Hz, 1H, C(18)H), 5.10 (dd, *J* = 10.2, 1.5 Hz, 1H, C(18)H), 4.99 – 4.89 (m, 1H, C(13)H), 4.23 (dd, *J* = 11.4, 3.2 Hz, 1H, C(20)H), 4.11 (dd, *J* = 11.4, 3.9 Hz, 1H, C(20)H), 4.03 (brs, 2H, C(16)H_2), 3.83 (s, 3H, OMe(21) -CH_3); ^{13}C NMR (101 MHz, chloroform-*d*) δ 171.66, 164.82, 158.86, 155.78 150.23,135.35, 133.52, 126.30, 120.76, 115.69, 111.21, 62.68, 56.43, 52.90, 43.93;

LRMS: *m/z*(%)= 337.1 (100), 339.1 (35) $[M + H]^+$; HRMS: calcd. $C_{15}H_{18}O_3N_4{}^{35}Cl$ $[M + H]^+$: 337.1062 ; found: 337.1063;

2-(2-Allylamino-6-chloroquinazolin-4-yl)amino-*N*,3-dihydroxypropanamide (51)

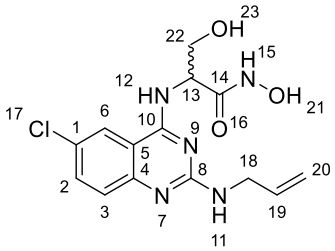

General procedure D using **50** (85 mg, 0.25 mmol, 1 equiv.). The product was purified using flash column chromatography (5−20% MeOH in DCM) to give 2-(2-Allylamino-6-chloroquinazolin-4-yl)amino-*N*,3-dihydroxypropanamide (47 mg, 0.14 mmol, 56%) as a white solid.

IR ν_{max}/cm^{-1}(solid): 3242 (O-H) and 1654 (C=O);

^{1}H NMR (500 MHz, DMSO-d_6) δ 10.59 (brs, 1H, O(21)H), 8.40 – 8.31 (m, 1H, C(6)H), 7.54 (d, *J* = 8.9 Hz, 1H, C(2)H), 7.30 (d, *J* = 8.9 Hz, 1H, C(3)H), 6.93 (brss, 1H, N(11)H), 6.06 – 5.83 (m, 1H, C(19)H), 5.20 (dd, *J* = 17.2, 1.8 Hz, 1H, C(20)H), 5.06 (dd, *J* = 10.3, 1.7 Hz, 1H, C(20)H), 4.67 (app. q, *J* = 6.6 Hz, 1H, C(13)H), 4.05 – 3.96 (m, 2H, C(18)H_2), 3.79 (app t, *J* = 5.2 Hz, 2H, C(22)H_2); ^{13}C NMR (126 MHz, DMSO-d_6) δ 172.51, 167.35, 163.68, 159.66, 158.69, 136.55, 124.65, 123.57, 115.59, 69.93, 61.64, 55.89, 43.53;

LRMS: *m/z*(%)= 338.1 (100), 340.1 (34) $[M + H]^+$; HRMS: calcd. $C_{14}H_{17}O_3N_5{}^{35}Cl$ $[M + H]^+$: 338.1016 ; found: 338.1014;

Methyl (2,6-dichloroquinazolin-4-yl)-valinate (52)

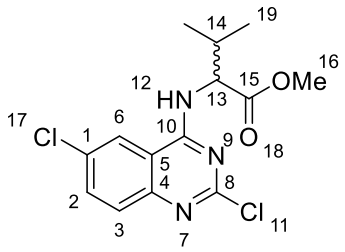

General procedure A using **22** (500 mg, 2.1 mmol, 1 equiv.) and valine methyl ester hydrochloride (540 mg, 3.4 mmol, 1.6 equiv.). Methyl (2,6-dichloroquinazolin-4-yl)-valinate (566 mg, 1,7 mmol, 82%) obtained as a yellow solid.

IR ν_{max}/cm^{-1}(thin film): 1722 (C=O);

^{1}H NMR (400 MHz, chloroform-*d*) δ 7.71 (app. t, *J* = 1.4 Hz, 1H, C(2)H), 7.64 (d, *J* = 1.4 Hz, 2H, C(2)H, C(6)H), 6.59 (d, *J* = 8.1 Hz, 1H, N(12)H), 5.03 (dd, *J* = 8.1, 5.4 Hz, 1H, (C13)H, 3.85 (s, 3H, OMe(16) -CH_3), 2.37 (app. pd, *J* = 6.9, 5.4 Hz, 1H, C(14)H), 1.06 (dd, *J* = 18.4, 6.9 Hz, 6H, $(C(19)H_3)_2$).^{13}C NMR (101 MHz, chloroform-*d*) δ 173.07, 159.84, 157.50, 149.35, 134.36, 131.85, 129.39, 120.41, 113.74, 58.86, 52.60, 31.34, 18.91, 18.48

LRMS: *m/z*(%)= 328.1 (100), 330.1 (68) $[M + H]^+$; HRMS: calcd. $C_{14}H_{16}O_2N_3{}^{35}Cl_2$ $[M + H]^+$: 328.0614 ; found: 328.0615;

Methyl (2-allylamino-6-chloroquinazolin-4-yl)-valinate (53)

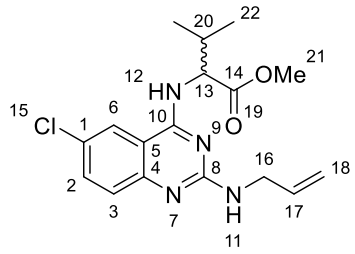

General procedure B using **52** (300 mg, 0.91 mmol, 1 equiv.). The product was purified using flash column chromatography (20−60% EtOAc in cyclohexane) to give methyl (2-allylamino-6-chloroquinazolin-4-yl)-valinate (168 mg, 0.48 mmol, 53%) as a white solid.

IR ν_{max}/cm^{-1}(thin film): 1735 (C=O);

^{1}H NMR (400 MHz, chloroform-*d*) δ 7.54 (d, *J* = 2.3 Hz, 1H, C(6)H), 7.45 (dd, *J* = 8.9, 2.3 Hz, 1H, C(2)H), 7.35 (d, *J* = 8.9 Hz, 1H, C(3)H), 6.10 – 5.86 (m, 2H, N(12)H, C(17)H), 5.24 (dd, *J* = 17.2, 1.7 Hz, 1H, C(18)H), 5.11 (dd, *J* = 10.3, 1.5 Hz, 1H, C(18)H), 5.05 (s, 1H, N(11)H), 4.86 (dd, *J* = 7.8, 5.4 Hz, 1H, C(13)H), 4.17 – 4.03 (m, 2H, C(16)H_2), 3.78 (s, 3H, OMe(21) -CH_3), 2.31 (app. pd, *J* = 6.9, 5.3 Hz, 1H, C(20)H), 1.05 (dd, *J* = 20.6, 6.9 Hz, 6H, (C(22)H_3)$_2$); ^{13}C NMR (101 MHz, chloroform-*d*) δ 173.10, 159.21, 159.13, 150.88, 135.66, 133.31, 127.23, 125.95, 120.38, 115.50, 111.47, 58.71, 52.20, 43.93, 31.28, 18.99, 18.64;

LRMS: *m/z*(%)= 349.2 (100), 351.1 (35) $[M + H]^+$; HRMS: calcd. $C_{17}H_{22}O_2N_4{}^{35}Cl_1$ $[M + H]^+$: 349.1426 ; found: 349.1426;

2-(2-allylamino-6-chloroquinazolin-4-ylamino)-*N*-hydroxy-3-methylbutanamide (54)

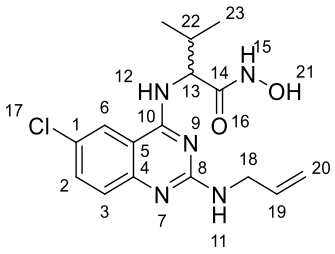

General procedure D using **53** (150 mg, 0.43 mmol, 1 equiv.). Purified using flash column chromatography (2−15% MeOH in DCM) to 2-(2-allylamino-6-chloroquinazolin-4-ylamino)-*N*-hydroxy-3-methylbutanamide (36 mg, 0.10 mmol, 24%) as a white solid.

IR ν_{max}/cm^{-1}(solid): 3236 (O-H) and 1649 (C=O);

^{1}H NMR (400 MHz, DMSO-d_6) δ 11.00 (s, 1H, O(21)H), 9.48 (d, *J* = 7.8 Hz, 1H, N(12)H), 8.82 (s, 1H, C(6)H), 8.39 (t, *J* = 5.7 Hz, 1H, N(11)H), 7.84 (dd, *J* = 8.9, 2.1 Hz, 1H, C(2)H), 7.50 (d, *J* = 8.8 Hz, 1H, C(3)H), 5.93 (app dt, *J* = 16.6, 6.2 Hz, 1H, C(19)H), 5.31 (d, *J* = 17.3 Hz, 1H, C(20)H), 5.16 (d, *J* = 10.4 Hz, 1H, C(20)H), 4.50 (app. t, *J* = 8.5 Hz, 1H, C(13)H), 4.29 – 4.02 (m, 2H, C(18)H_2), 2.37 – 2.19 (m, 1H, C(22)H), 0.96 (d, *J* = 6.8 Hz, 6H, (C(23)H_3)$_2$); ^{13}C NMR (101 MHz, DMSO-d_6) δ 172.92, 166.74, 159.72, 153.16, 138.42, 135.79, 134.75, 128.64, 124.78, 119.17, 116.85, 110.95, 60.03, 43.48, 30.13, 19.98, 19.58;

LRMS: *m/z*(%)= 350.2 (100), 352.1 (33) $[M + H]^+$; HRMS: calcd. $C_{16}H_{21}O_2N_5{}^{35}Cl$ $[M + H]^+$: 350.1378 ; found: 350.1380;

2-(2-allylamino-6-chloroquinazolin-4-yl)amino-*N*-hydroxy-4-methylpentanamide (55)

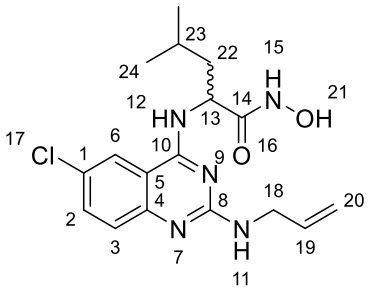

General procedure D using a racemic mixture of **24** and **29** (160 mg, 0.44 mmol, 1 equiv.). Purified using flash column chromatography (2−10% MeOH in DCM) to 2-(2-allylamino-6-chloroquinazolin-4-yl)amino-*N*-hydroxy-4-methylpentanamide (62 mg, 0.17 mmol, 39%) as a white solid.

IR ν_{max}/cm^{-1}(solid): 3303 (O-H) and 1629 (C=O);

^{1}H NMR (500 MHz, DMSO-d_6) δ 10.58 (brs, 1H, O(21)H), 8.84 (s, 1H, N(15)H), 8.35 (d, *J* = 2.6 Hz, 1H, C(6)H), 7.95 (brs, 1H, N(12)H), 7.50 (dd, *J* = 8.9, 2.4 Hz, 1H, C(2)H), 7.26 (d, *J* = 8.9 Hz, 1H, C(3)H), 6.80 (brs, 1H, N(11)H), 6.23 – 5.83 (m, 1H, C(19)H), 5.20 (dd, *J* = 17.2, 2.1 Hz, 1H, C(20)H), 5.05 (app. d, *J* = 10.2 Hz, 1H C(20)H), 4.77 – 4.60 (m, 1H, C(13)H) 3.97 (app d, *J* = 24.5 Hz, 2H, C(18)H), 1.89 – 1.74 (m, 1H, C(22)H), 1.75 – 1.52 (m, 2H, C(22)H, C(23)H), 0.93 (d, *J* = 6.4 Hz, 3H, C(24)H_3), 0.86 (d, *J* = 6.3 Hz, 3H, C(24)H_3); ^{13}C NMR (126 MHz, DMSO-d_6) δ 169.54, 159.55, 159.33, 150.69, 136.88, 135.68, 133.05, 126.96, 124.29, 123.32, 115.40, 112.21, 51.17, 43.55, 24.83, 23.37, 22.11;

LRMS: *m/z*(%)= 364.2 (100), 366.2 (35) $[M + H]^+$; HRMS: calcd. $C_{17}H_{23}O_2N_5{}^{35}Cl$ $[M + H]^+$: 364.1535 ; found: 364.1537;

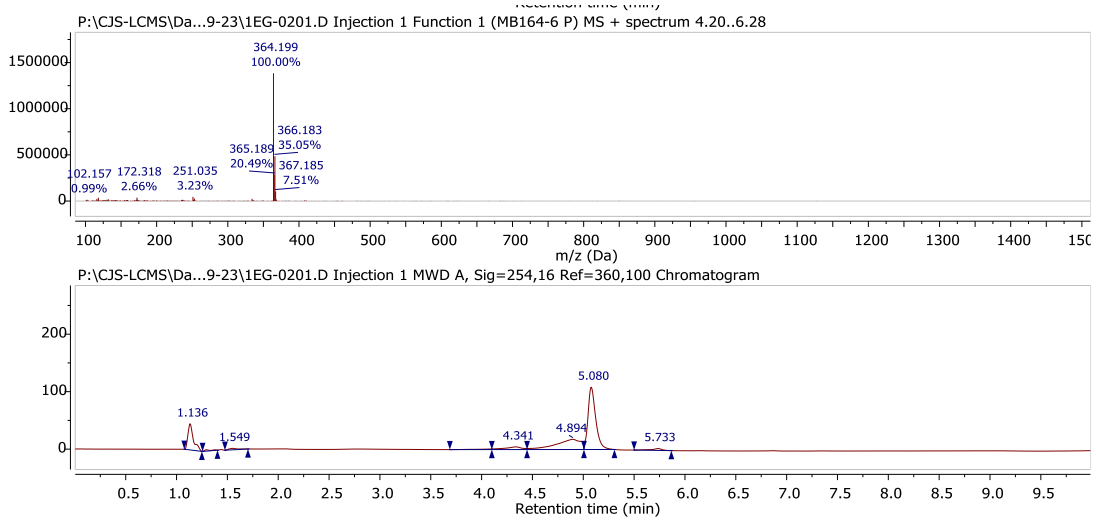

Ethyl (6-chloro-2-ethoxyquinazolin-4-yl)-*L*-alaninate (56)

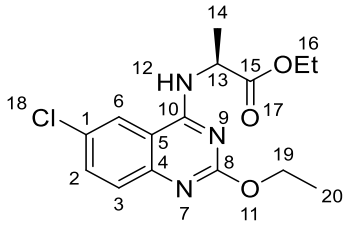

To a solution of **40** (200 mg, 0.67 mmol, 1 equiv.) in EtOH (2 mL), 4 M HCl in dioxane (2 mL) was added. The reaction mixture was stirred at 50 °C. Then, it was quenched with sat. $NaHCO_{3(aq)}$ (25 mL) and extracted with DCM (3 × 25 ml). The combined organic layer was washed with brine (30 mL), dried over Na_2SO_4, then concentrated *in vacuo* to give ethyl (6-chloro-2-ethoxyquinazolin-4-yl)-*L*-alaninate (182 mg, 0.56 mmol, 84%).

IR ν_{max}/cm^{-1}(thin film): 1722 (C=O);

^{1}H NMR (400 MHz, chloroform-*d*) δ 7.63 (dd, *J* = 2.2, 0.7 Hz, 1H, C(6)H), 7.51 (dd, *J* = 8.9, 2.0 Hz, 1H, C(2)H), 7.47 (dd, *J* = 8.9, 0.7 Hz, 1H, C(3)H), 6.55 (d, *J* = 7.0 Hz, 1H, N(12)H), 5.01 (app. p, *J* = 7.2 Hz, 1H, C(13)H), 4.44 (app. qt, *J* = 7.0, 3.5 Hz, 2H, C(19)H), 4.29 (app. qt, *J* = 7.1, 3.5 Hz, 2H, -OEt(16) –CH_2-), 1.59 (d, *J* = 7.1 Hz, 3H, C(14)H), 1.43

(t, *J* = 7.1 Hz, 3H C(20)H), 1.33 (t, *J* = 7.1 Hz, 3H, -OEt(16) –CH_3); ^{13}C NMR (101 MHz, chloroform-*d*) δ 174.01, 162.30, 160.01, 150.18, 133.48, 128.40, 128.35, 120.51, 112.56, 62.82, 61.83, 49.53, 18.22, 14.67, 14.18;

LRMS: *m/z*(%)= 324.2 (100), 326.2 (34) $[M + H]^+$; HRMS: calcd. $C_{15}H_{19}O_3N_3{}^{35}Cl$ $[M + H]^+$: 324.1109 ; found: 324.1110;

(*S*)-2-(6-Chloro-2-ethoxyquinazolin-4-yl)amino-*N*-hydroxypropanamide (57)

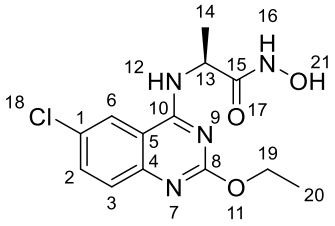

General procedure D using **56** (150 mg, 0.48 mmol, 1 equiv.). Purified using flash column chromatography (2−20% MeOH in DCM) to give (*S*)-2-(6-chloro-2-ethoxyquinazolin-4-yl)amino-*N*-hydroxypropanamide (123 mg, 0.40 mmol, 82%) as white solid.

IR ν_{max}/cm^{-1}(solid): 3223 (O-H) and 1666 (C=O);

^{1}H NMR (400 MHz, DMSO-d_6) δ 10.84 (s, 1H, O(21)H), 9.44 (s, 1H, N(12)H), 8.69 (d, *J* = 2.3 Hz, 1H, C(6)H), 7.88 (dd, *J* = 8.9, 2.3 Hz, 1H, C(2)H), 7.55 (d, *J* = 8.9 Hz, 1H, C(3)H), 5.02 – 4.69 (m, 1H, C(13)H), 4.52 (q, *J* = 7.1 Hz, 2H, C(19)H_2), 1.49 (d, *J* = 7.2 Hz, 3H, C(14)H_2), 1.37 (t, *J* = 7.1 Hz, 3H, C(20)H_3); ^{13}C NMR (101 MHz, DMSO-d_6) δ 168.55, 161.18, 159.58, 135.43, 129.19, 124.36, 123.44 112.62, 65.11, 49.93, 18.10, 14.69;

LRMS: *m/z*(%)= 311.1 (100), 313.1 (31) $[M + H]^+$; HRMS: calcd. $C_{13}H_{16}O_3N_4{}^{35}Cl$ $[M + H]^+$: 311.09054 ; found: 311.09055;

$[\alpha]_D^{25}$ = +29.2 (c = 0.6 in MeOH);

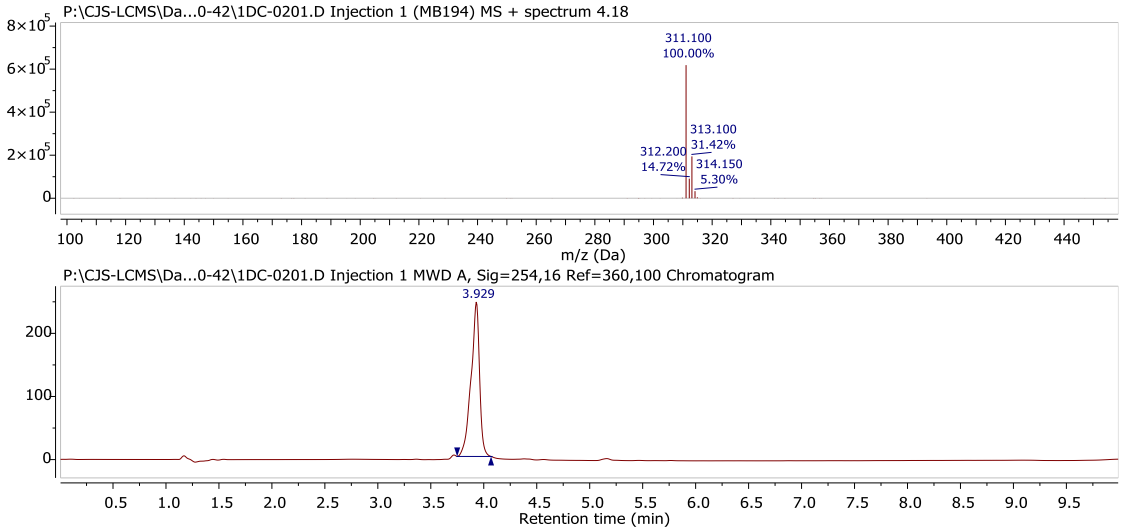

Methyl (6-chloro-2-morpholinoquinazolin-4-yl)-*L*-alaninate (58)

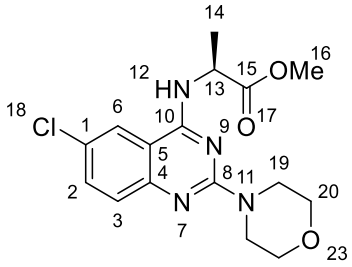

To a solution of **40** (400 mg, 1.3 mmol, 1 equiv.) in MeOH (4.5 mL), morpholine (0.5 mL, 5.7 mmol, 4.4 equiv.) was added. The reaction mixture was stirred for 20 min at 120 °C in a microwave reactor. Then, it was acidified to pH 2 with 4 M HCl in 1,4-dioxane and concentrated *in vacuo*. The product was purified using flash column chromatography (10−50% EtOAc in cyclohexane) to give methyl (6-chloro-2-morpholinoquinazolin-4-yl)-*L*-alaninate (352 mg, 1 mmol, 75%) as a yellow solid.

IR ν_{max}/cm^{-1}(thin film):1730 (C=O);

^{1}H NMR (400 MHz, chloroform-*d*) δ 7.49 (d, *J* = 2.3 Hz, 1H, C(6)H), 7.39 (dd, *J* = 8.9, 2.3 Hz, 1H, C(2)H), 7.30 (d, *J* = 8.8 Hz, 1H, C(3)H), 6.21 (d, *J* = 6.5 Hz, 1H, N(12)H), 5.10 – 4.64 (m, 1H, C(13)H), 3.83 (app. dd, *J* = 6.5, 4.2 Hz, 4H, $(C(20)H_2)_2$), 3.80 (s, 3H, OMe(16) $-CH_3$), 3.76 (app. ddd, *J* = 5.7, 3.3, 1.2 Hz, 4H, $(C(19)H_2)_2$), 1.58 (d, *J* = 7.2 Hz, 3H, C(14)H); ^{13}C NMR (101 MHz, chloroform-*d*) δ 174.65, 158.53, 158.28, 150.73, 133.21, 127.45, 125.96, 120.44, 110.75, 67.01, 52.44, 49.94, 44.31, 17.70;

LRMS: *m/z*(%)= 351.2 (100), 353.2 (33) $[M + H]^+$; HRMS: calcd. $C_{16}H_{20}O_3N_4{}^{35}Cl$ $[M + H]^+$: 351.1218 ; found: 351.1219;

(*S*)-2-(6-Chloro-2-morpholinoquinazolin-4-yl)amino-*N*-hydroxypropanamide (59)

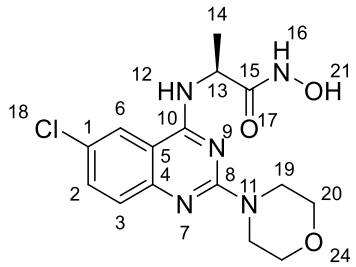

General procedure D using **58** (250 mg, 0.71 mmol). The product was purified using flash column chromatography (5−20% MeOH in DCM) to give (*S*)-2-(6-chloro-2-morpholinoquinazolin-4-yl)amino-*N*-hydroxypropanamide (224 mg, 59%) as a white solid.

IR ν_{max}/cm^{-1}(solid): 3208 (O-H) and 1644 (C=O);

^{1}H NMR (400 MHz, DMSO-d_6) δ 10.67 (d, *J* = 1.7 Hz, 1H, O(21)H), 8.76 (d, *J* = 1.7 Hz, 1H, N(16)H), 8.35 (d, *J* = 2.4 Hz, 1H, C(6)H), 8.03 (d, *J* = 6.6 Hz, 1H, N(12)H), 7.52 (dd, *J* = 8.9, 2.4 Hz, 1H, C(2)H), 7.28 (d, *J* = 8.9 Hz, 1H, C(3)H), 4.52 (app p, *J* = 7.0 Hz, 1H, C(13)H), 3.73 (dd, *J* = 5.9, 3.7 Hz, 4H, $(C(19)H_2)_2$), 3.63 (t, *J* = 4.7 Hz, 4H, $(C(20)H_2)_2$),

1.42 (d, J = 7.2 Hz, 3H, (C(14)H_3); ^{13}C NMR (101 MHz, DMSO-d_6) δ 170.14, 159.21, 158.97, 150.92, 133.11, 127.36, 124.69, 123.29, 111.75, 66.66, 48.91, 44.52, 18.39;

LRMS: *m/z*(%)= 352.2 (100), 354.2 (34) $[M + H]^+$; HRMS: calcd. $C_{15}H_{19}O_3N_5{}^{35}Cl$ $[M + H]^+$: 352.11706 ; found: 352.11740;

$[\alpha]_D^{25} = -6.9$ (c = 0.9 in MeOH);

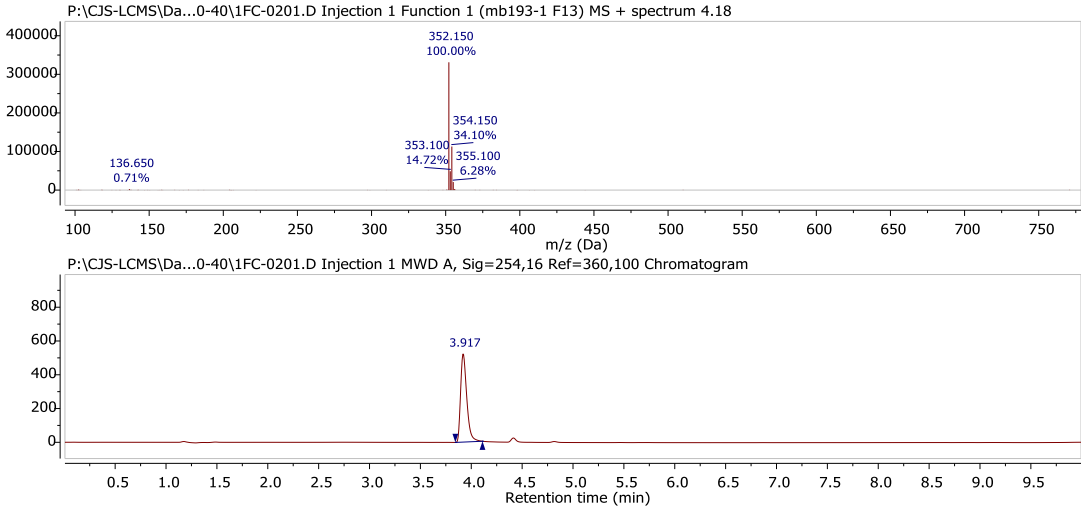

Methyl (6-chloro-2-diethylaminoquinazolin-4-yl)-*L*-alaninate (60)

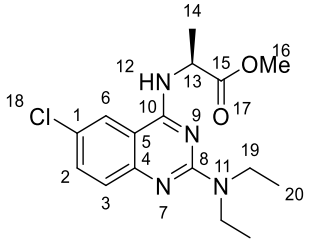

To a solution of **40** (300 mg, 1.00 mmol, 1 equiv.) in MeOH (3 mL), diethylamine (0.5 mL, 4.8 mmol, 4.8 equiv.) was added. The reaction mixture was stirred for 20 min at 120 °C in a microwave reactor. Then it was acidified to pH 2 with 4 M HCl in 1,4-dioxane and then concentrated *in vacuo*. Purified using flash column chromatography (10−50% EtOAc in

cyclohexane) to give methyl (6-chloro-2-(diethylamino)quinazolin-4-yl)-*L*-alaninate (208 mg, 0.62 mmol, 62%) as a yellow solid.

IR ν_{max}/cm^{-1}(thin film):1731 (C=O);

^{1}H NMR (400 MHz, chloroform-*d*) δ 7.49 (d, *J* = 2.3 Hz, 1H, C(6)H), 7.40 (dd, *J* = 9.0, 2.3 Hz, 1H, C(2)H), 7.33 (d, *J* = 9.0 Hz, 1H, C(3)H), 5.85 (d, *J* = 6.5 Hz, 1H, N(12)H) 4.81 (app p, *J* = 7.0 Hz, 1H, C(13)H), 3.78 (s, 3H, OMe(16) –CH_3), 3.65 (qd, *J* = 7.0, 4.6 Hz, 4H, (C(13)H_2)$_3$), 1.58 (d, *J* = 7.2 Hz, 3H, C(14)H), 1.19 (t, *J* = 7.0 Hz, 6H, (C(20)H_3)$_2$); ^{13}C NMR (101 MHz, chloroform-*d*) δ 174.35, 158.02, 151.48, 132.92, 127.43, 124.83, 120.30, 110.33, 52.39, 49.71, 41.52, 18.09, 13.53;

LRMS: *m/z*(%)= 337.2 (100), 339.2 (35) $[M + H]^+$; HRMS: calcd. $C_{16}H_{22}O_2N_4{}^{35}Cl$ $[M + H]^+$: 337.1426 ; found: 337.1426;

(*S*)-2-(6-chloro-2-diethylaminoquinazolin-4-yl)amino-*N*-hydroxypropanamide (61)

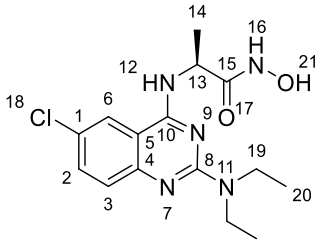

General procedure D using **60** (150 mg, 0.45 mmol, 1 equiv.). The product was purified using flash column chromatography (5−20% MeOH in DCM) to give (*S*)-2-(6-chloro-2-(diethylamino)quinazolin-4-yl)amino-*N*-hydroxypropanamide (133 mg, 0.39 mmol, 88%) as a white solid.

IR ν_{max}/cm^{-1}(solid): 3221 (O-H) and 1637 (C=O);

^{1}H NMR (400 MHz, DMSO-d_6) δ 10.82 (s, 1H, O(21)H), 9.31 (brs, 1H, N(16)H), 8.89 (brs, 1H, N(12)H), 8.61 (d, *J* = 2.2 Hz, 1H, C(6)H), 7.86 (dd, *J* = 8.9, 2.2 Hz, 1H, C(2)H), 7.76 (d, *J* = 9.0 Hz, 1H, C(3)H), 4.62 (app. p, *J* = 7.0 Hz, 1H, C(13)H), 3.67 (app. d, *J* = 7.2 Hz, 4H, $(C(19)H_2)_2$), 1.49 (d, *J* = 7.2 Hz, 3H, $(C(14)H_3)$, 1.20 (t, *J* = 7.0 Hz, 6H, $(C(20)H_3)_2$); ^{13}C NMR (101 MHz, DMSO-d_6) δ 168.59, 158.30, 151.06, 139.27, 135.13, 128.74, 124.45, 120.08, 111.04, 50.17, 18.11, 13.38;

LRMS: *m/z*(%)= 338.2 (100), 340.2 (27) $[M + H]^+$; HRMS: calcd. $C_{15}H_{21}O_2N_5{}^{35}Cl$ $[M + H]^+$: 338.13783 ; found: 338.13791;

$[\alpha]_D^{25}$ = +3.9 (c = 0.6 in MeOH);

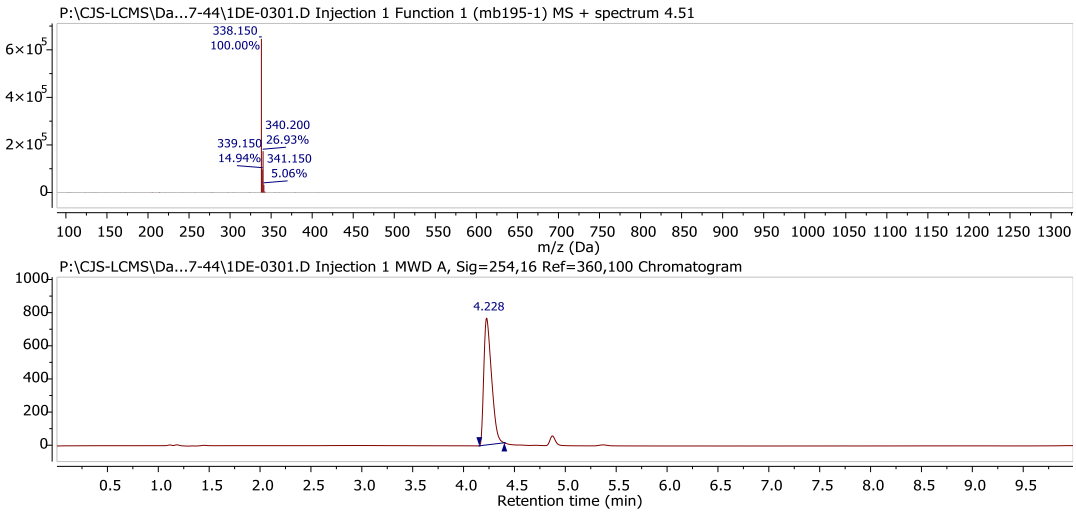

Methyl (6-chloro-2-methyl(propyl)aminoquinazolin-4-yl)-*L*-alaninate (62)

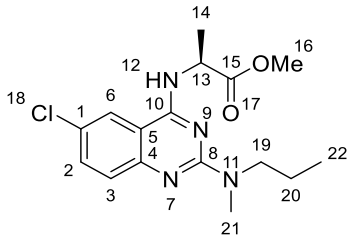

To a solution of **40** (300 mg, 1.00 mmol, 1 equiv.) in MeOH (3 mL), *N*-Methylpropylamine (0.29 mL, 3.0 mmol, 3 equiv.) was added. The reaction mixture was stirred for 20 min at 120 °C in a microwave reactor. The reaction mixture was acidified with 4 M HCl and then concentrated *in vacuo*. The product was purified using flash column chromatography (20-60% EtOAc in cyclohexane) to give methyl (6-chloro-2-methyl(propyl)aminoquinazolin-4-yl)-*L*-alaninate (247 mg, 0.73 mmol, 73%) as a white solid.

IR ν_{max}/cm^{-1}(thin film): 1732 (C=O);

^{1}H NMR (400 MHz, chloroform-*d*) δ 7.48 (d, *J* = 2.3 Hz, 1H, (C(6)H), 7.37 (dd, *J* = 9.0, 2.3 Hz, 1H, C(2)H), 7.32 (d, *J* = 8.9 Hz, 1H, C(3)H), 6.01 (d, *J* = 6.6 Hz, 1H, N(12)H), 4.78 (app. p, *J* = 7.1 Hz, 1H, C(13)H), 3.79 (s, 3H, OMe(16) -CH_3), 3.59 (app. tq, *J* = 13.6, 7.0, 6.5 Hz, 2H, C(19)H_2), 3.17 (s, 3H, C(21)H_2), 1.69 – 1.59 (m, 2H, C(20)H_2), 1.58 (d, *J* = 7.2 Hz, 3H, C(14)H_3), 0.93 (t, *J* = 7.4 Hz, 3H, C(22)H_3); ^{13}C NMR (101 MHz, chloroform-*d*) δ 174.59, 158.96, 157.94, 151.25, 132.95, 127.30, 124.98, 120.37, 110.29, 52.37, 50.92, 49.79, 35.10, 20.96, 17.89, 11.39;

LRMS: *m/z*(%)= 337.2 (100), 339.2 (33) $[M + H]^+$; HRMS: calcd. $C_{16}H_{22}O_2N_4{}^{35}Cl$ $[M + H]^+$: 337.1426 ; found: 337.1425;

(*S*)-2-(6-chloro-2-methyl(propyl)aminoquinazolin-4-yl)amino-*N*-hydroxypropanamide (63)

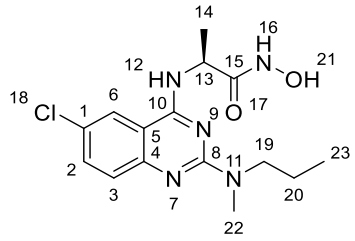

General procedure D using **62** (150 mg, 0.45 mmol, 1 equiv.). Purified using flash column chromatography (5−20% MeOH in DCM) to give (*S*)-2-(6-chloro-2-methyl(propyl)aminoquinazolin-4-yl)amino-*N*-hydroxypropanamide (127 mg, 0.38 mmol, 83%) as a white solid.

IR ν_{max}/cm^{-1}(solid): 3192 (O-H) and 1635 (C=O);

^{1}H NMR (400 MHz, DMSO-d_6) δ 10.88 (brs, 1H, O(21)H), 9.07 (brs, 1H, N(12)H), 8.59 (d, *J* = 2.3 Hz, 1H, C(6)H), 7.96 (d, *J* = 8.9 Hz, 1H, C(3)H), 7.73 (dd, *J* = 8.9, 2.3 Hz, 1H, C(2)H), 4.74 – 4.56 (m, 1H C(13)H), 3.68 – 3.64 (m, 2H, C(19)H$_2$) 3.22 (s, 3H, C(22)H$_3$), 1.67 – 1.50 (m, 2H, C(20)H$_2$), 1.47 (d, *J* = 7.2 Hz, 3H, C(14)H$_3$), 0.88 (t, *J* = 7.3 Hz, 3H, C(23)H); ^{13}C NMR (101 MHz, DMSO-d_6) δ 169.09, 163.52, 158.33, 153.74, 134.57, 127.58 124.19, 121.80, 111.05, 51.83, 49.96, 36.65, 20.57, 18.16, 11.38;

LRMS: *m/z*(%)= 338.2 (100), 340.2 (35) [M + H]$^+$; HRMS: calcd. $C_{15}H_{21}O_2N_5{}^{35}Cl$ [M + H]$^+$: 338.13783; found: 338.13782;

$[\alpha]_D^{25}$ = −6.9 (c = 1.1 in MeOH);

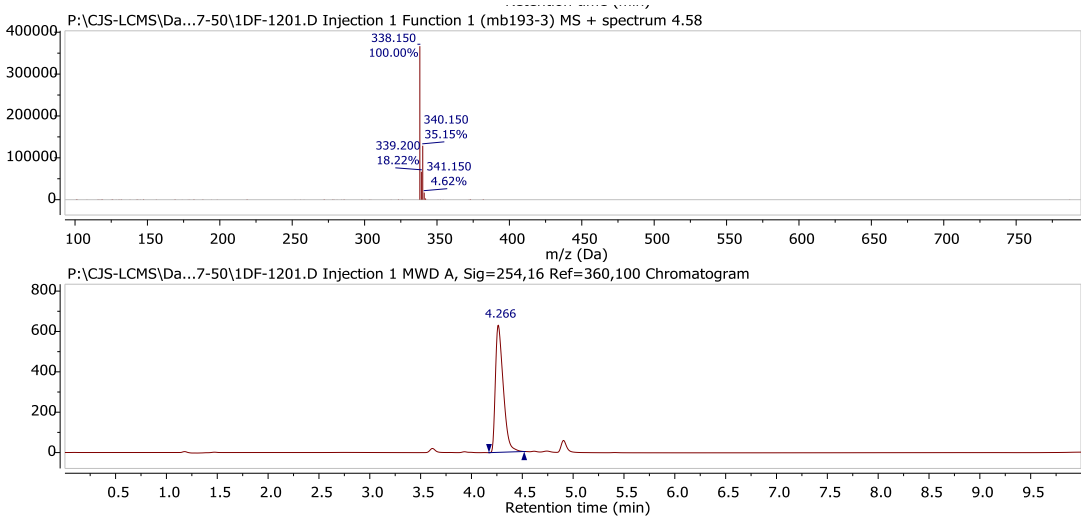

Methyl (6-chloro-2-benzylaminoquinazolin-4-yl)-*L*-alaninate (64)

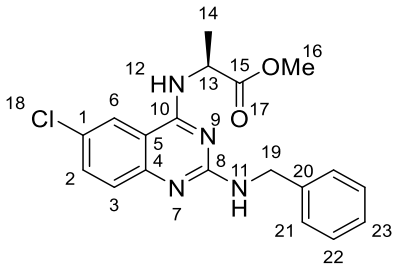

To a solution of **40** (400 mg, 1.3 mmol, 1 equiv.) in MeOH (3 mL), benzylamine (0.50 mL, 4.6 mmol, 4.6 equiv.) was added. The reaction mixture was stirred for 20 min at 120 °C in a microwave reactor. Then, it was acidified to pH 2 with 4 M HCl in 1,4-dioxane and concentrated *in vacuo*. The product was purified using flash column chromatography (10−50% EtOAc in cyclohexane) to give methyl (6-chloro-2-benzylaminoquinazolin-4-yl)-*L*-alaninate (237 mg, 0.68 mmol 48%) as a white solid.

IR ν_{max}/cm^{-1}(thin film):1718 (C=O);

^{1}H NMR (400 MHz, chloroform-*d*) δ 7.46 (d, *J* = 2.3 Hz, 1H, C(6)H), 7.36 (dd, *J* = 8.9, 2.3 Hz, 1H, C(2)H), 7.31 – 7.21 (m, 5H, C(3)H, $(C(21)H)_2$, $(C(22)H)_2$), 7.20 – 7.16 (m, 1H,

C(23)H), 6.14 (d, *J* = 6.8 Hz, 1H, N(12)H), 5.28 (brs, 1H, N(11)H), 4.75 (app. p, *J* = 7.0 Hz, 1H, C(13)H), 4.60 (d, *J* = 5.8 Hz, 2H, C(19)H_2), 3.68 (s, 3H, OMe(16) -CH_3), 1.45 (d, *J* = 7.2 Hz, 3H, C(14)H_3); ^{13}C NMR (101 MHz, chloroform-*d*) δ 174.38, 159.21, 158.58, 150.67, 139.82, 133.32, 128.51, 127.50, 127.05, 126.04, 120.55, 52.52, 49.56, 45.49, 18.02;

LRMS: *m/z*(%)= 371.1 (100), 373.2 (33) $[M + H]^+$; HRMS: calcd. $C_{19}H_{20}O_2N_4{}^{35}Cl$ $[M + H]^+$: 371.1269 ; found: 371.1270;

(*S*)-2-(6-Chloro-2-benzylaminoquinazolin-4-yl)amino-*N*-hydroxypropanamide (65)

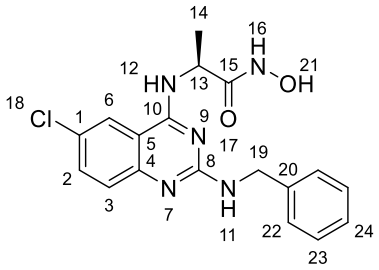

General procedure D using **64** (200 mg, 0.54 mmol, 1 equiv.). Purified using flash column chromatography (5-20% MeOH in DCM) to give (*S*)-2-(6-chloro-2-benzylaminoquinazolin-4-yl)amino-*N*-hydroxypropanamide (187 mg, 0.50 mmol, 93%) as a white solid.

IR ν_{max}/cm^{-1}(solid): 3218 (O-H) and 1644 (C=O);

^{1}H NMR (500 MHz, DMSO-d_6) δ 10.88 (s, 1H, O(21)H), 9.38 (brs, 1H, N(12)H), 8.62 (s, 1H, C(6)H), 8.57 (s, 1H, N(11)H), 7.82 (s, 1H, C(2)H), 7.50 (d, *J* = 9.0 Hz, 1H, C(3)H), 7.42 (app. d, *J* = 7.5 Hz, 2H, (C(22)$H)_2$), 7.36 (app. t, *J* = 7.5 Hz, 2H, (C(23)$H)_2$), 7.28 (app. t, *J* = 7.5 Hz, 1H, C(24)H), 4.74 (app. t, *J* = 7.0 Hz, 2H, C(19)H, C(14)H), 4.59 (app. d, *J* = 16.0 Hz, 1H, C(19)H), 1.47 (d, *J* = 7.0 Hz, 3H, C(14)H_3);

LRMS: *m/z*(%)= 372.2 (100), 374.2 (28) $[M + H]^+$; HRMS: calcd. $C_{18}H_{19}O_2N_5{}^{35}Cl$ $[M + H]^+$: 372.12218; found: 372.12231;

$[\alpha]_D^{25} = -15.2$ (c = 0.8 in MeOH);

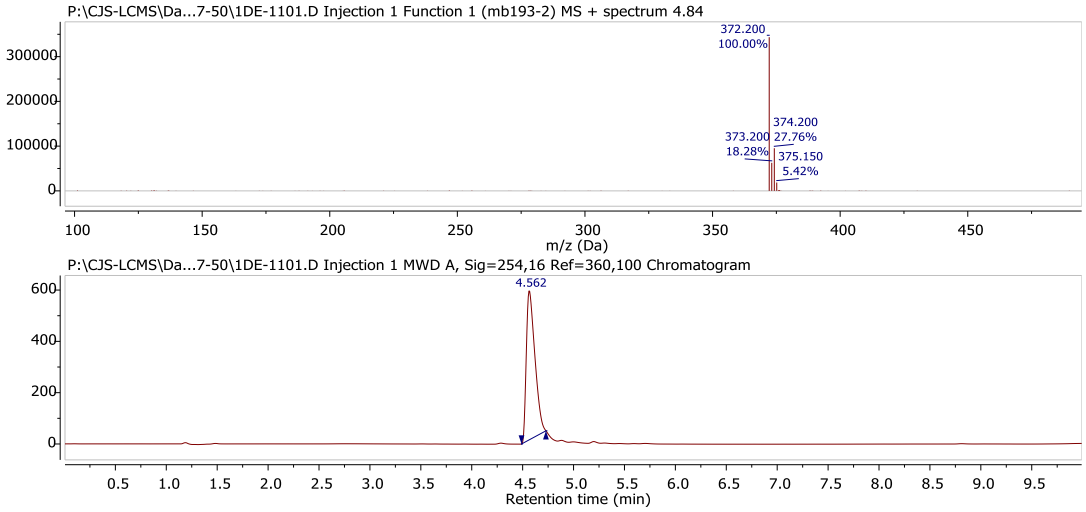

Methyl (6-chloro-2-(furan-2-ylmethyl)aminoquinazolin-4-yl-*L*-alaninate (66)

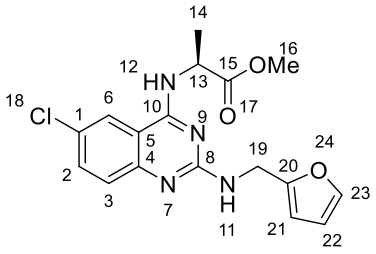

To a solution of **40** (300 mg, 1.0 mmol, 1 equiv.) in MeOH (3 mL), furfurylamine (0.3 mL, 3.4 mmol, 3.4 equiv.) was added. The reaction mixture was stirred for 20 min at 120 °C in a microwave reactor. Then, it was acidified to pH 2 with 4 M HCl in 1,4-dioxane and concentrated *in vacuo*. Purified using flash column chromatography (20−60% EtOAc in cyclohexane) to give methyl (6-chloro-2-(furan-2-ylmethyl)aminoquinazolin-4-yl)-*L*-alaninate (124 mg, 0.34 mmol, 34%) as a orange solid.

IR ν_{max}/cm^{-1}(thin film):1731 (C=O);

^{1}H NMR (400 MHz, chloroform-*d*) δ 7.54 (d, *J* = 2.0 Hz, 1H, C(6)H), 7.46 (dd, *J* = 9.0, 2.0 Hz, 1H, C(2)H), 7.42 – 7.33 (m, 2H, C(3)H, C(23), 6.31 (dd, *J* = 3.2, 1.9 Hz, 1H, C(22)H), 6.24 (d, *J* = 2.3 Hz, 1H, C(21)H), 6.13 (d, *J* = 6.5 Hz, 1H, N(12)H), 5.37 (brs, 1H, N(11)H), 4.87 (app. p, *J* = 7.1 Hz, 1H, C(13)H), 4.66 (d, *J* = 5.5 Hz, 2H, C(19)H_2), 3.79 (s, 3H, OMe(16) –CH_3), 1.57 (d, *J* = 7.1 Hz, 3H, C(14)H_3); ^{13}C NMR (101 MHz, chloroform-*d*) δ 174.23, 158.82, 158.53, 141.82, 133.39, 126.28, 120.51, 110.32, 106.65, 52.57, 38.66, 29.70, 18.10;

LRMS: *m/z*(%)= 361.1 (100), 363.2 (36) $[M + H]^+$; HRMS: calcd. $C_{17}H_{18}O_3N_4{}^{35}Cl$ $[M + H]^+$: 361.1062 ; found: 361.1063;

(*S*)-2-(6-Chloro-2-(furan-2-ylmethyl)aminoquinazolin-4-yl)amino-*N*-hydroxypropanamide (67)

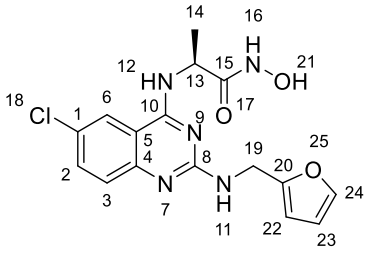

General procedure D using **66** (100 mg, 0.28 mmol, 1 equiv.). Purified using flash column chromatography (5−20% MeOH in DCM) to give (*S*)-2-(6-chloro-2-(furan-2-ylmethyl)aminoquinazolin-4-yl)amino-*N*-hydroxypropanamide (42 mg, 0.12 mmol, 42%) as a brown solid.

IR ν_{max}/cm^{-1}(solid): 3212 (O-H) and 1644 (C=O);

^{1}H NMR (500 MHz, DMSO-d_6)10.89 (s, 1H, O(21)H), 9.57 (d, J = 6.5 Hz, 1H, N(12)H), 8.96 (s, 1H, N(16)H), 8.66 (s, 1H, C(6)H), 8.63 (s, 1H, N(11)H), 7.85 (d, J = 8.5 Hz, 1H, C(2)H), 7.62 (s, 1H, C(24)H), 7.51 (d, J = 8.5 Hz, 1H, C(3)H), 6.45 (s, 1H, C(23)H), 6.42 (s, 1H, C(22)H), 4.80 – 4.71 (m, 2H, C(13)H, C(19)H), 4.61 (dd, J = 15.7, 5.0 Hz, 1H, C(19)H), 1.48 (d, J = 7.3 Hz, 3H, C(14)H); ^{13}C NMR (126 MHz, DMSO-d_6) δ 168.42, 159.39, 152.95, 151.36, 143.20, 138.47, 135.76, 128.69, 124.81, 119.51, 111.26, 111.11, 108.65, 50.14, 37.91, 18.01;

LRMS: *m/z*(%)= 362.2 (100), 363.2 (40) $[M + H]^+$; HRMS: calcd. $C_{16}H_{17}O_3N_5{}^{35}Cl$ $[M + H]^+$: 362.10144 ; found: 362.10138;

$[\alpha]_D^{25} = -27.6$ (c = 0.3 in MeOH);

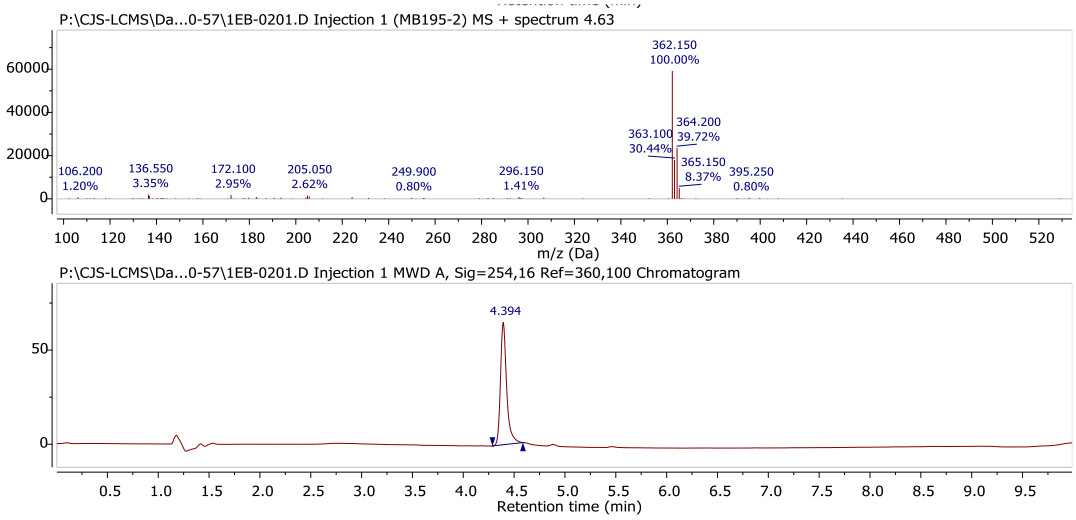

Methyl (6-chloro-2-(2-(pyridin-2-yl)ethyl)aminoquinazolin-4-yl)-*L*-alaninate (68)

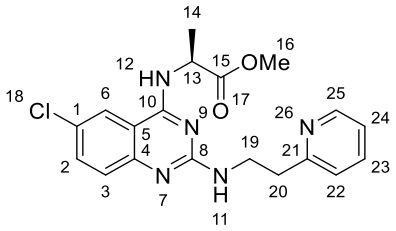

To a solution of **40** (300 mg, 1.0 mmol, 1 equiv.) in MeOH (3 mL), 2-(2-Pyridyl)ethylamine (0.36 mL, 3.0 mmol, 3 equiv.) was added. The reaction mixture was stirred for 30 min at 100 °C in a microwave reactor. Then, it was acidified to pH 2 with 4 M HCl in 1,4-dioxane and concentrated *in vacuo*. Purified using flash column chromatography (20−100% EtOAc with 1% TEA in cyclohexane) to give methyl (6-chloro-2-(2-(pyridin-2-yl)ethyl)aminoquinazolin-4-yl)-*L*-alaninate (124 mg, 0.32 mmol, 32%) as a white solid.

IR ν_{max}/cm^{-1}(thin film):1731 (C=O);

^{1}H NMR (400 MHz, chloroform-*d*) δ 8.48 (ddd, *J* = 4.9, 1.8, 0.9 Hz, 1H, C(25)H), 7.52 (app. td, *J* = 7.7, 1.9 Hz, 1H, C(2)H), 7.45 (d, *J* = 2.4 Hz, 1H, C(6)H), 7.34 (dd, *J* = 8.9, 2.2 Hz, 1H, C(2)H), 7.24 (d, *J* = 9.3 Hz, 1H, C(3)H), 7.12 (app. dt, *J* = 7.7, 1.1 Hz, 1H, C(22)H), 7.06 (ddd, *J* = 7.6, 4.9, 1.2 Hz, 1H, C(24)H), 6.17 (s, 1H, N(12)H), 5.39 (s, 1H, N(11)H), 4.81 (app p, *J* = 7.1 Hz, 1H, C(13)H), 3.79 (app q, *J* = 6.7 Hz, 2H, C(19)H_2), 3.72 (s, 3H, OMe(16) -CH_3), 3.03 (t, *J* = 6.7 Hz, 2H, C(20)H_2), 1.51 (d, *J* = 7.1 Hz, 2H, C(14)H_3).^{13}C NMR (101 MHz, chloroform-*d*) δ 174.47, 159.81, 159.16, 158.50, 149.36, 136.41, 133.99, 133.24, 125.83, 123.46, 121.38, 120.54, 52.52, 49.58, 41.01, 38.12, 18.05.

LRMS: *m/z*(%)= 193.6 (100), 194.6 (38) $[M + 2H]^{2+}$; 386.2 (7) $[M + H]^{+}$; HRMS: calcd. $C_{19}H_{21}O_2N_5{}^{35}Cl$ $[M + H]^{+}$: 386.1378; found: 386.1378;

(*S*)-2-(6-chloro-2-(2-(pyridin-2-yl)ethyl)aminoquinazolin-4-yl)amino-*N*-hydroxypropanamide (69)

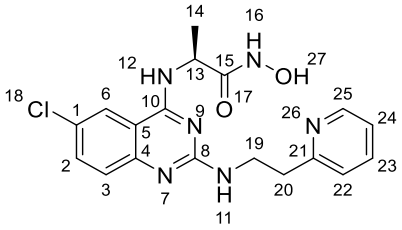

General procedure D using **68** (120 mg, 0.31 mmol, 1 equiv.). Purified using flash column chromatography (5−20% MeOH with 1% NH_2Me in DCM) to give (*S*)-2-(6-chloro-2-(2-(pyridin-2-yl)ethyl)aminoquinazolin-4-yl)amino-*N*-hydroxypropanamide (114 mg, 0.30 mmol, 95%) as a white solid.

IR ν_{max}/cm^{-1}(solid): 3020 (O-H) and 1645 (C=O);

^{1}H NMR (400 MHz, methanol-d_4) δ 8.42 (dd, *J* = 7.1, 2.1 Hz, 1H, C(25)H), 8.24 (app. t, *J* = 7.4 Hz, 1H,, C(23)H), 8.09 (s, 1H, C(6)H), 7.77 (app. t, *J* = 7.2 Hz, 1H, C(24)H), 7.63 (t, *J* = 6.5 Hz, 1H, C(22)H), 7.41 (dd, *J* = 8.8, 2.1 Hz, 1H, C(2)H), 7.09 (d, *J* = 9.0 Hz, 1H, C(3)H), 4.39 (m, 1H, C(13)H), 3.68 (app. ddt, *J* = 32.2, 25.8, 8.3 Hz, 2H, $C(19)H_2$), 3.18 – 3.07 (m, 2H, $C(20)H_2$), 1.33 (d, *J* = 7.1 Hz, 3H, $C(14)H_3$); ^{13}C NMR (101 MHz, methanol-d_4) δ 170.79, 164.65, 159.85, 153.91, 146.94, 141.15, 137.65, 135.60, 128.19, 125.42, 124.07, 123.89, 118.47, 51.00, 40.11, 32.99, 16.60;

LRMS: *m/z*(%)= 194.2 (100), 195.0 (46) $[M + 2H]^{2+}$; 387.1 (4) $[M + H]^{+}$; HRMS: calcd. $C_{18}H_{20}O_2N_6{}^{35}Cl$ $[M + H]^{+}$: 387.13308; found: 387.13293;

$[\alpha]_D^{25}$ = +3.6 (c = 1.5 in MeOH);

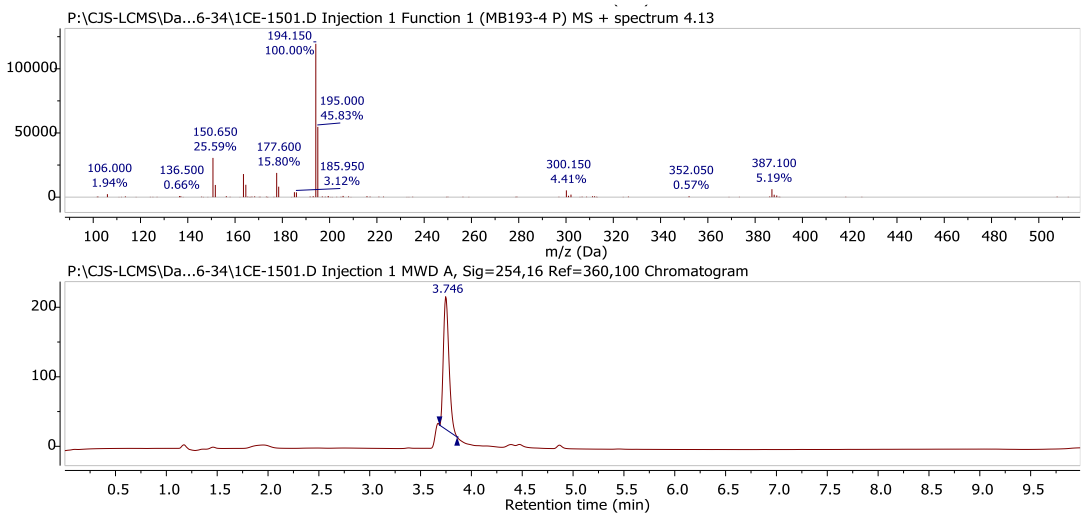

(*S*)-2-(6-chloro-2-(2-(dimethylamino)ethyl)aminoquinazolin-4-yl)amino-*N*-hydroxypropanamide trifluoroacetate (70)

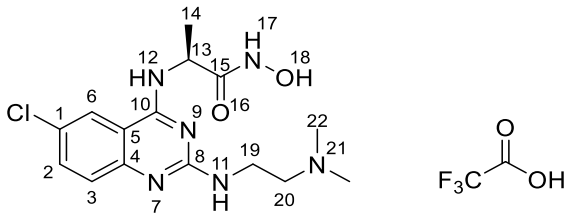

To a solution of **40** (300 mg, 1 mmol, 1 equiv.) in MeOH (2.5 mL), 2-(Dimethylamino)ethylamine (85 µL, 1.2 mmol, 1.2 equiv.) was added. The reaction mixture was stirred at 100 °C for 40 min in a microwave reactor. Then, crude intermediate was added to a solution of $NH_2OH{\cdot}HCl$ (210 mg, 3 mmol, 3 equiv.) and NaOMe 25 wt. % in MeOH (2.3 mL, 10 mmol, 10 equiv.) in MeOH (5 mL) and stirred at RT for 2 h. The product was purified using RP HPLC (MeCN in H_2O both with 0.1% TFA) and lyophilized to give (*S*)-2-(6-chloro-2-(2-(dimethylamino)ethyl)aminoquinazolin-4-yl)amino-*N*-hydroxypropanamide trifluoroacetate (64 mg, 0.14 mmol, 14% after 2 steps) as a white solid.

IR ν_{max}/cm^{-1}(solid): 3092 (O-H) and 1665 (C=O);

^{1}H NMR (400 MHz, methanol-d_4) δ 8.47 (d, J = 2.0 Hz, 1H, C(6)H), 7.83 (dd, J = 9.0, 2.0 Hz, 1H, C(2)H), 7.50 (d, J = 9.0 Hz, 1H, C(3)H), 4.62 (app. q, J = 7.0 Hz, 1H, C(14)H), 4.03 (app. dt, J = 15.0, 6.0 Hz, 1H, C(19)H), 3.80 (app dt, J = 15.0, 6.5 Hz, 1H, C(19)H), 3.40 (t, J = 6.3 Hz, 2H, C(20)H_2), 2.97 (s, 6H, (C(22)H_3)$_2$), 1.66 (d, J = 7.3 Hz, 3H, C(14)H_3); ^{13}C NMR (101 MHz, methanol-d_4) δ 170.47, 160.08, 138.01, 135.65, 130.10, 123.81, 118.50, 110.85, 55.85, 51.22, 42.42, 36.20, 16.30;

LRMS: m/z(%)= 177.2 (100), 178.0 (41) $[M + 2H]^{2+}$; 353.2 (8) $[M + H]^{+}$ $]^{+}$; HRMS: calcd. $C_{15}H_{22}O_2N_6{}^{35}Cl$ $[M + H]^{+}$: 353.1487; found: 353.1486;

$[\alpha]_D^{25}$ = +33.2 (c = 0.6 in MeOH);

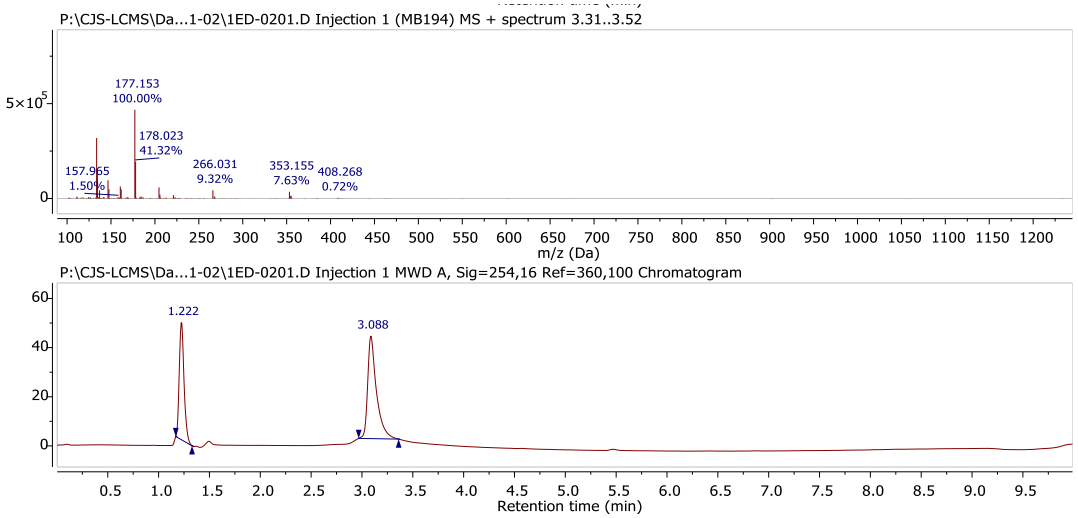

Ethyl 4-oxo-3,4-dihydroquinazoline-2-carboxylate (71)[13]

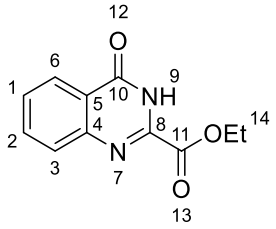

The compound was synthesised using a literature procedure.[13] A mixture of 2-aminobenzamide (6 g, 44 mmol, 1 equiv.) and diethyl oxalate (24 mL, 176 mmol, 4 equiv.) was stirred under reflux for 24 h, then the reaction mixture was concentrated *in vacuo*. The product was recrystallised in EtOH to give ethyl 4-oxo-3,4-dihydroquinazoline-2-carboxylate (6.3 g, 29 mmol, 66%) as a white solid.

^{1}H NMR (400 MHz, chloroform-*d*) δ 10.40 (s, 1H, N(9)H), 8.36 (ddd, *J* = 7.9, 1.6, 0.6 Hz, 1H, C(6)H), 7.96 (ddd, *J* = 8.2, 1.2, 0.6 Hz, 1H, C(3)H), 7.84 (ddd, *J* = 8.2, 7.2, 1.6 Hz, 1H, C(2)H), 7.62 (ddd, *J* = 7.9, 7.2, 1.2 Hz, 1H, C(1), 4.58 (q, *J* = 7.1 Hz, 2H, OEt(14) -CH_2-), 1.49 (t, *J* = 7.1 Hz, 3H, OEt(14) -CH_3); ^{13}C NMR (101 MHz, chloroform-*d*) δ 160.96, 160.60, 147.61, 141.62, 135.03, 129.30, 129.27, 126.82, 123.17, 64.17, 14.17;

LRMS: *m/z*(%)= 219.2 (100) $[M + H]^+$

Analytical data (^{1}H NMR) were in accord with those previously reported.[13]

4-Chloroquinazoline-2-carbonyl chloride (72)[14]

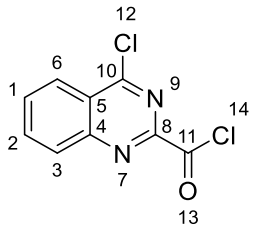

The compound was synthesised using a literature procedure.[14] A mixture of **71** (1.8 g, 8.3 mmol) and NaOH (1.65 g, 41 mmol, 5 equiv.) in a solution of H_2O/EtOH (1:1, 80 mL). The reaction mixture was stirred under reflux for 1 h. Then it was cooled, acidified to pH 2 with 2 M $HCl_{(aq)}$ and left in an ice bath for 1 h to crystalise. The precipitate was collected by filtration and dried to give intermediate 4-oxo-3,4-dihydroquinazoline-2-carboxylic acid.

Intermediate was added to a solution of $SOCl_2$ (1.2 mL, 16 mmol, 2 equiv.) in $CHCl_3$ (15 mL) and DMF (5 drops). The reaction mixture was stirred under reflux for 3 h, and then it was concentrated *in vacuo* to give 4-chloroquinazoline-2-carbonyl chloride (1.7 g, 7.5 mmol, 91% after 2 steps) as a yellow solid. The crude product was used straight for the subsequent reaction.

Methyl (4-allylaminoquinazoline-2-carbonyl)-*L*-alaninate (73)

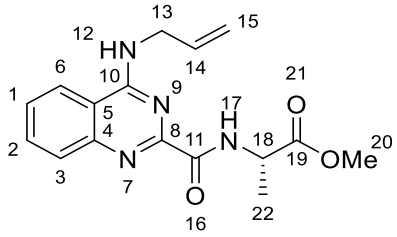

To a solution of **72** (650 mg, 2.9 mmol, 1 equiv.) and *L*-alanine methyl ester hydrochloride (480 mg, 3.5 mmol, 1.2 equiv.) in anhydrous DCM (10 mL) at −40°C, DIPEA (2 mL, 11

mmol, 3.8 equiv.) was added dropwise. The reaction mixture was stirred at −40°C under an inert atmosphere for 1 h, After 1 h, allylamine (430 µL, 5.8 mmol, 2 equiv.) was added dropwise, and the reaction mixture was stirred at RT for a further 16 h. Then, it was quenched with H_2O (25 mL) and extracted with EtOAc (3 × 25 mL). The combined organic layer was washed with brine (50 mL), dried over Na_2SO_4, then concentrated *in vacuo*. The product was purified using flash column chromatography (50−100% EtOAc in cyclohexane) to give methyl (4-allylaminoquinazoline-2-carbonyl)-*L*-alaninate (703 mg, 2.2 mmol, 78%) as a yellow solid.

IR ν_{max}/cm^{-1}(thin film): 1743 (C=O);

^{1}H NMR (400 MHz, chloroform-*d*) δ 8.72 (d, *J* = 7.7 Hz, 1H, N(17)H), 8.01 (ddd, *J* = 8.4, 1.3, 0.6 Hz, 1H, C(6)H 7.86 (dd, *J* = 8.6, 0.7 Hz, 1H, C(3)H) 7.75 (ddd, *J* = 8.4, 7.0, 1.3 Hz, 1H, C(2)H), 7.51 (ddd, *J* = 8.3, 7.0, 1.2 Hz, 1H, C(1), 6.32 (t, *J* = 5.6 Hz, 1H, N(12)H), 6.01 (ddt, *J* = 17.1, 10.2, 5.9 Hz, 1H, C(14)H), 5.34 (app. dq, *J* = 17.2, 1.6 Hz, 1H, C(15)H), 5.22 (app. dq, *J* = 10.2, 1.3 Hz, 1H, C(15)H), 4.91 – 4.80 (m, 1H, C(18)H), 4.36 (app. tt, *J* = 5.7, 1.5 Hz, 2H, C(13)H_2), 3.79 (s, 3H, OMe(20) -CH_3), 1.56 (d, *J* = 7.2 Hz, 3H, C(14)H_3).^{13}C NMR (101 MHz, chloroform-*d*) δ 173.48, 163.22, 159.71, 153.29, 149.56, 133.88, 133.03, 129.88, 127.35, 120.79, 117.47, 114.79, 52.49, 48.42, 44.02, 18.66.

LRMS: *m/z*(%)= 315.2 (100) $[M + H]^+$; HRMS: calcd. $C_{16}H_{19}O_3N_4$ $[M + H]^+$: 315.1452; found: 315.1447;

(4-Allylaminoquinazoline-2-carbonyl)-*L*-alanine (74)

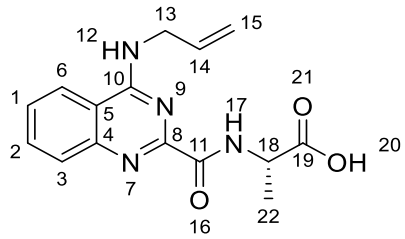

General procedure C using **73** (200 mg, 0.64 mmol, 1 equiv.). The product was purified using flash column chromatography (0−10% MeOH with 1% Formic acid in DCM) to (4-Allylaminoquinazoline-2-carbonyl)-*L*-alanine (163 mg, 0.54 mmol, 85%) as a white solid.

IR ν_{max}/cm^{-1}(solid): 3365 (O-H) and 1693 (C=O);

^{1}H NMR (400 MHz, DMSO-d_6) δ 11.04 (brs, 1H, N(12)H), 9.30 (d, *J* = 7.7 Hz, 1H, N(17)H), 8.88 (d, *J* = 8.2 Hz, 1H, C(6)H), 8.11 (d, *J* = 8.2 Hz, 1H, C(3)H), 8.02 (ddd, *J* = 8.3, 6.9, 1.2 Hz, 1H, C(2)H), 7.77 (ddd, *J* = 8.3, 7.0, 1.2 Hz, 1H, C(1)H), 6.02 (ddt, *J* = 17.2, 10.2, 5.7 Hz, 1H, C(14)H), 5.37 (app. dq, *J* = 17.2, 1.6 Hz, 1H, C(15)H), 5.20 (app. dq, *J* = 10.3, 1.4 Hz, 1H, C(15)H), 4.63 – 4.47 (m, 3H, C(18)H, C(13)H_2), 1.49 (d, *J* = 7.2 Hz, 3H, C(22)H_3);

^{13}C NMR (101 MHz, DMSO-d_6) δ 173.30, 160.75, 159.20, 150.21, 136.14, 134.03, 129.06, 125.18, 117.80, 114.06, 49.02, 48.88, 44.48, 17.37;

LRMS: *m/z*(%)= 301.2 (100) $[M + H]^+$; HRMS: calcd. $C_{15}H_{17}O_3N_4$ $[M + H]^+$: 301.12952; found: 301.12964;

$[\alpha]_D^{25}$ = +18.2 (c = 0.9 in MeOH);

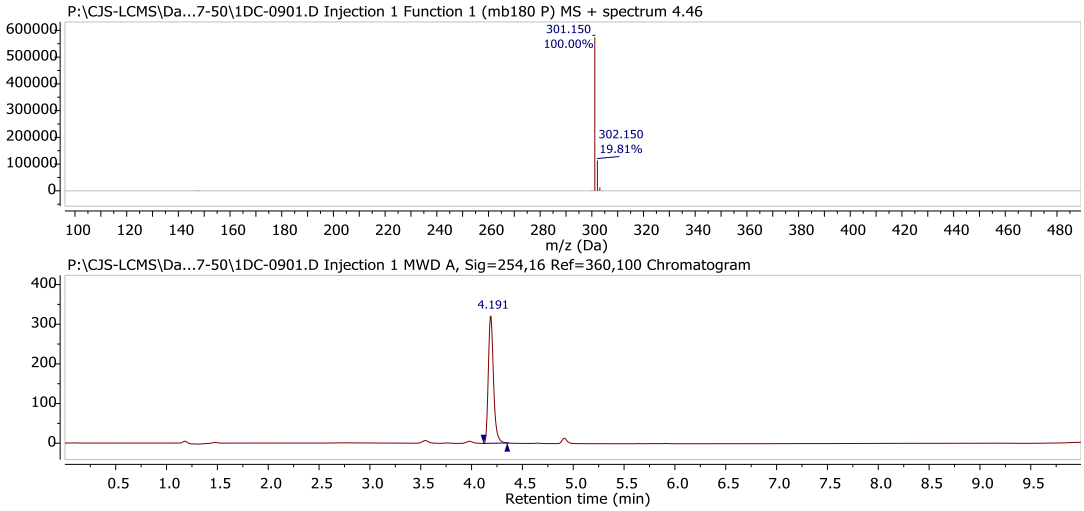

(*S*)-4-Allylamino-*N*-(1-hydroxyamino-1-oxopropan-2-yl)quinazoline-2-carboxamide (75)

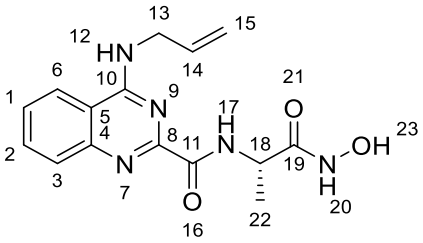

General procedure D using **73** (200 mg, 0.64 mmol, 1 equiv.). Purified using RP HPLC (MeCN in H_2O both with 0.1% TFA) and lyophilized to give (*S*)-4-allylamino-*N*-(1-hydroxyamino-1-oxopropan-2-yl)quinazoline-2-carboxamide (46 mg, 0.15 mmol, 23%) as a white solid.

IR ν_{max}/cm^{-1}(solid): 3296 (O-H) and 1630 (C=O);

^{1}H NMR (400 MHz, DMSO-d_6) 10.85 (brs, 1H, O(23)H), 10.13 (brs, 1H, N(12)H), 9.02 (d, *J* = 8.1 Hz, 1H, N(17)H), 8.49 (d, *J* = 8.3 Hz, 1H, C(6)H), 8.07 (d, *J* = 8.3 Hz, 1H, C(3)H), 8.01 (app. t, *J* = 7.7 Hz, 1H, C(2)H), 7.77 (app. t, *J* = 7.0 Hz, 1H, C(1)H), 6.28 – 5.89 (m,

1H, C(14)H), 5.39 (dd, *J* = 17.1, 1.7 Hz, 1H, C(15)H), 5.23 (dd, *J* = 10.3, 1.7 Hz, 1H, C(15)H), 4.48 (app. dt, *J* = 12.9, 8.0 Hz, 3H, C(18)H, C(15)H_2), 1.41 (d, *J* = 7.0 Hz, 3H, C(22)H_3); ^{13}C NMR (101 MHz, DMSO-d_6) δ 168.37, 160.74, 159.61, 158.50, 150.97, 135.86, 134.05, 128.98, 124.21, 123.34, 117.78, 114.05, 47.36, 44.48, 18.88;

LRMS: *m/z*(%)= 316.2 (100) $[M + H]^+$; HRMS: calcd. $C_{15}H_{18}O_3N_5$ $[M + H]^+$: 316.14042; found: 316.14050;

$[\alpha]_D^{25}$ = +29.3 (c = 0.6 in MeOH);

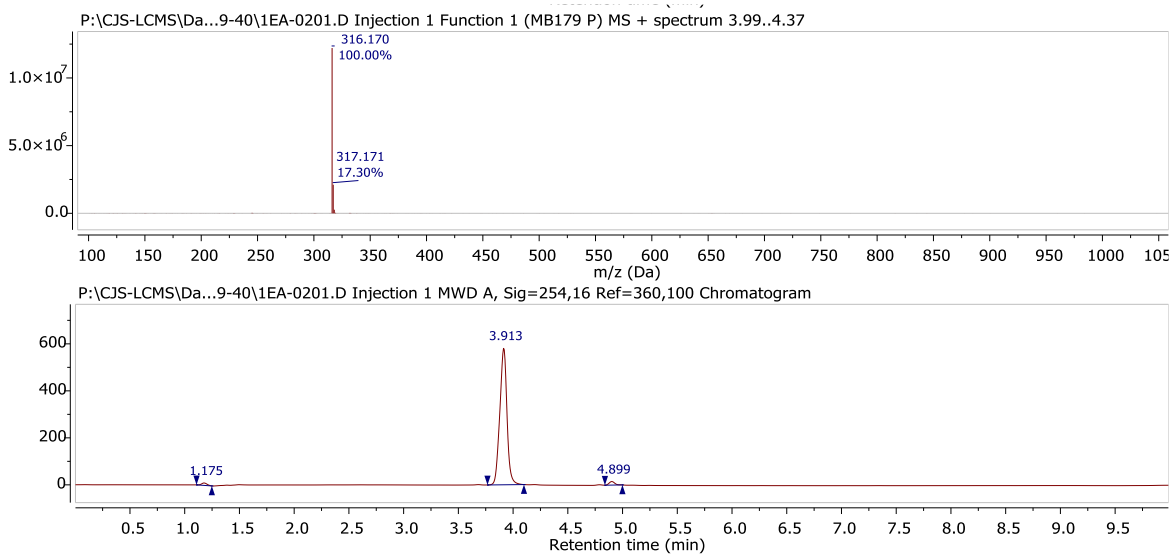

Methyl (2-(allylcarbamoyl)quinazolin-4-yl)-L-alaninate (76)

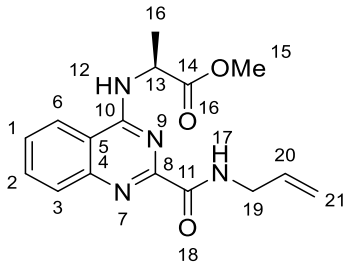

To a solution of **72** (650 mg, 2.9 mmol, 1 equiv.) in anhydrous DCM (10 mL) at −40°C, allylamine (300 µL, 4.1 mmol. 1.3 equiv.) and DIPEA (2 mL, 11 mmol, 3.8 equiv.) were added dropwise. The reaction mixture was stirred at −40°C under an inert atmosphere for 1 h. After 1 h, *L*-alanine methyl ester hydrochloride (800 mg, 5.8mmol, 2 equiv.) was added, the reaction mixture was stirred at RT for a further 16 h. Then, it was quenched with H_2O (25 mL) and extracted with EtOAc (3 × 25 mL). The combined organic layer was washed with brine (50 mL), dried over Na_2SO_4 and concentrated *in vacuo*. The product was purified using flash column chromatography (50−100% EtOAc in cyclohexane) to give impure methyl (4-allylaminoquinazoline-2-carbonyl)-*L*-alaninate (total mass 618 mg, but based on LCMS, only about 50% of the mixture was the desired product, 2.0 mmol, 68%) as a yellow solid. The product was contaminated with *N*-allyl-4-(allylamino)quinazoline-2-carboxamide, and it was used in the next step without further purification.

LRMS: *m/z*(%)= 315.2 (100) $[M + H]^+$

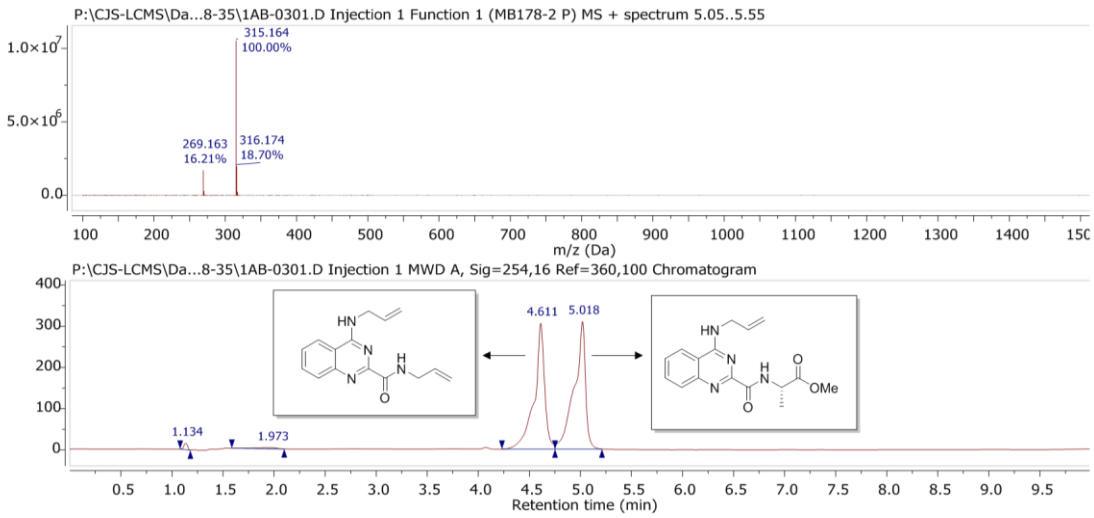

(2-(Allylcarbamoyl)quinazolin-4-yl)-*L*-alanine (77)

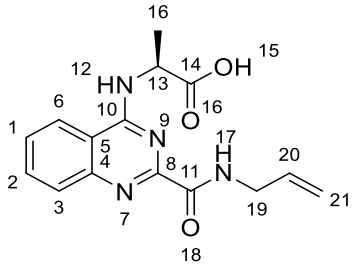

General procedure C using **76** (250 mg, 0.80 mmol, 1 equiv.). Purified using RP HPLC (MeCN in H_2O both with 0.1% TFA) and lyophilized to give to (2-(Allylcarbamoyl)quinazolin-4-yl)-L-alanine (44 mg, 15 mmol, 19%) as a white solid.

IR ν_{max}/cm^{-1}(solid): 3022 (O-H) and 1717 (C=O);

^{1}H NMR (400 MHz, DMSO-d_6) δ 9.89 (d, *J* = 7.9 Hz, 1H, N(12)H), 9.34 (t, *J* = 6.1 Hz, 1H, N(17)H), 8.58 (dd, *J* = 8.5, 1.3 Hz, 1H, C(6)H), 8.09 (dd, *J* = 8.5, 1.4 Hz, 1H, C(3)H), 8.04 (ddd, *J* = 8.4, 6.9, 1.2 Hz, 1H, C(2)H), 7.81 (ddd, *J* = 8.3, 6.8, 1.4 Hz, 1H, C(1)H), 5.93 (ddt, *J* = 17.2, 10.3, 5.2 Hz, 1H, C(20)H), 5.59 (app. p, *J* = 7.3 Hz, 1H, C(13)H), 5.24 (dd, *J* = 17.2, 1.7 Hz, 1H, C(21)H), 5.16 (dd, *J* = 10.3, 1.6 Hz, 1H, C(21)H), 4.00 (ddd, *J* = 8.0, 4.3,

1.7 Hz, 2H, C(19)H_2), 1.57 (d, *J* = 7.2 Hz, 3H, C(16)H_3); ^{13}C NMR (101 MHz, DMSO-d_6) δ 173.78, 160.50, 160.11, 151.17, 135.99, 134.74, 128.98, 124.36, 123.61, 116.25, 113.83, 50.32, 42.12, 17.16;

LRMS: *m/z*(%)= 301.2 (100) $[M + H]^+$; HRMS: calcd. $C_{15}H_{17}O_3N_4$ $[M + H]^+$: 301.12952; found: 301.12961;

$[\alpha]_D^{25}$ = +18.1 (c = 1.1 in MeOH);

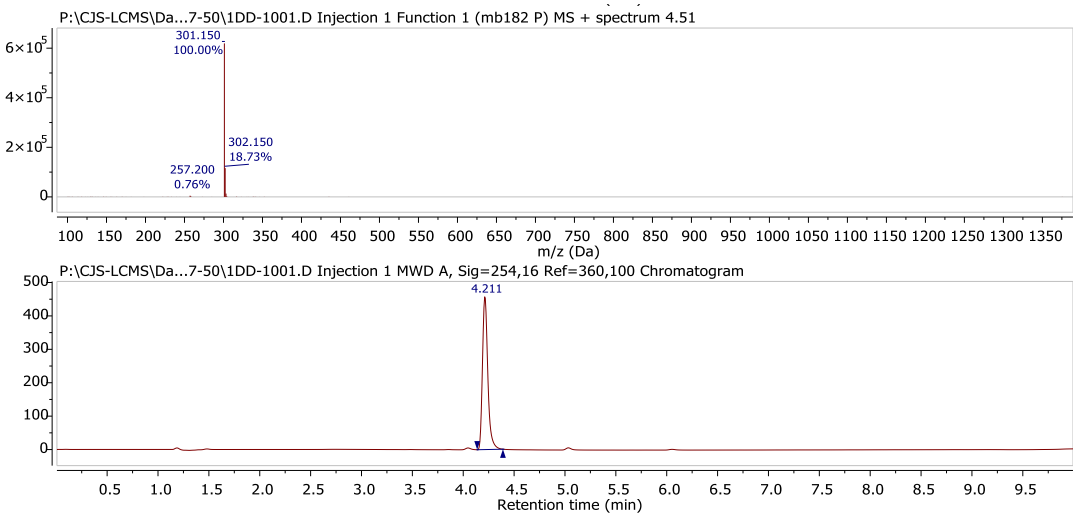

(*S*)-*N*-Allyl-4-(1-hydroxyamino-1-oxopropan-2-yl)aminoquinazoline-2-carboxamide (78)

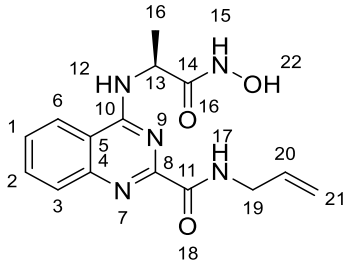

General procedure D using **76** (250 mg, 0.80 mmol, 1 equiv.). Purified using RP HPLC (MeCN in H_2O both with 0.1% TFA) and lyophilized to give (*S*)-*N*-allyl-4-(1-

hydroxyamino-1-oxopropan-2-yl)aminoquinazoline-2-carboxamide (47 mg, 0.15 mmol 19%) as a white solid.

IR ν_{max}/cm^{-1}(solid): 3226 (O-H) and 1648 (C=O);

^{1}H NMR (400 MHz, DMSO-d_6) δ 10.86 (brs, 1H, O(22)H, 9.86 (d, *J* = 7.4 Hz, 1H, N(12)H), 9.27 (t, *J* = 6.2 Hz, 1H, N(12)H), 8.63 (dd, *J* = 8.5, 1.3 Hz, 1H C(6)H), 8.09 (dd, *J* = 8.5, 1.4 Hz, 1H, C(3)H), 8.03 (ddd, *J* = 8.3, 6.9, 1.2 Hz, 1H, C(2)H), 7.80 (ddd, *J* = 8.3, 6.9, 1.4 Hz, 1H, C(1)H), 5.94 (ddt, *J* = 17.2, 10.3, 5.2 Hz, 1H, C(20)H), 5.33 (t, *J* = 7.2 Hz, 1H, C(21)H), 5.25 (dd, *J* = 17.2, 1.7 Hz, 1H, C(21)H), 5.16 (app. dd, *J* = 10.3, 1.6 Hz, 1H, C(13)H), 4.02 (app. tt, *J* = 5.2, 1.8 Hz, 2H, C(19)H_2), 1.53 (d, *J* = 7.1 Hz, 3H, C(16)H_3); ^{13}C NMR (101 MHz, DMSO-d_6) δ 168.49, 160.66, 159.99, 150.94, 135.98, 134.71, 128.89, 124.78, 123.29, 116.29, 114.11, 49.42, 42.21, 17.73;

LRMS: *m/z*(%)= 316.2 (100) $[M + H]^+$; HRMS: calcd. $C_{15}H_{18}O_3N_5$ $[M + H]^+$: 316.14042; found: 316.14044;

$[\alpha]_D^{25}$ = +33.3 (c = 0.8 in MeOH);

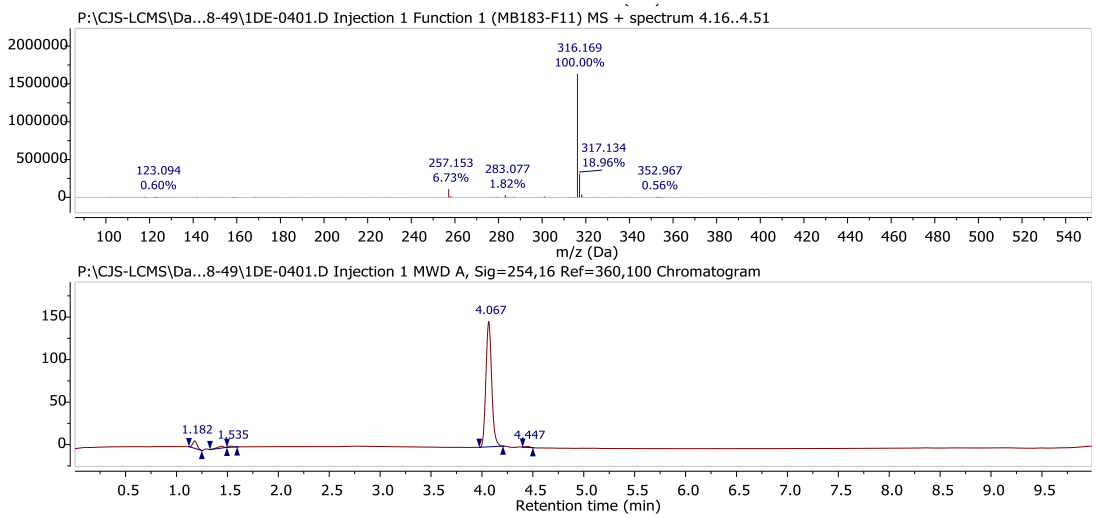

Methyl 6-(bromomethyl)picolinate (79)[15]

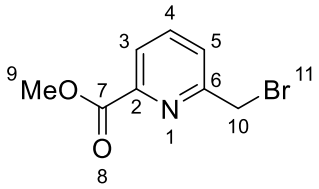

The compound was synthesised using a literature procedure.[15] To a solution of methyl 6-(hydroxymethyl)picolinate (860 mg, 5.1 mmol, 1 equiv.) in anhydrous $CHCl_3$ (10 mL) at 0°C, PBr_3 (500 µL, 5.2 mmol, 1 equiv.) was added dropwise. The reaction was stirred at 0°C under an inert atmosphere for 4 h, quenched with $NaHCO_{3(aq)}$ (25 mL), and extracted with DCM (3 × 25 mL). The combined organic layer was washed with brine (50 mL) and dried over Na_2SO_4. The product was purified using flash column chromatography (10−40% EtOAc in cyclohexane) to give methyl 6-(bromomethyl)picolinate (878 mg, 3.8 mmol, 71%) as a white-off solid.

IR ν_{max}/cm^{-1}(thin film):1714 (C=O);

^{1}H NMR (400 MHz, chloroform-*d*) δ 8.04 (dd, *J* = 7.8, 1.1 Hz, 1H, C(3)H), 7.85 (t, *J* = 7.8 Hz, 1H, C(4)H), 7.67 (dd, *J* = 7.8, 1.1 Hz, 1H, C(5)H), 4.63 (s, 2H, C(10)H_2), 3.99 (s, 3H, OMe(9) -CH_3); ^{13}C NMR (101 MHz, chloroform-*d*) δ 165.45, 157.53, 147.76, 138.26, 127.20, 124.53, 53.17, 33.25;

LRMS: *m/z*(%)= 230.1 (100), 232.1 (96) $[M + H]^+$; HRMS: calcd. $C_8H_9O_2N^{79}Br$ $[M + H]^+$: 229.9811; found: 229.9811;

Analytical data (^{1}H NMR and LRMS) were in accord with those previously reported.[15]

Methyl 6-((diethoxyphosphoryl)methyl)picolinate (80)[15]

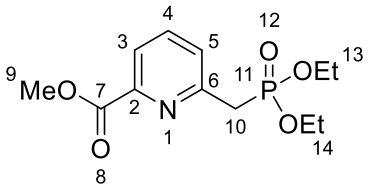

The compound was synthesised using a literature procedure.[15] A mixture of **79** (900 mg, 3.5 mmol, 1 equiv.) and $P(OEt)_3$ (6 mL, 35 mmol, 10 equiv.) in toluene (10 mL) was stirred under reflux for 2 h and then concentrated *in vacuo*. Purified using flash column chromatography (0−5% MeOH in EtOAc) to give methyl 6-((diethoxyphosphoryl)methyl)picolinate (910 mg, 3.2 mmol, 91%) as a yellow oil.

IR ν_{max}/cm^{-1}(thin film): 1743 (C=O);

^{1}H NMR (400 MHz, chloroform-*d*) δ 8.00 (ddd, *J* = 7.8, 1.9, 1.1 Hz, 1H, C(3)H), 7.79 (td, *J* = 7.8, 0.7 Hz, 1H, C(4)H), 7.61 (ddd, *J* = 7.8, 2.3, 1.1 Hz, 1H, C(5)H), 4.14 – 4.05 (m, 4H, OEt(13,14) -CH_2-), 3.98 (s, 3H, OMe(9) -CH_3), 3.52 (d, *J* = 21.9 Hz, 2H, C(10)H_2), 1.26 (td, *J* = 7.1, 0.5 Hz, 6H, OEt(13,14) -CH_3); ^{13}C NMR (101 MHz, chloroform-*d*) δ 165.63, 153.40 (d, *J* = 7.5 Hz), 147.79, 137.44 (d, *J* = 2.7 Hz), 127.69 (d, *J* = 4.4 Hz), 123.50 (d, *J* = 2.8 Hz), 62.35 (d, *J* = 6.5 Hz), 52.86, 36.55 (d, *J* = 135.3 Hz), 16.29 (d, *J* = 6.1 Hz); ^{31}P NMR (162 MHz, chloroform-*d*) δ 24.28;

LRMS: *m/z*(%)= 288.1 (100) $[M + H]^+$; HRMS: calcd. $C_{12}H_{19}O_5NP$ $[M + H]^+$: 288.0995; found: 288.0994;

Analytical data (^{1}H NMR and LRMS) were in accord with those previously reported.[15]

6-(Phosphonomethyl)picolinic acid hydrochloride (81)[16]

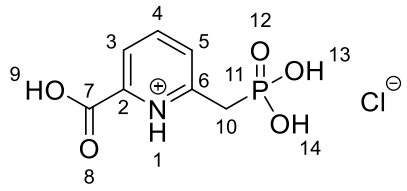

The compound was synthesised using a literature procedure.[16] A mixture of **80** (750 mg, 2.6 mmol, 1 equiv.) in 6M $HCl_{(aq)}$ (30 mL) was stirred under reflux for 16 h and then concentrated *in vacuo* to give 6-(phosphonomethyl)picolinic acid hydrochloride (622 mg, 2.5 mmol, 95%) as a white solid.

IR ν_{max}/cm^{-1}(solid): 1650 (C=O);

^{1}H NMR (400 MHz, DMSO-d_6) δ 9.70 (brs, 4H, N(1)H, O(9)H, O(13,14)H), 8.07 (t, *J* = 7.8 Hz, 1H, C(4)H), 7.99 (app. d, *J* = 7.8 Hz, 1H, C(3)H), 7.73 (app. d, *J* = 7.8, Hz, C(5)H), 3.40 (d, *J* = 21.8 Hz, 2H, C(10)H_2); ^{13}C NMR (101 MHz, DMSO-d_6) δ 165.02, 154.59 (d, *J* = 7.5 Hz), 146.24, 139.38, 128.35 (d, *J* = 4.0 Hz), 123.06, 37.39 (d, *J* = 127.2 Hz); ^{31}P NMR (162 MHz, DMSO-d_6) δ 18.04;

LRMS: *m/z*(%)= 218.1 (100) $[M - Cl]^+$; HRMS: calcd. $C_7H_8O_5NP^{23}Na$ $[M + Na]^+$: 240.9883; found: 240.9876;

Analytical data (^{1}H NMR and LRMS) were in accord with those previously reported.[16]

4-((Diethoxyphosphoryl)methyl)quinolin-2(1H)-one (82)[17]

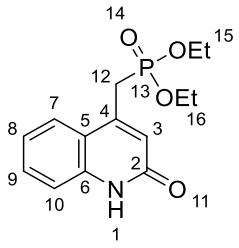

The compound was synthesised using a literature procedure.[17] A mixture of 4-(bromomethyl)quinolin-2(1H)-one (1.00 g, 4.2 mmol, 1 equiv.) and $P(OEt)_3$ (2.9 mL, 16.8 mmol, 4 equiv.) in 1,4-dioxane (4 mL) was stirred under reflux for 20 h.Then, the reaction mixture was concentrated *in vacuo* and purified using flash column chromatography (0−5% MeOH in DCM) to give 4-((diethoxyphosphoryl)methyl)quinolin-2(1H)-one (1.05 g, 3.6 mmol, 85%) as a white solid.

IR ν_{max}/cm^{-1}(thin film): 1613 (C=O);

^{1}H NMR (400 MHz, chloroform-*d*) δ 12.59 (s, 1H, N(1)H), 7.82 (dd, *J* = 8.3, 1.3 Hz, 1H, C(7)H), 7.54 – 7.42 (m, 2H, C(9)H, C(10)H), 7.25 (ddd, *J* = 8.3, 5.6, 1.4 Hz, 1H, C(8)H), 6.71 (s, 1H, C(3)H), 4.07 (q, *J* = 7.0 Hz, 4H, OEt(15,16) -CH_2-), 3.42 (s, 2H, C(12)H_2), 1.24 (t, *J* = 7.0 Hz, 6H, OEt(15,16) -CH_3); ^{13}C NMR (101 MHz, chloroform-*d*) δ 163.69 (d, *J* = 2.9 Hz), 143.74 (d, *J* = 9.2 Hz), 138.66, 130.87, 125.23, 122.66, 122.56, 119.47 (d, *J* = 3.7 Hz), 116.71, 62.61 (d, *J* = 6.8 Hz), 30.81 (d, *J* = 137.8 Hz), 16.35 (d, *J* = 6.0 Hz); ^{31}P NMR (162 MHz, chloroform-*d*) δ 23.33;

LRMS: *m/z*(%)= 296.1 (100) $[M + H]^+$; HRMS: calcd. $C_{14}H_{19}O_4NP$ $[M + H]^+$: 296.1046; found: 296.1048;

Analytical data (^{1}H NMR and LRMS) were in accord with those previously reported.[17]

4-(Phosphonomethyl)quinolin-2(1H)-one (83)[17]

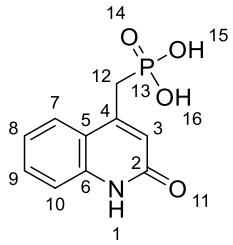

The compound was synthesised using a literature procedure.[17] A mixture of **82** (1.00 g, 3.4 mmol, 1 equiv.) and 4 M HCL in 1,4-dioxane (5 mL) was stirred under reflux for 24 h. Then the reaction mixture was concentrated in vacuo to give 4-(phosphonomethyl)quinolin-2(1H)-one (791 mg, 3.3 mmol, 98%) as a white solid.

IR ν_{max}/cm^{-1}(solid): 1604 (C=O);

^{1}H NMR (400 MHz, DMSO-d_6) δ 11.67 (s, 1H, N(1)H), 7.83 (dd, *J* = 8.3, 1.3 Hz, 1H, C(7)H), 7.48 (ddd, *J* = 8.3, 7.1, 1.3 Hz, 1H, C(9)H), 7.30 (dd, *J* = 8.3, 1.2 Hz, 1H, C(10)H), 7.17 (ddd, *J* = 8.3, 7.1, 1.2 Hz, 1H, C(8)H), 6.44 (s, 1H, C(3)H), 3.27 (s, 2H, C(12)H); ^{13}C NMR (101 MHz, DMSO-d_6) δ 161.52 (d, *J* = 2.9 Hz), 144.94 (d, *J* = 8.7 Hz), 138.88, 130.26, 126.01, 122.43 (d, *J* = 7.9 Hz), 121.50, 119.15 (d, *J* = 3.6 Hz), 115.44, 31.87 (d, *J* = 128.8 Hz); ^{31}P NMR (162 MHz, DMSO-d_6) δ 18.76.

LRMS: *m/z*(%)= 238.1 (100) $[M - H]^-$; HRMS: calcd. $C_{10}H_9O_4NP$ $[M - H]^-$: 238.0275; found: 238.0272;

Analytical data (^{1}H NMR and ^{13}C NMR) were in accord with those previously reported.[17]

Methyl (6-chloro-2-dimethylaminoquinazolin-4-yl)-*L*-alaninate (84)

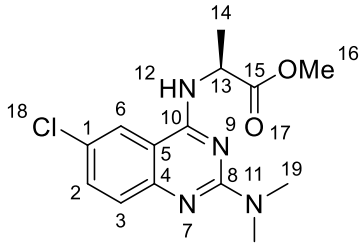

To a solution of **40** (200 mg, 0.67 mmol, 1 equiv.) in anhydrous DMF (3 mL), 2 M $NHMe_2$ in THF (1.0 mL, 2.0 mmol, 3 equiv.) was added. The reaction mixture was stirred for 4 h at 100 °C under an inert atmosphere, then concentrated in vacuo. The product was purified using flash column chromatography (40−80% EtOAc in cyclohexane) to give methyl (6-chloro-2-dimethylaminoquinazolin-4-yl)-*L*-alaninate (201 mg, 0.65 mmol, 98%) as a yellow solid.

IR ν_{max}/cm^{-1}(thin film):1729 (C=O);

^{1}H NMR (400 MHz, chloroform-*d*) δ 7.45 (d, *J* = 2.3 Hz, 1H, C(6)H), 7.34 (dd, *J* = 9.0, 2.3 Hz, 1H, C(2)H), 7.27 (d, *J* = 9.0 Hz, 1H, C(3)H) 6.18 (d, *J* = 6.5 Hz, 1H, N(12)H), 4.83 – 4.73 (m, 1H, C(13)H), 3.80 (s, 3H, OMe(16) -CH_3), 3.18 (s, 6H, $(C(19)H_3)_2$), 1.57 (d, *J* = 7.2 Hz, 3H, C14)H_3); ^{13}C NMR (101 MHz, chloroform-*d*) δ 175.11, 159.39, 158.12, 151.20, 133.09, 127.32, 125.20, 120.56, 110.25, 52.55, 50.03, 36.99, 17.85;

LRMS: *m/z*(%)= 309.1 (100), 311.1 (34) $[M + H]^+$; HRMS: calcd. $C_{14}H_{18}O_2N_4{}^{35}Cl$ $[M + H]^+$: 309.1113; found: 309.1111;

(*S*)-2-(6-Chloro-2-dimethylaminoquinazolin-4-yl)amino-*N*-hydroxypropanamide (85)

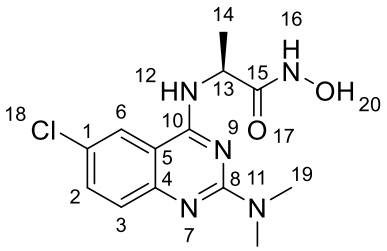

General procedure D using **84** (100 mg, 0.32 mmol, 1 equiv.). Purified using RP HPLC (MeCN in H_2O both with 0.1% TFA) and lyophilized to give (*S*)-2-(6-chloro-2-dimethylaminoquinazolin-4-yl)amino-*N*-hydroxypropanamide (30 mg, 0.01 mmol, 30%) as a white solid.

IR ν_{max}/cm^{-1}(solid): 3234 (O-H) and 1645 (C=O);

^{1}H NMR (400 MHz, methanol-d_4) δ 8.24 (d, *J* = 2.2 Hz, 1H, C(6)H), 7.71 (dd, *J* = 8.8, 2.0 Hz, 1H, C(2)H), 7.53 (d, *J* = 8.9 Hz, 1H, C(3)H), 4.67 (q, *J* = 7.2 Hz, 1H, C(3)H), 3.33 (s, 6H, $(C(19)H_3)_2$), 1.64 (d, *J* = 7.3 Hz, 3H, $C(14)H_3$); ^{13}C NMR (101 MHz, methanol-d_4) δ 171.67, 159.73, 153.53, 139.41, 136.39, 131.17, 124.74, 120.06, 111.73, 51.52, 38.74, 17.90;

LRMS: *m/z*(%)= 310.1 (100), 312.1 (33) $[M + H]^+$; HRMS: calcd. $C_{13}H_{17}O_2N_5{}^{35}Cl$ $[M + H]^+$: 310.1065; found: 310.1066;

$[\alpha]_D^{25}$ = +5.7 (c = 1.2 in MeOH);

Methyl (2-chloro-6-fluoroquinazolin-4-yl)-*L*-alaninate (86)

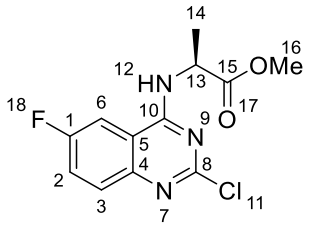

To a solution of 2,4-dichloro-6-fluoroquinazoline (500 mg, 2.3 mmol, 1 equiv.) and *L*-alanine methyl ester hydrochloride (480 mg, 3.4 mmol, 1.5 equiv.) in anhydrous DMF (5 mL) at 0 °C, anhydrous DIPEA (1.2 mL, 6.9 mmol, 3 equiv.) was added dropwise. The reaction mixture was stirred at RT under an inert atmosphere for 16 h and then diluted with cold H_2O (75 mL). The precipitate was collected by filtration and dried under vacuum to give methyl (2-chloro-6-fluoroquinazolin-4-yl)-*L*-alaninate (620 mg, 2.2 mmol, 94%) obtained as a yellowish-white solid.

IR ν_{max}/cm^{-1}(thin film): 1722 (C=O);

^{1}H NMR (400 MHz, chloroform-*d*) δ 7.65 (dd, *J* = 9.2, 5.1 Hz, 1H, C(6)H), 7.43 (ddd, *J* = 9.1, 8.1, 2.7 Hz, 1H, C(2)H), 7.33 (dd, *J* = 8.7, 2.7 Hz, 1H, C(3)H), 6.81 (d, *J* = 7.0 Hz, 1H. N(12)H), 5.01 (app. p, *J* = 7.2 Hz, 1H, C(13)H), 3.88 (s, 3H, OMe(16) -CH_3), 1.61 (d, *J* = 7.2 Hz, 3H, C(14)H_3); ^{13}C NMR (101 MHz, chloroform-*d*) δ 174.63, 161.29, 159.83, 158.81, 156.77, 147.67, 130.22 (d, *J* = 8.4 Hz), 123.23 (d, *J* = 24.6 Hz), 113.55 (d, *J* = 8.3 Hz), 105.80 (d, *J* = 23.5 Hz), 53.10, 49.91, 18.05; ^{19}F NMR (377 MHz, chloroform-*d*) δ -111.52;

LRMS: *m/z*(%)= 284.1 (100), 286.1 (34) $[M + H]^+$; HRMS: calcd. $C_{12}H_{12}O_2N_3{}^{35}ClF$ $[M + H]^+$: 284.0597; found: 284.0596;

Methyl (2-dimethylamino-6-fluoroquinazolin-4-yl)-*L*-alaninate (87)

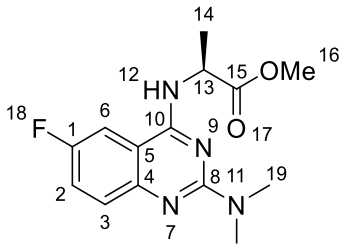

To a solution of **86** (200 mg, 0.70 mmol, 1 equiv.) in anhydrous DMF (3 mL), 2 M $NHMe_2$ in THF (1.0 mL, 2.0 mmol, 2.9 equiv.) was added. The reaction mixture was stirred at 100°C under an inert atmosphere for 4 h, then concentrated in vacuo. The product was purified using flash column chromatography (40−100% EtOAc in cyclohexane) to give methyl (2-dimethylamino-6-fluoroquinazolin-4-yl)-*L*-alaninate (192 mg, 0.66 mmol, 93%) as a white solid.

IR ν_{max}/cm^{-1}(thin film): 1731 (C=O);

^{1}H NMR (400 MHz, chloroform-*d*) δ 7.40 (dd, *J* = 9.2, 5.2 Hz, 1H, C(6)H), 7.24 (ddd, *J* = 9.2, 8.3, 2.8 Hz, 1H, C(2)H), 7.17 (dd, *J* = 9.0, 2.8 Hz, 1H, C(3)H), 5.94 (d, *J* = 6.4 Hz, 1H, N(12)H), 4.84 – 4.74 (m, 1H, C(13)H), 3.79 (s, 3H, OMe(16) -CH_3), 3.18 (s, 6H, $(C(19)H_3)_2$), 1.58 (d, *J* = 7.1 Hz, 3H, $C(14)H_3$); ^{13}C NMR (101 MHz, chloroform-*d*) δ 174.68, 159.23, 158.49 (d, *J* = 4.0 Hz), 158.04, 155.65, 149.52, 127.73 (d, *J* = 7.8 Hz), 121.87 (d, *J* = 24.1 Hz), 109.28 (d, *J* = 7.9 Hz), 105.43 (d, *J* = 22.8 Hz), 52.43, 49.97, 36.97, 17.92; ^{19}F NMR (376 MHz, chloroform-*d*) δ -121.13;

LRMS: *m/z*(%)= 293.1 (100) $[M + H]^+$; HRMS: calcd. $C_{14}H_{18}O_2N_4F$ $[M + H]^+$: 293.1408; found: 293.1407;

(*S*)-2-(2-Dimethylamino-6-fluoroquinazolin-4-yl)amino-*N*-hydroxypropanamide (88)

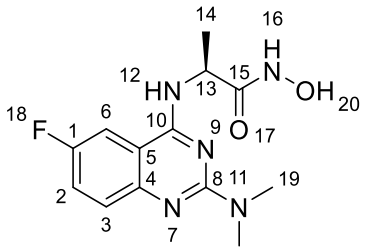

General procedure D using **87** (100 mg, 0.34 mmol, 1 equiv.). Purified using RP HPLC (MeCN in H_2O both with 0.1% TFA) and lyophilized to give (*S*)-2-(2-dimethylamino-6-fluoroquinazolin-4-yl)amino-*N*-hydroxypropanamide (42 mg, 0.14 mmol, 42%) as a white solid.

IR ν_{max}/cm^{-1}(solid): 3201 (O-H) and 1649 (C=O);

^{1}H NMR (400 MHz, methanol-d_4) δ 8.07 (dd, *J* = 9.1, 2.6 Hz, 1H, C(6)H), 7.70 – 7.54 (m, 2H, C(2)H, C(3)H), 4.65 (q, *J* = 7.2 Hz, 1H, C(13)H), 3.33 (s, 6H, $(C(19)H_3)_2$), 1.64 (d, *J* = 7.3 Hz, 3H, $C(14)H_3$); ^{13}C NMR (101 MHz, methanol-d_4) δ 171.64, 161.68, 160.30, 159.25, 153.71, 137.57, 124.69 (d, *J* = 24.7 Hz), 120.56 (d, *J* = 8.2 Hz), 111.67 (d, *J* = 8.5 Hz), 110.71 (d, *J* = 25.3 Hz), 51.59, 38.63, 17.86; ^{19}F NMR (376 MHz, methanol-d_4) δ -76.93;

LRMS: *m/z*(%)= 294.1 (100), $[M + H]^+$; HRMS: calcd. $C_{13}H_{17}O_2N_5F$ $[M + H]^+$: 294.1361; found: 294.1360;

$[\alpha]_D^{25} = -26.0$ (c = 1.0 in MeOH);

Methyl (2-chloro-6-methoxyquinazolin-4-yl)-*L*-alaninate (89)

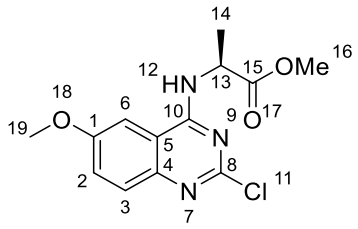

To a solution of 2,4-dichloro-6-methoxyquinazoline (500 mg, 2.2 mmol, 1 equiv.) and *L*-alanine methyl ester hydrochloride (480 mg, 3.4 mmol, 1.5 equiv.) in anhydrous DMF (5 mL) at 0 °C, anhydrous DIPEA (1.2 mL, 6.9 mmol, 3 equiv.) was added dropwise. The reaction mixture was stirred 16 h at RT under an inert atmosphere and then diluted with cold H_2O (75 mL). The precipitate was collected by filtration and dried under vacuum to give methyl (2-chloro-6-methoxyquinazolin-4-yl)-*L*-alaninate (470 mg, 1.6 mmol, 73%) obtained as a yellowish-white solid.

IR ν_{max}/cm^{-1}(solid): 1719 (C=O);

^{1}H NMR (400 MHz, methanol-d_4) δ 7.57 (d, *J* = 2.7 Hz, 1H, C(6)H), 7.49 (d, *J* = 9.1 Hz, 1H, C(3)H), 7.37 (dd, *J* = 9.2, 2.7 Hz, 1H, C(2)H), 4.86 (q, *J* = 7.3 Hz, 1H, C(13)H), 3.91 (s, 3H, C(19)H_3), 3.77 (s, 3H, OMe(16) -CH_3), 1.62 (d, *J* = 7.4 Hz, 3H, C(14)H_3); ^{13}C NMR (101 MHz, methanol-d_4) δ 175.45, 161.86, 159.53, 156.03, 146.64, 128.55, 126.22, 115.12, 102.94, 56.41, 52.88, 51.38, 17.10;

LRMS: *m/z*(%)= 296.1 (100), 298.1 (32) $[M + H]^+$; HRMS: calcd. $C_{13}H_{15}O_3N_3{}^{35}Cl$ $[M + H]^+$: 296.0796; found: 296.0798;

Methyl (2-dimethylamino-6-methoxyquinazolin-4-yl)-*L*-alaninate (90)

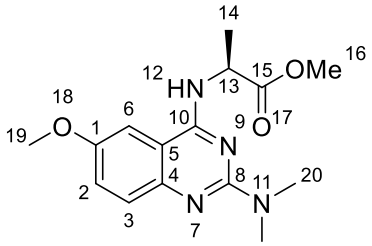

To a solution of **89** (200 mg, 0.68 mmol, 1 equiv.) in anhydrous DMF (3 mL), 2 M $NHMe_2$ in THF (1.0 mL, 2.0 mmol, 2.9 equiv.) was added. The reaction mixture was stirred for 4h at 100 °C under an inert atmosphere and concentrated in vacuo. The product was purified using flash column chromatography (40−100% EtOAc in cyclohexane) to give methyl (2-dimethylamino-6-methoxyquinazolin-4-yl)-*L*-alaninate (183 mg, 0.60 mmol, 89%) as a white solid.

IR ν_{max}/cm^{-1}(thin film): 1731 (C=O);

^{1}H NMR (400 MHz, chloroform-*d*) δ 7.40 (d, *J* = 9.1 Hz, 1H, C(3)H), 7.18 (dd, *J* = 9.1, 2.7 Hz, 1H, C(2)H), 6.85 (d, *J* = 2.8 Hz, 1H, C(6)H), 5.96 (d, *J* = 6.5 Hz, 1H, N(12)H), 4.83 (app. p, *J* = 7.0 Hz, 1H, C(13)H), 3.82 (s, 3H, C(19)H_3), 3.77 (s, 3H, OMe(16) -CH_3), 3.18 (s, 6H, (C(20)H_3)$_2$), 1.59 (d, *J* = 7.2 Hz, 3H, C(14)H_3); ^{13}C NMR (101 MHz, chloroform-*d*) δ 174.87, 158.58, 158.23, 153.81, 147.92, 127.29, 123.54, 109.31, 100.99, 55.65, 52.27, 49.89, 36.95, 17.91;

LRMS: *m/z*(%)= 305.1 (100) $[M + H]^+$; HRMS: calcd. $C_{15}H_{21}O_3N_4$ $[M + H]^+$: 305.1608; found: 305.1607;

(*S*)-2-(2-Dimethylamino-6-methoxyquinazolin-4-yl)amino-*N*-hydroxypropanamide (91)

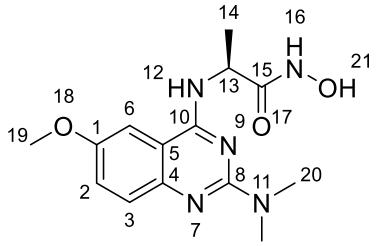

General procedure D using **90** (100 mg, 0.33 mmol, 1 equiv.). Purified using RP HPLC (MeCN in H_2O both with 0.1% TFA) and lyophilized to give (*S*)-2-(2-dimethylamino-6-methoxyquinazolin-4-yl)amino-*N*-hydroxypropanamide (33 mg, 0.11 mmol, 33%) as a white solid.

IR ν_{max}/cm^{-1}(solid): 3234 (O-H) and 1644 (C=O);

^{1}H NMR (400 MHz, methanol-d_4) δ 7.38 (s, 1H, C(6)H), 7.30 (d, *J* = 9.0 Hz, 1H, C(2)H), 7.22 (d, *J* = 8.3 Hz, 1H, C(3)H), 4.69 (q, *J* = 6.8 Hz, 1H, C(13)H), 3.78 (s, 3H, C(19)H_3), 3.32 (d, *J* = 3.1 Hz, 6H, (C(2)H_3)$_2$), 1.70 (d, *J* = 7.2 Hz, 3H, C(14)H_3); ^{13}C NMR (101 MHz, methanol-d_4) δ 172.22, 160.30, 158.01, 152.80, 134.69, 126.38, 119.87, 110.85, 104.61, 56.90, 51.36, 38.29, 18.09;

LRMS: *m/z*(%)= 306.2 (100) $[M + H]^+$; HRMS: calcd. $C_{14}H_{20}O_3N_5$ $[M + H]^+$: 306.1561; found: 306.1561;

$[\alpha]_D^{25}$ = +103.2 (c = 1.2 in MeOH);

Methyl (2-bromo-6-fluoroquinazolin-4-yl)-*L*-alaninate (92)

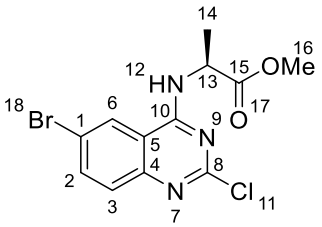

To a solution of 6-bromo-2,4-dichloroquinazoline (500 mg, 1.8 mmol, 1 equiv.) and *L*-alanine methyl ester hydrochloride (300 mg, 2.2 mmol, 1.2 equiv.) in anhydrous DMF (5 mL) at 0 °C, anhydrous DIPEA (630 µL, 3.6 mmol, 2 equiv.) was added dropwise. The reaction mixture was stirred at RT under an inert atmosphere for 16 h and then diluted with cold H_2O (75 mL). The precipitate was collected by filtration and dried under vacuum to give methyl (6-bromo-2-chloroquinazolin-4-yl)-*L*-alaninate (584 mg, 1.7 mmol, 94%) obtained as a white solid.

IR ν_{max}/cm^{-1}(thin film): 1724 (C=O);

^{1}H NMR (400 MHz, chloroform-*d*) δ 7.86 (d, *J* = 2.0 Hz, 1H, C(6)H), 7.70 (dd, *J* = 8.9, 2.0 Hz, 1H, C(2)H), 7.47 (d, *J* = 8.9 Hz, 1H, C(3)H), 7.12 (d, *J* = 7.2 Hz, 1H, N(12)H), 5.03 (app. p, *J* = 7.2 Hz, 1H, C(13)H, 3.89 (s, 3H, OMe(16) -CH_3), 1.60 (d, *J* = 7.2 Hz, 3H, C(14)H_3); ^{13}C NMR (101 MHz, chloroform-*d*) δ 174.69, 159.13, 157.49, 149.37, 136.81, 129.19, 123.93, 119.40, 114.09, 53.03, 49.75, 17.81;

LRMS: *m/z*(%)= 346.1 (100), 344.1 (74), 348.1 (27) $[M + H]^+$; HRMS: calcd. $C_{12}H_{12}O_2N_3{}^{81}Br{}^{35}Cl$ $[M + H]^+$: 345.9773; found: 345.9774;

Methyl (6-bromo-2-dimethylaminoquinazolin-4-yl)-*L*-alaninate (93)

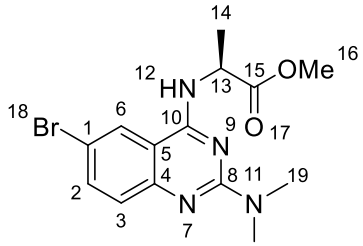

To a solution of **92** (300 mg, 0.87 mmol, 1 equiv.) in anhydrous DMF (4 mL), 2 M $NHMe_2$ in THF (1.3 mL, 2.6 mmol, 3 equiv.) was added. The reaction mixture was stirred for 4 h at 100 °C under an inert atmosphere, then concentrated *in vacuo*. The product was purified using flash column chromatography (20−60% EtOAc in cyclohexane) to give methyl (6-bromo-2-dimethylaminoquinazolin-4-yl)-*L*-alaninate (271 mg, 0.77 mmol, 88%) as a white solid.

IR ν_{max}/cm^{-1}(thin film):1736 (C=O);

^{1}H NMR (400 MHz, chloroform-*d*) δ 7.61 (d, *J* = 2.2 Hz, 1H, C(6)H), 7.46 (dd, *J* = 9.0, 2.2 Hz, 1H, C(2)H), 7.22 (d, *J* = 9.0, Hz, 1H, C(3)H), 6.21 (d, *J* = 6.5 Hz, 1H, N(12)H), 4.83 – 4.70 (m, 1H, C(13)H), 3.81 (s, 3H, OMe(16) -CH_3), 3.19 (s, 6H, $(C(19)H_3)_2$), 1.58 (d, *J* = 7.2 Hz, 3H, $C(14)H_3$); ^{13}C NMR (101 MHz, chloroform-*d*) δ 175.08, 159.36, 157.96, 151.45, 135.64, 127.54, 123.76, 112.48, 110.95, 52.55, 50.03, 37.01, 17.83;

LRMS: *m/z*(%)= 353.1 (100), 355.1 (98) $[M + H]^+$; HRMS: calcd. $C_{14}H_{18}O_2N_4{}^{79}Br$ $[M + H]^+$: 353.0608; found: 353.0606;

Methyl (2-dimethyl-6-phenylaminoquinazolin-4-yl)-*L*-alaninate (94)

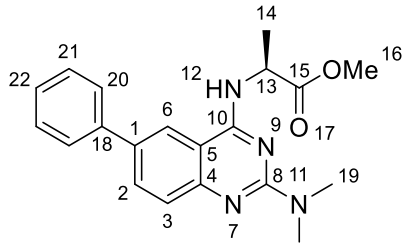

A mixture of **93** (250 mg, 0.71 mmol, 1 equiv.), phenylboronic acid (130 mg, 1.06 mmol, 1.5 equiv.), $NaHCO_3$ (300 mg, 3.5 mmol, 5 equiv.), and $Pd(dppf)Cl_2$ (52 mg, 0.07 mmol, 0.1 equiv.) in degassed 1,4-dioxane (4 mL) and H_2O (1 mL) was stirred for 1 h at 100 °C under inert atmosphere in microwave reactor. The reaction mixture was diluted with EtOAc (30 mL), washed with H_2O (2 × 15 mL) and dried over Na_2SO_4. Purified using flash column chromatography (20−60% EtOAc in cyclohexane) to give methyl (2-dimethyl-6-phenylaminoquinazolin-4-yl)-*L*-alaninate (221 mg, 0.63 mmol, 89%) as a white solid.

IR ν_{max}/cm^{-1}(thin film): 1730 (C=O);

^{1}H NMR (400 MHz, chloroform-*d*) δ 7.77 (dd, *J* = 8.7, 2.1 Hz, 1H, C(2)H), 7.71 (d, *J* = 2.0 Hz, 1H, C(6)H), 7.64 – 7.57 (m, 2H, $(C(20)H)_2$), 7.50 (d, *J* = 8.7 Hz, 1H. C(3)H), 7.46 – 7.38 (m, 2H, $(C(21)H)_2$), 7.36 – 7.29 (m, 1H, C(22)H), 6.16 (d, *J* = 6.5 Hz, 1H, N(12)H), 4.91 – 4.77 (m, 1H, C(13)H), 3.79 (s, 3H, OMe(16) -CH_3), 3.19 (s, 6H, -$(C(19)H_3)_2$), 1.61 (d, *J* = 7.2 Hz, 3H, C(14)H_3); ^{13}C NMR (101 MHz, chloroform-*d*) δ 174.80, 159.41, 158.96, 152.17, 140.90, 133.54, 132.07, 128.90, 127.00, 126.98, 126.30, 119.13, 109.92, 52.46, 50.01, 37.03, 18.06.

LRMS: *m/z*(%)= 351.2 (100) $[M + H]^+$; HRMS: calcd. $C_{20}H_{23}O_2N_3$ $[M + H]^+$: 351.1816; found: 351.1818;

(*S*)-2-(2-Dimethylamino-6-phenylquinazolin-4-yl)amino-*N*-hydroxypropanamide (95)

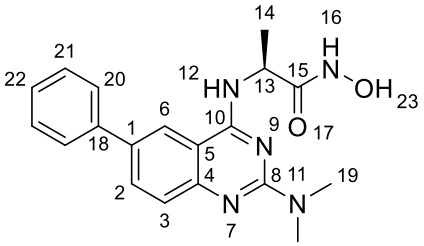

General procedure D using **94** (100 mg, 0.33 mmol, 1 equiv.). Purified using RP HPLC (MeCN in H_2O both with 0.1% TFA) and lyophilized to give (*S*)-2-(2-dimethylamino-6-phenylquinazolin-4-yl)amino-*N*-hydroxypropanamide (21 mg, 0.06 mmol, 21%) as a white solid.

IR ν_{max}/cm^{-1}(solid): 3235 (O-H) and 1642 (C=O);

^{1}H NMR (400 MHz, methanol-d_4) δ 8.20 (brs, 1H, C(6)H), 7.95 (brs, 1H, C(2), 7.73 (brs, 2H, $C(20)H)_2$), 7.51 (app. d, J = 7.0 Hz, 2H, $(C(21)H)_2$), 7.42 – 7.19 (m, 2H, C(3)H, C(22)H), 4.68 (app. d, J = 6.3 Hz, 1H, C(13)H), 2.85 (s, 6H, $(C(19)H_3)_2$), 1.71 (d, J = 7.1 Hz, 3H, $C(14)H_3$); ^{13}C NMR (101 MHz, methanol-d_4) δ 170.75, 158.85, 151.19, 137.95, 136.50, 135.58, 131.82, 129.05, 127.89, 125.49, 119.71, 117.51, 109.21, 49.84, 37.40, 16.82;

LRMS: *m/z*(%)= 352.1 (100) $[M + H]^+$; HRMS: calcd. $C_{20}H_{23}O_2N_3$ $[M + H]^+$: 352.1768; found: 352.1768;

$[\alpha]_D^{25}$ = +72.4 (c = 1.5 in MeOH);

Ethyl 4-chloroquinazoline-2-carboxylate (96)[18]

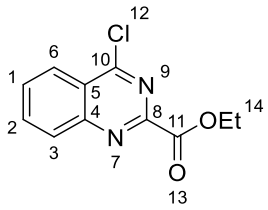

The compound was synthesised using a literature procedure.[18] To a solution of **71** (6.0g, 27 mmol, 1 equiv.) and $SOCl_2$ (20 mL, 275 mmol, 10 equiv.) in chloroform (60 mL), DMF (5 drops) was added. The reaction mixture was stirred under reflux for 3 h, then concentrated *in vacuo* to give ethyl 4-chloroquinazoline-2-carboxylate (6.5 g, 27 mmol, quantitative) as a yellow solid.

IR ν_{max}/cm^{-1}(solid): 1734 (C=O);

^{1}H NMR (400 MHz, DMSO-d_6) δ 8.17 (ddd, *J* = 8.0, 1.6, 0.6 Hz, 1H, C(6)H), 7.89 (ddd, *J* = 8.5, 7.0, 1.6 Hz, 1H, C(2)H), 7.82 (ddd, *J* = 8.5, 1.3, 0.6 Hz, 1H, C(3)H), 7.64 (ddd, *J* = 8.0, 7.0, 1.3 Hz, 1H, C(1)H), 4.38 (q, *J* = 7.1 Hz, 2H, OEt(14) -CH_2-), 1.35 (t, *J* = 7.1 Hz, 3H OEt(14) -CH_3); ^{13}C NMR (101 MHz, DMSO-d_6) δ 161.49, 160.61, 147.61, 143.95, 135.29, 129.13, 128.77, 126.52, 123.39, 63.14, 14.37;

LRMS: *m/z*(%)= 237.1 (100), 239.1 (35) $[M + H]^+$;

A variance between analytical data (^{1}H NMR) and previously reported data has been observed, caused by the use of different solvents.[18]

Ethyl (*S*)-4-((1-(tert-butoxy)-1-oxopropan-2-yl)amino)quinazoline-2-carboxylate (97)

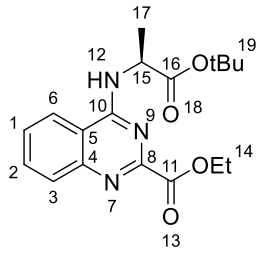

To a solution of **96** (6.5 g, 27 mmol, 1 equiv.) and *L*-alanine tert-butyl ester hydrochloride (7.5 g, 41 mmol, 1.5 equiv.) in anhydrous DCM (60 mL) at 0 °C, TEA (11.5 mL, 82 mmol, 3 equiv.) was added dropwise. The reaction mixture was stirred at RT under an inert atmosphere for 72 h, diluted with DCM (200 mL), washed with: 0.1 M citric $acid_{(aq)}$ (100 mL), H_2O (100 ml), and brine (100 mL), then dried over Na_2SO_4. Purified using flash column chromatography (20−60% EtOAc in cyclohexane) to give ethyl (*S*)-4-((1-(tert-butoxy)-1-oxopropan-2-yl)amino)quinazoline-2-carboxylate (8.2 g, 24 mmol, 87%) as a yellowish solid.

IR ν_{max}/cm^{-1}(solid): 1739 and 1711 (C=O);

^{1}H NMR (400 MHz, methanol-d_4) δ 8.25 (ddd, *J* = 8.3, 1.4, 0.7 Hz, 1H, C(6)H), 7.87 (ddd, *J* = 8.4, 1.5, 0.7 Hz, 1H, C(3)H), 7.82 (ddd, *J* = 8.4, 6.7, 1.4 Hz, 1H, C(2)H), 7.58 (ddd, *J* = 8.3, 6.7, 1.5 Hz, 1H, C(1)H), 4.84 (q, *J* = 7.0 Hz, 1H, C(15)H), 4.44 (q, *J* = 7.1 Hz, 2H, OEt(14) -CH_2-), 1.59 (d, *J* = 7.3 Hz, 3H, OEt(14) -CH_3), 1.45 (s, 9H, OtBu(19) (-CH_3)$_3$); ^{13}C NMR (101 MHz, methanol-d_4) δ 174.41, 166.13, 161.89, 154.30, 150.03, 134.62, 128.87 (d, *J* = 3.9 Hz), 123.66, 116.11, 82.59, 63.11, 52.08, 28.25, 17.13, 14.57;

LRMS: *m/z*(%)= 346.2 (100) $[M + H]^+$; HRMS: calcd. $C_{18}H_{24}O_4N_3$ $[M + H]^+$: 346.1761; found: 346.1761;

Ethyl (*S*)-4-((1-((benzyloxy)amino)-1-oxopropan-2-yl)amino)quinazoline-2-carboxylate (98)

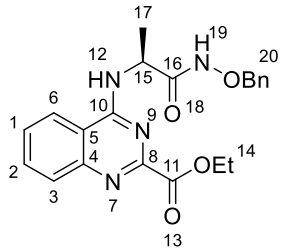

To a solution of **97** (8.0g, 23 mmol, 1 equiv.) in DCM (20 mL), 4 M HCl in 1,4-dioxane (20 mL, 81 mmol, 3.5 equiv.) was slowly added. The reaction mixture was stirred at RT for 16 h, then concentrated *in vacuo* to give intermediate (2-(ethoxycarbonyl)quinazolin-4-yl)-*L*-alanine (6.7 g, 23 mmol) as a yellow solid. Crude intermediate was used for the next step without purification.

To a solution of intermediate (2-(ethoxycarbonyl)quinazolin-4-yl)-*L*-alanine (6.0 g, 21 mmol, 1 equiv.), HATU (7.9 g, 21 mmol, 1 equiv.), *O*-benzylhydroxylamine hydrochloride (4.0 g, 25 mmol, 1.2 equiv.) in anhydrous DCM (50 mL) at 0 °C, DIPEA (10.8 mL, 62 mmol, 3 equiv.) was added dropwise. The reaction mixture was stirred at RT under inert atmosphere for 16 h, diluted with DCM (150 mL), washed with 1 M $HCl_{(aq)}$ (100 mL), sat. $NaHCO_{3(aq)}$ (100 ml), and brine (100 mL), then dried over Na_2SO_4. Purified using flash column chromatography (40−100% EtOAc in cyclohexane) to give Ethyl (*S*)-4-((1-((benzyloxy)amino)-1-oxopropan-2-yl)amino)quinazoline-2-carboxylate (6.5 g, 16 mmol, 79% after 2 steps) as a white solid.

IR ν_{max}/cm^{-1}(solid): 1724 and 1676 (C=O);

^{1}H NMR (400 MHz, methanol-d_4) δ 8.26 (d, J = 8.1 Hz, 1H, C(6)H), 7.96 – 7.77 (m, 2H, C(2)H, C(3)H), 7.62 (ddd, J = 8.1, 6.7, 1.4 Hz, 1H, C(1)H), 7.29 – 7.22 (m, 2H, OBn(20) ArH_2), 7.18 – 7.06 (m, 3H, OBn(20) ArH_3), 4.90 – 4.76 (m, 3H, C(15)H, OBn(20) -CH_2-), 4.42 (q, J = 7.1 Hz, 2H, OEt(14) -CH_2-), 1.55 (d, J = 7.1 Hz, 3H, C(17)H_3), 1.43 (t, J = 7.1 Hz, 3H, OEt(14) -CH_3); ^{13}C NMR (101 MHz, methanol-d_4) δ 170.69, 164.56, 160.14, 152.12, 148.72, 135.36, 133.44, 128.96, 128.20, 127.81, 127.78, 127.64, 122.40, 114.88, 77.22, 62.02, 48.23, 15.69, 13.10;

LRMS: *m/z*(%)= 395.1 (100) $[M + H]^+$; HRMS: calcd. $C_{21}H_{23}O_4N_4$ $[M + H]^+$: 395.1714; found: 395.1714;

(*S*)-4-((1-((Benzyloxy)amino)-1-oxopropan-2-yl)amino)quinazoline-2-carboxylic acid (99)

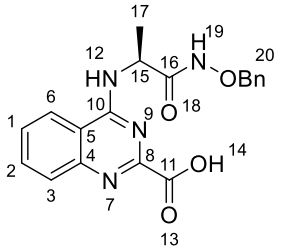

To a solution of **98** (6.5 g, 16 mmol, 1 equiv.) in THF (30 mL), 2 M $KOH_{(aq)}$ (33 mL, 66 mmol, 4 equiv.) was added slowly. Reaction mixture was stirred for 2 h, cooled to 0 °C, acidified with 2 M $HCl_{(aq)}$ (50 mL) and extracted with $CHCl_3$/*i*-PrOH (4:1, 3 × 100 mL). Combine organic layer was washed with brine (150 mL), dried over Na_2SO_4, then concentrated *in vacuo* to give (*S*)-4-((1-((benzyloxy)amino)-1-oxopropan-2-yl)amino)quinazoline-2-carboxylic acid (5.7 g, 15 mmol, 94%) as a white solid.

IR ν_{max}/cm^{-1}(solid): 3327 (O-H), 1645 (C=O) and 1637 (C=O);

^{1}H NMR (400 MHz, DMSO-d_6) δ 11.34 (s, 1H, N(19)H), 8.60 (d, J = 7.0 Hz, 1H, C(6)H), 8.49 (d, J = 8.3 Hz, 1H, N(12)H), 7.92 – 7.81 (m, 2H, C(2)H, C(3)H), 7.66 (ddd, J = 8.2, 6.3, 1.9 Hz, 1H, C(1)H), 7.39 – 7.27 (m, 5H, OBn(20) ArH_5), 4.85 – 4.75 (m, 3H, C(15)H, OBn(20) -CH_2-), 1.46 (d, J = 7.2 Hz, 3H, C(17)H_3); ^{13}C NMR (101 MHz, DMSO-d_6) δ 169.67, 165.76, 160.32, 154.20, 148.58, 136.30, 134.01, 129.36, 128.68, 128.03, 127.65, 124.01, 115.00, 77.34, 48.74, 17.95;

LRMS: m/z(%)= 367.1 (100) $[M + H]^+$; HRMS: calcd. $C_{19}H_{19}O_4N_4$ $[M + H]^+$: 367.1401; found: 367.1402;

2,5-Dioxopyrrolidin-1-yl (*S*)-4-((1-((benzyloxy)amino)-1-oxopropan-2-yl)amino) quinazoline-2-carboxylate (100)

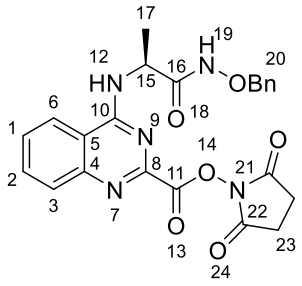

To a solution of **99** (5.7 g, 15 mmol, 1 equiv.) and *N*-hydroxysuccinimide (2.3 g, 20 mmol, 1.3 equiv.) in anhydrous DMF (30 mL) at 0 °C, DCC (4.0 g, 19 mmol, 1.2 equiv.) was added. The reaction mixture was stirred at RT under an inert atmosphere for 16 h. A white precipitate (dicyclohexylurea) was removed using filtration, and the filtrate was concentrated *in vacuo.* The product was purified by flash column chromatography (60−100% EtOAc in cyclohexane) to give 2,5-dioxopyrrolidin-1-yl (*S*)-4-((1-((benzyloxy)amino)-1-oxopropan-2-yl)amino)quinazoline-2-carboxylate (4.8 g, 10 mmol, 67%) as a white-off solid.

IR ν_{max}/cm^{-1}(solid): 1781, 1733 and 1658 (C=O);

^{1}H NMR (400 MHz, DMSO-d_6) δ 11.32 (s, 1H, N(19)H), 8.72 (d, *J* = 7.0 Hz, 1H, N(12)H), 8.55 (d, *J* = 8.3 Hz, 1H, C(6)H), 7.98 – 7.90 (m, 2H, C(2)H, C(3)H), 7.76 (ddd, *J* = 8.4, 5.4, 2.6 Hz, 1H, C(1)H), 7.43 – 7.24 (m, 5H, OBn(20) ArH_5), 4.81 – 4.70 (m, 3H, C(15)H, OBn(20) -CH_2-), 2.89 (s, 4H, $(C(23)H_2)_2$), 1.48 (d, *J* = 7.3 Hz, 3H, $C(17)H_3$); 170.12, 168.83, 159.98, 159.69, 149.26, 148.45, 135.82, 133.83, 128.79, 128.46, 128.43, 128.16, 123.71, 115.29, 76.88, 48.53, 25.58, 17.50;

(*S*)-((4-((1-(Hydroxyamino)-1-oxopropan-2-yl)amino)quinazoline-2-carboxamido) methyl)phosphonic acid (101)

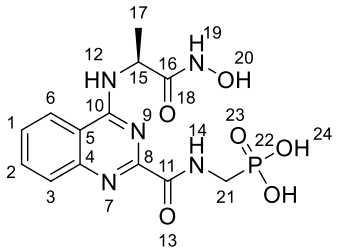

To a solution of (aminomethyl)phosphonic acid (200 mg, 1.80 mmol, 4.2 equiv.) in 0.4 M $Na_2CO_{3(aq)}$ (3 mL), **100** (200 mg, 0.43 mmol, 1 equiv.) in DMF (2 mL) was added dropwise. The reaction mixture was stirred at RT for 3 h, acidified with 1 M HCl (3 mL), degassed with argon and palladium on carbon (100 mg, 10 wt. %) was added. The reaction mixture was stirred for another 3 h under an H_2 atmosphere, filtered through Celite, then concentrated *in vacuo.* Purified using RP HPLC (MeCN in H_2O both with 0.1% TFA) and lyophilized to give (*S*)-((4-((1-(Hydroxyamino)-1-oxopropan-2-yl)amino)quinazoline-2-carboxamido)methyl)phosphonic acid (22 mg, 0.06 mmol, 14% after 2 steps) as a white solid.

IR ν_{max}/cm^{-1}(solid): 1660 and 1633 (C=O);

^{1}H NMR (400 MHz, deuterium oxide) δ 7.95 (d, *J* = 8.3 Hz, 1H, C(6)H), 7.76 (t, *J* = 7.7 Hz, 1H, C(2)H), 7.69 (d, *J* = 8.3 Hz, 1H, C(3)H), 7.51 (t, *J* = 7.7 Hz, 1H, C(1)H), 4.84 (q, *J* = 7.2 Hz, 1H, C(15)H), 3.47 (app. qd, *J* = 14.8, 1.5 Hz, 2H, C(21)H_2), 1.50 (d, *J* = 7.0 Hz, 3H, C(17)H_3); ^{13}C NMR (151 MHz, deuterium oxide) δ 167.33, 165.00 (d, *J* = 6.3 Hz), 159.41, 153.17, 147.97, 133.77, 127.79, 127.32, 122.14, 114.39, 48.96 (d, *J* = 4.9 Hz), 39.19 (d, *J* = 137.2 Hz), 17.76; ^{31}P NMR (162 MHz, deuterium oxide) δ 13.30;

LRMS: *m/z*(%)= 370.1 (100) $[M + H]^+$; HRMS: calcd. $C_{13}H_{17}O_6N_5P$ $[M + H]^+$: 370.0911; found: 370.0911;

$[\alpha]_D^{25}$ = +2.1 (c = 0.7 in H_2O);

(*S*)-(2-(4-((1-(Hydroxyamino)-1-oxopropan-2-yl)amino)quinazoline-2-carboxamido) ethyl)phosphonic acid (102)

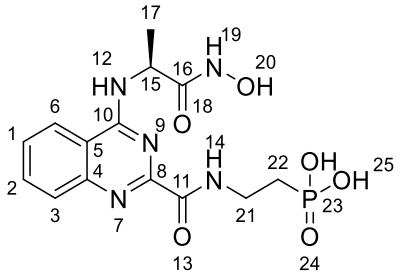

To a solution of 2-aminoethylphosphonic acid (200 mg, 1.60 mmol, 3.7 equiv.) in 0.4 M $Na_2CO_{3(aq)}$ (3 mL), **100** (200 mg, 0.43 mmol, 1 equiv.) in DMF (2 mL) was added dropwise. The reaction mixture was stirred at RT for 3 h, acidified with 1 M HCl (3 mL), degassed with argon and palladium on carbon (100 mg, 10 wt. %) was added. The reaction mixture was stirred for another 3 h under an H_2 atmosphere, filtered through Celite, then concentrated

in vacuo. Purified using RP HPLC (MeCN in H_2O both with 0.1% TFA) and lyophilized to give (*S*)-(2-(4-((1-(hydroxyamino)-1-oxopropan-2-yl)amino)quinazoline-2-carboxamido)ethyl)phosphonic acid (51 mg, 0.13 mmol, 31% after 2 steps) as a white solid.

IR ν_{max}/cm^{-1}(solid): 1671 and 1628 (C=O);

^{1}H NMR (400 MHz, deuterium oxide) δ 7.75 (d, *J* = 8.3 Hz, 1H, C(6)H), 7.61 (t, *J* = 7.8 Hz, 1H, C(2)H), 7.50 (d, *J* = 8.3 Hz, 1H, C(3)H), 7.36 (t, *J* = 7.7 Hz, 1H, C(1)H), 4.52 (q, *J* = 6.7 Hz, 1H, C(15)H), 3.53 (q, *J* = 7.5 Hz, 2H, C(21)H_2), 1.83 – 1.70 (m, 2H, C(22)H), 1.45 (d, *J* = 7.1 Hz, 3H, C(17)H_3); ^{13}C NMR (151 MHz, deuterium oxide) δ 167.30, 164.80, 158.97, 152.66, 147.71, 133.57, 127.63, 127.17, 121.93, 113.99, 49.18, 36.64, 29.18 (d, *J* = 125.9 Hz), 17.67; ^{31}P NMR (162 MHz, deuterium oxide) δ 18.40;

LRMS: *m/z*(%)= 382.1 (100) $[M - H]^-$; HRMS: calcd. $C_{14}H_{17}O_6N_5P$ $[M - H]^-$: 382.0922; found: 382.0916;

$[\alpha]_D^{25}$ = +18.7 (c = 1.5 in H_2O);

(*S*)-(3-(4-((1-(Hydroxyamino)-1-oxopropan-2-yl)amino)quinazoline-2-carboxamido) propyl)phosphonic acid (103)

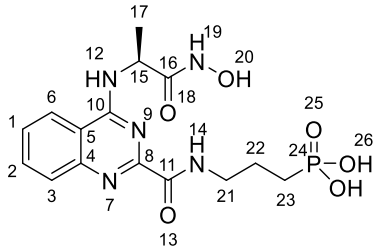

To a solution of 3-aminopropylphosphonic acid (200 mg, 1.44 mmol, 3.3 equiv.) in 0.4 M $Na_2CO_{3(aq)}$ (3 mL), **100** (200 mg, 0.43 mmol, 1 equiv.) in DMF (2 mL) was added dropwise.

The reaction mixture was stirred at RT for 3 h, acidified with 1 M HCl (3 mL), degassed with argon and palladium on carbon (100 mg, 10 wt. %) was added. The reaction mixture was stirred for another 3 h under an H_2 atmosphere, filtered through Celite, then concentrated *in vacuo.* Purified using RP HPLC (MeCN in H_2O both with 0.1% TFA) and lyophilized to give (*S*)-(3-(4-((1-(hydroxyamino)-1-oxopropan-2-yl)amino)quinazoline-2-carboxamido)propyl)phosphonic acid (64 mg, 0.16 mmol, 37% after 2 steps) as a white solid.

IR ν_{max}/cm^{-1}(solid): 1664 and 1628 (C=O);

^{1}H NMR (400 MHz, deuterium oxide) δ 7.74 (d, *J* = 8.3 Hz, 1H, C(6)H), 7.61 (t, *J* = 7.3 Hz, 1H, C(2)H), 7.51 (d, *J* = 8.3 Hz, 1H, C(3)H), 7.36 (t, *J* = 7.7 Hz, 1H, C(1)H), 4.48 (q, *J* = 7.6 Hz, 1H, C(15)H), 3.41 – 3.28 (m, 2H, C(21)H_2), 1.82 – 1.69 (m, 2H, C(22)H_2), 1.45 – 1.36 (m, 5H, C(17)H_3, C(23)H_2); ^{13}C NMR (151 MHz, deuterium oxide) δ 167.54, 165.18, 159.00, 152.74, 147.70, 133.58, 127.63, 127.19, 121.95, 114.02, 49.30, 41.34 (d, *J* = 19.1 Hz), 26.71 (d, *J* = 130.4 Hz), 24.31, 17.75 (d, *J* = 5.3 Hz); ^{31}P NMR (162 MHz, deuterium oxide) δ 21.69;

LRMS: *m/z*(%)= 396.1 (100) $[M - H]^-$; HRMS: calcd. $C_{15}H_{19}O_6N_5P$ $[M - H]^-$: 396.1078; found: 396.1071;

$[\alpha]_D^{25}$ = +24.8 (c = 1.2 in H_2O);

(*S*)-(4-(4-((1-(Hydroxyamino)-1-oxopropan-2-yl)amino)quinazoline-2-carboxamido) butyl)phosphonic acid (104)

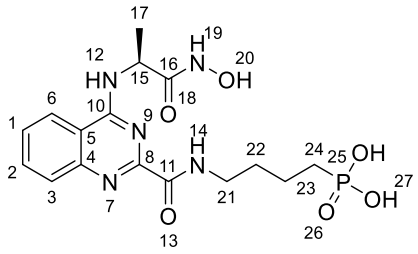

To a solution of 4-aminobutylphosphonic acid (200 mg, 1.31 mmol, 3.0 equiv.) in 0.4 M $Na_2CO_{3(aq)}$ (3 mL), **100** (200 mg, 0.43 mmol, 1 equiv.) in DMF (2 mL) was added dropwise. The reaction mixture was stirred at RT for 3 h, acidified with 1 M HCl (3 mL), degassed with argon and palladium on carbon (100 mg, 10 wt. %) was added. The reaction mixture was stirred for another 3 h under an H_2 atmosphere, filtered through Celite, then concentrated *in vacuo.* Purified using RP HPLC (MeCN in H_2O both with 0.1% TFA) and lyophilized to give (*S*)-(4-(4-((1-(hydroxyamino)-1-oxopropan-2-yl)amino)quinazoline-2-carboxamido)butyl)phosphonic acid (44 mg, 0.11 mmol, 25% after 2 steps) as a white solid.

IR ν_{max}/cm^{-1}(solid): 1673 and 1636 (C=O);

^{1}H NMR (400 MHz, deuterium oxide) δ 7.81 (d, *J* = 8.3 Hz, 1H. C(6)H), 7.68 (t, *J* = 7.7 Hz, 1H, C(2)H), 7.59 (d, *J* = 8.3 Hz, 1H, C(3)H), 7.43 (t, *J* = 7.6 Hz, 1H, C(1)H), 4.57 – 4.45 (m, 1H, C(15)H), 3.45 – 3.26 (m, 2H, C(21)H_2), , 1.75 – 1.61 (m, 2H, C(22)H_2), 1.60 – 1.50 (m, 1H, C(23)H_2), 1.47 (d, *J* = 7.1 Hz, 3H, C(17)H_3), 1.44 – 1.38 (m, 2H, C(24)H_2); ^{13}C NMR (151 MHz, deuterium oxide) δ 167.59, 165.14, 159.06, 152.84, 147.80, 133.62, 127.72, 127.28, 122.01, 114.10, 49.36, 39.82, 30.68, 29.04 (d, *J* = 130.2 Hz), 21.86, 17.72; ^{31}P NMR (162 MHz, deuterium oxide) δ 22.52;

LRMS: *m/z*(%)= 410.1 (100) $[M - H]^-$; HRMS: calcd. $C_{16}H_{21}O_6N_5P$ $[M - H]^-$: 410.1229; found: 410.1235;

$[\alpha]_D^{25}$ = +2.1 (c = 1.0 in H_2O);

(*S*)-4-((1-(Hydroxyamino)-1-oxopropan-2-yl)amino)-*N*-(2-sulfamoylethyl)quinazoline-2-carboxamide (105)

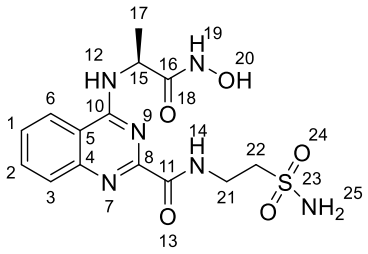

To a solution of 2-aminoethane-1-sulfonamide (200 mg, 1.61 mmol, 3.7 equiv.) and TEA (180 µL, 1.29 mmol, 3 equiv.) in DMF (3 mL), **100** (200 mg, 0.43 mmol, 1 equiv.) in DMF (2 mL) was added dropwise. The reaction mixture was stirred at RT for 3 h, then concentrated *in vacuo*. Crude intermediate was redissolved in MeOH (5 mL), degassed with argon and palladium on carbon (100 mg, 10 wt. %) was added. The reaction mixture was stirred for another 3 h under an H_2 atmosphere, filtered through Celite, then concentrated *in vacuo.* Purified using RP HPLC (MeCN in H_2O both with 0.1% TFA) and lyophilized to give (*S*)-4-((1-(hydroxyamino)-1-oxopropan-2-yl)amino)-*N*-(2-sulfamoylethyl)quinazoline -2-carboxamide (72 mg, 0.19 mmol, 44% after 2 steps) as a white solid.

IR ν_{max}/cm^{-1}(solid): 3247 (O-H), 1670 (C=O), 1628 (C=O) and 1320 (S=O);

^{1}H NMR (600 MHz, methanol-d_4) δ 8.48 (d, *J* = 8.5 Hz, 1H, C(6)H), 8.07 – 7.98 (m, 2H, C(2)H, C(3)H), 7.83 – 7.75 (m, 1H, C(1)H), 5.08 (q, *J* = 7.1 Hz, 1H, C(15)H), 4.01 – 3.93

(m, 2H, C(21)H_2), 3.47 (t, *J* = 6.5 Hz, 2H, C(22)H_2), 1.67 (d, *J* = 7.1 Hz, 3H, C(17)H_3); ^{13}C NMR (151 MHz, methanol-d_4) δ 171.37, 162.21, 160.96, 151.48, 142.40, 137.25, 130.42, 125.09, 123.48, 115.01, 54.38, 51.50, 36.29, 17.68;

LRMS: *m/z*(%)= 383.1 (100) $[M + H]^+$; HRMS: calcd. $C_{14}H_{19}O_5N_6S$ $[M + H]^+$: 383.1132; found: 383.1131;

$[\alpha]_D^{25}$ = +17.9 (c = 1.1 in MeOH);

(*S*)-4-((1-(Hydroxyamino)-1-oxopropan-2-yl)amino)-*N*-(3-sulfamoylpropyl) quinazoline-2-carboxamide (106)

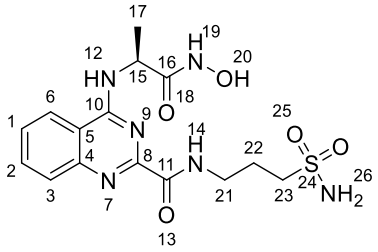

To a solution of 3-aminopropane-1-sulfonamide (200 mg, 1.45 mmol, 3.4 equiv.) and TEA (180 µL, 1.29 mmol, 3 equiv.) in DMF (3 mL), **100** (200 mg, 0.43 mmol, 1 equiv.) in DMF (2 mL) was added dropwise. The reaction mixture was stirred at RT for 3 h, then concentrated *in vacuo*. Crude intermediate was redissolved in MeOH (5 mL), degassed with argon and palladium on carbon (100 mg, 10 wt. %) was added. The reaction mixture was stirred for another 3 h under an H_2 atmosphere, filtered through Celite, then concentrated *in vacuo.* Purified using RP HPLC (MeCN in H_2O both with 0.1% TFA) and lyophilized to give (*S*)-4-((1-(hydroxyamino)-1-oxopropan-2-yl)amino)-*N*-(3-sulfamoylpropyl) quinazoline-2-carboxamide (66 mg, 0.17 mmol, 39% after 2 steps) as a white solid.

IR ν_{max}/cm^{-1}(solid): 3241 (O-H), 1670 (C=O), 1627 (C=O) and 1321 (S=O);

^{1}H NMR (600 MHz, methanol-d_4) δ 8.53 (d, J = 8.4 Hz, 1H, C(6)H), 8.10 – 8.03 (m, 2H, C(2)H, C(3)H), 7.83 (ddd, J = 8.3, 6.1, 2.1 Hz, 1H, C(1)H), 5.13 (q, J = 7.1 Hz, 1H, C(15)H), 3.73 – 3.57 (m, 2H, C(21)H_2), 3.26 – 3.21 (m, 2H, C(23)H_2), 2.25 – 2.18 (m, 2H, C(22)H), 1.69 (d, J = 7.1 Hz, 3H, C(17)H_3); ^{13}C NMR (151 MHz, methanol-d_4) δ 171.34, 162.49, 160.55, 151.35, 141.30, 137.60, 130.60, 125.30, 122.63, 114.86, 53.62, 51.83, 39.73, 25.11, 17.57;

LRMS: m/z(%)= 397.1 (100) $[M + H]^+$; HRMS: calcd. $C_{15}H_{21}O_5N_6S$ $[M + H]^+$: 397.1289; found: 397.1290;

$[\alpha]_D^{25}$ = +20.7 (c = 1.2 in MeOH);

(*S*)-3-(4-((1-(Hydroxyamino)-1-oxopropan-2-yl)amino)quinazoline-2-carboxamido) propane-1-sulfonic acid (107)

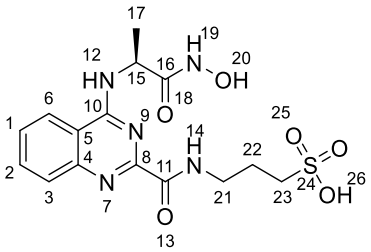

To a solution of 3-amino-1-propanesulfonic acid (200 mg, 1.44 mmol, 3.3 equiv.) in 0.4 M $Na_2CO_{3(aq)}$ (3 mL), **100** (200 mg, 0.43 mmol, 1 equiv.) in DMF (2 mL) was added dropwise. The reaction mixture was stirred at RT for 3 h, acidified with 1 M HCl (3 mL), degassed with argon and palladium on carbon (100 mg, 10 wt. %) was added. The reaction mixture was stirred for another 3 h under an H_2 atmosphere, filtered through Celite, then concentrated

in vacuo. Purified using RP HPLC (MeCN in H_2O both with 0.1% TFA) and lyophilized to give (*S*)-3-(4-((1-(hydroxyamino)-1-oxopropan-2-yl)amino)quinazoline-2-carboxamido) propane-1-sulfonic acid (41 mg, 0.10 mmol, 24% after 2 steps) as a white solid.

IR ν_{max}/cm^{-1}(solid): 1663 (C=O), 1628 (C=O) and 13284 (S=O);

^{1}H NMR (400 MHz, deuterium oxide) δ 7.68 (d, *J* = 7.9 Hz, 1H, C(6)H), 7.59 (t, *J* = 7.6 Hz, 1H, C(2)H), 7.48 (d, *J* = 8.3 Hz, 1H, C(3)H), 7.34 (t, *J* = 7.6 Hz, 1H. C(1)H), 4.41 – 4.35 (m, 1H, C(15)H), 3.58 – 3.33 (m, 2H, C(21)H_2), 3.03 – 2.90 (m, 2H, C(23)H_2), 2.12 – 1.91 (m, 2H, C(22)H_2), 1.43 (d, *J* = 7.1 Hz, 3H, C(17)H); ^{13}C NMR (151 MHz, deuterium oxide) δ 167.63, 165.23, 158.84, 152.42, 147.67, 133.52, 127.66, 127.22, 121.92, 113.96, 49.40 (d, *J* = 5.3 Hz), 48.66, 38.44, 24.25, 17.70;

LRMS: *m/z*(%)= 396.1 (100) $[M - H]^-$; HRMS: calcd. $C_{15}H_{18}O_6N_5S$ $[M - H]^-$: 396.0983; found: 396.0982;

$[\alpha]_D^{25}$ = +2.5 (c = 1.0 in H_2O);

(3-Azidopropyl)phosphonic acid (108)[19]

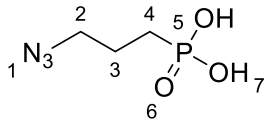

The compound was synthesised using a modified version of a literature procedure.[19] A mixture of diethyl (3-bromopropyl)phosphonate (2.0 mL, 10 mmol, 1 equiv.) and NaN_3 (1.3 g, 20 mmol, 2 equiv.) in anhydrous acetone (20 mL) was stirred under reflux for 24 h. Then the reaction mixture was cooled to RT, and the precipitate was removed by filtration. The filtrate was concentrated *in vacuo* to give intermediate diethyl (3-azidopropyl)

phosphonate as a colourless oil. Intermediate was used in the next step without further purification. Intermediate was dissolved in anhydrous MeCN (20 mL), and bromotrimethylsilane (6.6 mL, 50 mmol, 5 equiv.) was slowly added. The reaction mixture was stirred at RT under an inert atmosphere for 24 h, concentrated *in vacuo* and diluted with MeOH/H_2O (9:1, 20 mL) stirred. The reaction mixture was stirred at RT for a further 16 h, then concentrated *in vacuo* and co-evaporated with toluene to remove H_2O to give (3-azidopropyl)phosphonic acid (1.6 g, 10 mmol, 96% after 2 steps) as a colourless oil.

IR ν_{max}/cm^{-1}(thin film): 2110 (N=N=N);

^{1}H NMR (400 MHz, methanol-d_4) δ 3.45 – 3.34 (m, 2H, C(2)H_2), 2.02 – 1.65 (m, 4H, C(3)H_2, C(4)H_2); ^{13}C NMR (101 MHz, methanol-d_4) δ 51.94 (d, J = 16.8 Hz), 24.39 (d, J = 139.1 Hz), 23.01; ^{31}P NMR (162 MHz, methanol-d_4) δ 29.06;

LRMS: *m/z*(%)= 164.1 (100) $[M - H]^-$; HRMS: calcd. $C_3H_7O_3N_3P$ $[M - H]^-$: 164.0231; found: 164.0223;

Analytical data (^{1}H NMR, ^{13}C NMR, and ^{31}P NMR) were in accord with those previously reported.[19]

(((3-Azidopropyl)phosphoryl)bis(oxy))bis(methylene) bis(2,2-dimethylpropanoate) (109)

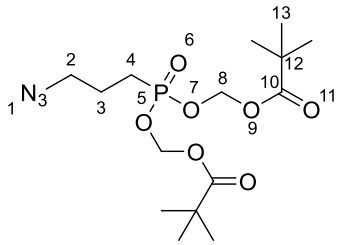

To a solution of **108** (1.5 g, 9.1 mmol, 1 equiv.) and TEA (8.7 mL, 64 mmol, 7 equiv.) in anhydrous MeCN (25 mL) at RT, chloromethyl pivalate (5.2 mL, 36 mmol, 4 equiv.) was added slowly. The reaction mixture was stirred at 60 °C under an inert atmosphere for 40 h. After the first 24 h, additional chloromethyl pivalate (2.6 mL, 18 mmol, 2 equiv.) was added. After 40 h, the reaction mixture was concentrated *in vacuo*. The crude product was diluted with EtOAc (50 mL), then washed with H_2O (3 × 25 mL), washed with brine (30 mL) and dried over Na_2SO_4. The product was purified using flash column chromatography (10−40% EtOAc in cyclohexane) to give (((3-azidopropyl)phosphoryl)bis(oxy))bis(methylene) bis(2,2-dimethylpropanoate) (2.6 g, 6.6 mmol, 73%) as a colourless oil.

IR ν_{max}/cm^{-1}(thin film): 2099 (N=N=N) and 1751 (C=O);

^{1}H NMR (400 MHz, chloroform-*d*) δ 5.32 (s, 4H, $(C(8)H_2)_2$), 3.02 (td, *J* = 6.3, 2.0 Hz, 2H, $C(2)H_2$), 1.60 – 1.47 (m, 4H, $C(3)H_2$, $C(4)H_2$), 0.88 (s, 18H, $(C(13)H_3)_6$); ^{13}C NMR (101 MHz, chloroform-*d*) δ 176.98, 81.51 (d, *J* = 6.3 Hz), 51.32 (d, *J* = 17.4 Hz), 38.85, 26.95, 23.88 (d, *J* = 142.6 Hz), 22.14 (d, *J* = 4.9 Hz); ^{31}P NMR (162 MHz, chloroform-*d*) δ 31.66;

LRMS: *m/z*(%)= 394.1 (100) $[M + H]^+$; HRMS: calcd. $C_{15}H_{29}O_7N_3P$ $[M + H]^+$: 394.1738; found: 394.1731;

(*S*)-(((3-(4-((1-((Benzyloxy)amino)-1-oxopropan-2-yl)amino)quinazoline-2-carboxamido)propyl)phosphoryl)bis(oxy))bis(methylene)bis(2,2-dimethylpropanoate) (110)

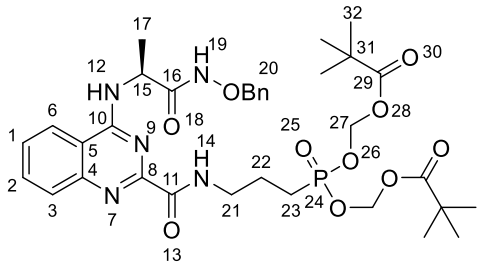

A mixture of **109** (500 mg, 1.3 mmol, 1 equiv.), PPh_3 (334 mg, 1.3 mmol, 1 equiv.) and H_2O (30 uL, 1.7 mmol, 1.3 equiv.) in THF (10 mL) was stirred for 12 h. Reaction mixture was dried first under flow of $N_{2(g)}$ and then using Schlenk line to give crude intermediate (((3-aminopropyl)phosphoryl)bis(oxy))bis(methylene) bis(2,2-dimethylpropanoate) as a white solid. Crude intermediate was dissolved in anhydrous DMF (5 mL), cooled down to −20 °C and **100** (590 mg, 1.3 mmol, 1 equiv.) was added followed by dropwise addition of TEA (180 µL, 1.3 mmol, 1 equiv.). Reaction mixture was stirred at −20 °C under inert atmosphere for 5 h, diluted with EtOAc (50 mL), washed with 0.2 M citric $acid_{(aq)}$ (2 × 10 mL), washed with brine (20 mL) and dried over $Na2SO_4$. Purified twice using flash column chromatography (first: 0–5% MeOH in EtOAc, second 0–7% MeOH in DCM) to give (*S*)-(((3-(4-((1-((Benzyloxy)amino)-1-oxopropan-2-yl)amino)quinazoline-2-carboxamido) propyl)phosphoryl)bis(oxy))bis(methylene) bis(2,2-dimethylpropanoate) (390 mg, 0.54 mmol, 43% after 2 steps) as a white solid.

IR ν_{max}/cm^{-1}(thin film): 1754, 1672 and 1618 (C=O);

^{1}H NMR (500 MHz, DMSO-d_6) δ 11.36 (s, 1H, N(19)H), 8.69 (t, *J* = 6.2 Hz, 1H, N(14)H), 8.53 (d, *J* = 6.6 Hz, 1H, C(6)H), 8.47 (d, *J* = 8.3 Hz, 1H, N(12)H), 7.89 – 7.81 (m, 2H, C(2)H, C(3)H), 7.63 (ddd, *J* = 8.3, 6.2, 2.1 Hz, 1H, C((1)H), 7.35 – 7.25 (m, 5H, OBn(20) ArH_5), 5.63 – 5.54 (m, 4H, $(C(27)H_2)_2$), 4.78 – 4.72 (m, 3H, C(15)H, OBn(20) -CH_2-), 3.37 – 3.30 (m, 2H, $C(21)H_2$), 1.95 – 1.86 (m, 2H, $C(23)H_2$), 1.80 – 1.71 (m, 2H, $C(22)H_2$), 1.47 (d, *J* = 7.1 Hz, 3H, $C(17)H_3$), 1.13 (s, 18H, $(C(32)H_3)_6$); ^{13}C NMR (126 MHz, 363K, DMSO-d_6) δ 175.76, 163.26, 159.27, 153.69, 148.92, 135.68, 132.81, 128.34, 127.91, 127.77, 127.72, 126.41, 123.01, 114.39, 81.35 (d, *J* = 6.1 Hz), 78.82, 48.29, 38.97, 37.90, 26.23, 23.31 (d, *J* = 139.3 Hz), 21.85 (d, *J* = 5.0 Hz), 16.76; ^{31}P NMR (162 MHz, DMSO-d_6) δ 32.52;

LRMS: *m/z*(%)= 716.2 (100), 717.2 (39) $[M + H]^+$; HRMS: calcd. $C_{34}H_{47}O_{10}N_5P$ $[M + H]^+$: 716.3055; found: 716.3046;

(*S*)-(((3-(4-((1-(Hydroxyamino)-1-oxopropan-2-yl)amino)quinazoline-2-carboxamido) propyl)phosphoryl)bis(oxy))bis(methylene) bis(2,2-dimethylpropanoate) (111)

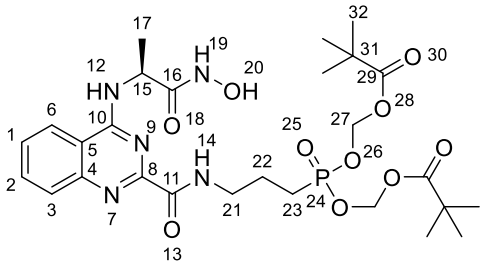

A mixture of **110** (350 mg, 0.49 mmol, 1 equiv.), palladium on carbon (100 mg, 10 wt. %) in MeOH (10 mL) was stirred at RT under H_2 atmosphere for 3 h, then concentrated *in vacuo*.

Purified twice using flash column chromatography (2 × 2–15% MeOH in DCM) to give (*S*)-(((3-(4-((1-(hydroxyamino)-1-oxopropan-2-yl)amino)quinazoline-2-carboxamido)propyl) phosphoryl)bis(oxy))bis(methylene) bis(2,2-dimethylpropanoate) (202 mg, 0.32 mmol, 66%) as a white solid.

IR ν_{max}/cm^{-1}(solid): 3256 (O-H), 1754 (C=O) and 1670 (C=O)

^{1}H NMR (400 MHz, DMSO-d_6) δ 10.78 (d, *J* = 1.8 Hz, 1H, N(19)H), 8.85 (d, *J* = 1.8 Hz, 1H, O(20)H), 8.68 (t, *J* = 6.2 Hz, 1H, N(14)H), 8.48 (app. d, *J* = 7.9 Hz, 2H, C(6)H, N(12)H), 7.84 (app. dd, *J* = 6.3, 1.5 Hz, 2H, C(2)H, C(3)H), 7.62 (ddd, *J* = 8.3, 6.1, 2.2 Hz, 1H, C(1)H), 5.63 – 5.58 (m, 4H, $(C(27)H_2)_2$), 4.85 (app. p, *J* = 7.1 Hz, 1H, C(15)H), 3.36 (td, *J* = 6.8, 3.0 Hz, 2H, $C(21)H_2$), 1.92 (app. dd, *J* = 10.1, 6.1 Hz, 2H, $C(23)H_2$), 1.76 (app. dq, *J* = 14.3, 7.1 Hz, 2H, $C(22)H_2$), 1.48 (d, *J* = 7.0 Hz, 3H, $C(17)H_3$), 1.14 (s, *J* = 1.2 Hz, 18H, $(C(32)H_3)_6$); ^{13}C NMR (151 MHz, DMSO-d_6) δ 176.12, 169.58, 163.33, 159.29, 153.69, 149.08, 133.22, 128.22, 126.78, 123.46, 114.54, 81.32 (d, *J* = 6.0 Hz), 48.12, 39.52, 38.16, 26.45, 23.34 (d, *J* = 139.3 Hz), 22.06 (d, *J* = 4.8 Hz), 17.63; ^{31}P NMR (162 MHz, DMSO-d_6) δ 32.79;

LRMS: *m/z*(%)= 626.1 (100), 627.1 (31) $[M + H]^+$; HRMS: calcd. $C_{27}H_{41}O_{10}N_5P$ $[M + H]^+$: 626.2586; found: 626.2579;

$[\alpha]_D^{25}$ = +4.1 (c = 0.8 in MeOH);

6.3. References

[1] C. K. Allerston, S. Y. Lee, J. A. Newman, C. J. Schofield, P. J. Mchugh and O. Gileadi, *Nucleic Acids Research*, 2015, **43**, 11047–11060.

[2] Y. Yosaatmadja, H.T Baddock, J. A. Newman, M. Bielinski, A. E. Gavard, S. M. M. Mukhopadhyay, A. A. Dannerfjord, C. J. Schofield, P. J. McHugh and O. Gileadi, *Nucleic Acids Research*, 2021, **49**, 9310-9326.
[3] S. Y. Lee, J. Brem, I. Pettinati, T. D. W. Claridge, O. Gileadi, C. J. Schofield and P. J. Mchugh, *Chemical Communications*, 2016, **52**, 6727–6730.
[4] WO 9819648
[5] A. J. Birch, M. Salahud-Din and D. C. C. Smith, *Journal of the Chemical Society C: Organic*, 1966, **0**, 523–527.
[6] S. Takada, T. Sasatani, N. Chomei, M. Adachi, T. Fujishita, M. Eigyo, S. Murata, K. Kawasaki and A. Matsushita, *Journal of Medicinal Chemistry*, 1996, **39**, 2844–2851.
[7] R. R. Deore, G. S. Chen, P.-T. Chang, T.-R. Chern, S.-Y. Lai, M.-H. Chuang, J.-H. Lin, F.-L. Kung, C.-S. Chen, C.-T. Chiou and J.-W. Chern, *ChemMedChem*, 2012, **7**, 850–860.
[8] M. Falsini, L. Squarcialupi, D. Catarzi, F. Varano, M. Betti, L. Di Cesare Mannelli, B. Tenci, C. Ghelardini, M. Tanc, A. Angeli, C. T. Supuran and V. Colotta, *Journal of Medicinal Chemistry*, 2017, **60**, 6428–6439.
[9] J. Tang, K. Maddali, M. Metifiot, Y. Y. Sham, R. Vince, Y. Pommier and Z. Wang, *Journal of Medicinal Chemistry*, 2011, **54**, 2282–2292.
[10] P. S. Khokhlov, V. N. Osipov and A. V. Roshchin, *Russian Chemical Bulletin*, 2011, **60**, 153–156.
[11] R. A. Smits, I. J. P. De Esch, O. P. Zuiderveld, J. Broeker, K. Sansuk, E. Guaita, G. Coruzzi, M. Adami, E. Haaksma and R. Leurs, *Journal of Medicinal Chemistry*, 2008, **51**, 7855–7865.
[12] L. Purushottam, S. R. Adusumalli, U. Singh, V. B. Unnikrishnan, D. G. Rawale, M. Gujrati, R. K. Mishra and V. Rai, *Nature Communications*, 2019, **10**.
[13] H.-B. Zhou, G.-S. Liu and Z.-J. Yao, *The Journal of Organic Chemistry*, 2007, **72**, 6270–6272.
[14] C. Hao, F. Zhao, H. Song, J. Guo, X. Li, X. Jiang, R. Huan, S. Song, Q. Zhang, R. Wang, K. Wang, Y. Pang, T. Liu, T. Lu, W. Huang, J. Wang, B. Lin, Z. He, H. Li, F. Li, D. Zhao and M. Cheng, *Journal of Medicinal Chemistry*, 2018, **61**, 265–285.
[15] A. Y. Chen, P. W. Thomas, Z. Cheng, N. Y. Xu, D. L. Tierney, M. W. Crowder, W. Fast and S. M. Cohen, *ChemMedChem*, 2019, **14**, 1271–1282.
[16] G. Labbé, A. P. Krismanich, S. De Groot, T. Rasmusson, M. Shang, M. D. R. Brown, G. I. Dmitrienko and J. G. Guillemette, *Journal of Inorganic Biochemistry*, 2012, **112**, 49–58.
[17] O. A. Pemberton, P. Jaishankar, A. Akhtar, J. L. Adams, L. N. Shaw, A. R. Renslo and Y. Chen, *Journal of Medicinal Chemistry*, 2019, **62**, 8480–8496.
[18] Y. Yuan, S. A. Zaidi, D. L. Stevens, K. L. Scoggins, P. D. Mosier, G. E. Kellogg, W. L. Dewey, D. E. Selley and Y. Zhang, *Bioorganic & Medicinal Chemistry*, 2015, **23**, 1701–1715.
[19] A. K. Tucker-Schwartz and R. L. Garrell, *Chemistry – A European Journal*, 2010, **16**, 12718–12726.

Chapter 7. Appendix

7.1. Inhibitors developed in this project.

Table containing the inhibitors that were synthesised and tested during this project:

Number	Structure	Number	Structure
3	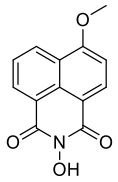	**5**	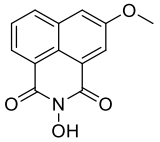
9	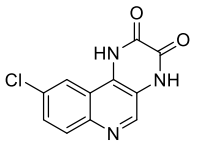	**12**	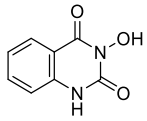
14	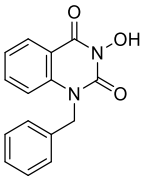	**15**	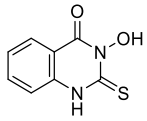
18	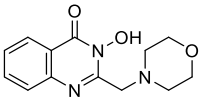	**20**	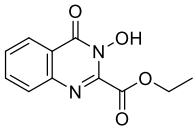
24	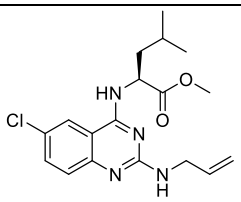	**25**	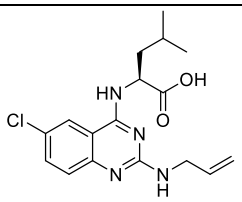
27	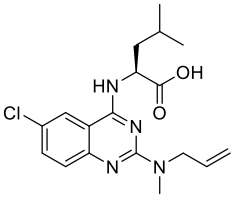	**30**	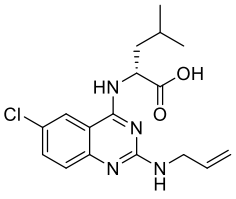

31	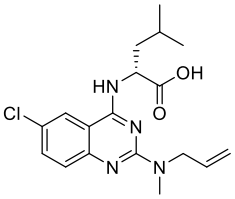	**34**	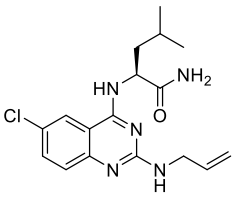
36	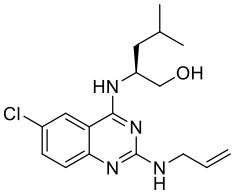	**39**	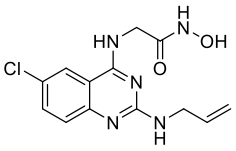
42	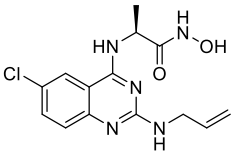	**45**	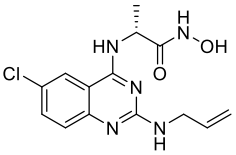
48	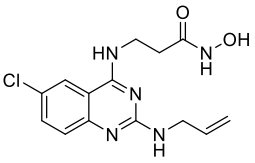	**51**	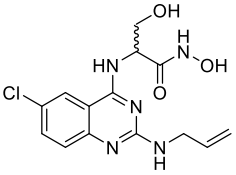
54	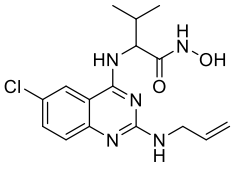	**55**	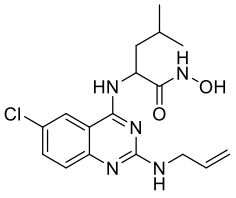
57	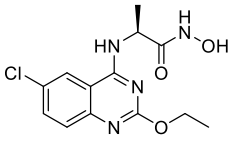	**59**	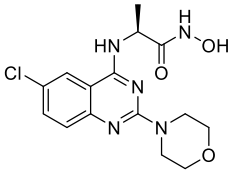
61	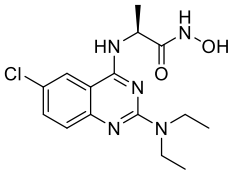	**63**	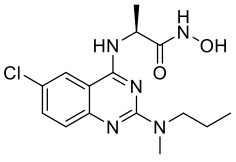
65	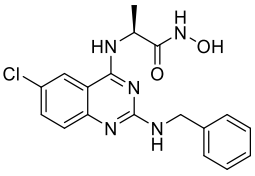	**67**	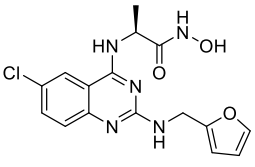

69	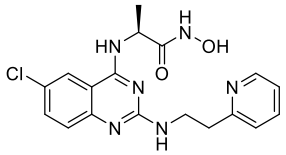	**70**	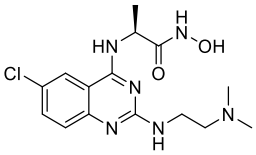
74	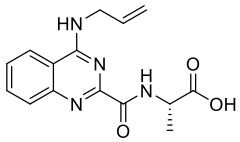	**75**	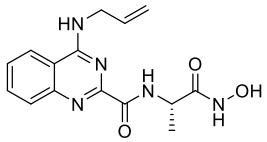
77	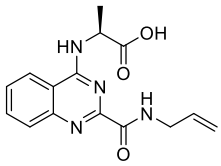	**78**	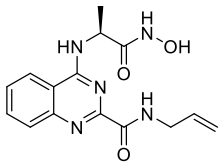
81	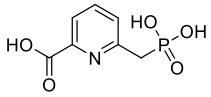	**83**	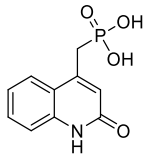
85	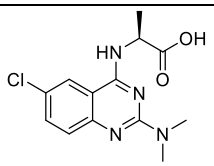	**88**	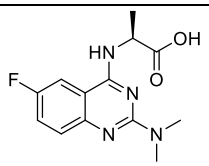
91	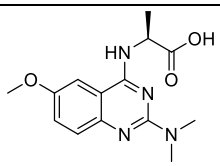	**95**	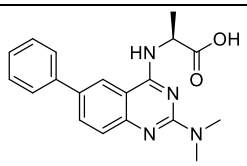
101	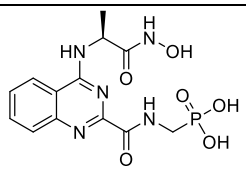	**102**	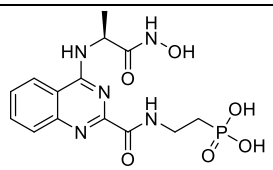
103	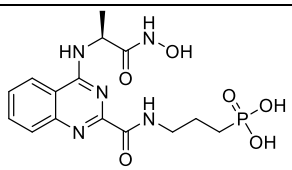	**104**	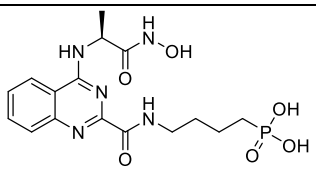

105	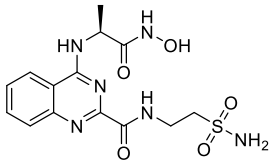	**106**	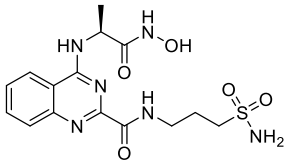
107	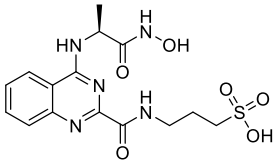	**111**	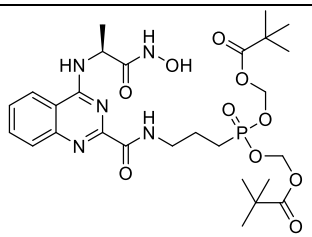

Table 7.1: Table of compounds developed in this project

7.2. Screening of metal chelators and metalloenzyme inhibitors

Throughout the project, commercially available and in-house compounds were screened against SNM1A and SNM1B. Primarily metal chelators and metalloenzyme inhibitors were tested in an attempt to find other potent pharmacophores active against SNM1A and SNM1B.

Boronates were tested because they are known inhibitors of protistan CPSF73, bacterial MBLs and phosphodiesterase, amongst other enzymes.[1,2,3] Additionally, boronates can act as phosphate bioisostere and might potentially mimic the phosphodiester bond in substrates for SNM1A and SNM1B.[4]

Name	Structure	Description	Testing vs SNM1A	Testing vs SNM1B
B1	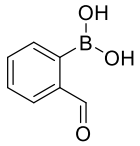	Boronate fragment	No inhibition observed at 100 μM	No inhibition observed at 100 μM
B2	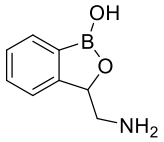	Boronate fragment	No inhibition observed at 100 μM	No inhibition observed at 100 μM
B3	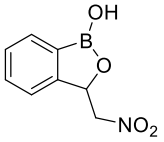	Boronate fragment	No inhibition observed at 100 μM	No inhibition observed at 100 μM
B4	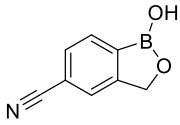	Boronate fragment	No inhibition observed at 100 μM	No inhibition observed at 100 μM
B5	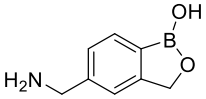	Boronate fragment	No inhibition observed at 100 μM	No inhibition observed at 100 μM
Bortezomib	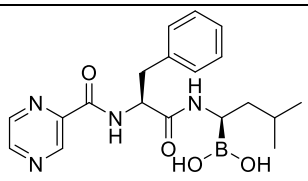	Clinically use boronate-based proteasome inhibitor	No inhibition observed at 100 μM	No inhibition observed at 100 μM
SCYX-6759	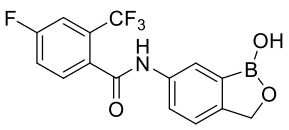	Protistan CPSF73 inhibitor, currently in clinical studies	No inhibition observed at 100 μM	No inhibition observed at 100 μM

Table 7.2: *Results from screening boronates.*

Sulfonamides were tested as they are good Zinc (II) chelators.[5] Sulfonamide functional group is commonly found in many metalloenzyme inhibitors, including bacterial MBL and carbonic anhydrase inhibitors.[6,7]

Name	Structure	Description	Testing vs SNM1A	Testing vs SNM1B
NSPC 6	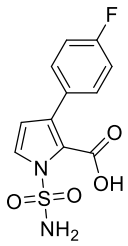	Bacterial MBL inhibitor	No inhibition observed at 100 μM	No inhibition observed at 100 μM
Famotidine	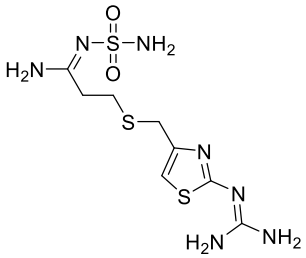	Clinically used antiulcer drug but also carbonic anhydrase inhibitor	No inhibition observed at 100 μM	No inhibition observed at 100 μM
Hydrochlorothiazide	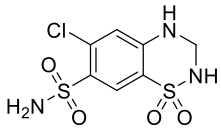	Clinically used carbonic anhydrase inhibitor	No inhibition observed at 100 μM	Not Tested
Acetazolamide	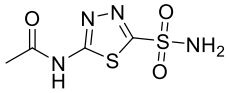	Clinically used carbonic anhydrase inhibitor	No inhibition observed at 100 μM	Not Tested

Table 7.3: *Results from screening sulfonamides.*

N-Heterocyclic carboxylic acids were tested because they are common metal ion chelators. Pyridine carboxylic acids inhibit multiple enzymes, including histone demethylases and bacterial MBLs.[8,9] The indole-3-carboxylate core is present in AP nuclease and bacterial MBL inhibitors.[10,11]

Name	Structure	Description	Testing vs SNM1A	Testing vs SNM1B
Pyridine-2,4-dicarboxylic acid	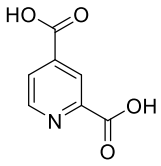	Common metal ion chelator	Apparent enhancement of activity	No inhibition observed at 100 μM
Pyridine-2,6-dicarboxylic acid	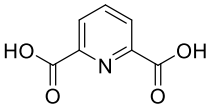	Common metal ion chelator	Apparent enhancement of activity	No inhibition observed at 100 μM
3-(Phenylsulfonamido) picolinic acid	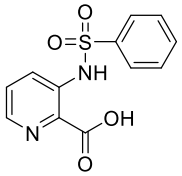	Bacterial MBL inhibitor	Apparent enhancement of activity	No inhibition observed at 100 μM
ANT431	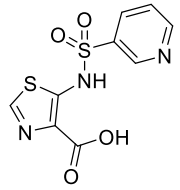	Bacterial MBL inhibitor, an analogue of 3-(Phenylsulfonamido) picolinic acid	Apparent enhancement of activity	No inhibition observed at 100 μM
Indole-2-carboxylate	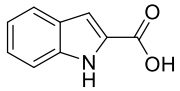	Indole-3-carboxylate, present in AP nuclease and bacterial MBL inhibitors	No inhibition observed at 100 μM	No inhibition observed at 100 μM
Indole-2-acetic acid	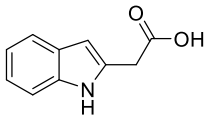	Metal ion chelator	No inhibition observed at 100 μM	No inhibition observed at 100 μM

Table 7.4: *Results from screening N-heterocyclic carboxylic acids.*

After observing that hydroxamate-based inhibitors inhibited SNM1A and SNM1B, in **Chapter 2** and **Chapter 3**, other commercially available hydroxamates were tested against SNM1A and SNM1B. In **Section 3.3.3**, testing of hydroxamate-based HDAC inhibitors was shown.

Name	Structure	Description	Testing vs SNM1A	Testing vs SNM1B
Zileuton	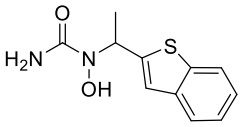	Clinical used 5-Lipoxygenase inhibitor	No inhibition was observed at 100 μM	No inhibition was observed at 100 μM
Fosmidomycin	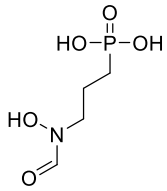	Antibiotic and DXP reductoisomerase inhibitor	No inhibition was observed at 100 μM	No inhibition was observed at 100 μM
N-Hydroxyphthalimide	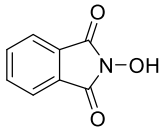	Cyclic hydroxamate	No inhibition was observed at 100 μM	No inhibition was observed at 100 μM

Table 7.5: *Results from testing hydroxamates.*

Screening of metal chelators and metalloenzyme was unfruitful. No new hit or pharmacophore against either SNM1A or SNM1B was identified. While no inhibition was observed, three more enhancers of SNM1A have been identified. All compounds that showed enhancement of enzyme activity had a picolinic acid core.

7.3. Enhancement of SNM1A activity by picolinic acid analogues

All the enhancers identified in the screening process were tested at 1 μM, 10 μM and 100 μM concentrations against SNM1A.

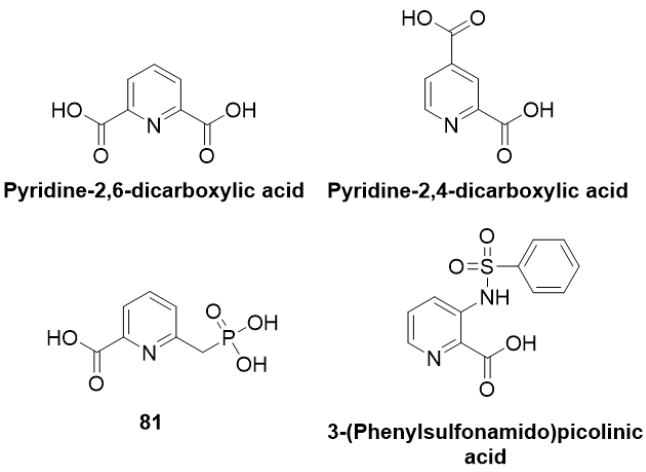

Figure 7.1: *Structure of SNM1A enhancers.*

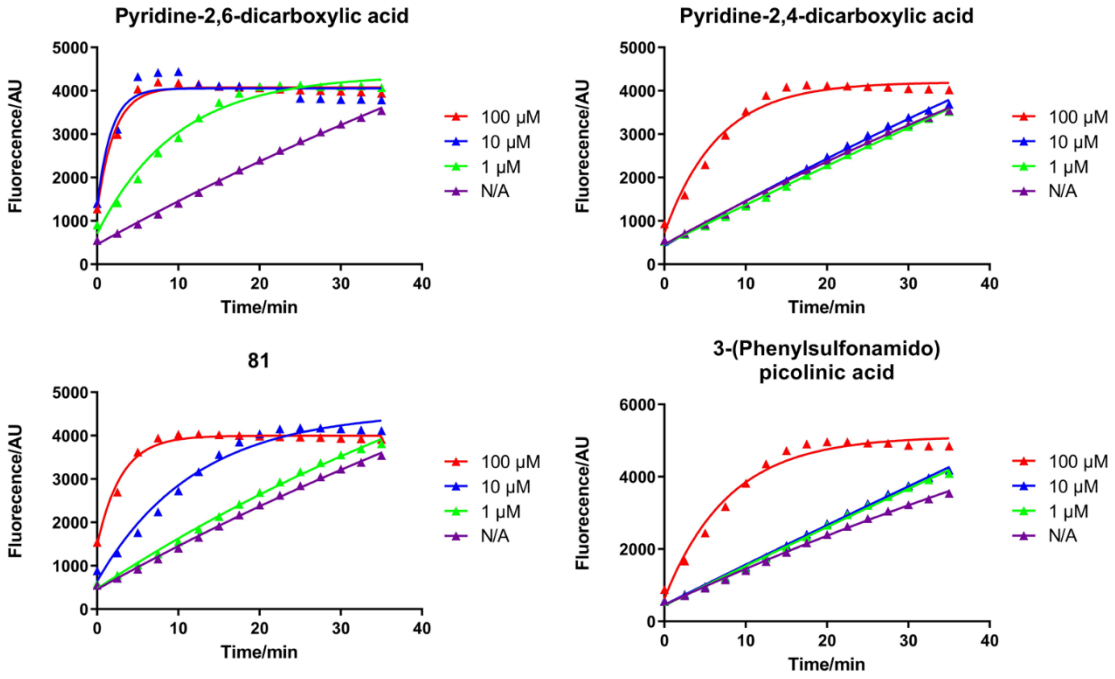

Figure 7.2: *Enzyme activity assay with SNM1A. Mesearument of fluorescence emission released upon digestion of modified DNA by SNM1A. The fluorescence emission is proportional to the extent of digestion of DNA substrate. [SNM1A] = 0.5 nM and [DNA] = 25 nM.*

The most potent enhancer out of the four enzyme enhancers, which were tested, was pyridine-2,6-dicarboxylic acid. Pyridine-2,6-dicarboxylic acid increased the enzyme activity at 1 µM, 10 µM and 100 µM although, at 1 µM concentration, the increase in enzyme activity was lower than at 10 µM and 100 µM. An increase in enzyme activity was not observed

when these compounds were tested against SNM1B. The mechanism through which the compounds present in **Figure 7.1** enhance the activity of SNM1A is unknown.

7.4. β-Citryl-*L*-glutamate

In addition to work on nuclease inhibitors, β-Citryl-*L*-glutamate (**β-CG**) was synthesised**. B-CG** is a known metabolite initially observed in the brains of newborn rats.[12] Although the function of this metabolite remains unknown, studies show that it is linked to oxidative stress.[13] β-Citryl-*L*-glutamate can also act as an iron chaperone.[14] **β-CG** was synthesised using a previously reported synthetic scheme (**Figure 7.3**).[12] Unfortunately, due to the use of strong basic conditions for the final step, deprotection of methyl esters, the citryl-*L*-glutamate was synthesised as a mixture of two isomers: α-citryl-*L*-glutamate (**α-CG**) and **β-CG**. Isomers were separated using RP-HPLC. After synthesis, both compounds were given to McCullagh Group (Department of Chemistry, University of Oxford) to be used as an internal standard for metabolomics studies.

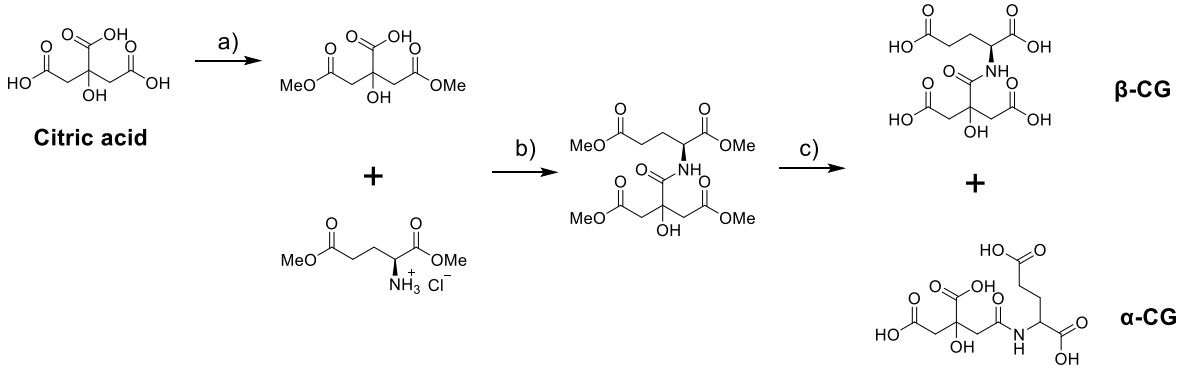

Figure 7.3: *Synthesis of* ***α-CG*** *and* ***β-CG****. Reaction conditions:* ***a)*** *$B(OH)_3$, MeOH, Acetone, RT, 72 h;* ***b)*** *NHS, DCC, 1,4-dioxane, RT, 12 h;* ***c)*** *NaOH, water, 1,4-dioxane RT, 4h.*

7.5. References

[1] R. J. Wall, E. Rico, I. Lukac, F. Zuccotto, S. Elg, I. H. Gilbert, Y. Freund, M. R. K. Alley, M. C. Field, S. Wyllie and D. Horn, *Proceedings of the National Academy of Sciences*, 2018, **115**, 9616–9621.

[2] P. A. Lang, A. Parkova, T. M. Leissing, K. Calvopiña, R. Cain, A. Krajnc, T. D. Panduwawala, J. Philippe, C. W. G. Fishwick, P. Trapencieris, M. G. P. Page, C. J. Schofield and J. Brem, *Biomolecules*, 2020, **10**, 899.

[3] D. M. Paton, *Drugs Today (Barc)*, 2017, **53**, 239-245.

[4] A. R. Martin, K. Mohanan, D. Luvino, N. Floquet, C. Baraguey, M. Smietana and J.-J. Vasseur, *Organic & Biomolecular Chemistry*, 2009, **7**, 4369.

[5] A. Tanakit, M. Rouffet, D. P. Martin and S. M. Cohen, *Dalton Transactions*, 2012, **41**, 6507.

[6] A. J. M. Farley, Y. Ermolovich, K. Calvopiña, P. Rabe, T. Panduwawala, J. Brem, F. Björkling and C. J. Schofield, *ACS Infectious Diseases*, 2021, **7**, 1809–1817.

[7] A. Bonardi, A. Nocentini, S. Bua, J. Combs, C. Lomelino, J. Andring, L. Lucarini, S. Sgambellone, E. Masini, R. Mckenna, P. Gratteri and C. T. Supuran, *Journal of Medicinal Chemistry*, 2020, **63**, 7422–7444.

[8]N. R. Rose, S. S. Ng, J. Mecinović, B. M. R. Liénard, S. H. Bello, Z. Sun, M. A. Mcdonough, U. Oppermann and C. J. Schofield, *Journal of Medicinal Chemistry*, 2008, **51**, 7053–7056.

[9] S. Leiris, A. Coelho, J. Castandet, M. Bayet, C. Lozano, J. Bougnon, J. Bousquet, M. Everett, M. Lemonnier, N. Sprynski, M. Zalacain, T. D. Pallin, M. C. Cramp, N. Jennings, G. Raphy, M. W. Jones, R. Pattipati, B. Shankar, R. Sivasubrahmanyam, A. K. Soodhagani, R. R. Juventhala, N. Pottabathini, S. Pothukanuri, M. Benvenuti, C. Pozzi, S. Mangani, F. De Luca, G. Cerboni, J.-D. Docquier and D. T. Davies, *ACS Infectious Diseases*, 2019, **5**, 131-140.

[10] S. Madhusudan, F. Smart, P. Shrimpton, J. L. Parsons, L. Gardiner, S. Houlbrook, D. C. Talbot, T. Hammonds, P. A. Freemont, M. J. E. Sternberg, G. L. Dianov and I. D. Hickson, *Nucleic Acids Research*, 2005, **33**, 4711–4724.

[11] J. Brem, T. Panduwawala, J. U. Hansen, J. Hewitt, E. Liepins, P. Donets, L. Espina, A. J. M. Farley, K. Shubin, G. G. Campillos, P. Kiuru, S. Shishodia, D. Krahn, R. K. Leśniak, J. Schmidt, K. Calvopiña, M.-C. Turrientes, M. E. Kavanagh, D. Lubriks, P. Hinchliffe, G. W. Langley, A. F. Aboklaish, A. Eneroth, M. Backlund, A. G. Baran, E. I. Nielsen, M. Speake, J. Kuka, J. Robinson, S. Grinberga, L. Robinson, M. A. Mcdonough, A. M. Rydzik, T. M. Leissing, J. C. Jimenez-Castellanos, M. B. Avison, S. Da Silva Pinto, A. D. Pannifer, M. Martjuga, E. Widlake, M. Priede, I. Hopkins Navratilova, M. Gniadkowski, A. K. Belfrage, P. Brandt, J. Yli-Kauhaluoma, E. Bacque, M. G. P. Page, F. Björkling, J. M. Tyrrell, J.

Spencer, P. A. Lang, P. Baranczewski, R. Cantón, S. P. Mcelroy, P. S. Jones, F. Baquero, E. Suna, A. Morrison, T. R. Walsh and C. J. Schofield, *Nature Chemistry*, 2022, **14**, 15–24.

[12] M. Miyake, Y. Kakimoto and M. Sorimachi, *Biochimica et Biophysica Acta (BBA) - General Subjects*, 1978, **544**, 656–666.

[13] T. Vallianatou, W. Lin, N. B. Bèchet, M. S. Correia, N. C. Shanbhag, I. Lundgaard and D. Globisch, *Journal of Cerebral Blood Flow & Metabolism*, 2021, **41**, 3324–3338.

[14] M. Hamada-Kanazawa, M. Narahara, M. Takano, K. S. Min, K. Tanaka and M. Miyake, *Biological and Pharmaceutical Bulletin*, 2011, **34**, 1455–1464.